NASA Contractor Report 172322

JT15D SIMULATED FLIGHT DATA EVALUATION

R.G. Holm

Aircraft Engine Business Group
General Electric Company
Cincinnati, Ohio 45215

Contract NAS1-16776
September 1984

NASA

National Aeronautics and
Space Administration

Langley Research Center
Hampton, Virginia 23665.

ABS: The noise characteristics of the JT15D turbofan engine was analyzed with
      the objectives of: (1) assessing the state-of-art ability to simulate
      flight acoustic data using test results acquired in wind tunnel and
      outdoor (turbulence controlled) environments; and (2) predicting the
      farfield noise directivity of the blade passage frequency (BPF) tonal
      components using results from rotor blade mounted dynamic pressure
      instrumentation. Engine rotor tip speeds at subsonic, transonic, and
      supersonic conditions were evaluated. The ability to simulate flight
      results was generally within 2-3 dB for both outdoor and wind tunnel
      acoustic results. Some differences did occur in the broadband noise level
      and in the multiple-pure-tone harmonics at supersonic tip speeds. The
      prediction of blade passage frequency tone directivity from dynamic
ENTER:

NASA Contractor Report 172322

JT15D SIMULATED FLIGHT DATA EVALUATION

R.G. Holm

Aircraft Engine Business Group
General Electric Company
Cincinnati, Ohio 45215

NASA

National Aeronautics and
Space Administration

Langley Research Center
Hampton, Virginia 23665

N85- 32387 #

TABLE OF CONTENTS

TABLE OF CONTENTS (Concluded)

LIST OF FIGURES

SECTION 1.0

SUMMARY

1.0 SUMMARY

The noise characteristics of the JT15D turbofan engine were analyzed in detail to make assessments of (1) the ability to simulate flight results using wind tunnel and outdoor (turbulence controlled) acoustic test data and (2) the prediction of the far field tonal noise directively using internal blade and vane mounted instrumentation. The data sets utilized to perform these analyses were obtained from various NASA or NASA-sponsored test programs at the NASA Ames 40 x 80 Foot Wind Tunnel, the NASA Ames Outdoor Test Facility and at the NASA Wallops Island Flight Test Center.

The initial task of projecting the simulated flight data to particular flight configurations involved a variety of corrections and adjustments each of which may have introduced added uncertainty. These uncertainties were not dealt with in this program, and thus the methodology associated with these projections represents state-of-the-art techniques. The projections themselves were performed using averaging techniques which attempt to produce minimized statistical errors, i.e., ±0.5 dB. The flight data to which the projections are compared was analyzed in time segments of 0.2 seconds which yields adequate narrowband resolution to make useful narrowband comparisons. Four microphones were ensemble-averaged to improve the statistical errors associated with this form of data analysis.

The results of these comparisons demonstrated that at subsonic conditions the broadband energy of the projected (flight simulated) data was typically on the order of 3 dB higher for wind tunnel cases and 5 dB higher for outdoor turbulence control cases when the fan was operating at subsonic tip speeds and over the angular range from 40 to 70°. For the projected results the tone energy associated with the fan blade passing frequency was, in general, higher at angles of 50° to 90° and lower for angles less than 50°. Generally the wind tunnel agreement was superior to the outdoor TCS agreement.

At supersonic fan tip speeds the Blade Passage Frequency (BPF) tone was considerably higher for the flight case than the projected results, while the multiple pure tones were considerably lower than the projected results.

SECTION 2.0

INTRODUCTION

2.0 INTRODUCTION

The measurement of aircraft flyover noise data which exhibits significant differences in characteristics from that obtained under static conditions has led to an expanded research effort toward understanding these differences. Directly related to the problem of what caused the observed noise differences between flight and static testing is the question of what techniques to use to simulate flight. The research effort to date has produced information suggesting that inflow turbulence is the primary cause of the observed differences between static and flight fan source noise. Thus, in-flow turbulence control devices and wind tunnels are being utilized to attempt to simulate in-flow turbulence characteristics that the fan would encounter in flight. This should in turn allow the fan to generate noise on the ground which is similar to that generated in flight.

A detailed understanding of the flight effects and flight simulation techniques can proceed only as rapidly as an adequate acoustic data base becomes available and understood. In the past, systematic far-field noise data obtained from controlled research tests of fully instrumented engines operated under several test environments, i.e., static, simulated flight and flight, has been difficult to obtain. However, as a result of the recent NASA OV-1B program and several other test programs, such acoustic data sets on the JT15D engine have become available. Therefore, an evaluation of the flight effect differences and flight simulation capabilities utilizing this important data base appear to be timely and appropriate.

The overall objective of this effort was to conduct a limited assessment of the detailed noise characteristics of the JT15D engine representing flight simulation capabilities of various non-flight test techniques. This was accomplished through systematic analyses of several sets of measured far-field acoustic data and blade mounted transducer (BMT) data already obtained by NASA and by the General Electric Co. under NASA-sponsored programs on the JT15D engine. Specifically, the use of an in-flow turbulence control structure (TCS) and the use of two different inlet geometries tested in the NASA Ames 12 x 24 m wind tunnel were evaluated for their flight simulation capabilities.

3

The analysis and comparison of data obtained from two test environments, static with TCS and wind tunnel, was performed. The data comparisons utilize measurements obtained with a hardwall diffusing inlet and both a treated and an untreated bypass exhaust duct. Flight effects and simulation capabilities were initially determined through analysis and comparison of far-field acoustic data in terms of conventional parameters, e.g., spectral and directivity characteristics. To the extent practical, BMT data were analyzed as appropriate to lend added understanding to the possible causes of observed far-field noise differences associated with the different test environments. The statistical significance of each data set was analyzed to verify that conclusions reached using the above comparisons were soundly based.

Findings concerning flight effects and simulation capabilities will be reviewed and discussed in terms of available theories and prior data regarding in-flow turbulence and aerodynamically induced distortion effects, convective amplification effects (dynamic) associated with acoustic source types, possible effects due to inlet designs and other propagation and installation effects. The anomalies identified in the tunnel data will be examined in-depth to determine, where possible, relative refraction and reflective effects or other effects that may be significant.

It is anticipated that accomplishment of the objectives of this program will assist NASA in conducting the final comprehensive determination of the adequacy of current flight simulation techniques. The potential for future applications of BMT information shall also be assessed.

4

SECTION 3.0

TEST DESCRIPTION

3.0 TEST DESCRIPTION

3.1   TEST FACILITIES

The test NASA facilities utilized to perform the acoustic evaluations which comprise this study were located at Moffet Field, California; Hampton, Virginia; and Wallops Island, Virginia. The test programs were all performed using a JT15D turbofan engine to make the data sets compatible. The test efforts were directed toward the ability to simulate flight acoustics in wind tunnel and outdoor test environments.

3.1.1 NASA WALLOPS ISLAND FLIGHT TEST CENTER

The flight tests of the JT15D turbofan engine installed on an aircraft were accomplished at the NASA Wallops Island Flight Test Center located in Wallops Island, Virginia. A typical flight profile for the testing is displayed in Figure 3-1. The Wallops facility possessed the capability to track the aircraft position very precisely using an FPS-16 radar in conjunction with a co-locating laser. The system focused on a laser reflector located in a fairing directly under the nose of the aircraft and provided an estimated accuracy of ±15.2 cm (6 in) in range and 0.1 milliradian in angle.

3.1.2 NASA-ARC 40 x 80 FOOT WIND TUNNEL

The simulated-flight tests were conducted in the Large-Scale 40 x 80 Foot Wind Tunnel at the Ames Research Center (ARC). A plan-view sketch of the 40 x 80 is shown in Figure 3-2. This facility has the capability, with an engine installed in the test section, to simulate flight speeds up to 91 m/s (300 ft/s). However, due to the fact that the wind tunnel is a closed-circuit facility, operation of an engine with the wind off circulates airflow around the circuit creating a minimum forward velocity range of 4 m/s (13.5 ft/s) to 8 m/s (26.3 ft/s), depending on the fan airflow. The wind-off operation provided quasi-static conditions of a low speed flow across the test section.

5

500' - 1000' AGL

400' - 300' AGL   3/4 - 1-1/2 NM   500' - 1000' AGL

3 - 5 NM

Test Runway

300' AGL   10   28   Climb to
                                               Downwind,
                                               Altitude

AGL = above ground level
NM = Nautical Miles
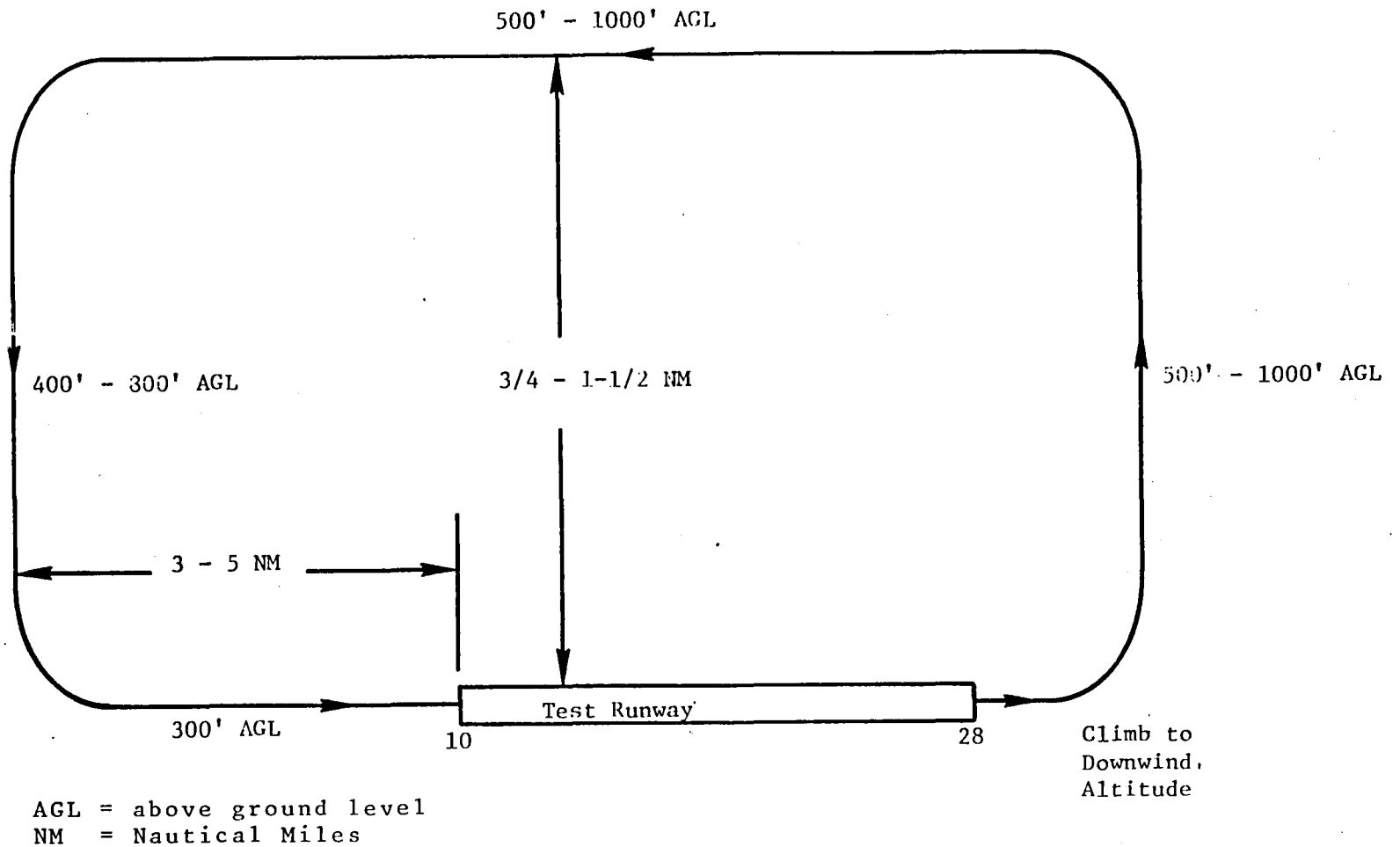
Figure 3-1. Typical Flight Profile for 300 ft. Flyover.

Six 12.2 m (40 ft) Diameter Fans

Flow

A

A

Test Section

Top View

24.4 m (80 ft)

12.2 ft(40 ft) R

12.2 m (40 ft)

Section A-A

Flow

24.4 m (80 ft)

Side View
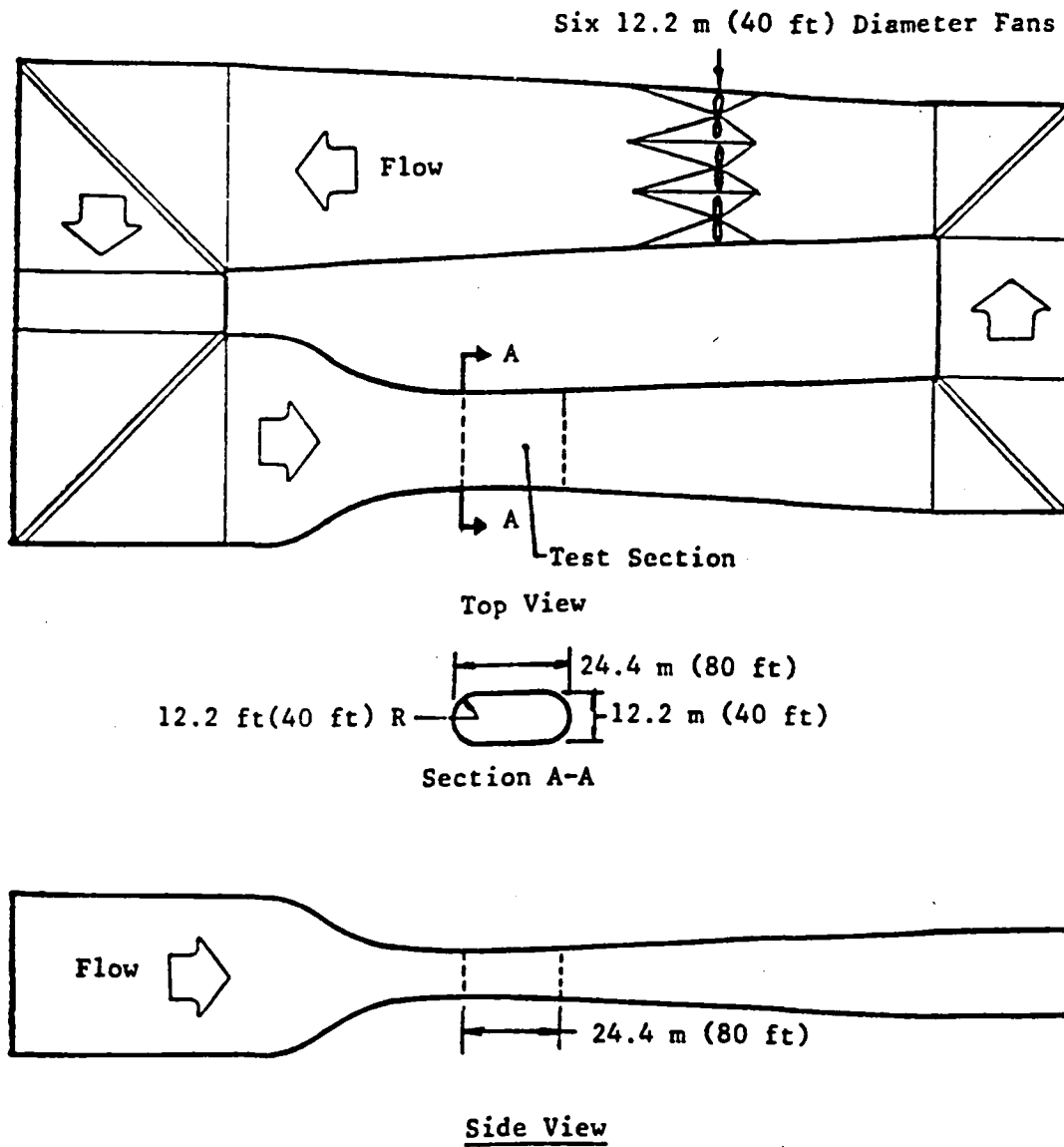
Figure 3-2. NASA-ARC 40 by 80 Wind Tunnel.

The use of the 40 by 80 for previous acoustic testing was significantly enhanced by lining the floor and part of the walls of the test section with a 7.62-cm (3-inch) layer of polyurethane foam. The foam mat virtually removed reverberant reflections from the noise data at all frequencies above 500 Hz. To ensure consistency in the noise measurements, the same foam was placed on the ground between the microphone and the engine during outdoor static tests.

3.1.3 NASA-ARC OUTDOOR TEST STAND

Outdoor static tests were performed on the NASA-ARC large-scale aerodynamics test stand. These tests were conducted during early morning hours to take advantage of calm wind conditions and to avoid background noise contamination from an active runway adjacent to the test site. A plan-view sketch of the test stand is shown in Figure 3-3. The operations, which include the engine operator's console and data acquisition systems, are housed underground to provide a reflection-free test-bed for acoustic measurements.

3.2 TEST VEHICLE

3.2.1 JT15D TURBOFAN ENGINE

The test vehicle supplied by ARC was a modified JT15D turbofan engine; a cross section is shown in Figure 3-4. The physical and aerodynamic parameters for the modified JT15D engine are listed in Table 3-1. The JT15D is a moderate bypass ratio engine with a single-stage, supersonic tip speed fan. With regard to forward radiated fan noise, the JT15D has many of the design features incorporated into the approximately four-times-larger modern turbofan engines in commercial service. Features such as the absence of inlet guide vanes (IGV's), large spacing between the fan blades and outlet guide vanes (OGV's), and at least twice as many OGV's as fan blades are common design features between the JT15D and the CF6, JT9D, and RB211 turbofan engines. The engine utilized for this series of tests was modified by ARC as a result of the research of Hodder (Reference 3-1). The inlet temperature sensor was made flush with the wall in order to eliminate the tone noise from the interaction of its wake with the fan blades. Also, the number of core stator vanes was increased and spaced further downstream from the fan to

8

Concrete Pad

TCS
Support
Crane

Underground
Operations
Facility

JT15D
Engine

Access
Road
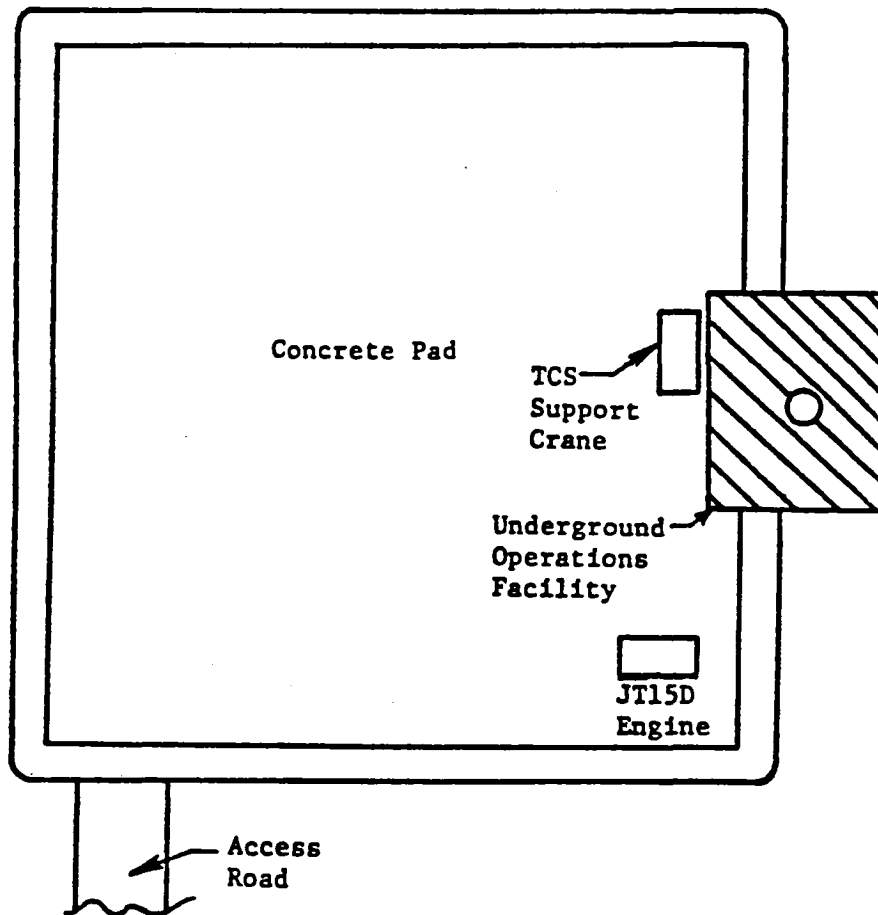
Figure 3-3. NASA-ARC Test Stand.

9

*Fan
(28 Blades)

(66 Vanes)

*HP Compressor
(16 Blades)

*Rotating Parts Are Shaded

Core (71 Vanes)

6 Support Struts
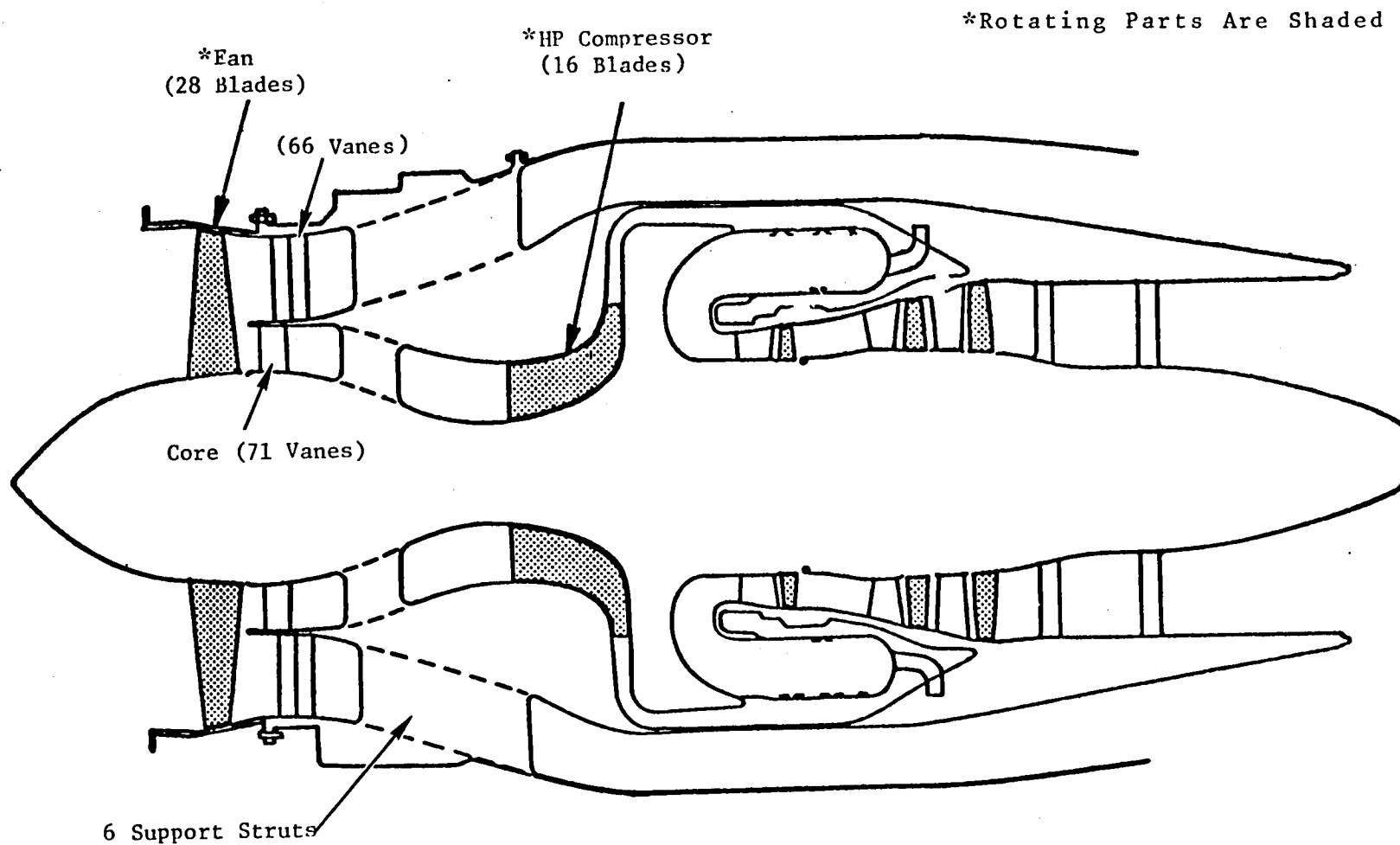
Figure 3-4. Modified JT15D Turbofan Engine.

TABLE 3-1

MODIFIED JT15D PARAMETERS

Fan Pressure Ratio	1.5
Bypass Ratio	3.3
Hub/Tip Ratio	0.405
Rotor Diameter, cm (in.)	53 (21)
Maximum Fan, rpm	16,000
Rotor Blades	28
Bypass Stator Vanes	66
Core Stator Vanes	71
Bypass Vane/Blade Ratio	2.36
Core Vane/Blade Ratio	2.54
Bypass Rotor/Stator Spacing	1.65
Core Rotor/Stator Spacing	0.85

diminish the impact of the fan blade wakes impinging on the vanes. The increase in core vane number produced a cutoff of tonal noise generated from this interaction.

3.2.2 NACELLE, NOZZLE, AND MOUNTING ASSEMBLY

JT15D engine used during the advanced inlet testing was housed in a special quiet nacelle designed by ARC engineers. The nacelle was completely lined with sound-absorbent material to minimize the radiation of engine casing noise to the forward quadrant. Also designed by ARC engineers was a new co-annular nozzle system for the JT15D. The new fan nozzle included a larger exit area to provide more flow to accommodate the operating line studies and had both walls lined with acoustic treatment to suppress the aft radiated fan noise. A cross section of the JT15D, with its nacelle and nozzle system, is shown in Figure 3-5, and the complete assembly is shown on the mount in Figure 3-6.

The mount is a leaned strut that supports the engine assembly 4.6 m (15 ft) over the wind tunnel floor as shown by the photo in Figure 3-7. The strut carries all the plumbing and instrumentation lines to the engine assembly and is fastened to a turntable. The axis of rotation is through the fan face which allows angle of attack to be accomplished by rotating the engine assembly about this vertical axis without changing the distances from the fan face to the noise measurement field. The engine assembly and its mount were installed on a nonrotating frame at the outdoor test stand to duplicate the wind tunnel setup during outdoor static testing.

3.2.3 AIRCRAFT

Figures 3-8(a) and (b) show photographs of the modified OV-1B aircraft which was used to perform the JT15D engine flight tests. Figure 3-9 is a sketch of the modified aircraft illustrating the mounting of the JT15D engine under the right wing. The mounting station normally carries an auxiliary fuel tank; therefore, the existing fuel system could be used with only minor modifications. Additional details regarding the aircraft with its JT15D installed performance are provided in Reference 3-2. The aircraft was heavily instrumented during the test program which provided aircraft and engine

Modified Core Stator   Fan-Exhaust Acoustic Treatment

Modified T_1 Sensor

Sound-Absorbing Lining
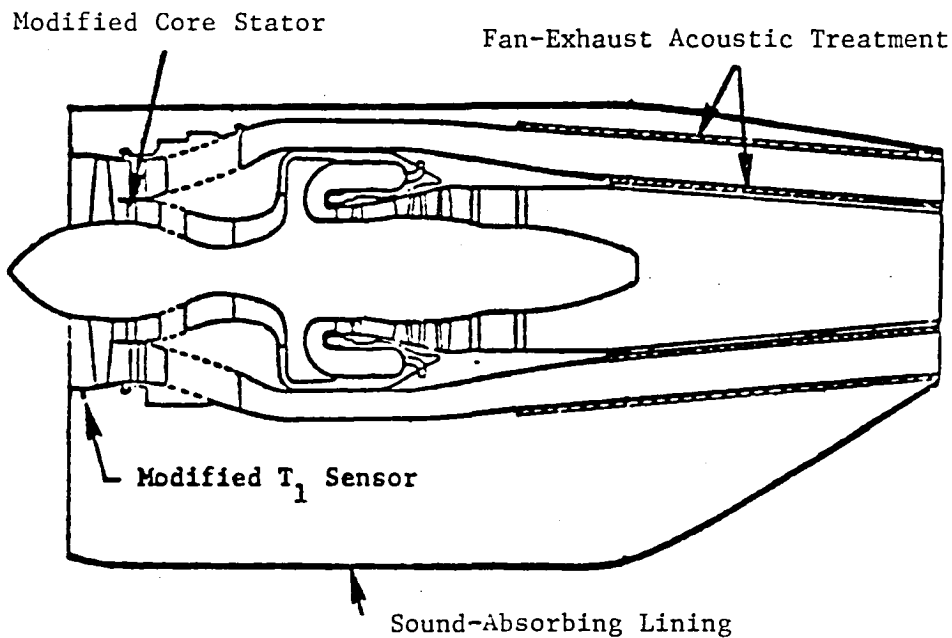
Figure 3-5. Modified NASA Test Engine Installed in the Quiet Nacelle.

40 by 80

4.6 m (15 ft)

7.62 cm (3 in.)
Foam Lining
on 40 by 80 Floor
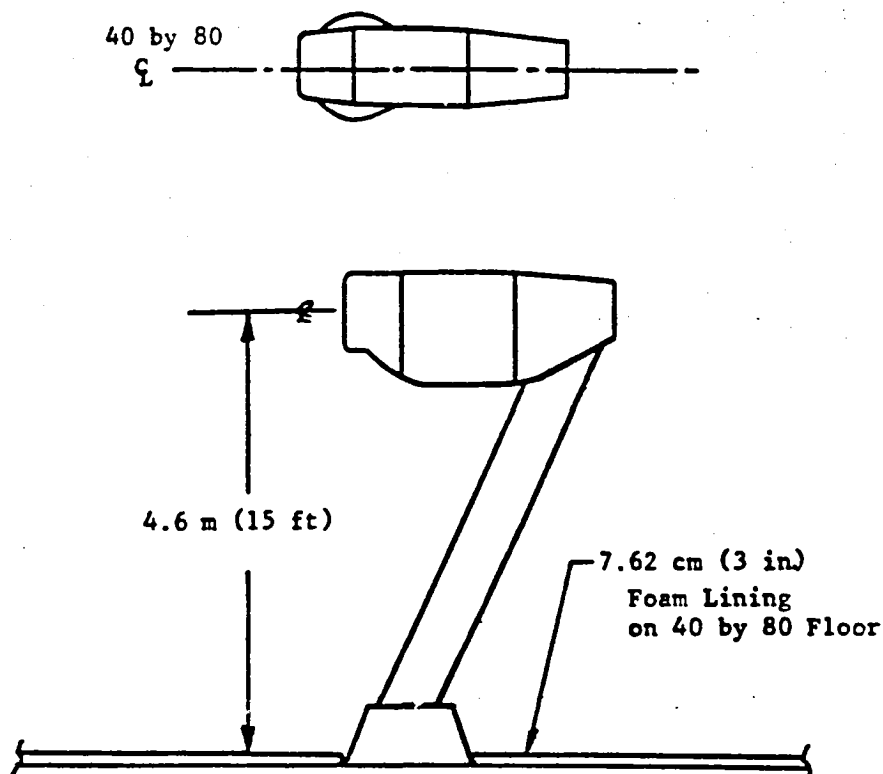
Figure 3-6. JT15D/Quiet Nacelle and Mount Assembly Schematic.

13
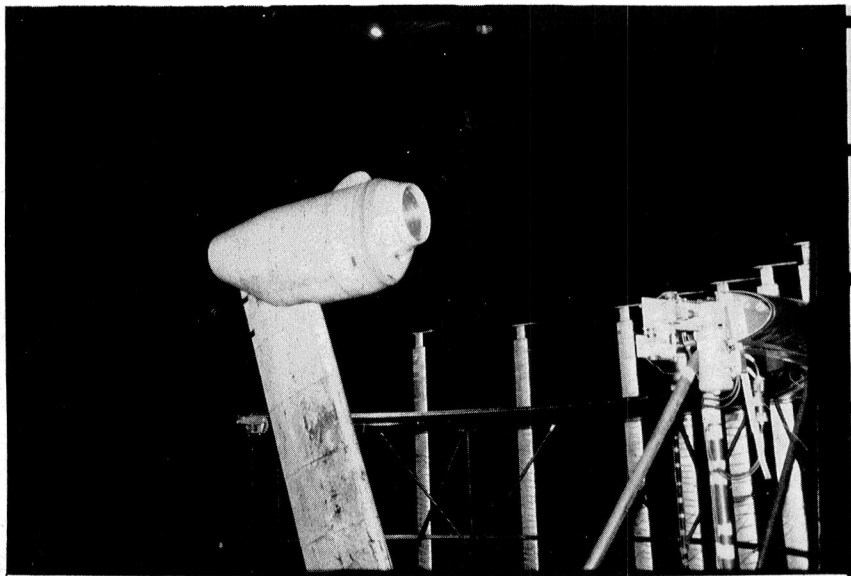
Figure 3-7. Engine Support Assembly.

(a)
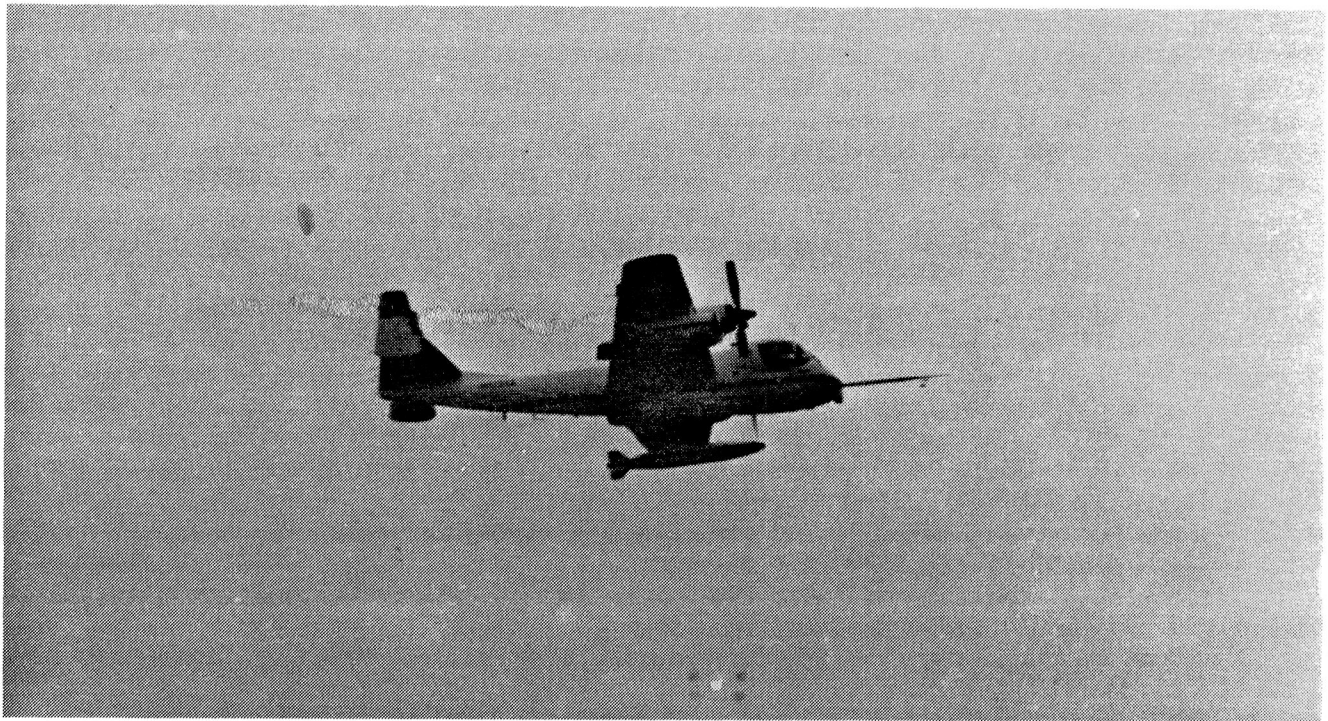
(b)

Figure 3-8. Modified OV-1B Aircrafts

C-Band Beacon and
Laser Reflectors
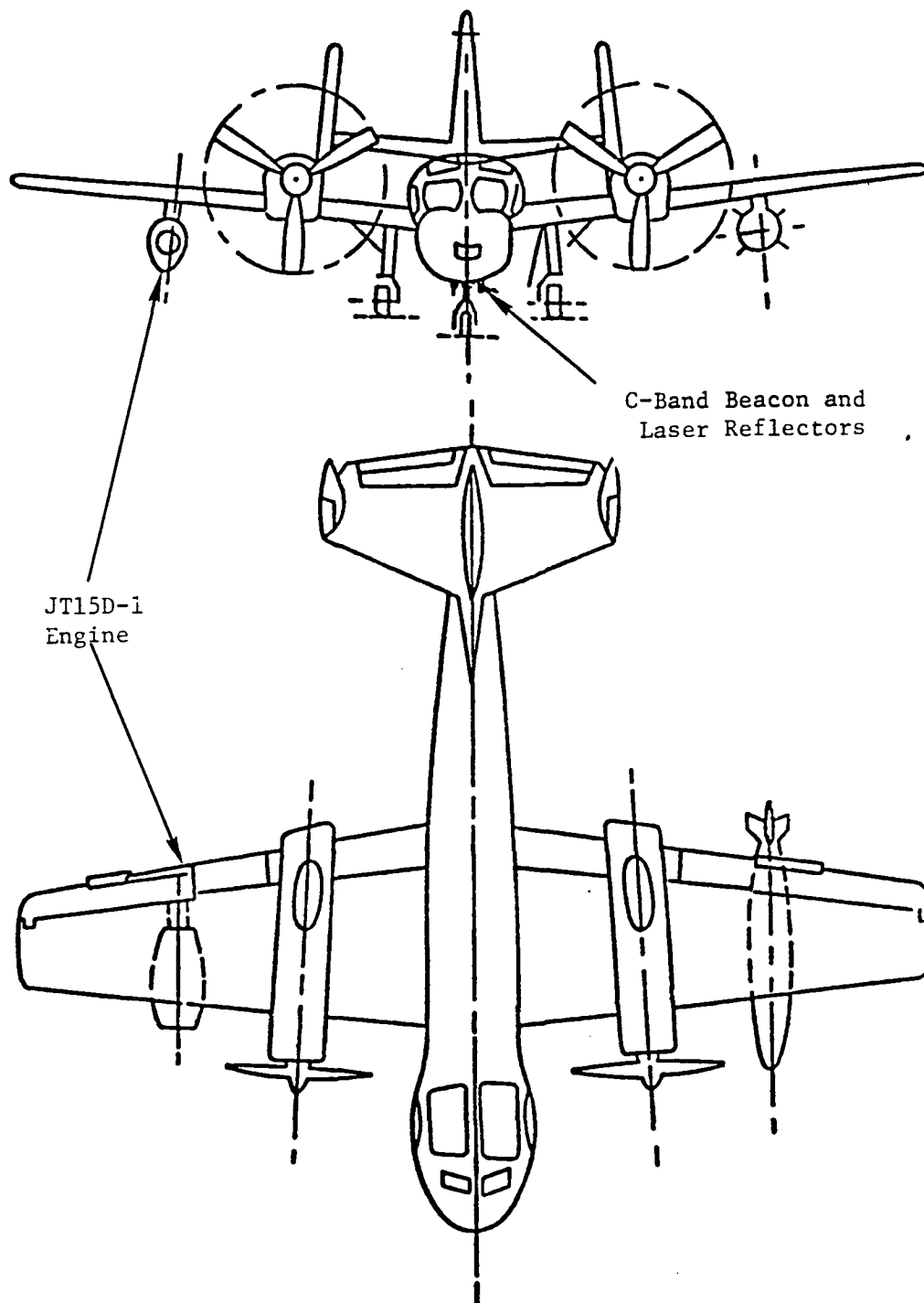
JT15D-1
Engine

Figure 3-9. Sketch of Test Aircraft Showing Location of JT15D-1 Engine.

performance data. These data in addition to the high frequency dynamic data were recorded using a complex on-board system which had its own signal conditioning.

3.3 INLET CONFIGURATIONS

3.3.1 NASA INLET

The inlet utilized by NASA Langley to perform their flight and wind tunnel tests was basically a Cessna Citation design. It possessed the same internal contours from the throat back while from the throat forward to the highlight a 2:1 ellipse was used. From the highlight outward the external body followed a bi-super elliptical shape. A schematic of the inlet is shown in Figure 3-10(a).

3.3.2 G.E. INLET CONFIGURATIONS

The inlet hardware tested in this program was fabricated under the supervision of the General Electric Co. The aerodynamic and mechanical designs were provided by General Electric, as was the acoustic treatment design. The inlets were selected to be representative of conventional commercial engines, apart from advanced aerodynamic concepts and advanced acoustic treatment designs. The aerodynamic design points for all inlets are listed in Table 3-2. The throat Mach number listed for each inlet is the one-dimensional calculation based on airflow and physical area. The acoustic design goals for the program were to achieve maximum perceived noise level (PNL) suppression when scaled to larger turbofan engines typical of those on modern commercial aircraft. There was also a goal to design as much of the hardware as possible to be common between the inlets, with configuration changes capable of being made simply and efficiently.

3.3.2.1 Baseline Cylindrical Inlet

The baseline inlet is cylindrical in shape with a length-to-diameter ratio of 1.01. The inlet attaches to the JT15D fan casing with four drag links which compress a rubber seal around the circumference to ensure no leaks in the flowpath at the interface.
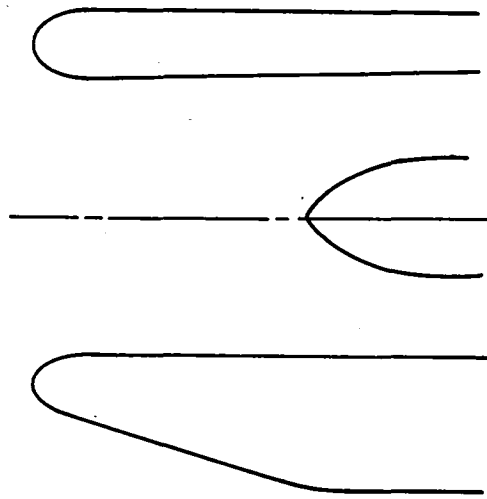
a. NASA Langley Inlet
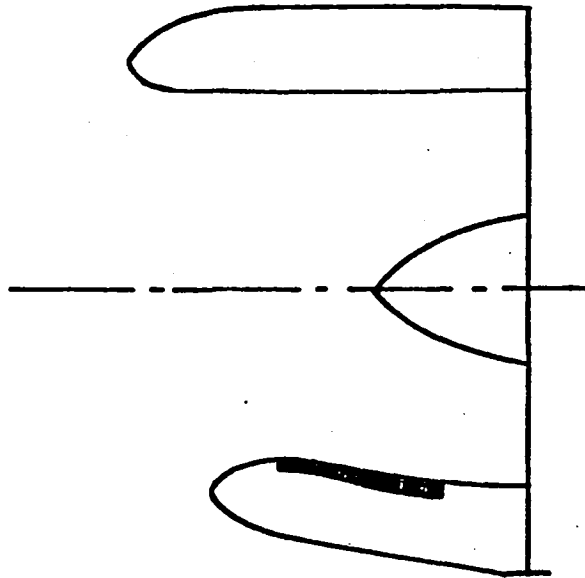
b. Baseline Cylindrical (Upper) and Straight Diffusing (Lower) Inlets

Figure 3-10. Schematic of Langley and GE Wind Tunnel Inlets.

TABLE 3-2

INLET DESIGN PARAMETERS

	Baseline	Diffusing
V_0, m/s (ft/s)	82 (270)	82 (270)
α, degrees	15	15
$\dot{w}$, kg/s (lb/s)	34 (75)	32.9 (73)
M_{th}	0.40	0.59
V_T, m/s (ft/s)	405 (1330)	405 (1400)
N_c, rpm	14,520	16,000
L/D	1.01	0.70
L/D Treated	---	0.38

The baseline inlet was tested in the previous series of tests reported in Reference 3-3 and was retested in a similar wind tunnel configuration in order to provide a common data link between the two test programs.

3.3.2.2 Straight Diffusing Inlet

The straight diffusing inlet has a diffusion rate consistent with designs found in commercial service. The fan area to throat area ratio is 1.26 with a length-to-diameter ratio of 0.70. A schematic comparison of the baseline inlet and the straight diffusing inlet is shown in Figure 3-10(b).

The straight diffusing inlet is equipped with a flight lip for wind tunnel testing and a reverse cone aeroacoustic lip for outdoor static testing. A schematic of the two configurations is presented in Figure 3-11. The reverse cone outdoor configuration is designed to mate to the turbulence control screen (TCS) device which is utilized in the outdoor testing. A schematic of the TCS installed on the reverse cone is displayed in Figure 3-12.

The attachment of the straight diffusing inlet to the fan casing is similar to the baseline inlet configuration. Any imperfections in the mating of the inlet hardware to the fan casing were smoothed over by using an RTV compound to ensure the flow field was aerodynamically as clean as possible when entering the fan.

3.4   TEST SET-UP

3.4.1 FLIGHT TEST

The OV-1B aircraft was configured with an instrumented and modified JT15D-1 turbofan engine below the right wing pylon which normally carries a drop tank. The aircraft contains all the research measurement and recording units necessary to record the JT15D-1 engine data as well as the most pertinent aircraft operational and aerodynamic data. The cockpit of the OV-1B aircraft had been modified to support the safe operation of the JT15D-1 engine.
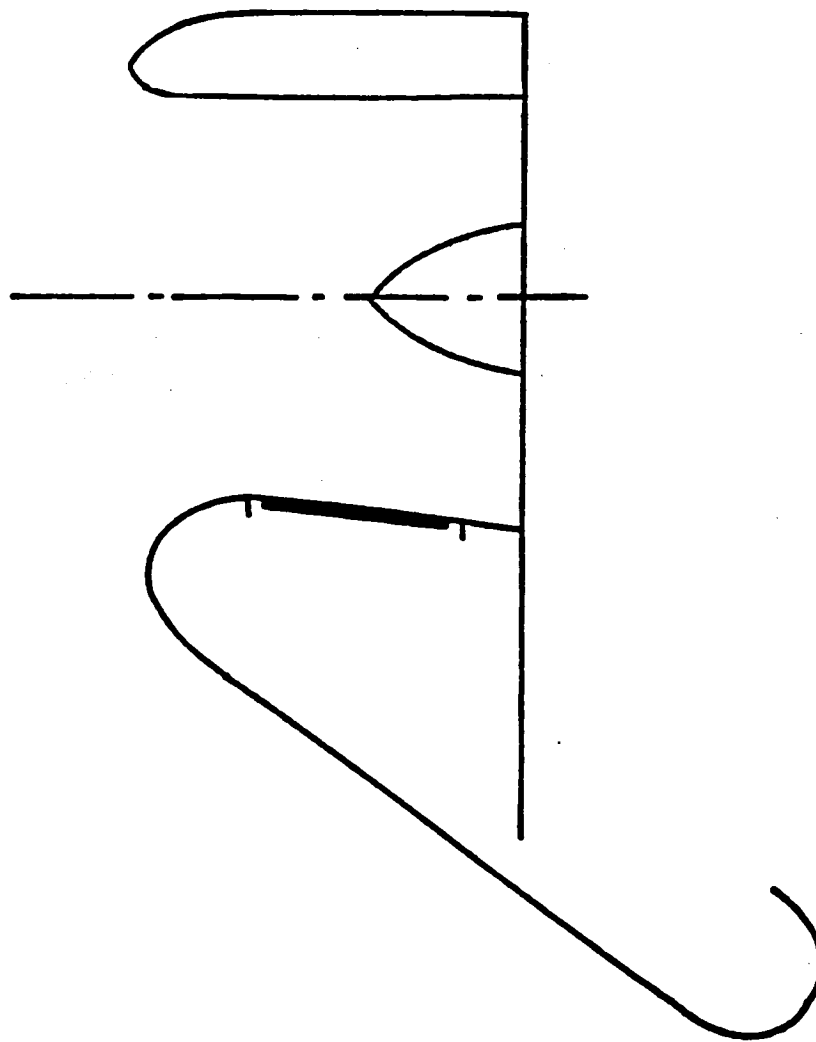
Figure 3-11. Schematic of GE Wind Tunnel (Upper) and Outdoor
Test (Lower) Configurations.
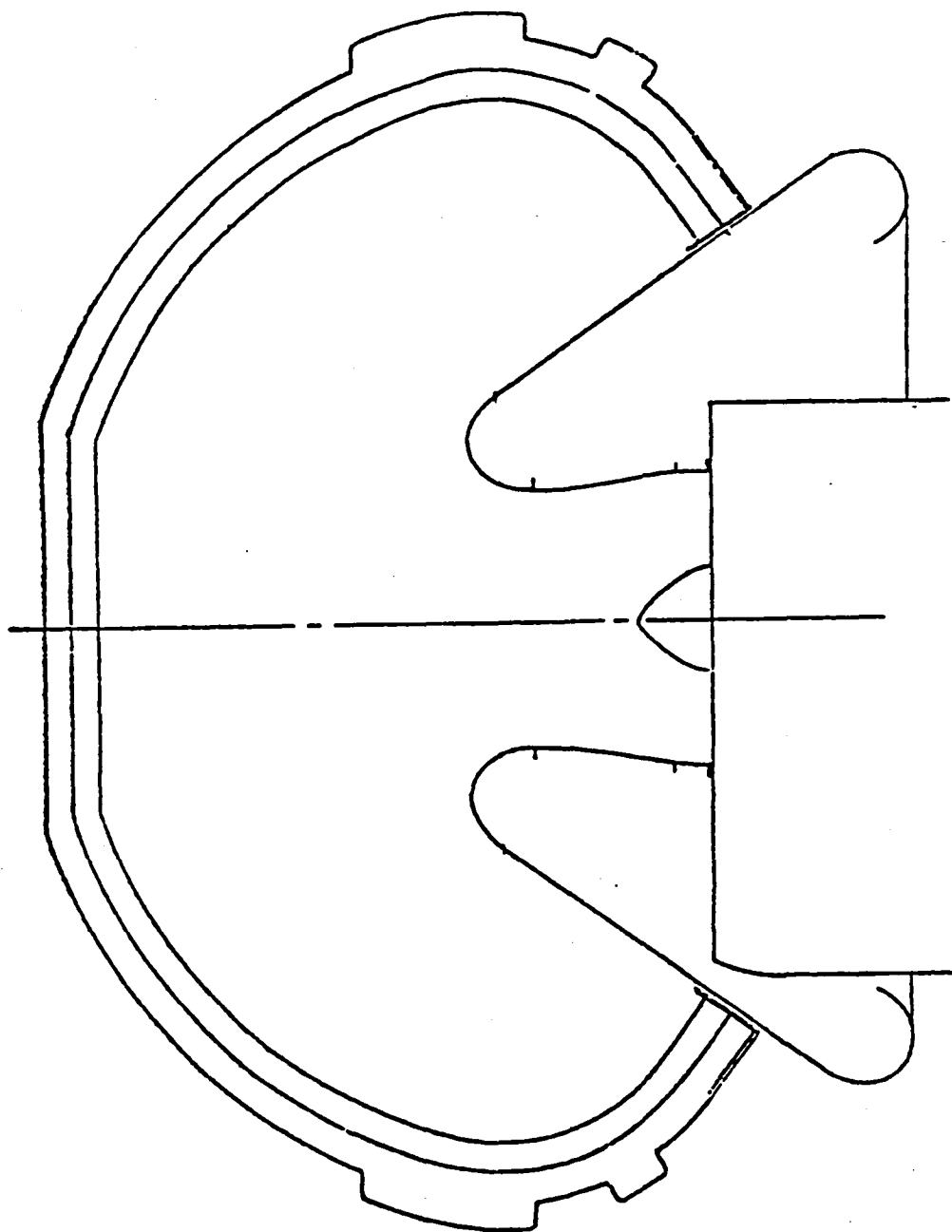
Figure 3-12. Schematic of TCS Installed on JT15D Engine.

The ground instrumentation for the noise measurements consists of an array of microphones located on runway 10-28 at a distance of 914.4 m (3000 ft) from the threshold of the runway (see Figure 3-13). Details of the array are shown in Figure 3-14(a). Three different microphone arrangements were used for the test series. For the first arrangement, which corresponds to flight tests 1, 2, and 3, the primary microphones were mounted on 9.14 m (30 ft) poles. There are 8 of these arranged in a line 4.6 m (15 ft) from, and parallel to, the runway centerline. The first pole microphone is 914.4 m (3000 ft) from the runway threshold and the spacing between the primary microphones is 9.14 m (30 ft). Four other microphones are mounted on groundboards. As shown in Figure 3-14(b), these microphones are also uniformly offset 4.6 m (15 ft) from the centerline of the runway with a spacing of 9.14 m (30 ft) between each.

3.4.2 WIND TUNNEL TESTS

The test vehicle was mounted during the wind tunnel tests by bolting the support strut to a turntable located in the center of the 40 x 80 test section. The engine centerline was 4.6 m (15 ft) above the wind tunnel floor with the turntable capable of yawing the test vehicle up to 40° for angle-of-attack operation. The floor and part of the walls were covered with foam to minimize reflection interference in the noise data. Noise measurements were made using a traversing microphone that covered angles from -5° to 138° on a 3.7 m (12 ft) arc. In addition, fixed microphones on a 4.5 m (14.5 ft) arc relative to the fan plane were located 30°, 50°, 60°, 70°, 90°, and 110° relative to the tunnel centerline. A schematic of the test setup is shown in Figure 3-15 with a photograph overview in Figure 3-16. Two other photographs showing the test setup are presented in Figures 3-17 and 3-18.

3.4.3 OUTDOOR STATIC TESTS

The test vehicle was mounted during the outdoor static tests by bolting the support strut to a support frame located in the southwest corner of the test area (see Figure 3-3). The engine centerline was 4.6 m (15 ft) above the ground and pointed in a northerly direction. The noise measurements were made at the same arc and fixed locations as those used in the wind tunnel tests.

23
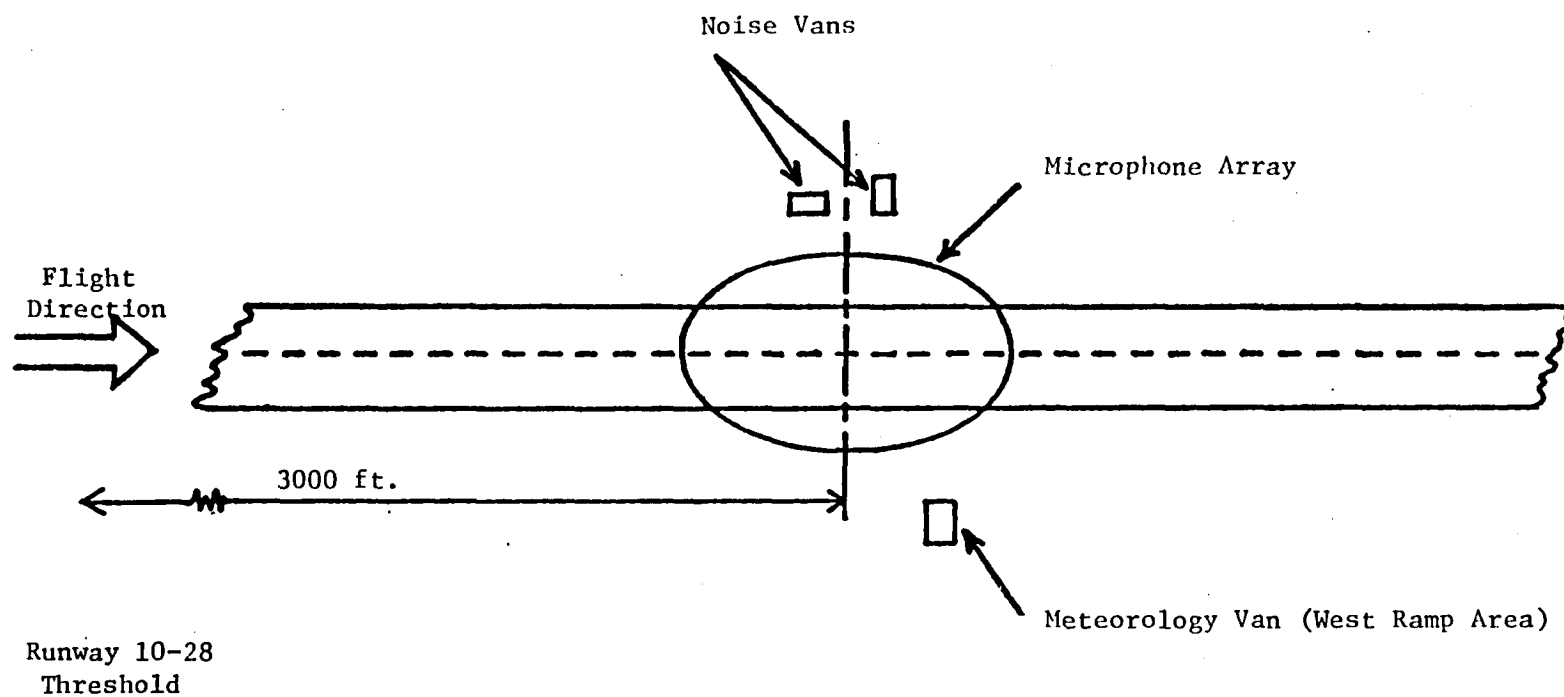
Figure 3-13.   Location of Ground Based Instrumentation on Runway 10-28.

No. 1 pole-mounted
microphone is at 914.4m
(3000 ft) mark on
runway; also origin
of x-y-z radar
coordinates

○ Microphones on 9.14m (30 ft) poles

□ Microphones on ground boards

Flight Direction

C_L

9.14m
(30ft)

4.6m
(15 ft)

100.6m
(330 ft)
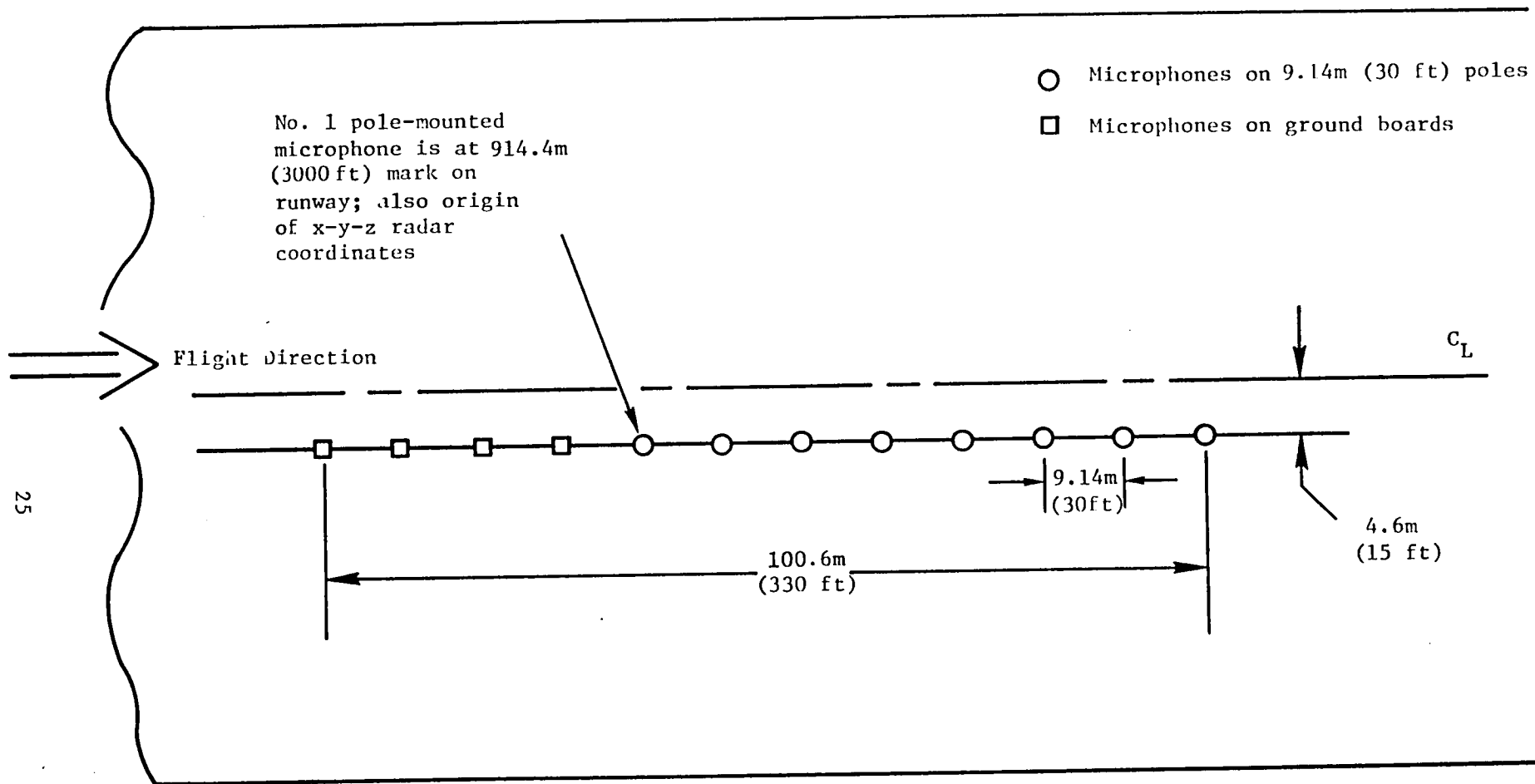
Figure 3-14a. Details of Microphone Array on Runway 10-28.

Figure 3-14b. Photo of Microphone Array

JT15D Far-Field Microphones
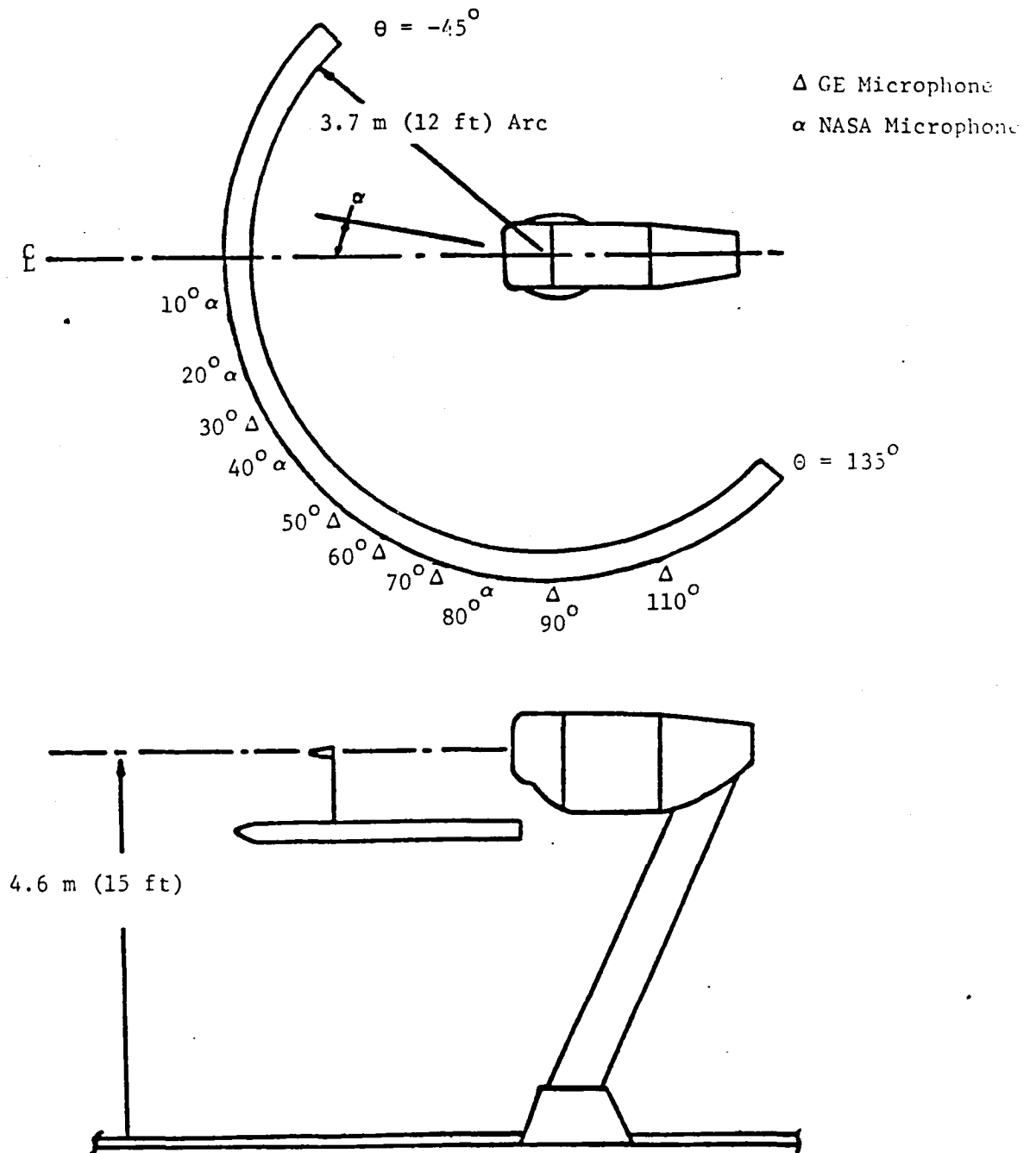
Figure 3-15. Test Setup for Wind Tunnel and Outdoor Static Tests.

27
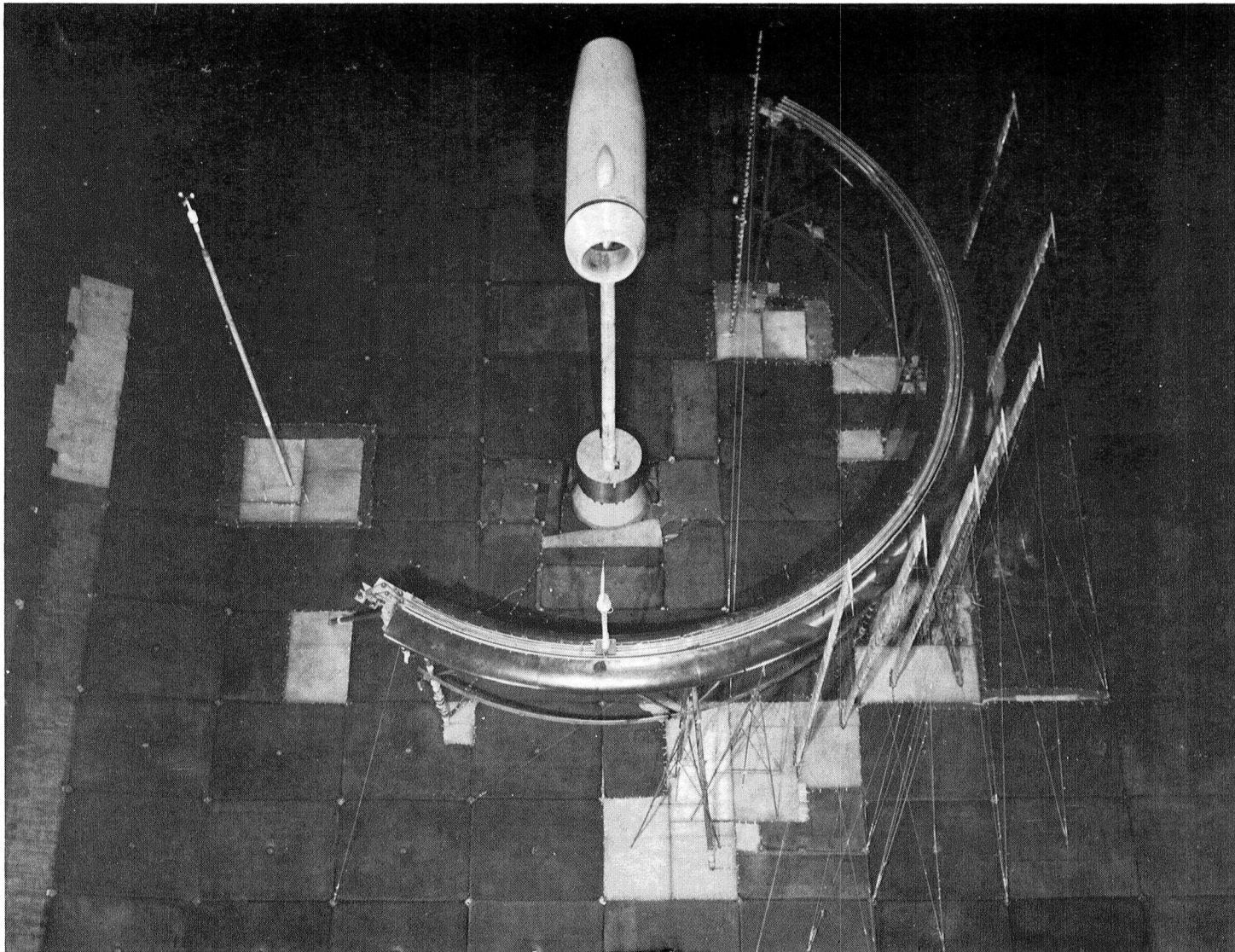
Figure 3-16. Photo of Wind Tunnel Test Configuration.
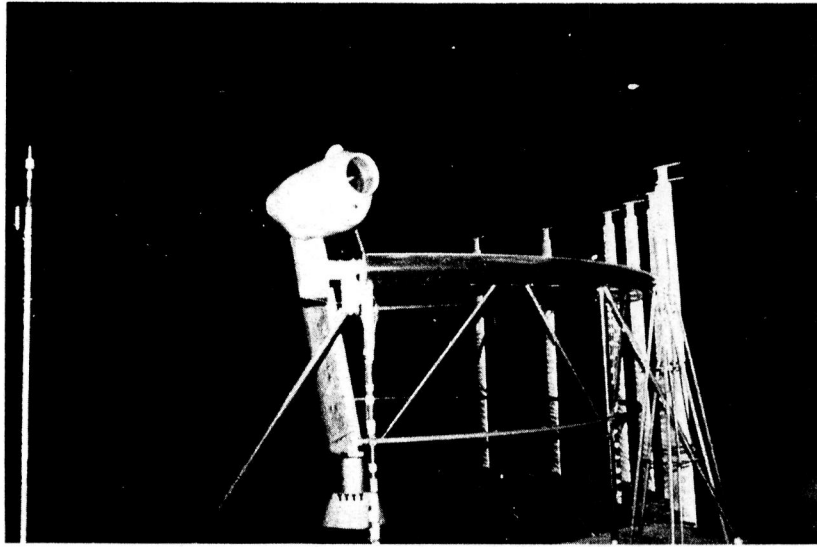
Figure 3-17.   Frontal View of Microphone Deployment
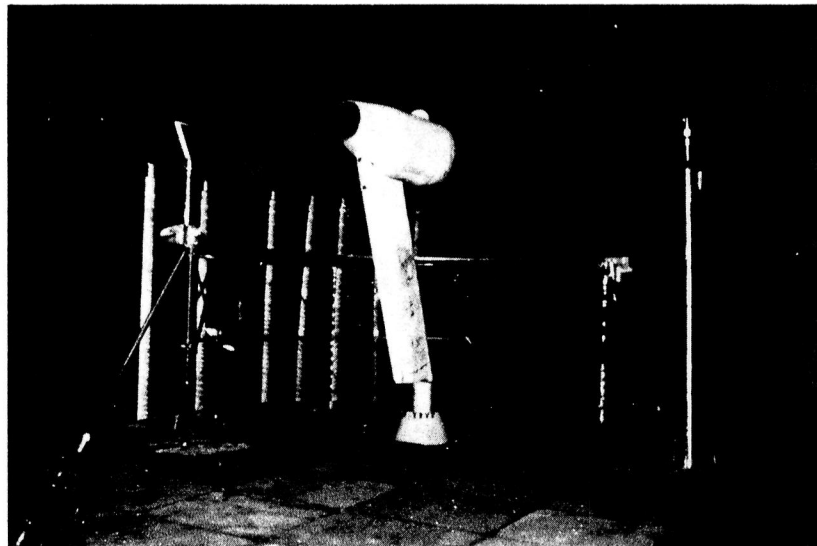
Figure 3-18.   Aft View of Microphone Deployment

To minimize ground reflection interference in the noise measurements, large pieces of the wind tunnel foam were used to cover the ground between the engine and microphones. Two photographs of the test setup are presented in Figures 3-19 and 3-20.

3.5   INSTRUMENTATION

3.5.1   ACOUSTICS

All noise measurements were made with B&K microphones. During all GE tests the microphones used were 0.64 cm (0.25 in.) B&K 4135's with B&K UA0385 nose cones attached. By using the same microphone/nose cone configuration for both outdoor static and wind tunnel tests, direct comparisons of the data can be made. However, B&K provides correction curves for noise arriving at the microphone at incidence angles from 0° to 180° and for the presence of nose cones. These curves were used to correct all the 1/3-octave-band data so that absolute sound pressure levels could be determined.

During the outdoor static and wind tunnel tests the fixed microphones were oriented pointing forward, parallel to the engine centerline or wind tunnel centerline. The circular traversing microphone used during the tests was attached to a movable vane that kept the microphone pointed upstream during forward speed testing in the wind tunnel. However, during quasi-static wind tunnel and outdoor static testing, the vane was locked so that the microphone pointed toward the engine at all angles. Photos of the microphone locations are shown as follows: Figures 3-16 through 3-18, wind tunnel; Figures 3-20 and 3-21, outdoor configuration; Figures 3-14b and 3-23, flight test configuration..

3.5.2   AERODYNAMIC PERFORMANCE

Static pressure distributions along the surfaces of each inlet at various circumferential positions were an essential part of the data acquired for each test condition. In addition, eight static pressure taps mounted circumferentially 67.3 cm (2.65 in) ahead of the fan face were closely monitored on-line during the testing. The static pressure tap locations for each of the inlets are tabulated in Table 3-3.
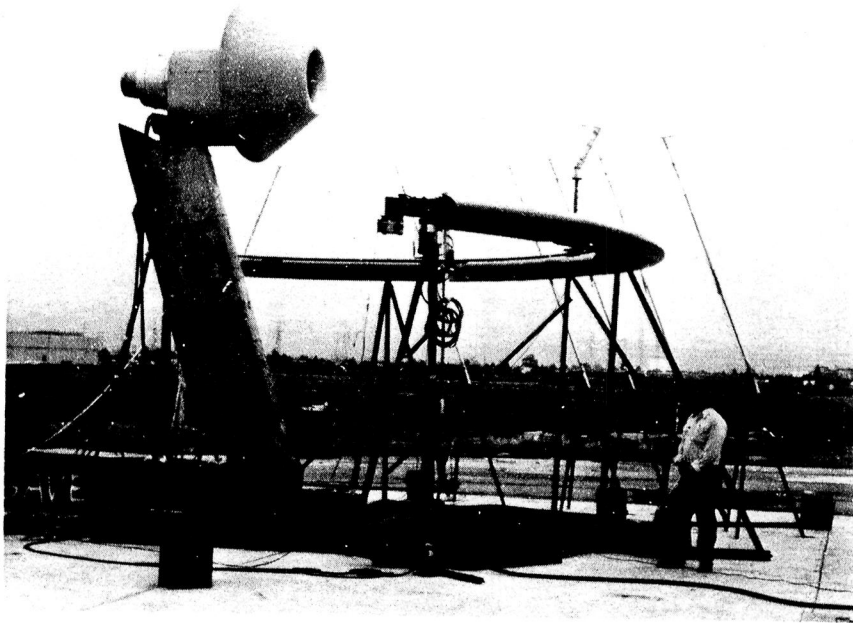
Figure 3-19. Photo of Outdoor Support Assembly

Figure 3-20. Photo of TCS Installation

31
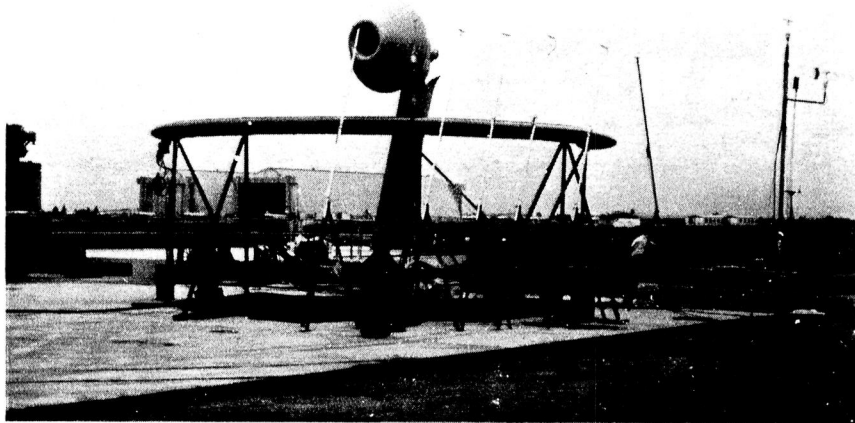
Figure 3-21. Photo of Outdoor Microphone Deployment
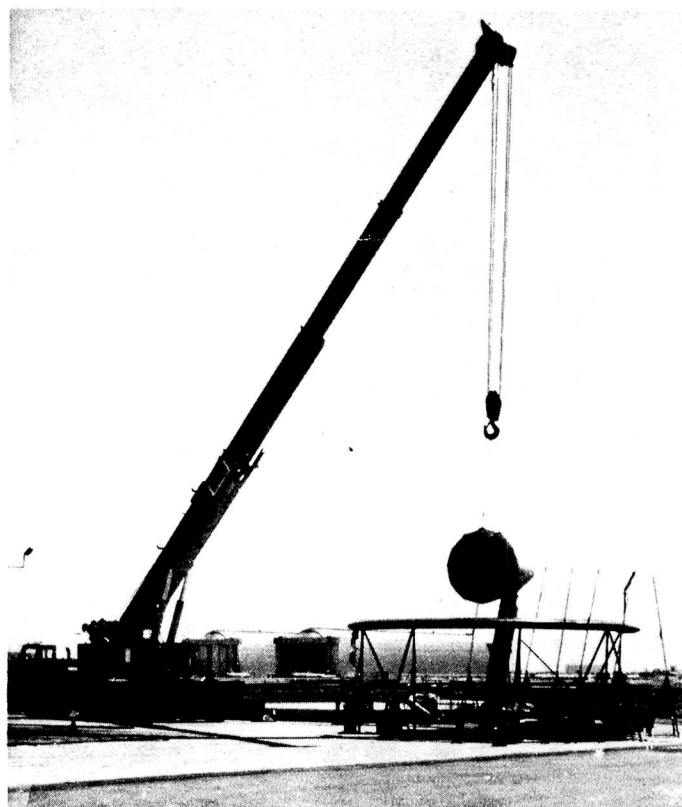
Figure 3-22. Photo of TCS and Instrumented Sound Field

Figure 3-23. Photo of Microphone Location for Flight Test Configuration

TABLE 3-3

INLET STATIC PRESSURE TAP LOCATIONS (FAN CASING REFERENCE X = 0)

Tap No.	Location θ	Location X		Tap No.	Location θ	Location X
				Flight Lip (Wind Tunnel)		
1	0	-0.72		33	270	-12.0
2	45	-0.72		34	90	-12.0
3	90	-0.72		35	270	-12.4
4	135	-0.72		36	270	-12.8
5	180	-0.72		37	0	-12.8
6	225	-0.72		38	90	-12.8
7	270	-0.72		39	180	-12.8
8	315	-0.72		40	270	-13.2
9	0	-2.65		41	270	-14.1
10	45	-2.65		42	270	-14.7
11	90	-2.65		43	270	-14.1
12	135	-2.65		44	270	-13.2
13	180	-2.65		45	270	-12.4
14	225	-2.65		46	270	-11.5
15	270	-2.65				
16	315	-2.65				
17	270	-4.0		**Aeroacoustic Lip (Outdoor)**		
18	270	-5.3				
19	270	-6.6		Tap No.	Location θ	Location X
20	90	-6.6				
21	270	-7.6				
22	270	-8.6		33	270	-12.0
23	270	-9.6		34	90	-12.0
24	0	-9.6		35	270	-12.4
25	90	-9.6		36	270	-12.8
26	180	-9.6		37	0	-12.8
27	270	-10.3		38	90	-12.8
28	270	-10.9		39	180	-12.8
29	0	-10.9		40	270	-13.2
30	90	-10.9		41	270	-13.9
31	180	-10.9		42	270	-14.8
32	270	-11.45		43	270	-16.2
				44	270	-16.79
				45	270	-16.1
				46	270	-14.1

(Flight Lip taps 42–46 marked: External)

(Aeroacoustic Lip taps 44–46 marked: External)

The JT15D fan pressure ratio was also of central concern during fan noise testing. The fan operating line was monitored during the wind tunnel testing utilizing a set of three NASA-supplied 6-headed total pressure rakes installed in the bypass duct.

3.5.3 BLADE/VANE-MOUNTED TRANSDUCERS

A special blade/vane-mounted instrumentation package, operated by NASA-Langley Research Center personnel, was provided for the test series. The locations and installation details of these transducers are shown in Figures 3-24 and 3-25. A more detailed discussion of this instrumentation can be found in References 3-4 and 3-5.

In general, the transducer system was a set of 14 Kulites - 8 blade-mounted and 6 vane-mounted. The blade-mounted transducers (BMT) were activated by a light switch, and information was telemetered to a receiving antenna mounted axially in the wall of the inlet. A schematic of the system installation details is also provided in Figure 3-24.

3.5.4 HOT FILM PROBE

During the outdoor static test program, a single hot film probe, TSI Model 1054A, was inserted at a station approximately 2.54 cm (1.0 in.) upstream of the fan rotor. Tests were conducted with this probe to measure axial turbulence parameters with and without the turbulence control device installed to determine its impact on the flow impinging onto the fan. Three radial immersions were tested coincidental with the BMT radial locations of 0.64, 1.9, and 5.1 cm (0.25, 0.75, and 2.0 in). Subsonic, transonic, and supersonic fan tip speeds were investigated with this hot film instrumentation.

3.6   TEST SUMMARY

3.6.1   FLIGHT TESTS

The flight tests analyzed during this program were conducted on June 18, 1981 as part of an extensive test series being performed by

KULITE Pressure Transducers
(20 - 20 kHz; 120 - 170 dB)

- 8 Rotating Blade
- 6 Stator Vanes

Transducers

Telemetry
Package

Transmitting
Antenna

Receiving Antenna

Transducer	Distance From Wall, cm (in.)	Surface Measured	Mounting Style
I	0.64 (0.25)	Pressure	Surface
J	1.90 (0.75)		
H	↓	↓	↓
K		Suction	
G	5.08 (2.00)	Pressure	
L	8.89 (3.50)		
M	0.64 (0.25)		Hole
N	12.7 (5.00)	↓	Surface
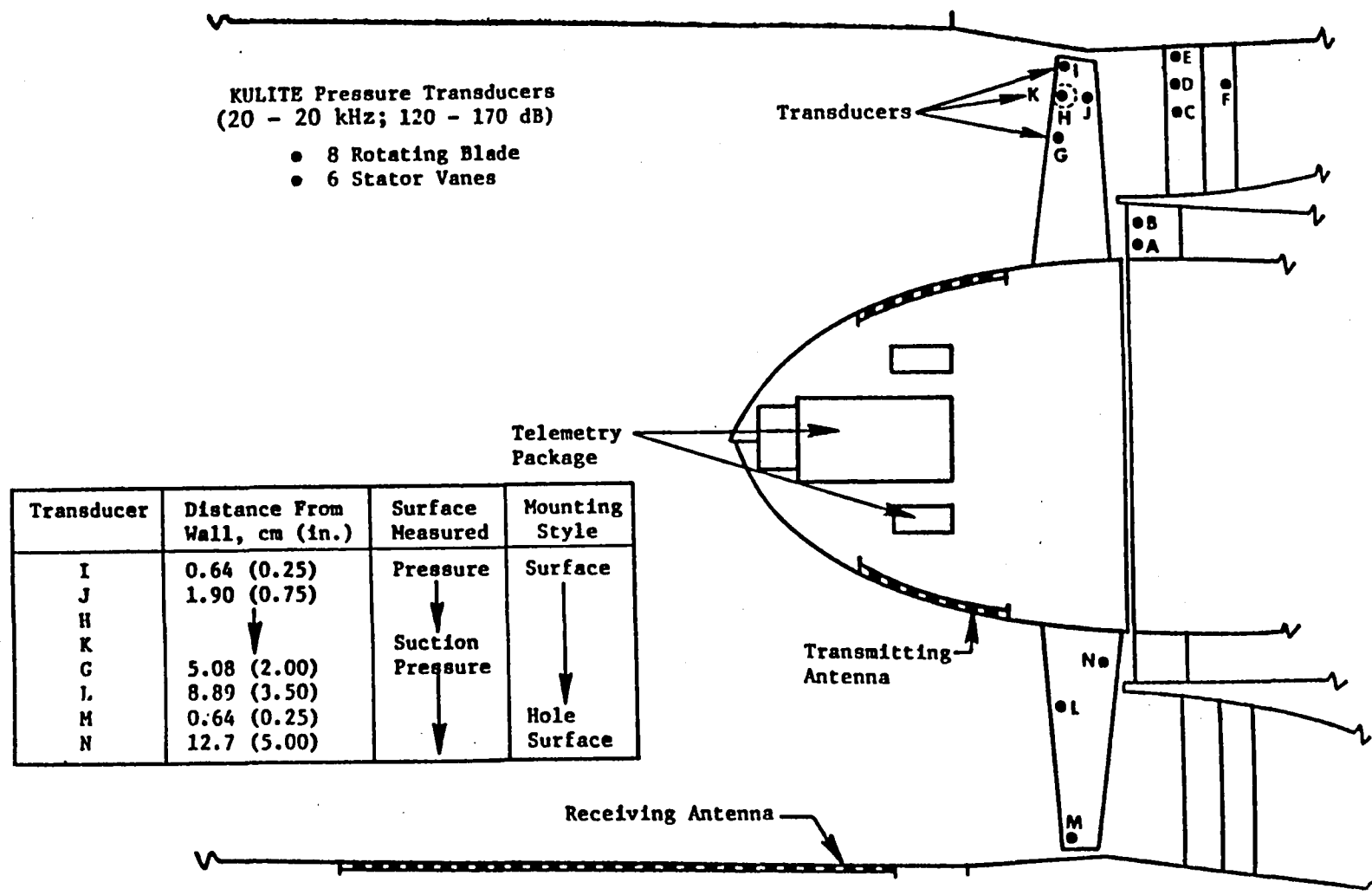
Figure 3-24. Schematic of Internal Dynamic Instrumentation.
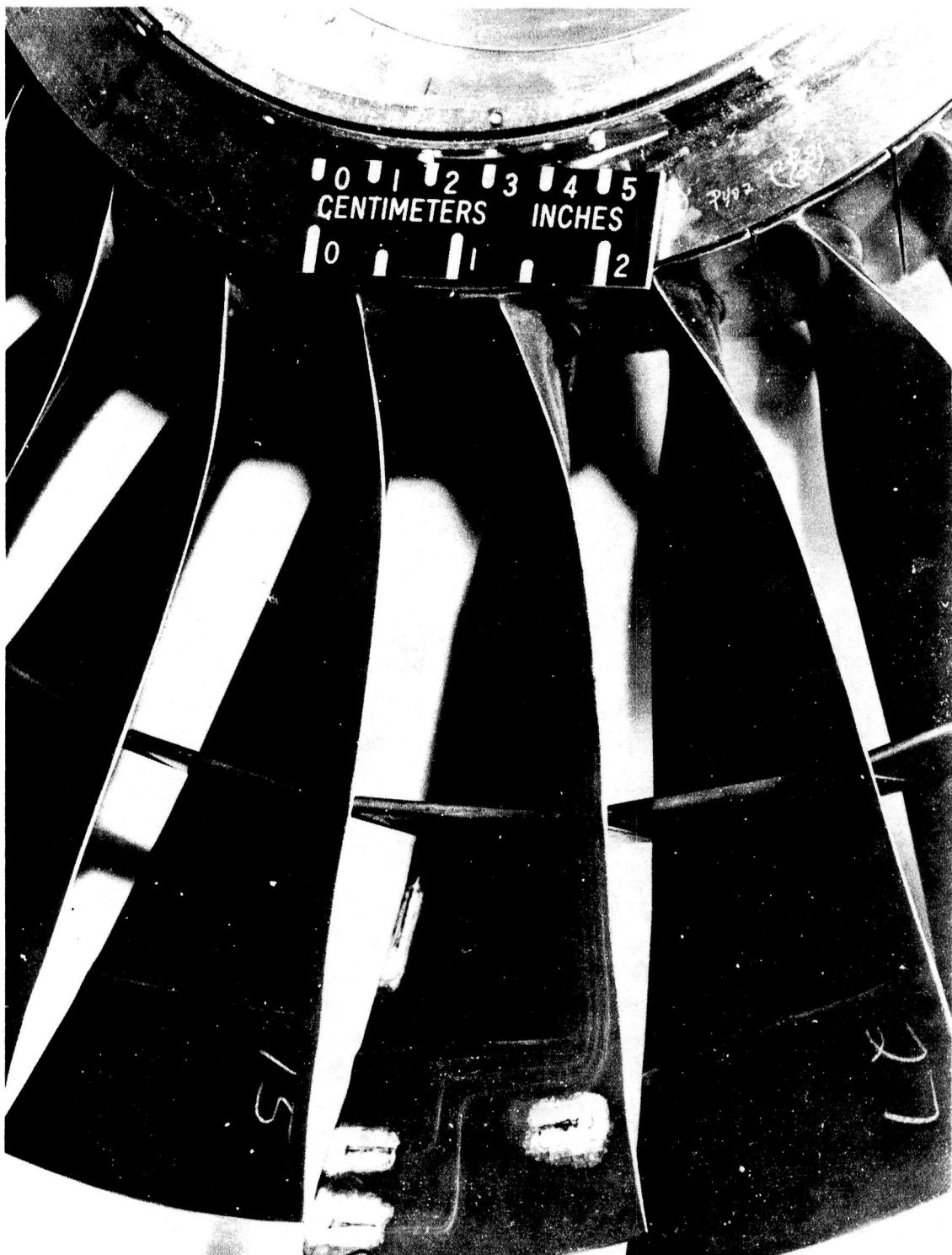
Figure 3-25. Photo of BMT Installation

37

NASA-Langley. The flight run numbers assigned to this investigation were
1461, 1471, and and 1481. The entire test series log is presented in
Table 3-4. The procedures utilized to record the acoustic information were
discussed in detail in Reference 3-6.

3.6.2 WIND TUNNEL TESTS

The Wind Tunnel tests (refer to References 3-7 and 5-3) were conducted
in the 40 × 80 during March, 1980. A summary of the test program is contained
in Table 3-5. The primary objectives of the program were to obtain a complete
characterization of the inlets tested, both aerodynamically and acoustically.
The tests were conducted over the entire operating range of the JT15D engine;
however, an emphasis was placed on obtaining the noise characteristics at
10,500, 12,000 and 13,500 rpm.

For each noise data point, the fan corrected speed was set based on
aeroacoustic considerations and allowed to stabilize. All amplifier gain
settings were optimized for internal and external noise measurements and then
at least 30 seconds of internal dynamic data was tape recorded with the
traversing microphone in the 138° position. An aerodynamic data sample was
computer printed during this recording time. The traverse microphone sweep
was then initiated and the recorders ran continuously for the approximate 4
minutes required to complete the traverse.

3.6.3 OUTDOOR STATIC TESTS

The outdoor static tests were conducted at the test stand during April
and May of 1980. A summary of the tests are contained in Table 3-6 which
includes the details of the test program. The initial objective of the
outdoor static tests was to compare the difference in aeroacoustic performance
which resulted from using a production exhaust configuration as opposed to
that produced by modifying the quiet nacelle engine to the production fan
operating line. The other objectives were to operationally check out the
turbulence control structure's aeroacoustic performance and obtain noise data
for comparisons with the wind tunnel noise data.

TABLE 3-4

FLIGHT TEST LOG

Run No.	No. of Passes	AGL (feet)	Air Speed (knots)	JT15D N_1	Flaps
1401	1	300	max.	13500	0°
1411				12000	
1421				10500	
1431			160	13500	
1441				12000	
1451				10500	
1461			130	13500	
1471				12000	
1481				10500	
1491			max.	0	
1501			130	0	

TABLE 3-5

LANGLEY WIND TUNNEL LOG

Run	Tunnel Speed kts	Angle Attack	RPM	RH	Temp °F	Air Speed
7-1	0	0	12000	62.2	52.4	10.7
7-2	-	-	10500	57.9	55.7	10.4
7-3	-	-	6750	60.3	53.5	5.7
7-4	20.5	0	12000	59.3	55.0	-
7-5	19.0	-	10500	57.0	57.0	-
7-6	20.3	-	6750	58.9	57.5	-
7-7	60	0	12000	52.3	59.8	-
7-8	60	-	10500	51.6	60.2	-
7-9	60	-	6750	51.9	59.9	-
7-10	84	-	12000	48.6	62.1	-
7-11	-	-	10500	47.7	62.6	-
7-12	-	-	6750	47.5	67.5	-

GE WIND TUNNEL LOG

Run	Tunnel Speed kts	Angle Attack	RPM	RH	Temp °F	Air Speed
8-1	-	-	0	20.2	71.3	-
8-2	-	-	12000	20.1	71.2	8.62
8-3	-	-	12000	19.6	72.1	12.69
8-4	80	-	9000	16.8	75.4	-
8-5	-	-	11080	16.6	76.2	-
8-6	-	-	14360	16.4	76.8	-
8-7	-	-	14750	15.9	77.7	-
8-8	-	-	14500	14.8	79.0	-
8-9	-	-	14500	14.2	79.8	-
8-10	-	-	13500	13.6	81.0	-
8-11	-	-	13500	12.9	81.4	-
8-12	-	-	12320	12.5	81.9	-
8-13	-	-	12320	12.4	82.1	-
8-14	-	-	12000	12.1	82.5	-
8-15	-	-	12000	11.9	83.0	-
8-16	-	-	11800	11.8	83.0	-
8-17	-	-	11800	11.5	83.2	-
8-18	-	-	11500	11.4	83.5	-
8-19	-	-	11500	11.2	83.7	-
8-20	-	-	11135	11.1	83.9	-
8-21	-	-	11135	11.1	83.9	-
8-22	-	-	10500	11.2	84.0	-
8-23	-	-	10500	11.2	84.0	-

TABLE 3-6

RUN LOG - OUTDOOR STATIC TEST

Run	Inlet	Lip†	Treatment	Test Points	Operating Line
1	Straight	Reverse Cone*	No	13	Design
2	Straight	RC/TCS	No	13	Design
3	Straight	RC/TCS	No	13	Upper

*Denoted as RC in other runs.
†TCS implies Turbulence Control Structure.

ENGINE SPEEDS

Test Pt	Run 1 (4-23-80)	Run 2 (4-23-80)	Run 3 (4-24-80)
1	14,460	14,411	14,402
2	13,307	13,436	13,425
3	12,764	12,729	12,763
4	12,227	12,236	12,322
5	11,993	11,929	11,981
6	11,721	11,726	11,771
7	11,440	11,422	11,488
8	12,230	11,200	11,270
9	10,751	10,721	10,818
10	10,453	10,449	10,501

For each noise data point the fan corrected speed was set by throat Mach number, if applicable, and allowed to stabilize. All amplifier gain settings were optimized for the internal/external noise measurements and then at least 30 seconds of data were tape recorded. During traverse operation of each outdoor static test, the recorders ran continuously for the 3 to 4 minutes required to complete the traverse. To minimize errors in data reduction the traverse microphone amplifier gain settings, which were pre-established based on peak overall noise levels, were not changed during data acquisition.

3.7 DATA REDUCTION

The reduction and processing of test data were shared by NASA and General Electric. Steady-state aerodynamic performance data for the inlets and the test facilities were calculated by the NASA computers. Data editing and correcting were performed by GE and NASA engineers, and the final computed post-test results were supplied by NASA to GE. The noise measurements were monitored on-line during the tests by GE and NASA personnel to ensure signal validity. Post-test noise data reduction and processing under this contract were accomplished at GE facilities.

3.7.1 AERODYNAMIC PERFORMANCE DATA

As part of the pretest effort, GE engineers conducted a compressible flow analysis of the inlets. This analysis determined the relationships between the airflow rate, the surface pressure distribution, and the throat Mach number for each inlet at outdoor static and wind tunnel test and flight conditions. The results of this analysis were incorporated into the on-line aerodynamic performance computer program used for all wind tunnel testing. This program computed throat Mach number for all zero angle-of-attack test points using selected wall static pressures from each inlet. The computer program also computed the average total pressure distortion and the area-weighted average total pressure for all test points. These computer programs were a valuable asset to the wind tunnel testing because preliminary results were available on-line for each test point and final checked results were available at the completion of the tests.

SECTION 4.0

FLIGHT PROJECTION PROCEDURES

4.0 FLIGHT PROJECTION PROCEDURES

The flight projection of acoustic data measured in turbulence controlled outdoor static or wind tunnel environments involves a multiplicity of adjustments and corrections being systematically applied to the measured data. The utilization of a minicomputer in this processing becomes a very valuable tool since the acoustic information can be digitally adjusted as appropriate to account for the numerous computations required to produce a resultant flight simulation. This process is shown schematically in Figure 4.0.

The adjustments and corrections which typically apply to this process can be divided into two categories. The initial corrections which compensate acoustic information recorded on magnetic tape are associated with the instrumentation characteristics. The recorded data need to be adjusted for microphone response, microphone protective nosecone (grid), diffraction and insertion loss, and system response traits. This information needs to be supplied by the manufacturer and/or determined at the time the acoustic information is recorded.

The second area of adjustment occurs as a results of the intrinsic physics associated with the propagation of sound through an atmosphere. These effects need to be incorporated into the flight projection of acoustic data and are summarized in the following:

- inverse square law
- atmospheric absorption
- convective amplification
- ground impedance
- Doppler shift
- background noise

These corrections are based on well established procedures, and GE has formulated and refined these procedures to produce simple yet reliable estimates.
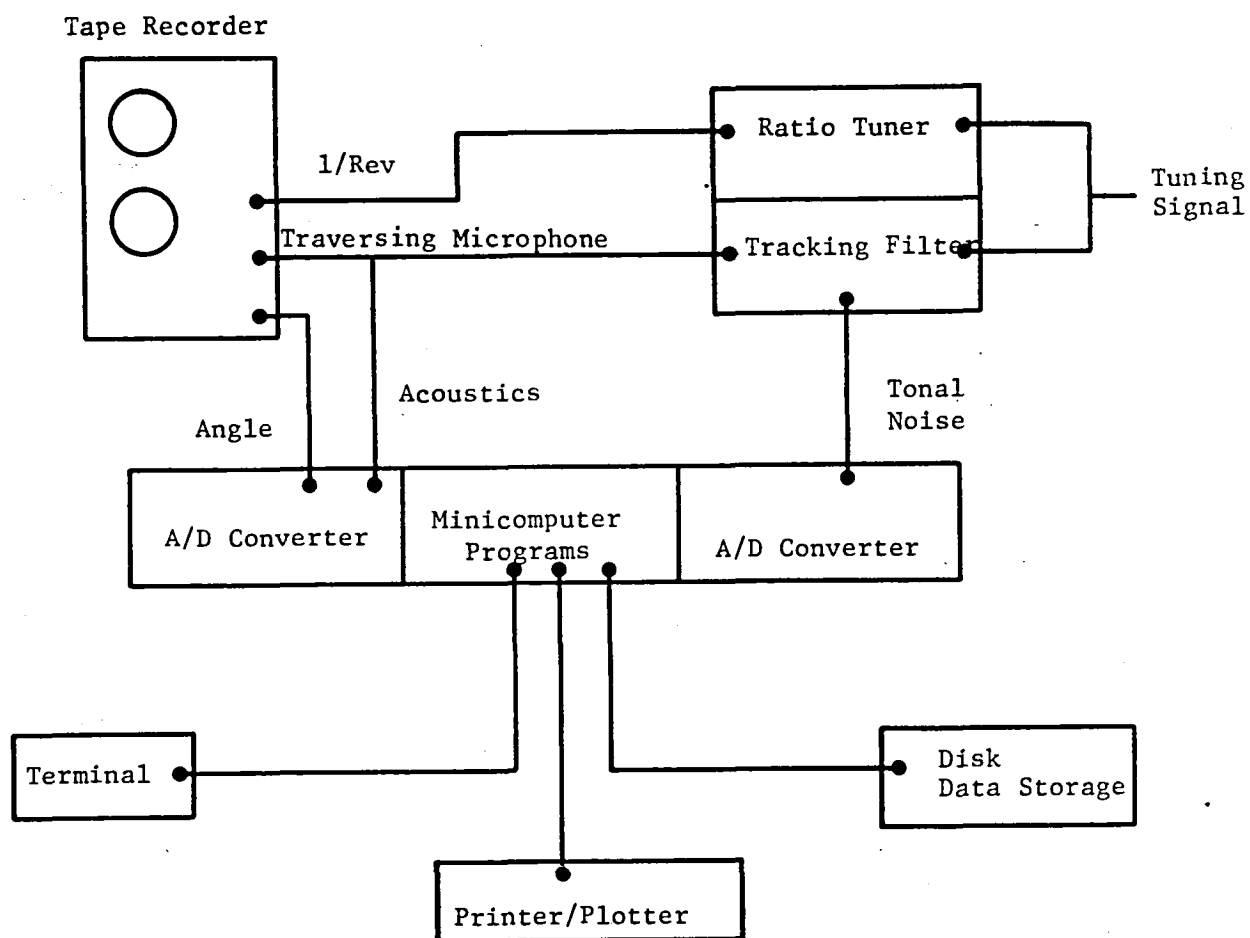
Figure 4-0. Data Reduction Instrumentation Schematic.

4.1   FLIGHT PATH DEFINITION

The initial consideration was the flight path to which the projection needed to be made. The definition of the flight path and flight conditions are illustrated in Figure 4-1. The projection is made for specific times and specific time increments, relative to a defined time scale with time t = 0.0 occurring when the aircraft engine is directly overhead of the reference microphone. The emission time (t_e) of the sound arriving at time t can be determined by using the following expression:

$$t_e = \frac{\left(c_o^{\ 2}t - V_o D \sin \alpha\right) + \sqrt{\left(c_o^{\ 2}t - V_o D \sin \alpha\right)^2 - \left(c_o^{\ 2} - V_o^{\ 2}\right)\left(c_o^{\ 2}t^2 - D^2\right)}}{\left(c_o^{\ 2} - V_o^{\ 2}\right)} \quad : \quad (1)$$

where c_o is the speed of sound. For a time increment Δt, the emission times $(t_2$ and $t_1)$ for t $\pm \Delta t/2$ are computed. These times are used to derive the angular range of the simulated flight spectrum being projected.

4.2   SIMULATED FLIGHT DATA PREPARATION

The simulated flight data is converted from analog to digitial at an effective sampling rate of 51,200 samples per second with an anti-aliasing filter set at 20 kHz. The data is stored in a manner which allows the angular location relative to the engine fan face to be known for each data sample. The data was measured over the angular range from 0 to 137.6 degrees at a distance r_o = 3.66 m (12 ft) relative to the fan face. However, in the case of forward radiated or aft radiated noise, an angular adjustment to the inlet plane or exhaust plane needs to be made prior to making the flight projection. This angular adjustment is illustrated in Figure 4-2.

The equations for angular location θ defined from the inlet and exhaust planes are as follows:

$$\tan \theta = r_i \sin\phi_i / (r_i \cos\phi_i + \Delta x_i) \text{ or } r_e \sin\phi_e / (r_e \cos\phi_e + \Delta x_e) \quad (2a)$$

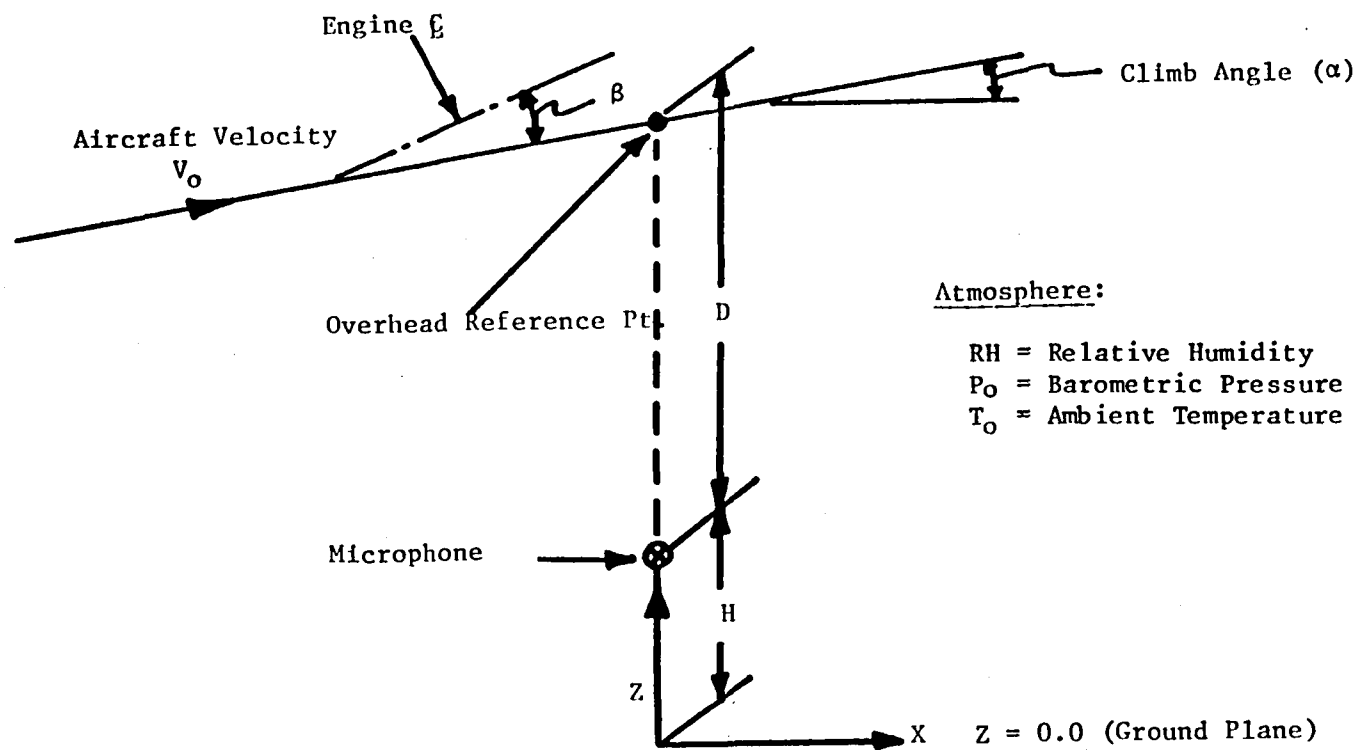$$\text{where } r_i = -\Delta x_i \sin \phi_i + \sqrt{r_o^{\ 2} - (\Delta x_i \sin \phi_i)^2},$$

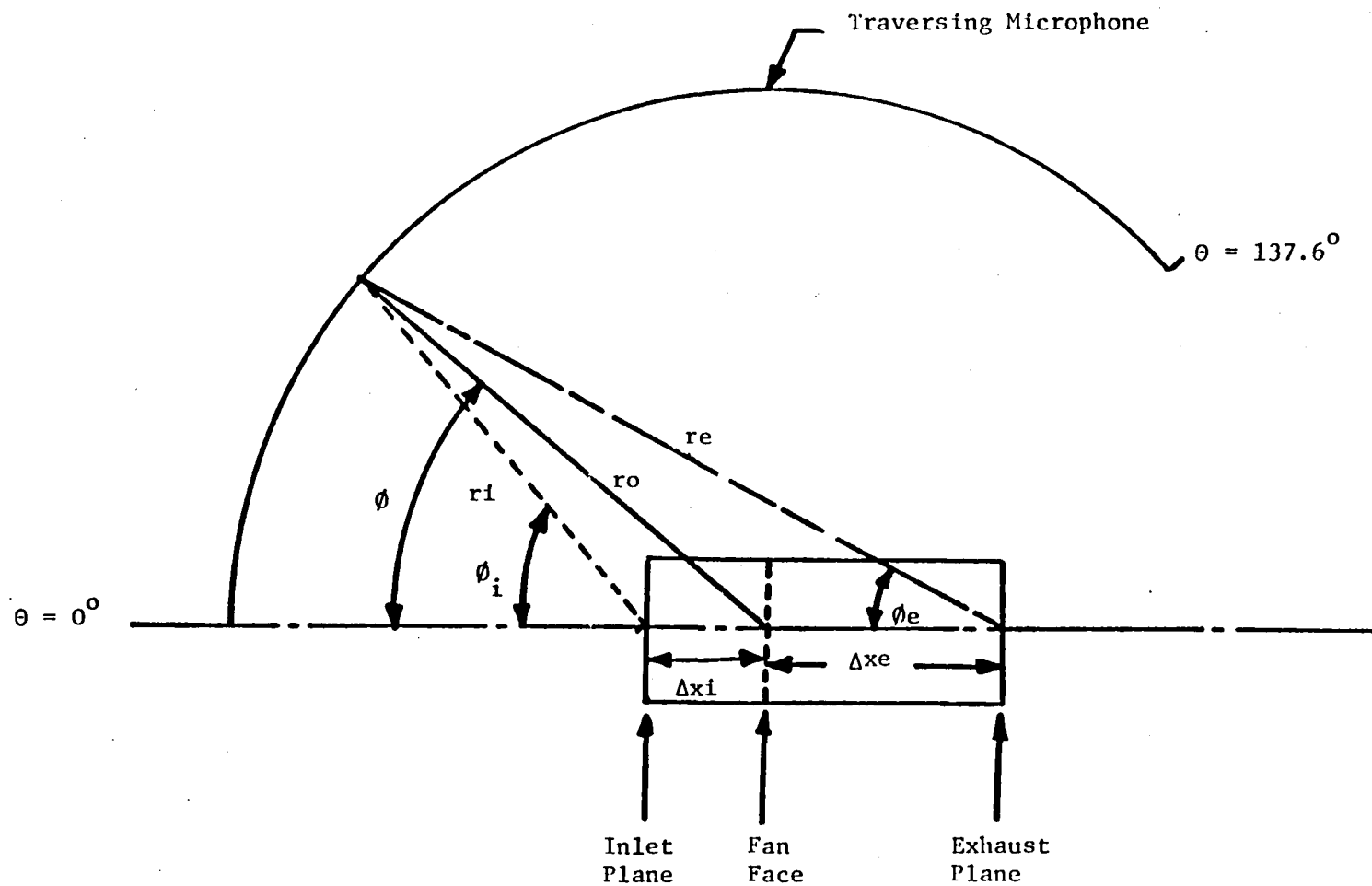Figure 4-1. Flight Path Definition Parameters.

Figure 4-2. Simulated Flight Measurement Parameters

and $r_e = \Delta x_e \sin\phi_e + \sqrt{r_o{}^2 - (\Delta x_e \sin\phi_e)^2}$

The assumption is made that for $\theta_e \leq 90°$, the (r_i, ϕ_i) coordinate system shall be used in the flight projections and for $\theta_e > 90°$, the (r_e, θ_e) coordinate system shall be used. The term ϕ_e is used to apply to the aircraft acoustic emission angle at time t_e. The angle θ_e is defined by:

$$\theta_e = \tan^{-1}\left[(D+V_o t_e \sin\alpha) \bigg/ V_o t_e \cos\alpha\right] + \beta \tag{3}$$

where β is the engine ₵ angle relative to the aircraft trajectory.

4.3 SPECTRAL PROJECTION

The definition of the values $\theta_e 1$ and $\theta_e 2$ using Equation 1, with t_e set equal to t_1 and t_2 respectively, allows for the spectral projection of the simulated flight acoustic data to proceed. Using the values of $\theta_e 1$ and $\theta_e 2$ as the minimum and maximum angles, the simulated flight data over the range θ_1 to θ_2 is spectrally averaged. The term spectrally averaged means that spectral results are computed using 2048 point digital data samples between the angles θ_1 and θ_2. Generally, the traverse rate of the microphone was on the order of one degree per two seconds such that 50 independent spectral averages of 2048 point samples can be obtained for each one degree of travel. If a flight time increment Δt of 0.2 seconds is used, then the number of averages of the simulated flight data will vary with time t which adjusts the acoustic emission angle. This variation for $V_o = 250$ ft/sec assuming $c_o = 1100$ ft/sec and D = 270 ft is displayed in Figure 4-3.

To obtain good confidence in the data sample, at least 40 averages are recommended, and to produce 90% confidence levels on the order of ± 0.5 dB, 100 averages are required.
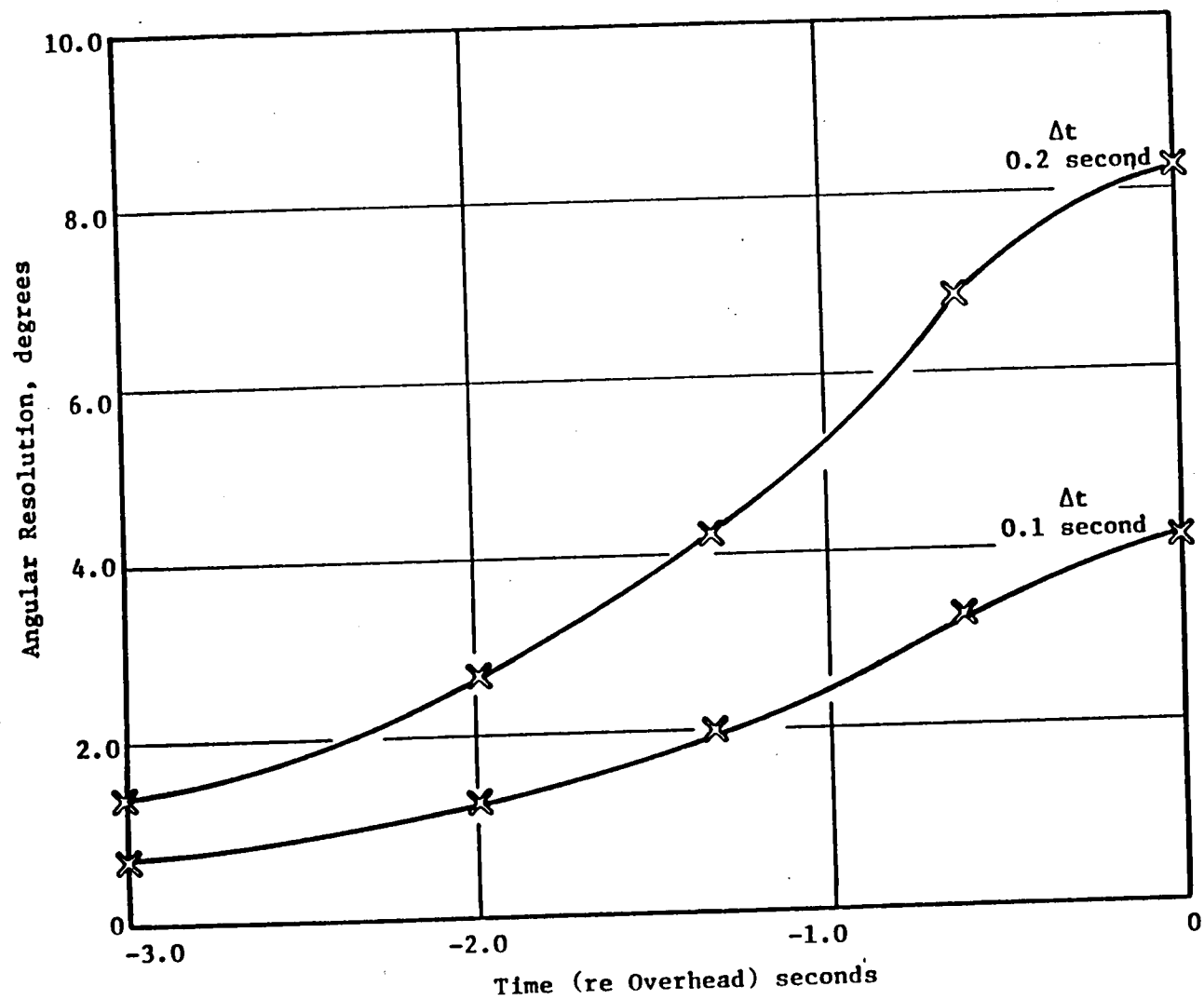
Figure 4-3. Angular Resolution for Various Time Increments Δt.

4.4   FLIGHT DATA ANALYSIS

The analysis of flight data also requires spectral averaging. However, the averaging procedure becomes one of time domain as opposed to the angular domain for the simulated flight case. In general, as many averages as can be acquired in as short a time increment as possible is desirable. Again, a time increment of 0.2 seconds is assumed. The flight data being evaluated under this contract was acquired using multi-microphones, hence an ensemble averaging procedure was used to improve the statistical confidence of the resultant averaged spectral determination. In addition to using multiple microphones, the sample rate was increased to 4 times the 51,200 samples/second used for the simulated flight data case. Hence, by recombining the data samples after they are digitized, one effectively acquires 4 times as much information. An anti-aliasing filter at 20 kHz is again utilized in the flight data case. Another technique to improve the statistics is to overlap the data samples by a factor of 50%. This effectively provides an increase of $(2N-1)/N$ times the number of samples. Figure 4-4 illustrates this process.

Hence, for a 0.2 sec time increment and a sampling rate of 204.8 kHz, 36 averages can be obtained which is a significant improvement over the 5 which would be obtained using a non-overlapped sampling procedure. The overlapping does provide statistically independent results as was shown in Reference 4-1, while the increased sampling rate improves the quantification of individual samples. The result is a 12 dB improvement in signal to noise resolution capability.

4.5   SPECTRAL ADJUSTMENTS

The spectral adjustments required prior to comparing flight spectra with the simulated flight spectra are delineated in the following:

- The flight data and simulated flight data are adjusted for instrumentation effects which include microphone pressure response, system response, wind screen and nose cone effects. These are shown in Figures 4-5a and 4-5b.

- The simulated flight data is adjusted for atmospheric absorption using the procedure outlined in Appendix I.

Data Record 1: 1, 5, 9, 13 ...
Data Record 2: 2, 6, 10, 14 ...
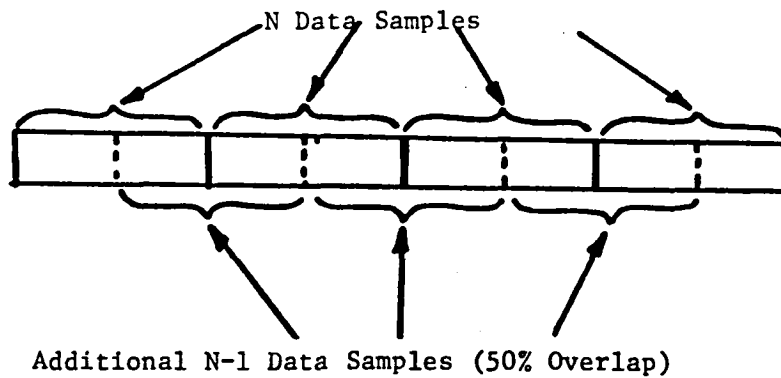Data Record 3: 3, 7, 11, 15 ...
Data Record 4: 4, 8, 12, 16 ...
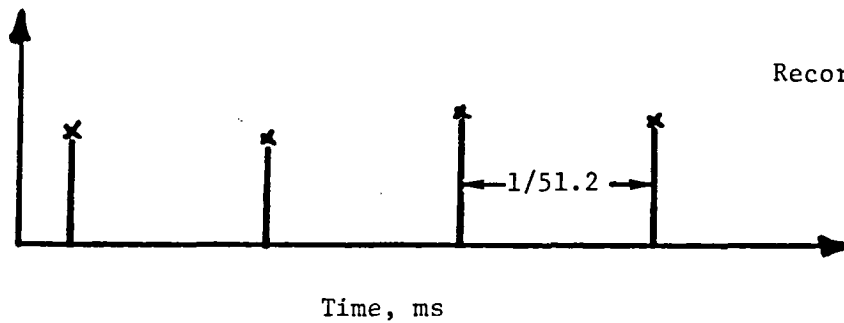

Sample No. (Sample Rate = 204.8k Hz)

Sample Nos.
Record 1: 1, 5, 9, 13 ...

1/51.2

Time, ms

N Data Samples

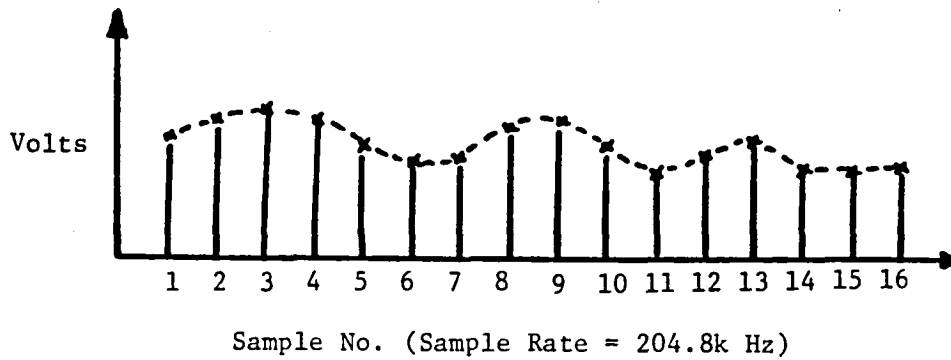Additional N-1 Data Samples (50% Overlap)

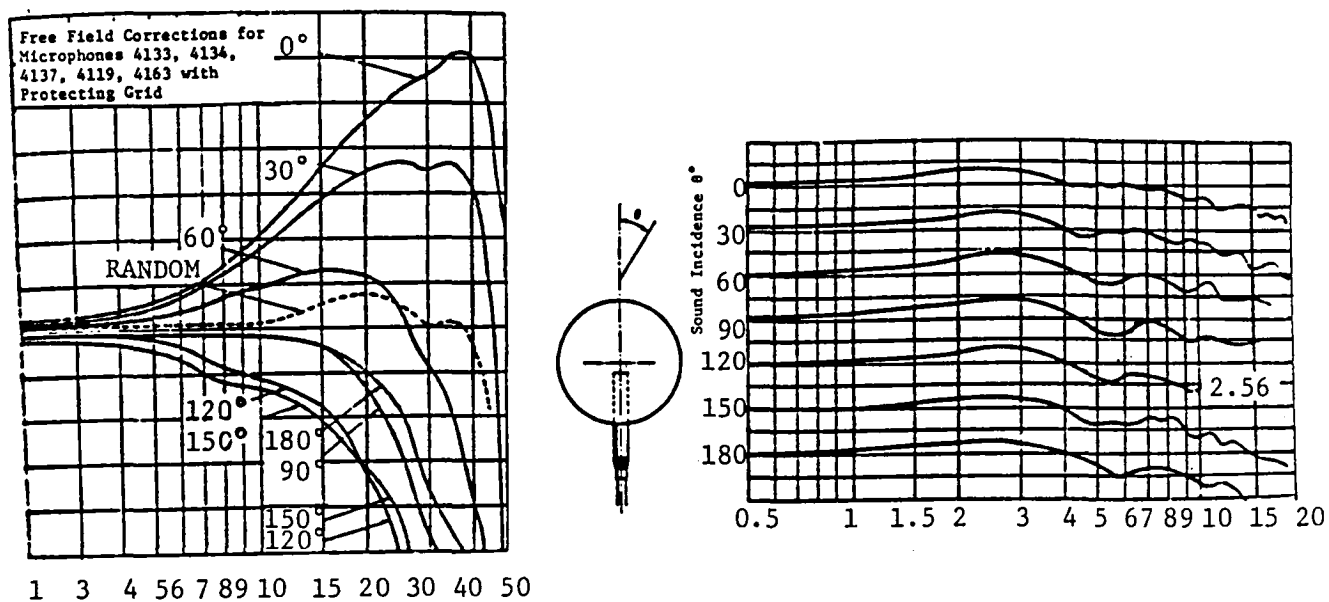Figure 4-4. Improvement by Factor of 8N/(N-1) in Number of Averages.

51

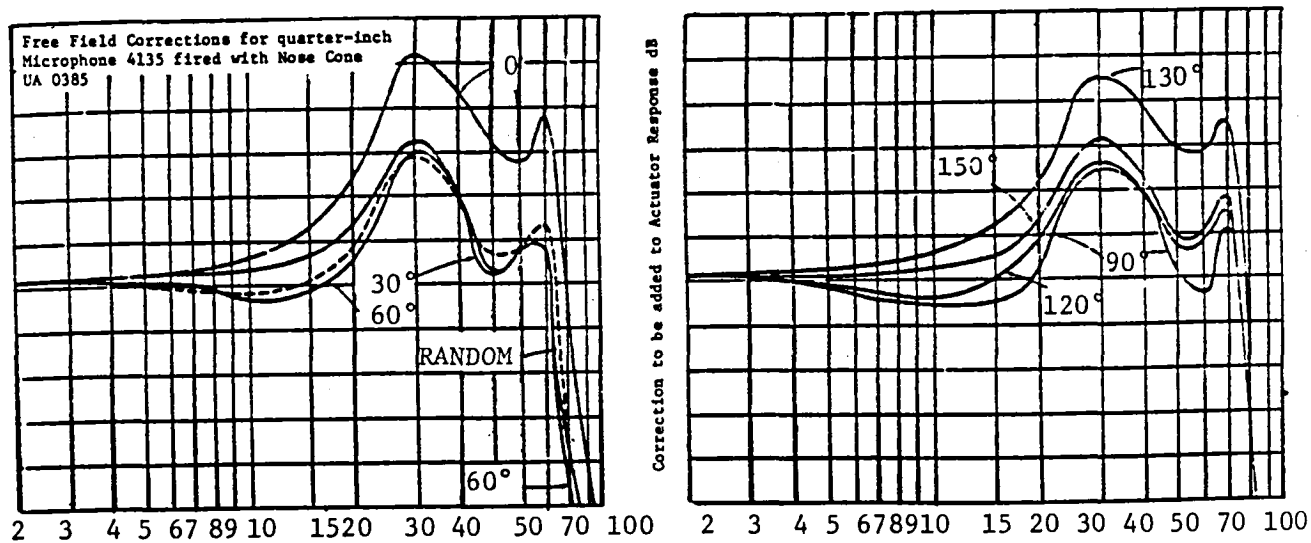Figure 4-5a.   Flight Microphone Corrections

Figure 4-5b.   Wind Tunnel and Outdoors Microphone Corrections
for General Electric Tests

- The simulated flight data is adjusted for ground reflection effects. The effective increase in the spectral value is computed using the following factor:

$$10 \log \left\{ 1 + R(f)/\left[1 + 4 \left[(H/D) + (H/D)^2 \right] \sin^2 \theta \right] \right\}$$

An assumption is made that the reflected signal is emitted at the same angle as the direct signal and that the signals are not correlated such that logrithmic energy addition is applicable and the factor R(f) is set equal to 1.0.

- The simulated flight data is adjusted for bandwidth effects using the standard doppler shift technique. Each spectral result estimated for a bandwidth (bw) of the sampling rate (51,200 Hz) divided by the blocksize (2048), i.e. 25 Hz is adjusted by the factor,

$$10 \log \left\{ bw / \left[1. - (Vo/co) \cos (\theta_e - \beta) \right] \right\} \tag{4}$$

for each $\theta_e(t)$, to arrive at 25 Hz bandwidth estimates for the flight spectrum. This energy redistribution is discussed in Reference 4-2.

- The simulated flight spectra is adjusted for forward velocity effects using the following equations:

$$\phi = \cos^{-1} \left[\frac{(\cos\phi - M_\infty)}{\sqrt{1+M_\infty^2 - 2M_\infty \cos\phi}} \right] \tag{5a.}$$

ϕ' is then used in Equation 2a replacing ϕ_i or ϕ_e where M_∞ is the uniform Mach number.

Also,

$$r' = r/ \sqrt{1+M_\infty^2 - 2M_\infty \cos \theta} \tag{5b.}$$

and r is either r_i or r_e as appropriate from Equation 2b.

53

- The simulated flight spectra are adjusted for spherical divergence using the factor:

$$10 \log (r'^2/R^2),$$

where $R^2 = (D - V_o t_e \sin\alpha)^2 + (V_o t_e \cos\alpha)^2$, and r' is defined in Equation 5b.

- The simulated flight spectra are adjusted for convective amplification using the standard monopole correction factor of Reference 4-3. This term is

$$40 \log \left[1 - M_\infty \cos (\theta_e - \beta) / 1 - (V_o/c_o) \cos\theta_e \right]$$

4.6 SPECTRAL COMPARISONS

The spectral results for times 1.0 seconds prior to overhead are displayed in Subsection 5.1. The time increment of 0.2 seconds was utilized. The matrix of test points and fan speeds which were flight projected are summarized in Table 4-1.

TABLE 4-1

SIMULATED FLIGHT JT15D ANALYSIS

LRC (Flight) (N_c)	GE (TCS) (N_c)	GE (TCS) (N_c)	GE (WT) (N_c)	LRC (WT) (N_c)
1461 (13,224)	1.03 (13,307)	3.03 (13,425)	8.10 (13,448)	–
1471 (11,768)	1.07 (11,721)	3.07 (11,771)	8.16 (11,778)	7.07 (~11,900)
1481 (10,301)	1.11 (10,453)	3.11 (10,501)	8.22 (10,479)	7.08 (~10,500)

4.7 ONE-THIRD OCTAVE EVALUATION

The narrowband results are reconstituted into one-third octave results. For one-third octave bands above 400 Hz, the reconstitution technique produces excellent one-third octave filter characteristics for the

25 Hz bandwidth analysis. Since in the flight case the low frequency JT15D engine noise was masked by the prop noise of the OV-1 aircraft and a high pass filter was set at 1000 Hz, the low frequency information is not available for direct comparison. Also, the introduction of a 1000 Hz tone component in the simulated flight testing as a result of a fan exhaust nozzle modification makes these low-frequency comparisons of limited value. Consequently, the method to investigate the high-frequency fan noise impact on system noise parameters such as PNLT and PNL is to equate the flight and simulated flight values below the 1250 Hz one-third octave band. This was accomplished with the tabulated one-third octave results presented in Subsection 5.3.

4.8   TONAL COMPARISONS

Although the previous comparisons yield quite detailed information of the quality of flight projection results, even more detailed resolution is required to evaluate the tonal structure. Alternate analysis methodologies are required to provide this resolution. In the simulated flight case, each tonal component of interest is filtered using a 50 Hz bandwidth, converted from analog to digital and stored. The angular information is also stored such that by applying the flight projection methodology previously discussed the projected flight time history of tone component may be created. Results of these analyses are presented in Subsection 5.3.

Regarding the flight data, the analysis problem arises in tracking the frequency of the tone due the doppler shift effect. When the tone amplitude is well above the broadband such as in the supersonic case, this method is available. However, at subsonic flight conditions an alternate technique is needed. The method chosen is again spectral averaging. However, improvement over the 36 averages/0.2 second interval is required. An initial improvement is made by reducing the block size to 512 points and formulating 8 records from the single data record. This provides for an effective sampling rate of 25,600 Hz with a 50 Hz bandwidth. Using these improvements, 32 spectral averages may be obtained in a time interval of 0.05 seconds from a single microphone. Shifting by only .01 seconds in the time domain, allows a tone amplitude value to be determined every 0.01 seconds with an averaging time of 0.05 seconds. The results of this analysis technique are displayed in Subsection 5.3.

When the previous technique cannot be implemented, one has to resort to plotting the narrowband values from the analysis previously described in Subsection 4.4. Thus, when this alternative procedure is used, only 16 data points are obtained for the 3.0 second time interval prior to overhead. This technique was resorted to for the Blade Passage frequency tone at an engine speed of 10,500 RPM and the compressor tone at an engine speed of 13,500 RPM.

SECTION 5.0

FLIGHT/SIMULATED FLIGHT COMPARISONS

5.0 FLIGHT/SIMULATED FLIGHT COMPARISONS

The results of the data analysis procedures discussed in Section 4.0 are presented in this section. The results may be separated into four separate categories for convenience. These categories are the following:

- Narrowband Data Analysis
- One-third octave band Data Analysis
- Tonal Data Analysis
- BMT Data Analysis

The separate areas of analysis formulate the next four subsections.

5.1   NARROWBAND DATA ANALYSIS

Selected examples of the spectral characteristics are displayed for subsonic, transonic, and supersonic fan tip speeds in Figures 5-1 through 5-3 respectively. In each case the projected spectral results are compared and differenced from the actual flight measured data at a time of 1.0 seconds prior to the aircraft overhead position. A distinct feature noted in the subsonic spectral data is the band spreading of the flight tonal data. Due to the projection method, the time energy is not band spread over many bands as is the flight data, hence the spectral difference plot does not produce alignment of the tones in many situations. The difference plots are thus more valuable in the resolution of broadband details as opposed to tone details. If many more microphones could have been utilized and the aircraft path could have been controlled precisely, then flight data averaging times shorter than 0.2 seconds could have been utilized and the flight tone energy could have been band spread to lesser degrees.

Another feature evident in the subsonic results is the appearence of a BPF tone in the projected to flight case for each simulated flight data set. The flight spectra on the other hand does not indicate a BPF tone, partly. because of the band spreading just indicated but also potentially due to differences in the noise source mechanisms which may exist between simulated flight and flight environments.
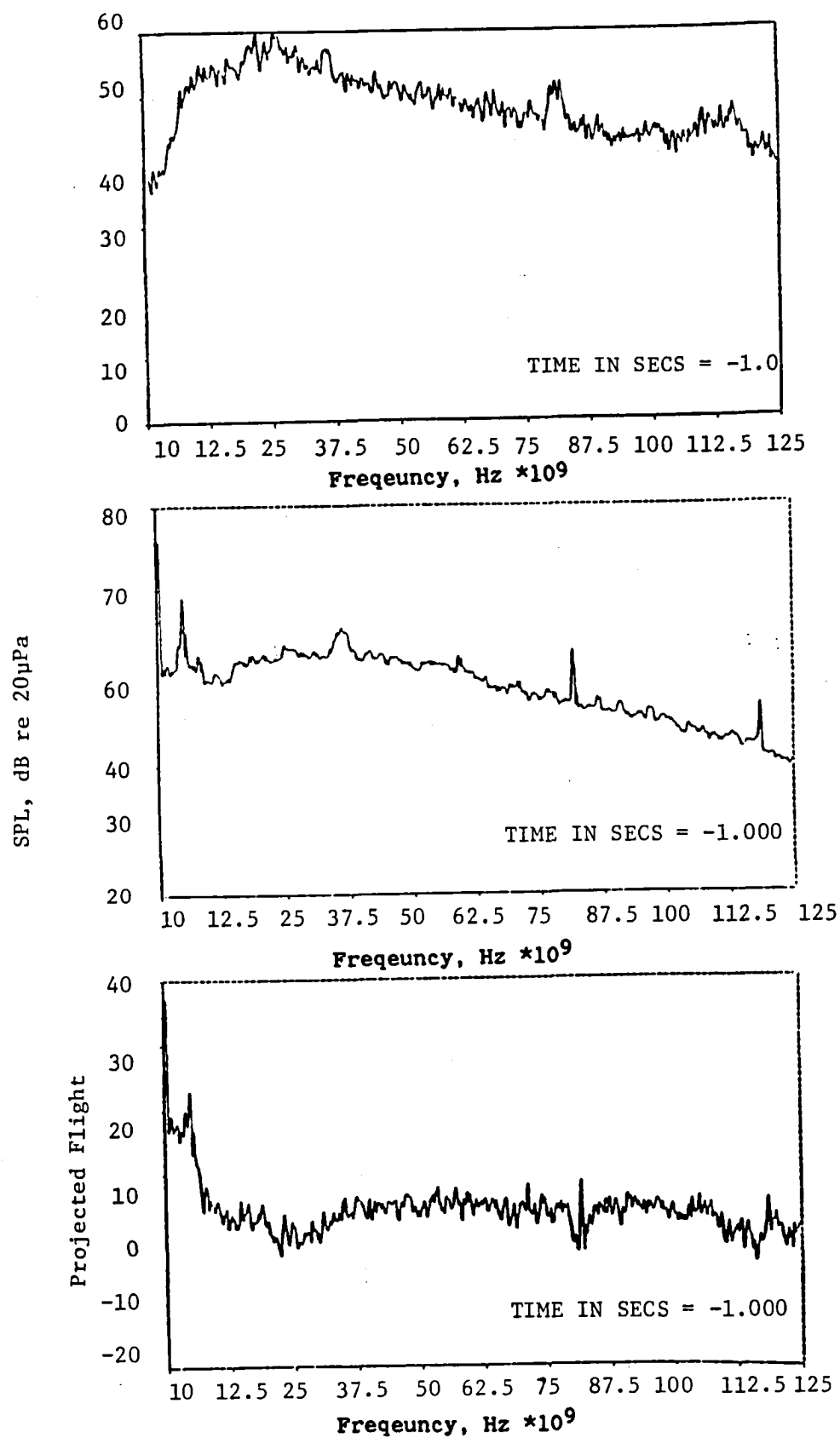
Figure 5.1(a). Comparison of Flight and Flight Projected Narrowband Spectra with Spectral Difference for Subsonic Fan Speed
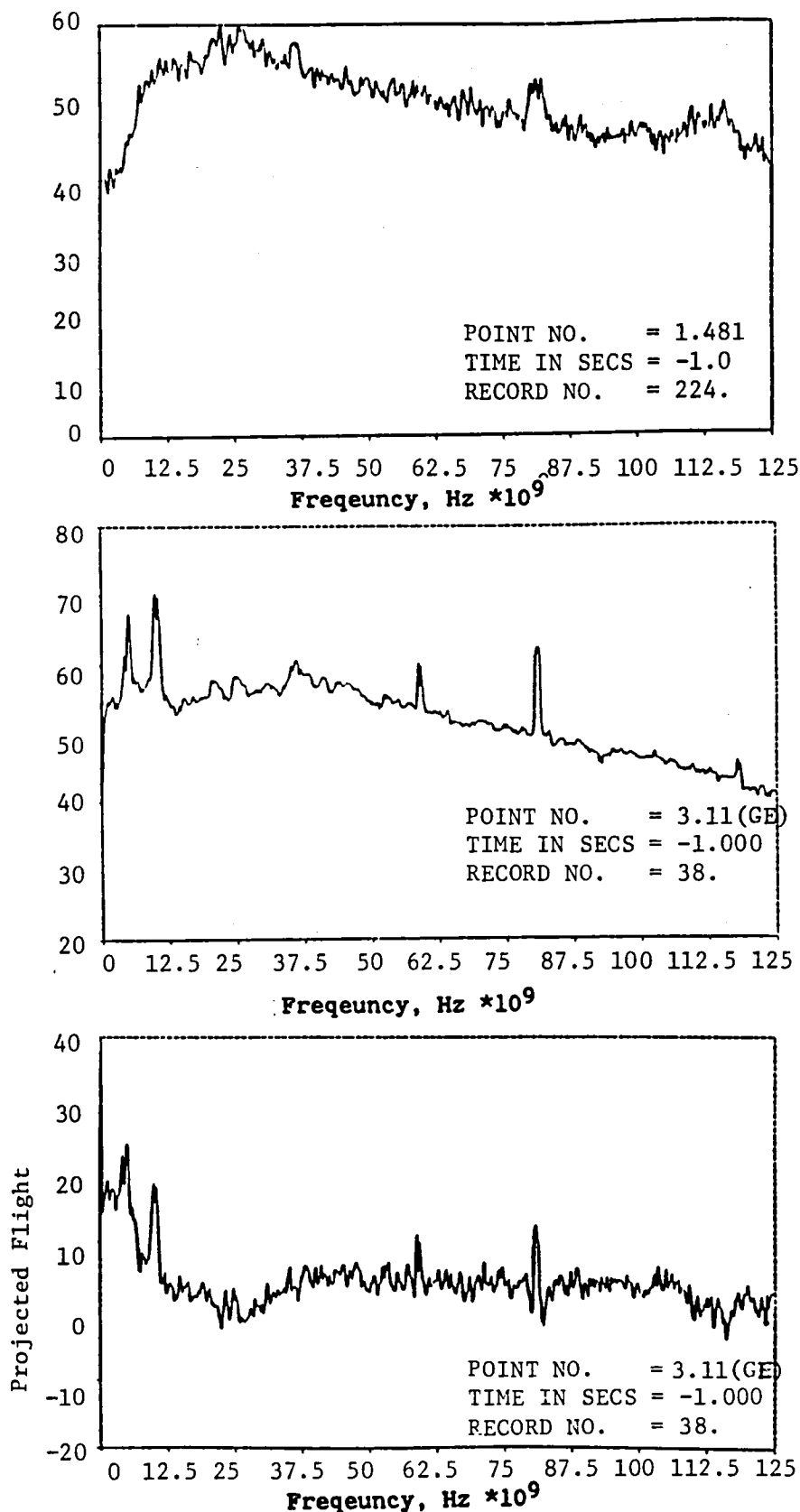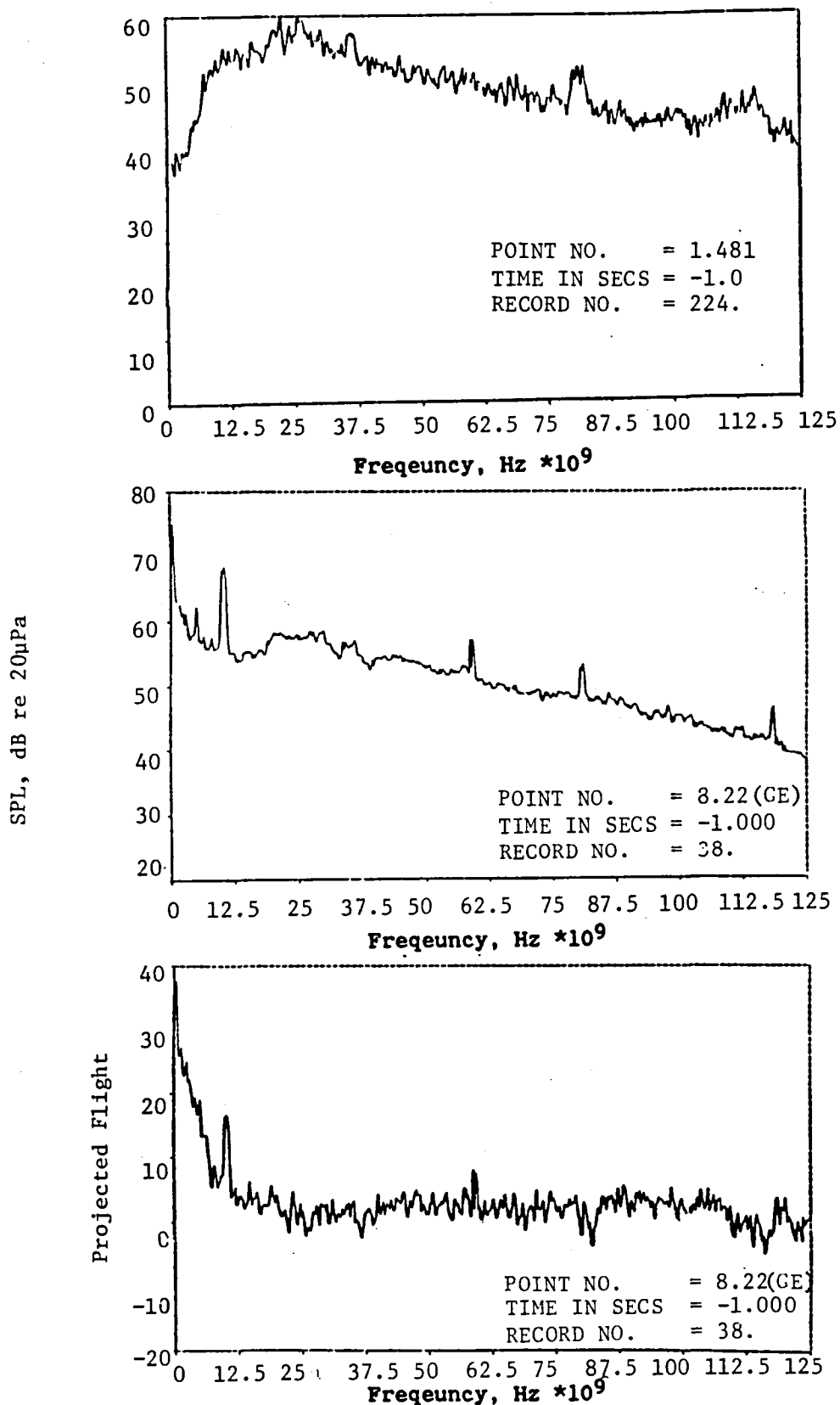
Figure 5.1(b). Comparison of Flight and Flight Projected Narrowband Spectra
With Spectral Difference for Subsonic Fan Speed

Figure 5.1(c). Comparison of Flight and Flight Projected Narrowband Spectra
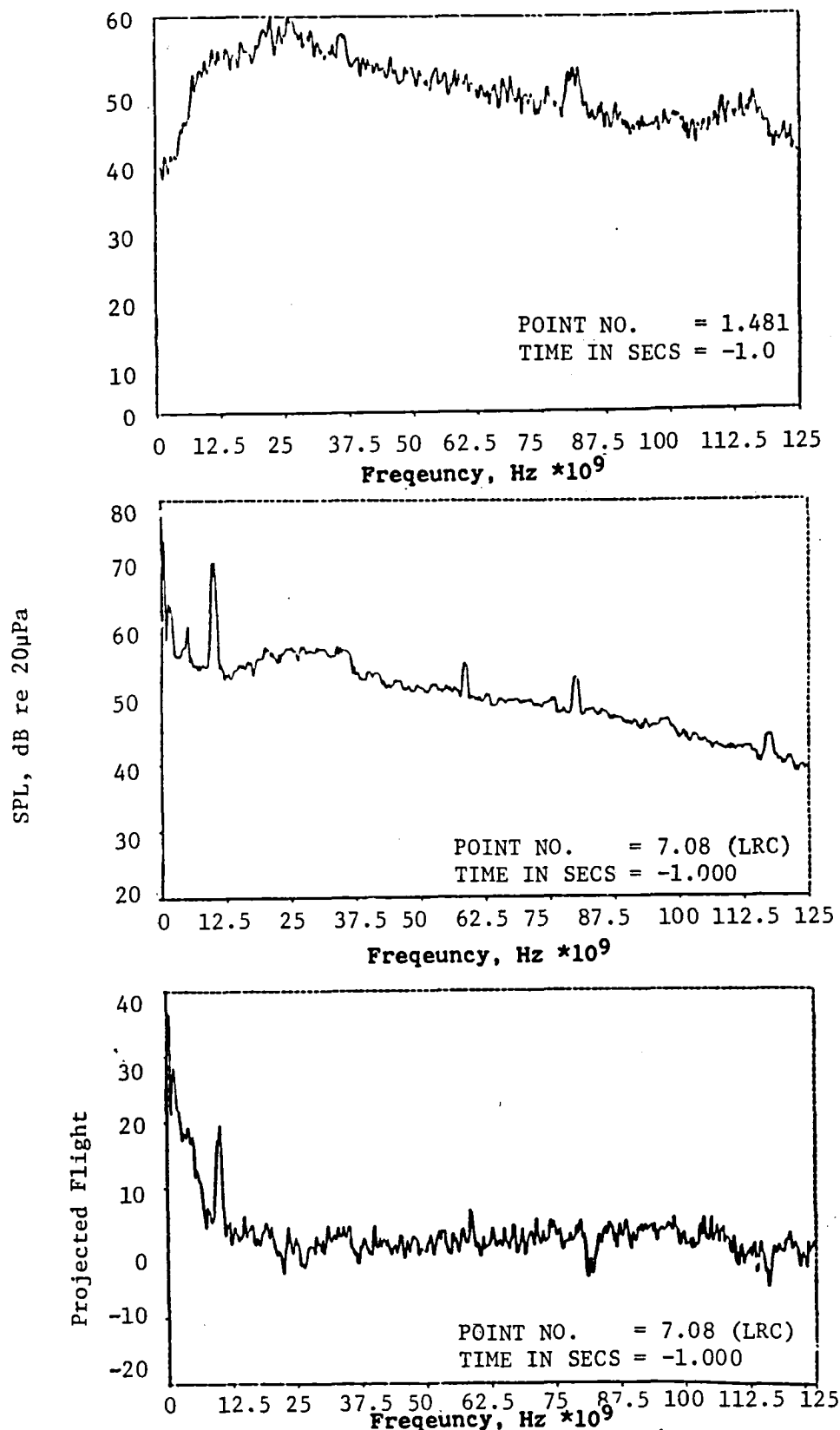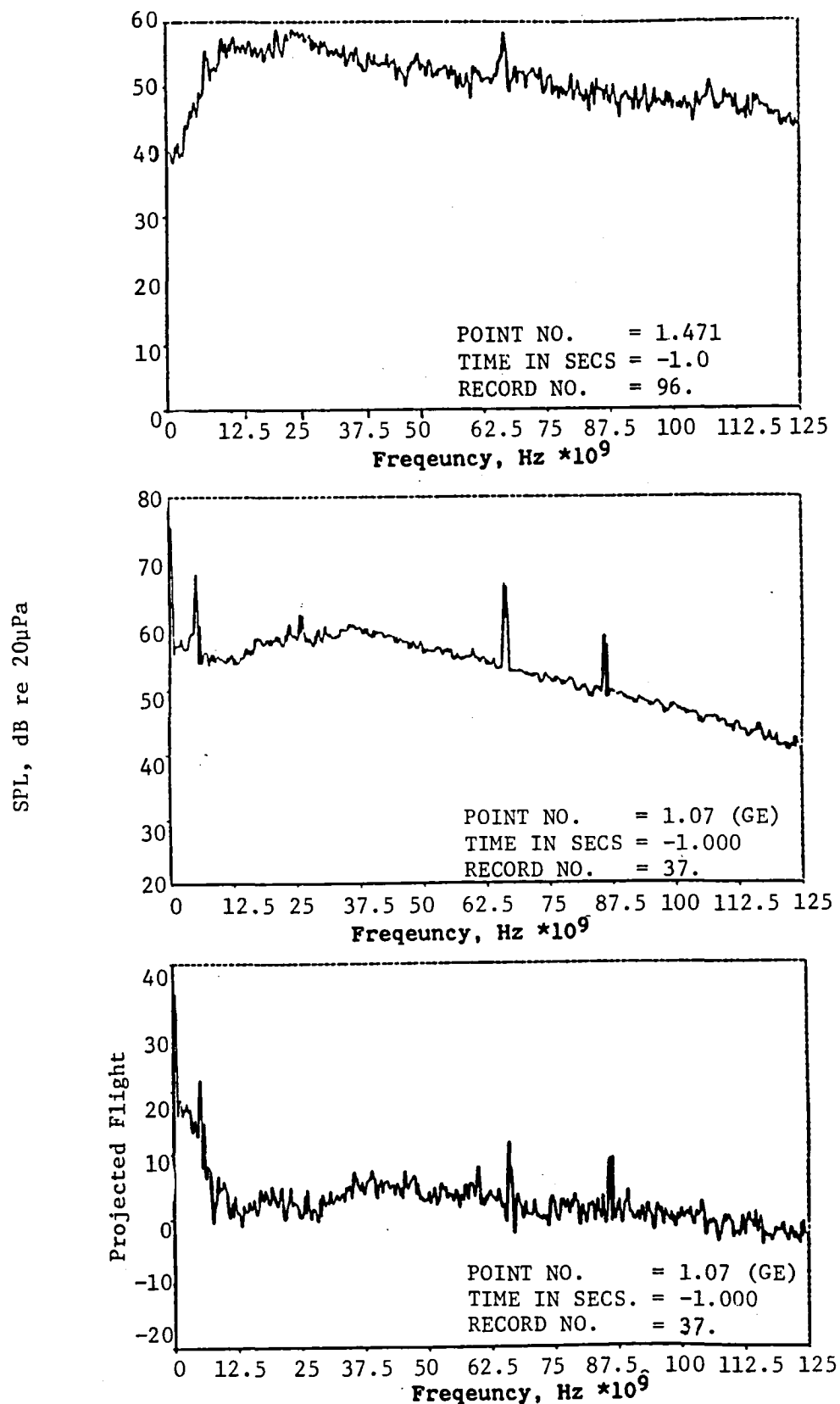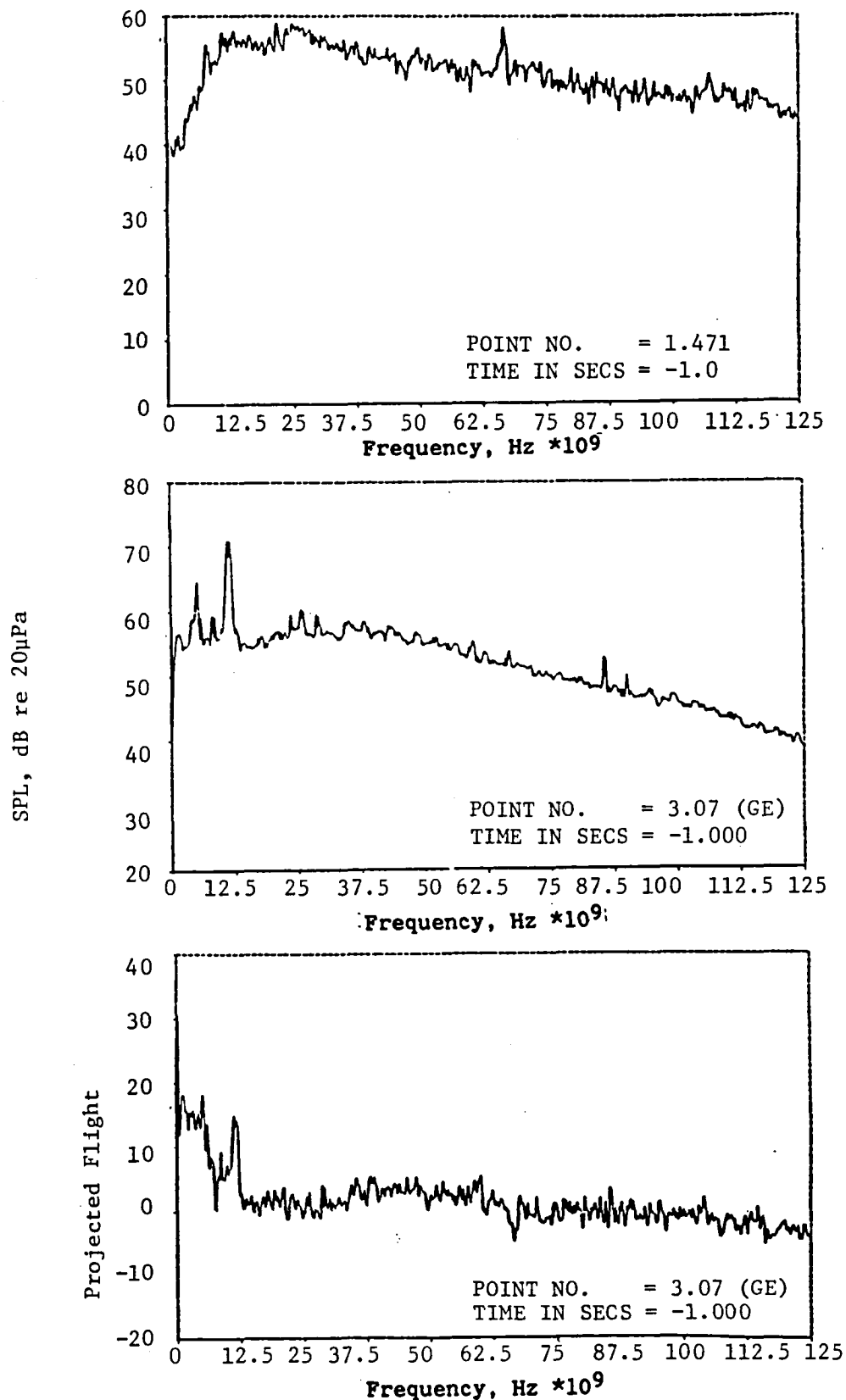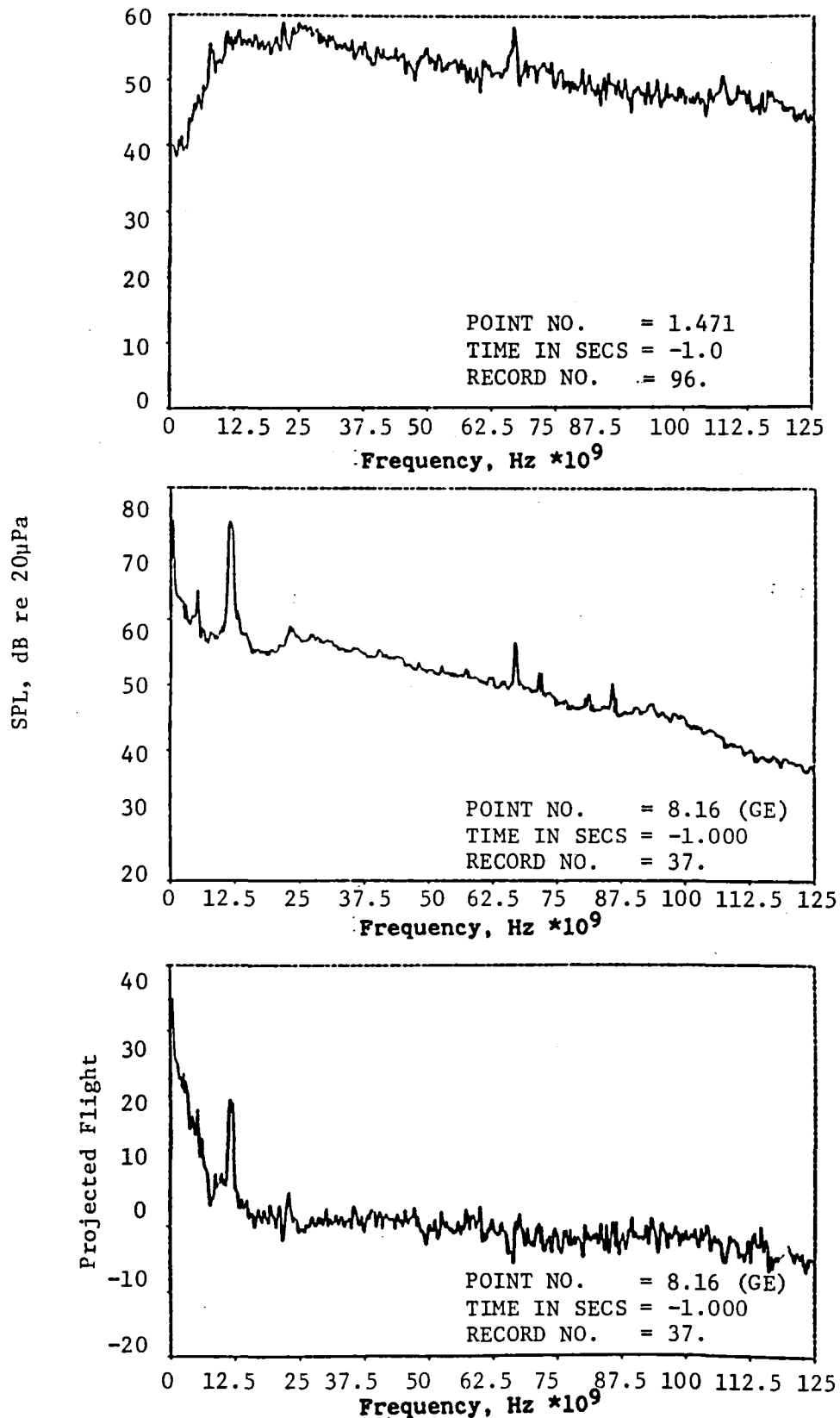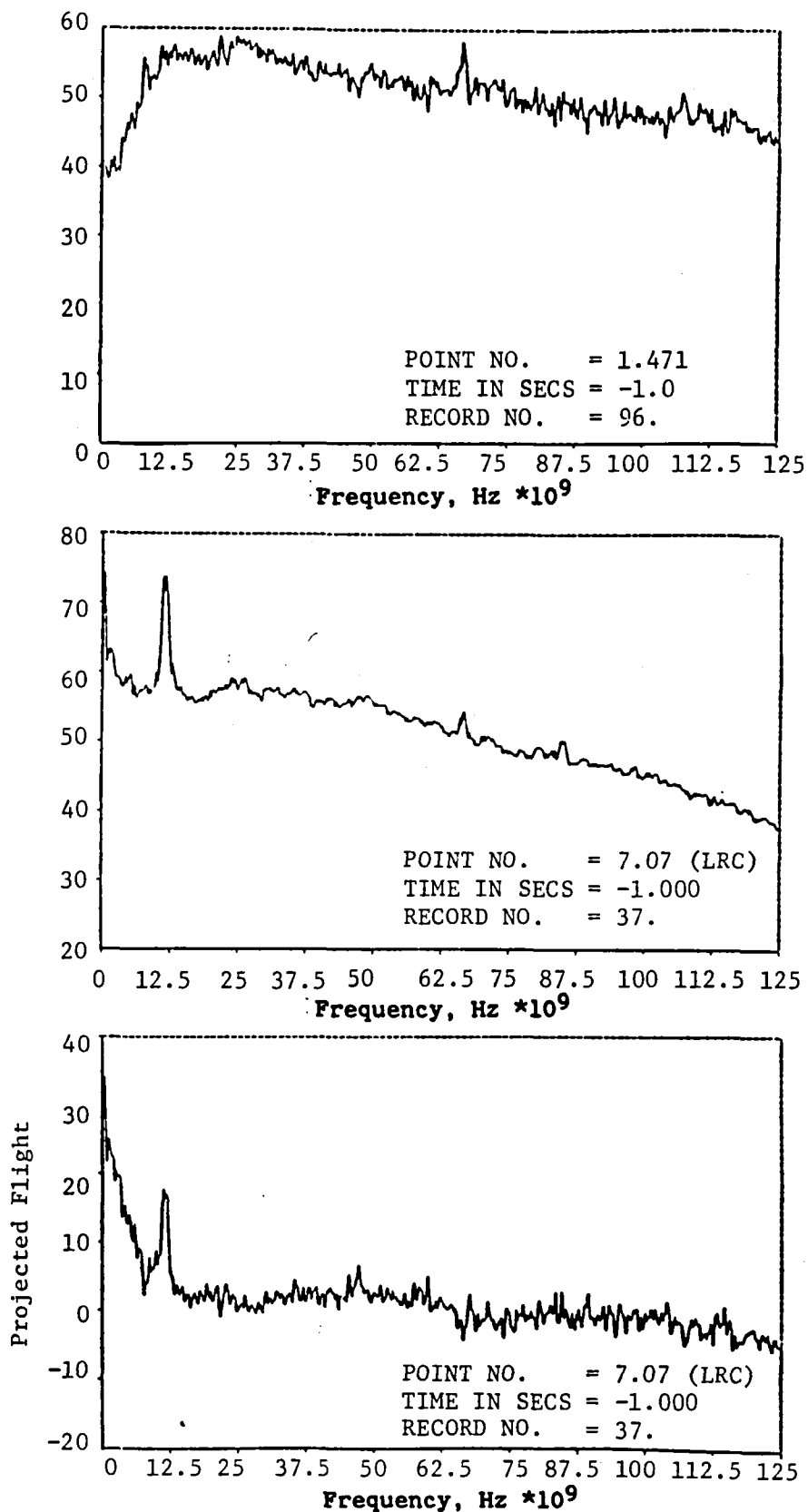With Spectral Difference for Subsonic Fan Speed

Figure 5.1(d). Comparison of Flight and Flight Projected Narrowband Spectra With Spectral Difference for Subsonic Fan Speed
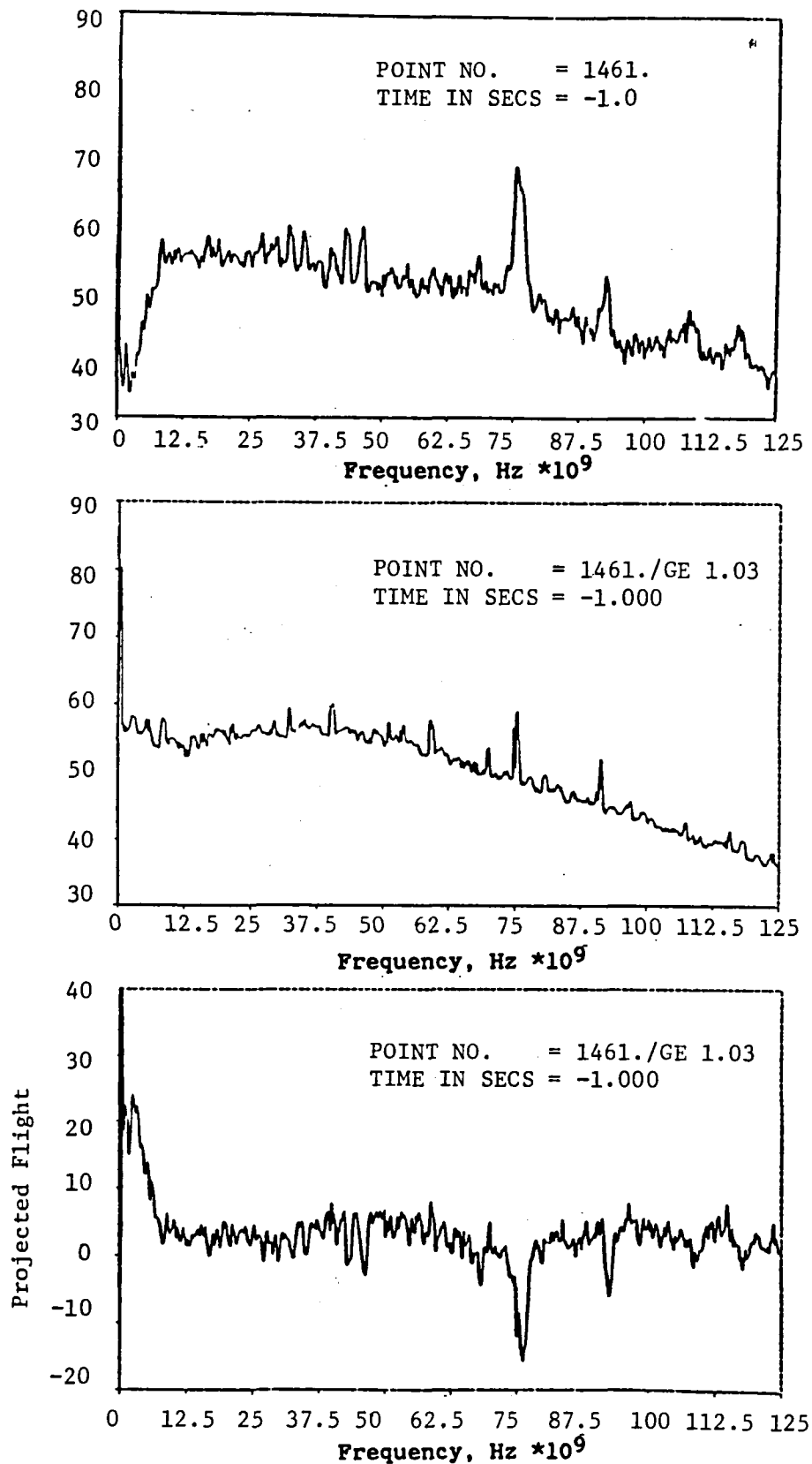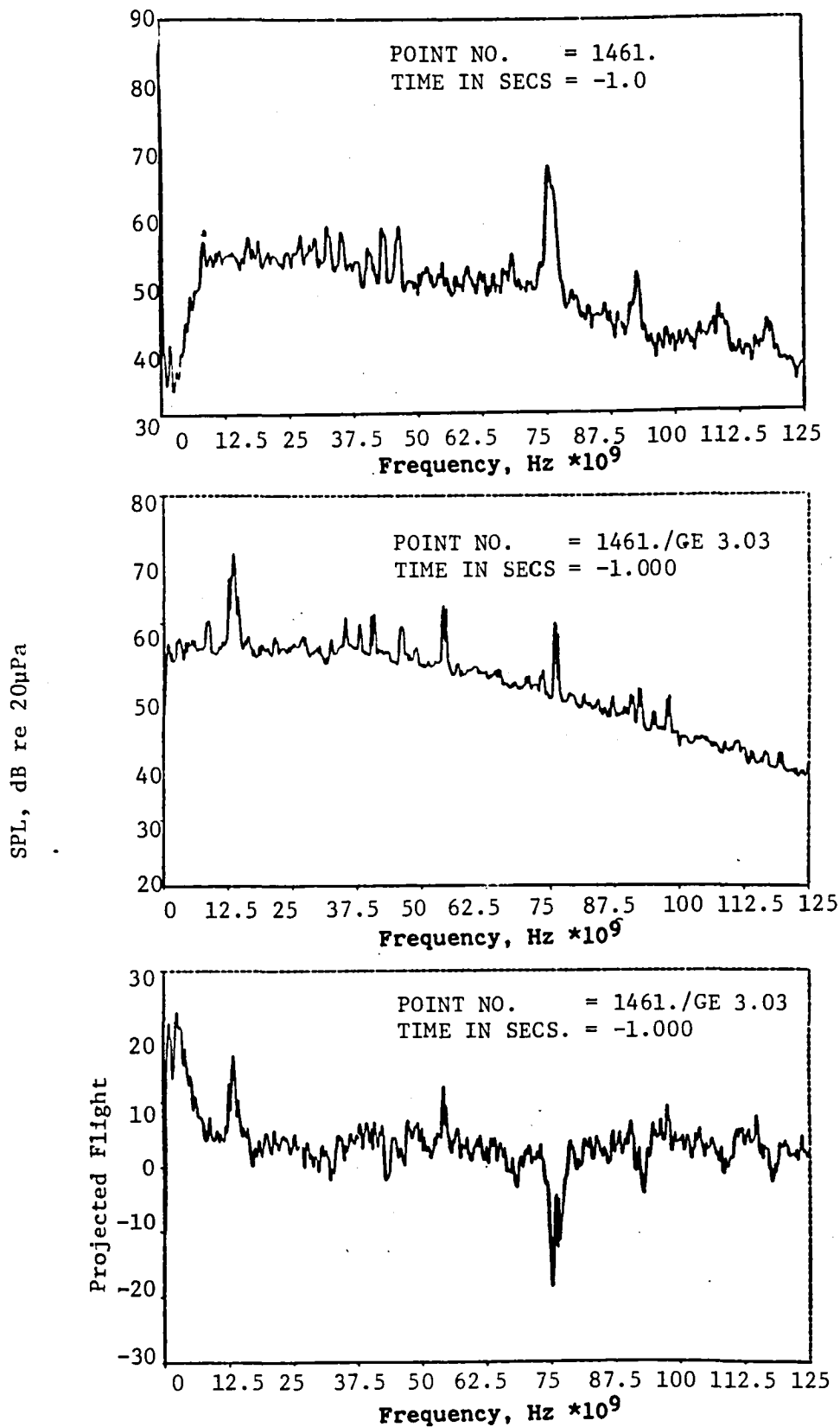
Figure 5.2(a).   Comparison of Flight and Flight Projected Narrowband Spectra
With Spectral Difference for Transonic Fan Speed

Figure 5.2(b). Comparison of Flight and Flight Projected Narrowband Spectra With Spectral Difference for Transonic Fan Speed

POINT NO.   = 1.471
TIME IN SECS = -1.0
RECORD NO.   = 96.

SPL, dB re 20μPa

Frequency, Hz *10^9

POINT NO.   = 8.16 (GE)
TIME IN SECS = -1.000
RECORD NO.   = 37.

Frequency, Hz *10^9

Projected Flight

POINT NO.   = 8.16 (GE)
TIME IN SECS = -1.000
RECORD NO.   = 37.

Frequency, Hz *10^9

Figure 5.2(c).   Comparison of Flight and Flight Projected Narrowband Spectra
With Spectral Difference for Transonic Fan Speed

Figure 5.2(d). Comparison of Flight and Flight Projected Narrowband Spectra
With Spectral Difference for Transonic Fan Speed

65

Figure 5.3(a). Comparison of Flight and Flight Projected Narrowband Spectra
With Spectral Difference for Supersonic Fan Speed

66

Figure 5.3(b). Comparison of Flight and Flight Projected Narrowband Spectra
With Spectral Difference for Supersonic Fan Speed

67
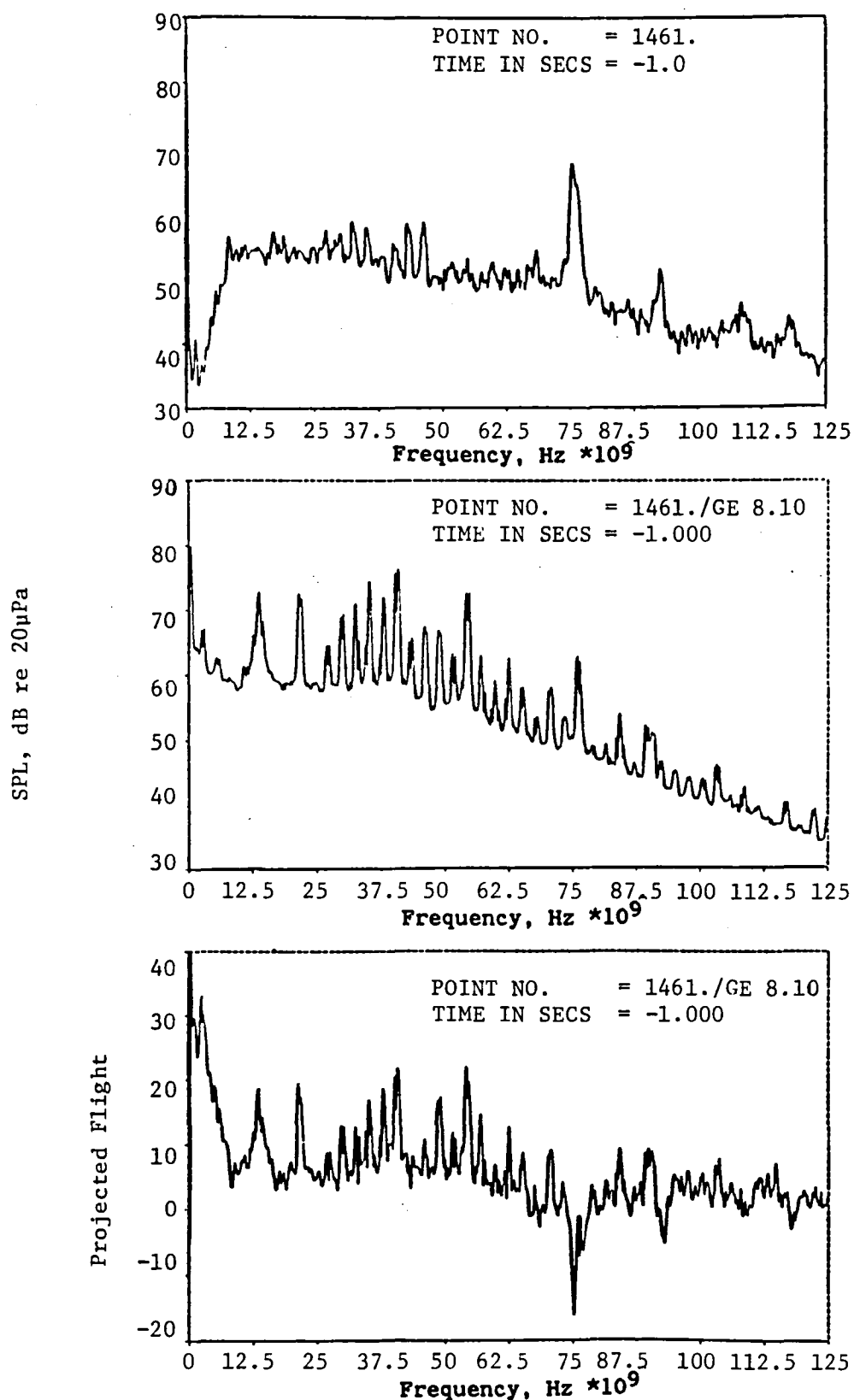
Figure 5.3(c). Comparison of Flight and Flight Projected Narrowband Spectra
With Spectral Difference for Supersonic Fan Speed

68

Noise generated by turbofan engine components has been described as a complex spectrum of tones and broadband noise. It is now recognized that the noise consists of a collection of interactive source mechanisms, each having unique directional and/or spectral characteristics and a particular dependence on design parameters and operating conditions. It is important that the characteristics of each of these sources be understood in detail so that accurate assessments of total turbomachinery noise spectral and directional characteristics can be made.

The conditions of a strong compressor tone component and a weak Blade Passage Frequency tone component in the flight spectra which occur at subsonic speeds indicated a near reversal as the fan tip speed becomes transonic as indicated by the Figure 5-2 results. It is noted that the projected spectra in these cases denote a relatively strong compressor tone component while the flight spectra denote a much lesser predominance to this spectral feature. These transonic speeds better agreement is denoted between the projected BPF tone and the flight measured tone.

The supersonic fan tip speed cases are presented in Figure 5-3. The BPF in the case is the dominant feature of the flight spectrum, whereas for the projected flight results the Multiple Pure Tones (MPT) are prevalent. These tonal features are representative of the differences between flight and projected to flight results at other angular locations.

5.1.1 SUBSONIC TIP SPEED

A time history of spectral difference results between projected to flight spectra and actual flight measured data for subsonic fan tip speed cases are displayed in Figures 5-4 through 5-7. For these situations the JT15D engine was nominally operating at 10,500 RPM. The figures in general indicate relatively good spectral agreement over a wide frequency range between the projected to flight and actual flight situations. Broadband noise differences at the 0.6 seconds to overhead position are most pronounced with projected to flight data 3-4 dB higher than actual measured results for the outdoor simulated flight conditions. In the wind tunnel projection to flight lesser broadband and spectral differences are observed, i.e. 1-2 dB higher for
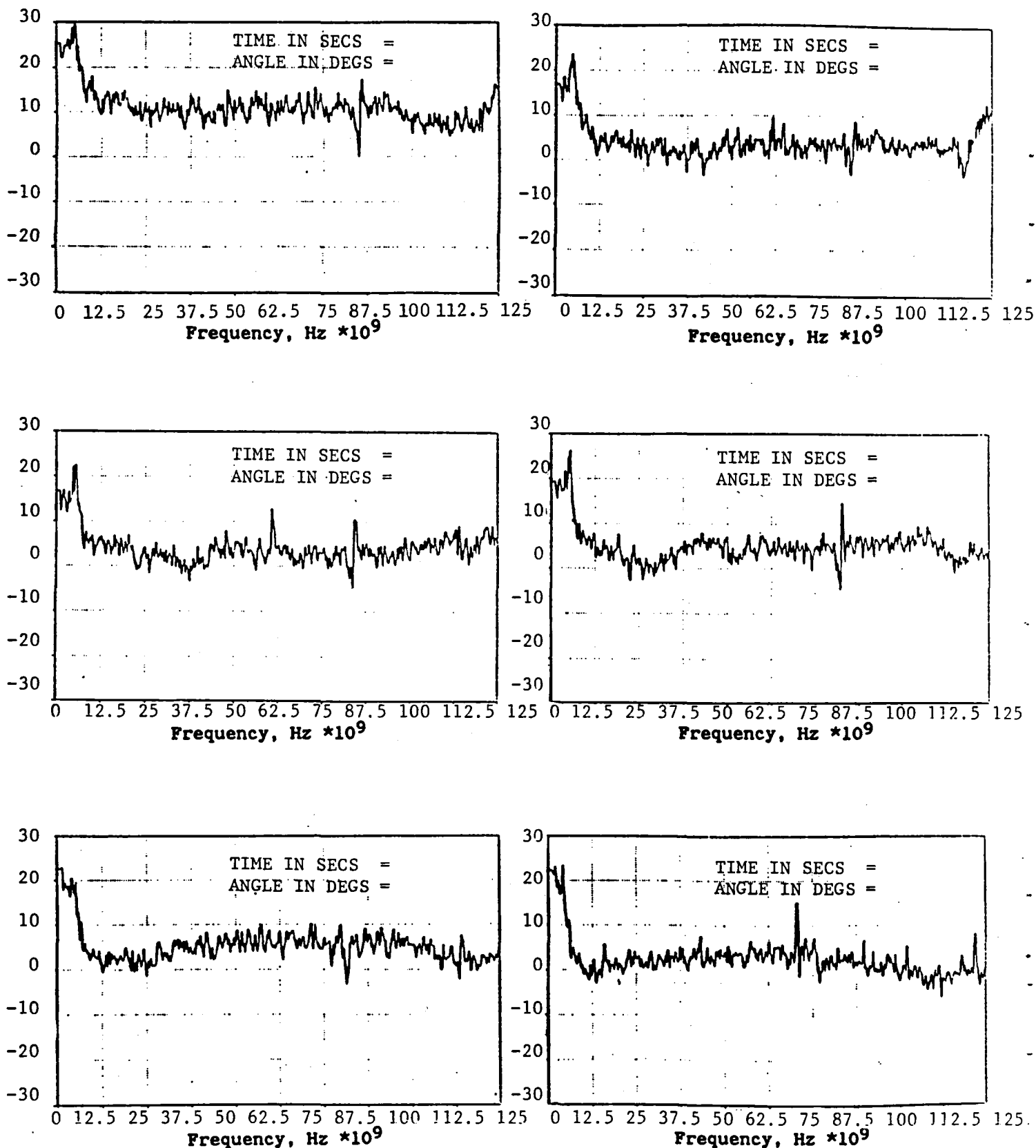
69

Figure 5-4. Spectral Difference Time History for Run GE.1.11
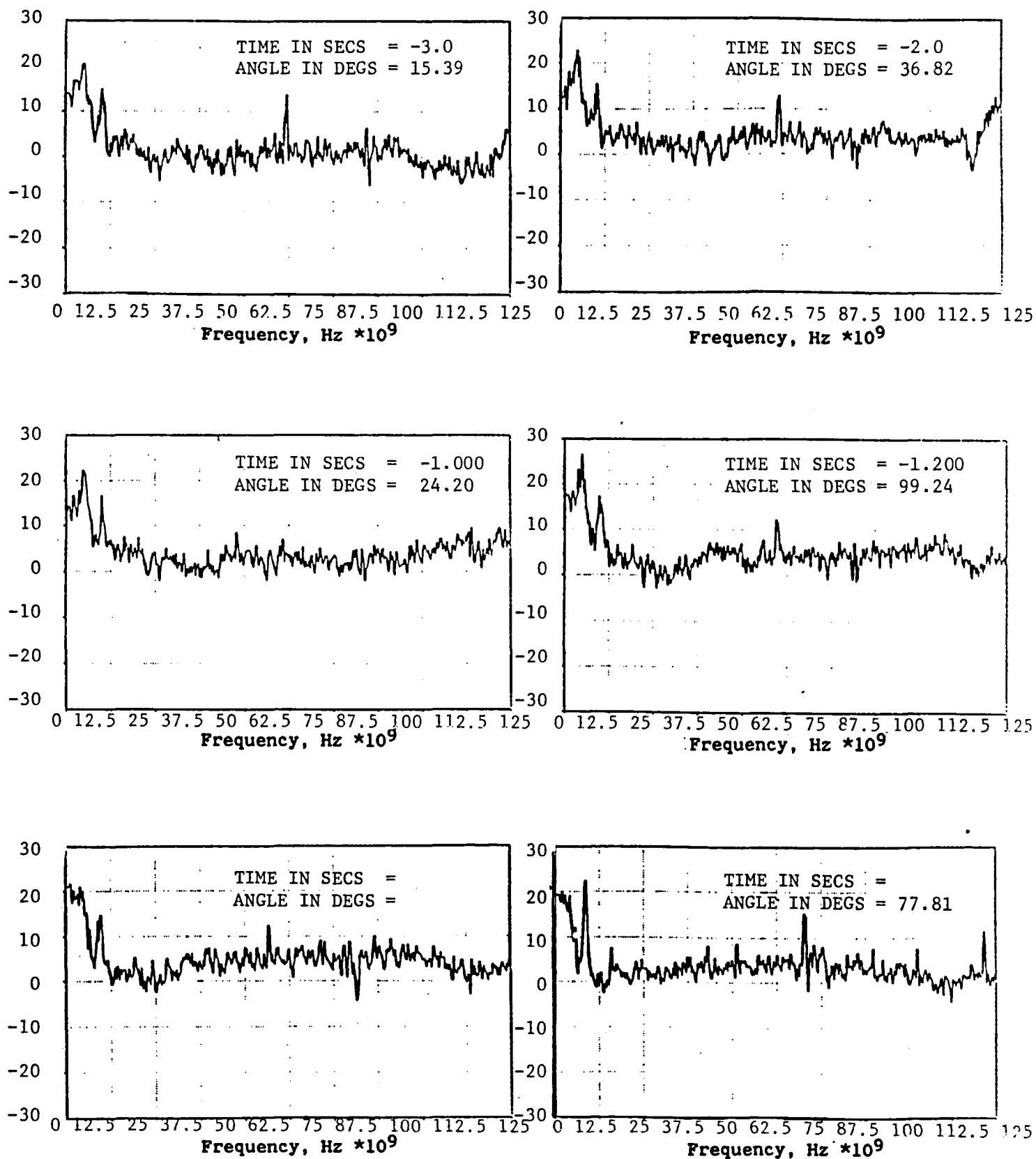Projected to Flight 1481

70

Figure 5-5. Spectral Difference Time History for Run GE.3.11
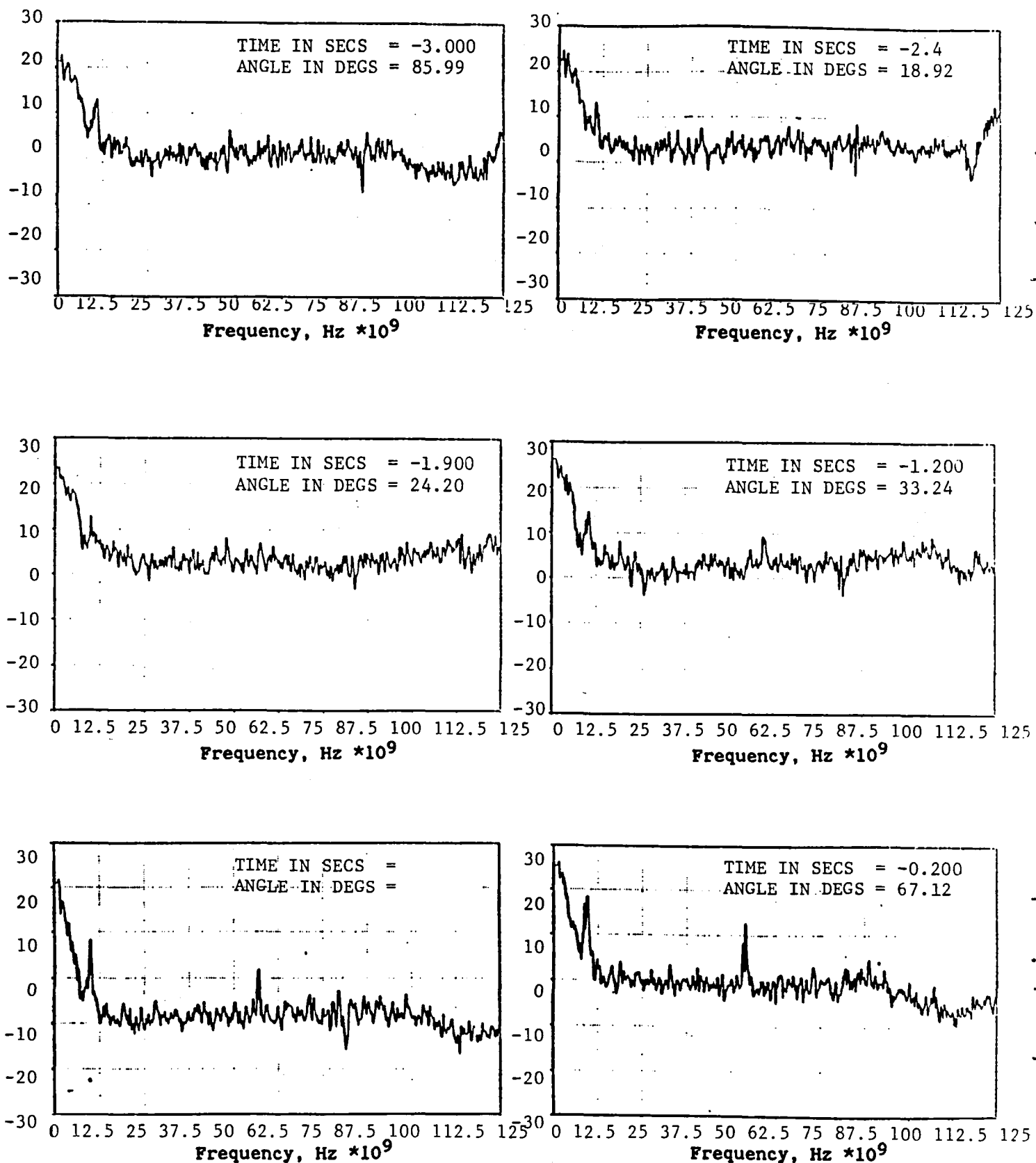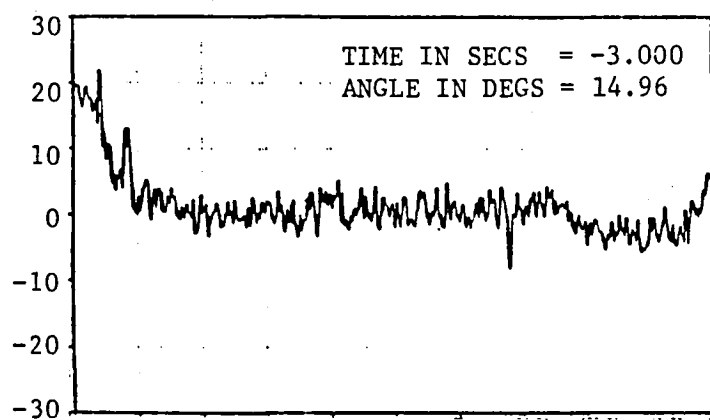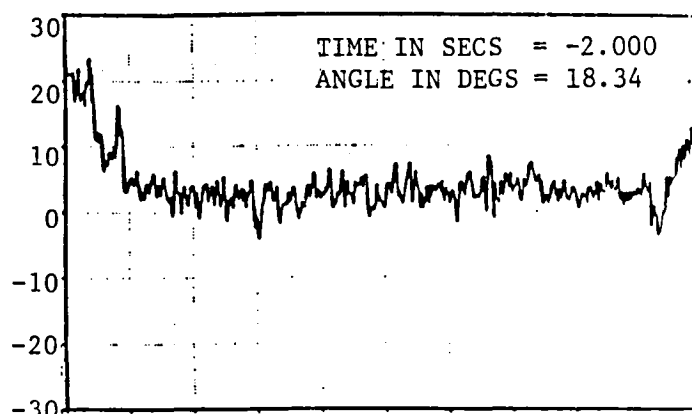Projected to Flight 1481

71

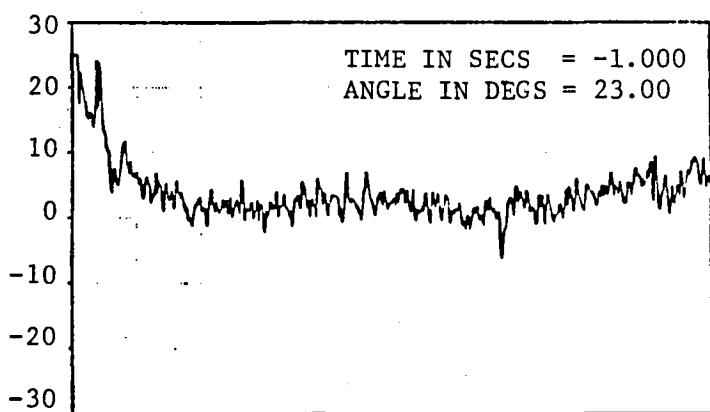Figure 5-6. Spectral Difference Time History for Run GE.8.22
Projected to Flight 1481

72
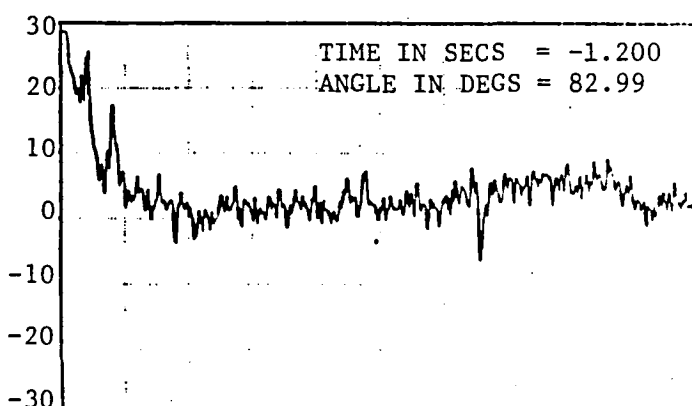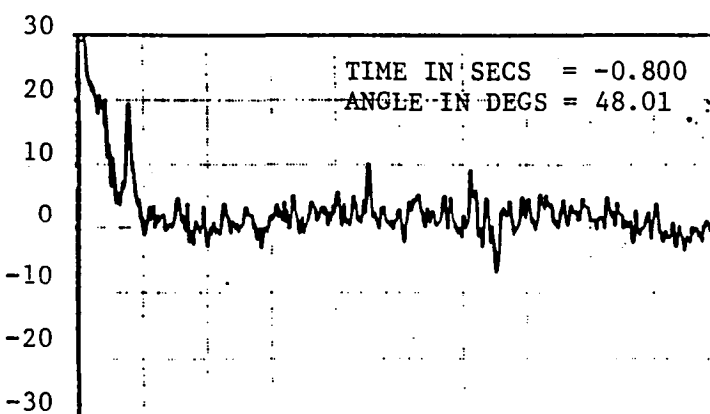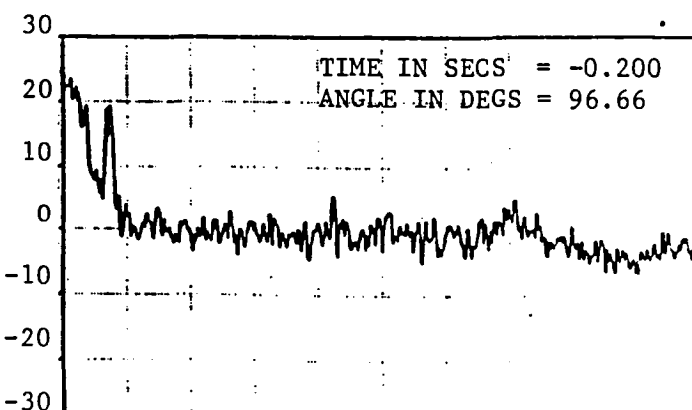
Figure 5-7. Spectral Difference Time History for Run LRC 7.08
Projected to Flight 1481

73

the projected condition. Significant broadband differences occur only in the 40-70 degree angular locations relative to the engine centerline with very small differences at shallow angles between 15 and 25 degrees and directly overhead, i.e., 90 degrees.

5.1.2 TRANSONIC TIP SPEED

The spectral differences time histories between projected (simulated flight) data and flight data are presented in Figures 5-8 through 5-11 for the JT15D operating at a nominal speed of 11,800 RPM. This fan speed produces a tip speed of 1081 ft/sec. and a blade tip relative Mach No. of 1.02. The broadband spectral differences denoted in the subsonic case, Subsection 5.1.1, are more pronounced for the transonic tip speed case. This is again particularly evident at the 0.6 seconds relative to overhead condition. Part of the explanation for this discrepancy is attributable to the aircraft noise background level which was measured with the JT15D shutdown. This background is added to the simulated flight data to achieve the overall projected result. Since the JT15D engine produces additional thrust when it is operating, the aircraft must be operated with higher flap settings to produce more drag and maintain a constant flight speed of 130 knots. These higher flap settings are known to produce additional broadband noise which consequently increases with JT15D fan speed.

The tone components generally are in agreement between projected to flight and flight data. The wind tunnel differences (Figures 5-10 and 5-11) are particularly small at all points along the spectral difference time history. The compressor tone is larger in flight data at the 1.8 seconds to overhead condition as compared to the GE wind tunnel data; however, it agrees well with the Langley wind tunnel data, Figure 5-11. The tone components in Figures 5-8 and 5-9 exhibit similiar trends to 5-10 and 5-11; however, differences are more pronounced, particularly the compressor tone at 0.6 seconds to overhead.

5.1.3 SUPERSONIC TIP SPEED

The spectral difference time history between flight projected and flight measured results for the supersonic tip speed case are presented in
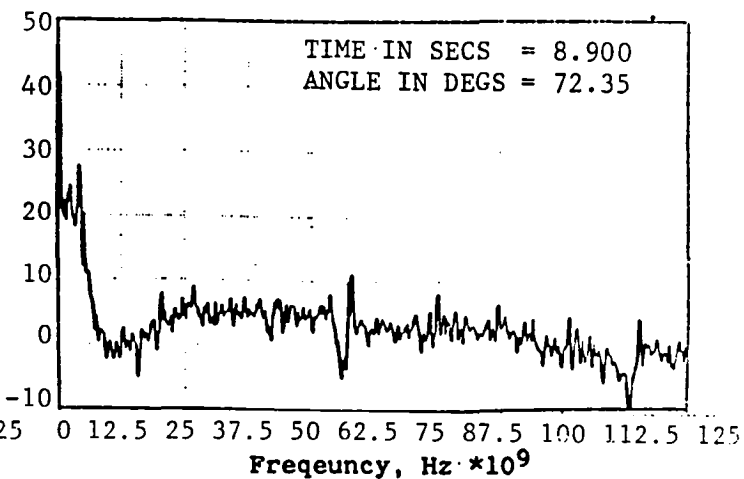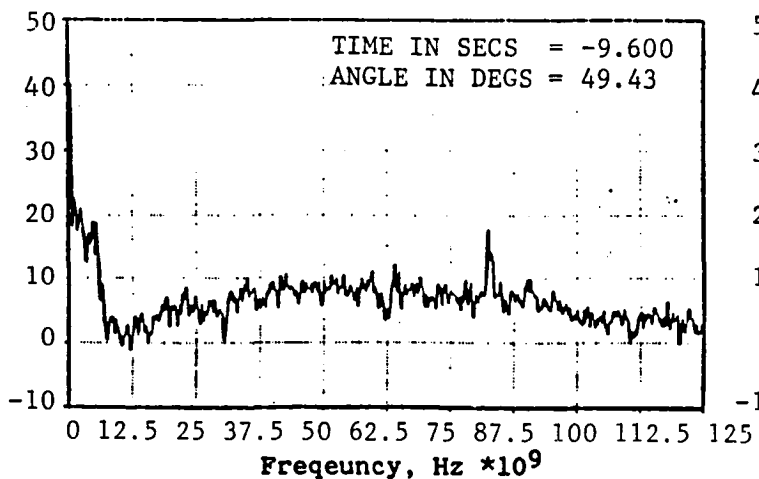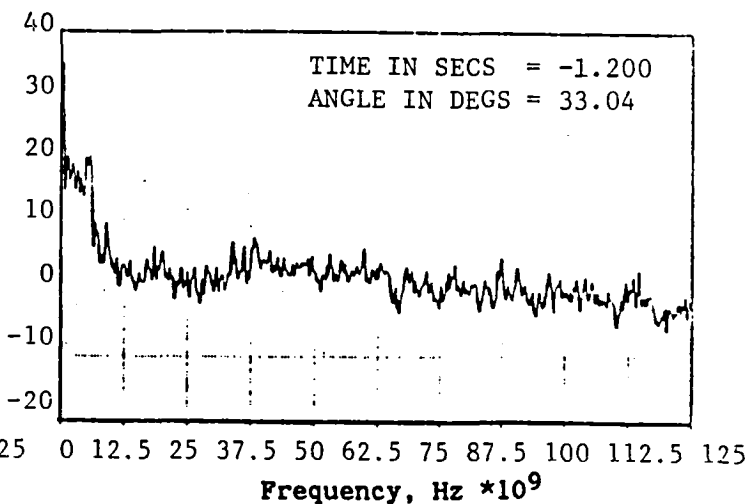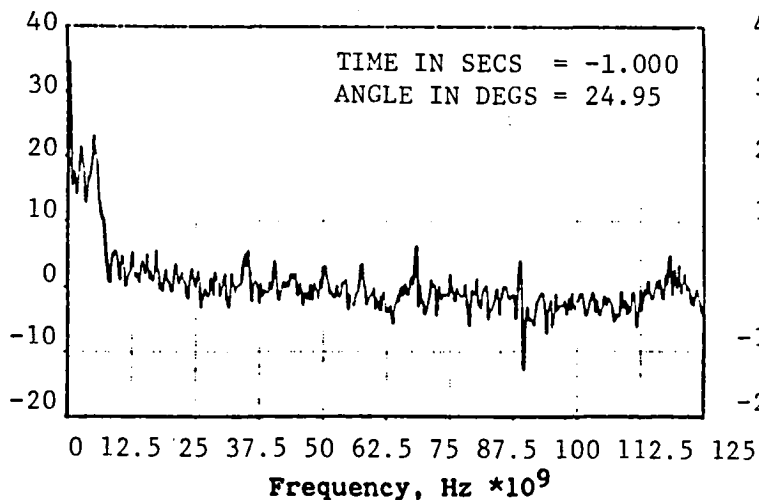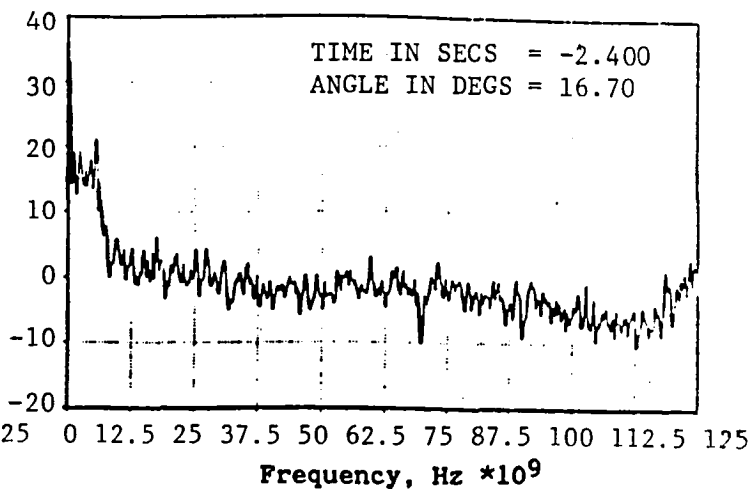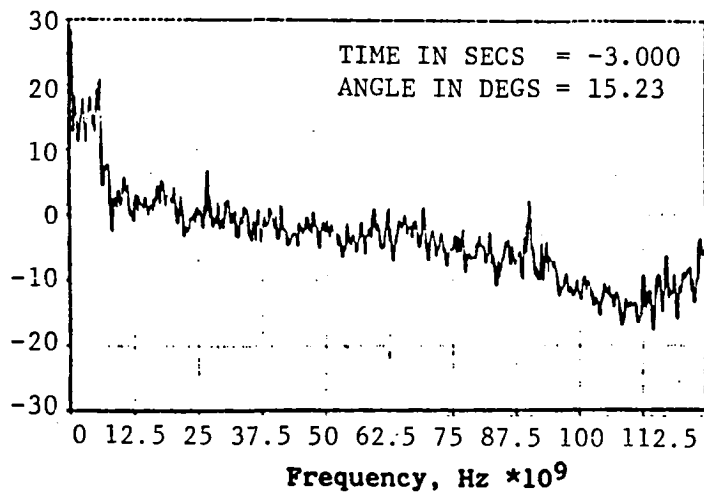
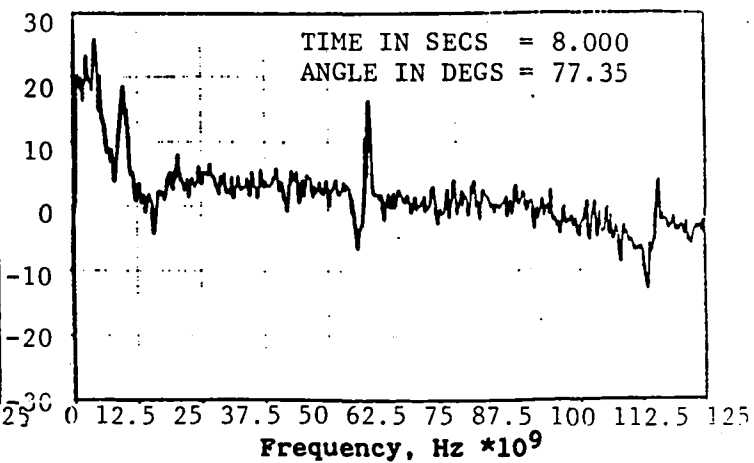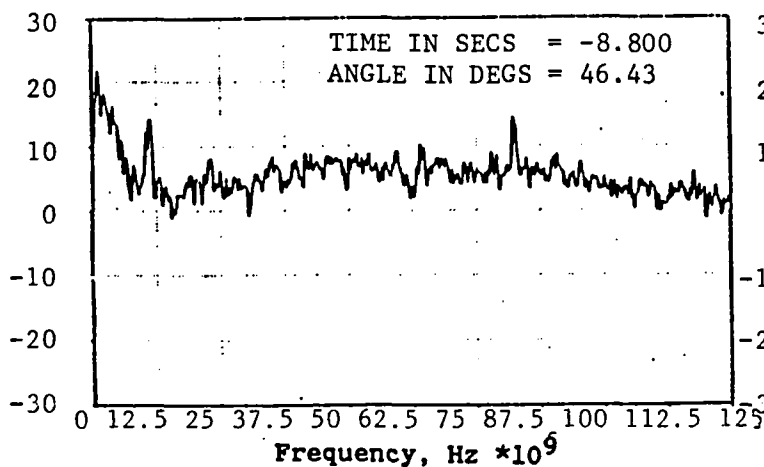Figure 5-8. Spectral Difference Time History for Run GE.1.07
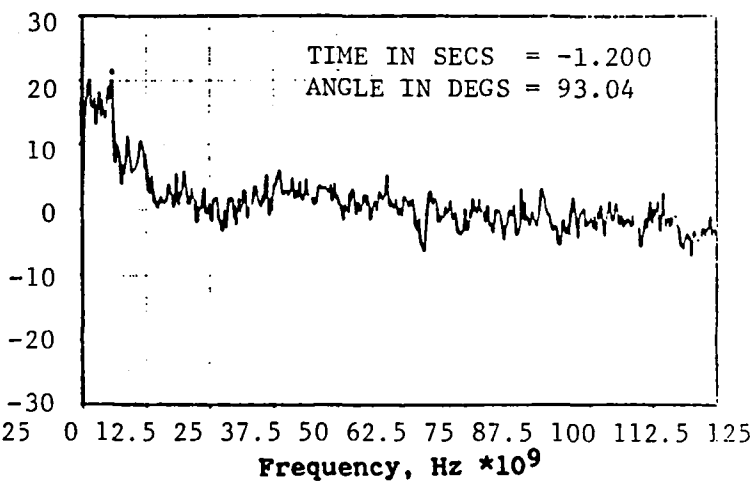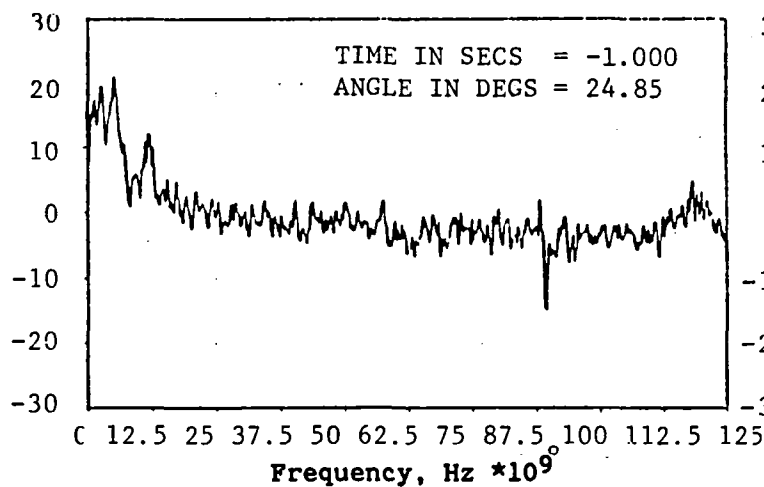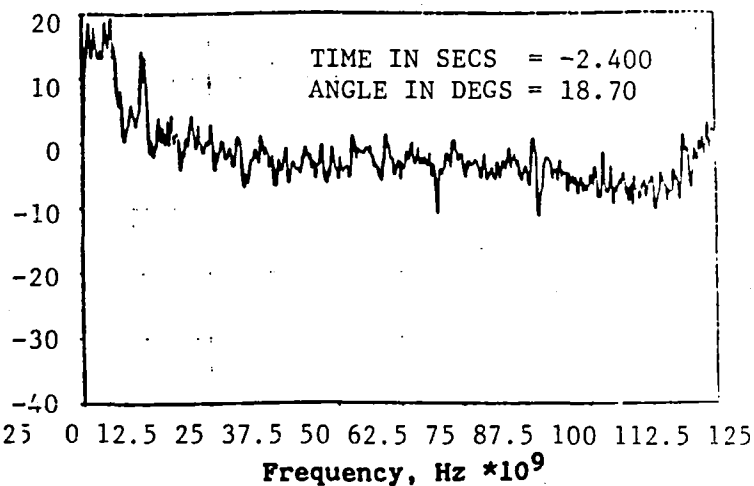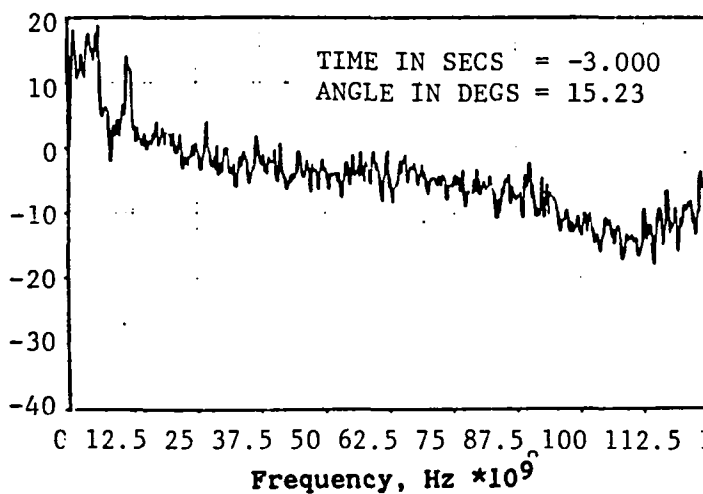Projected to Flight 1471

75

Figure 5-9. Spectral Difference Time History for Run GE.3.07
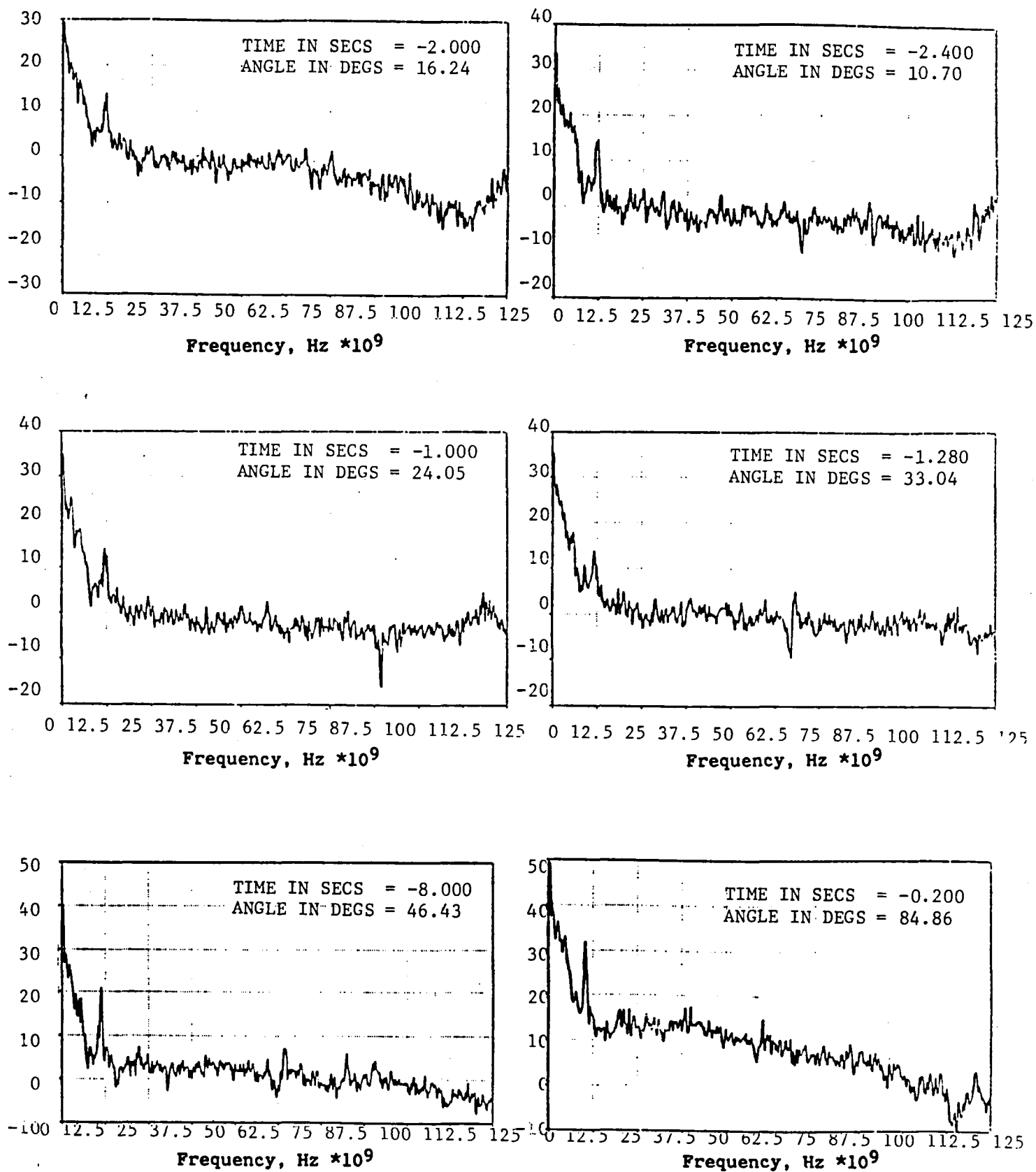Projected to Flight 1471

Figure 5-10. Spectral Difference Time History for Run GE.8.16
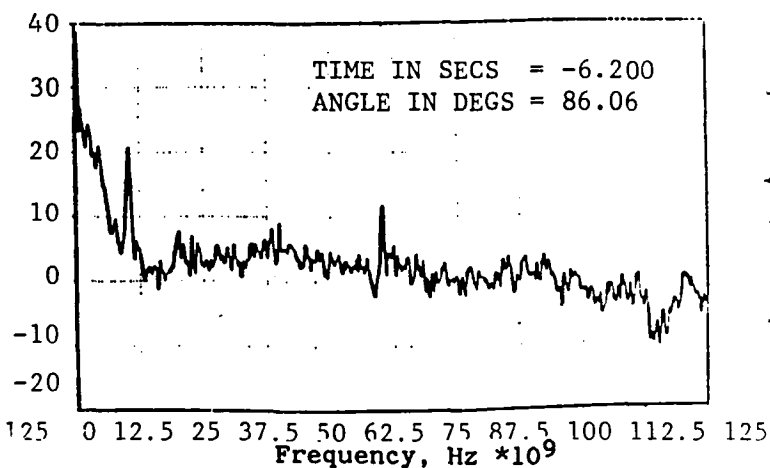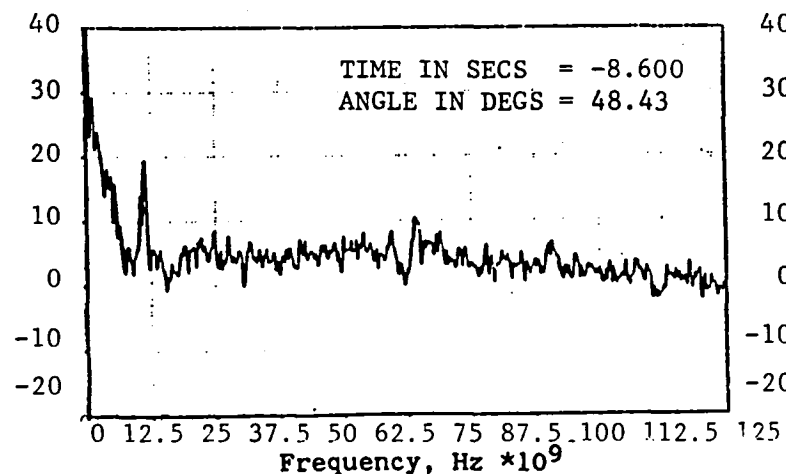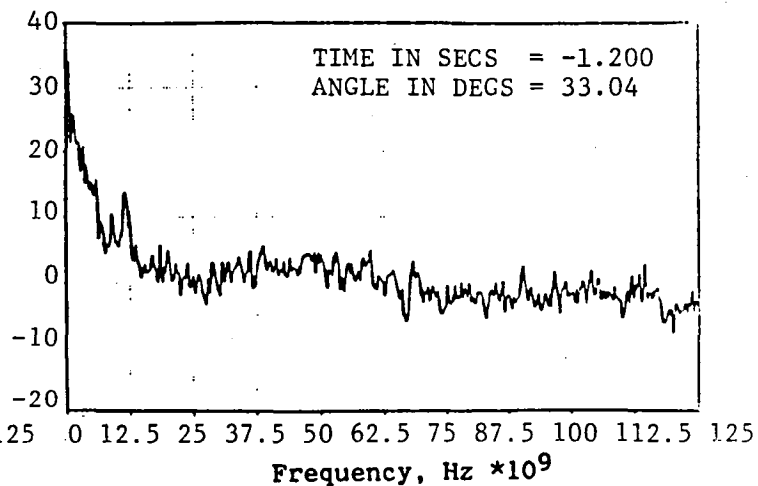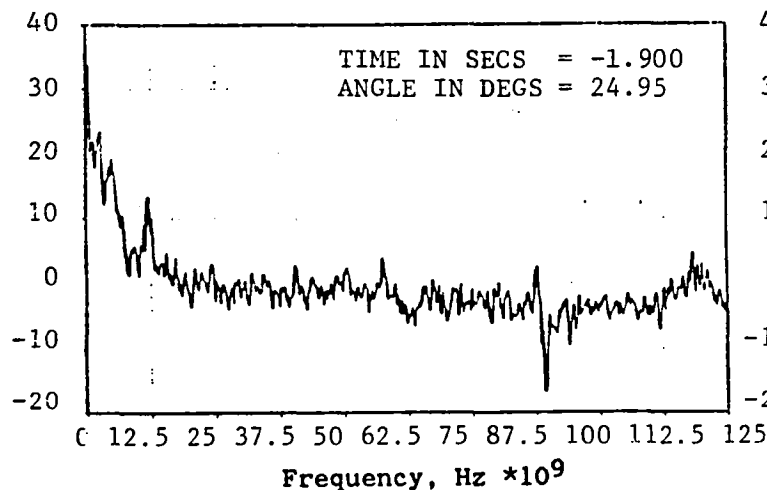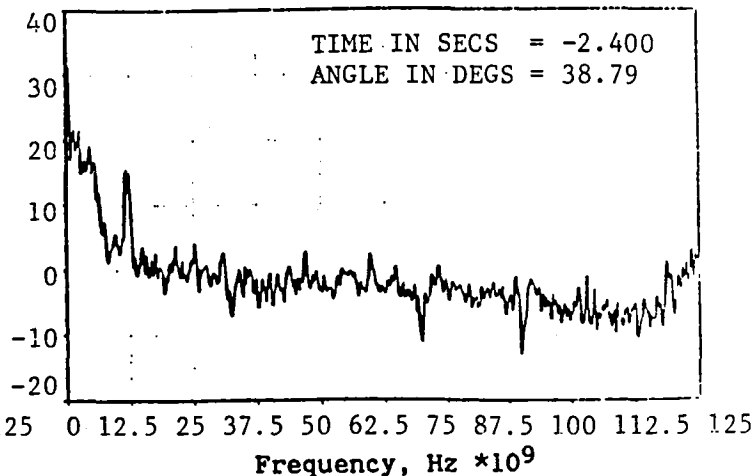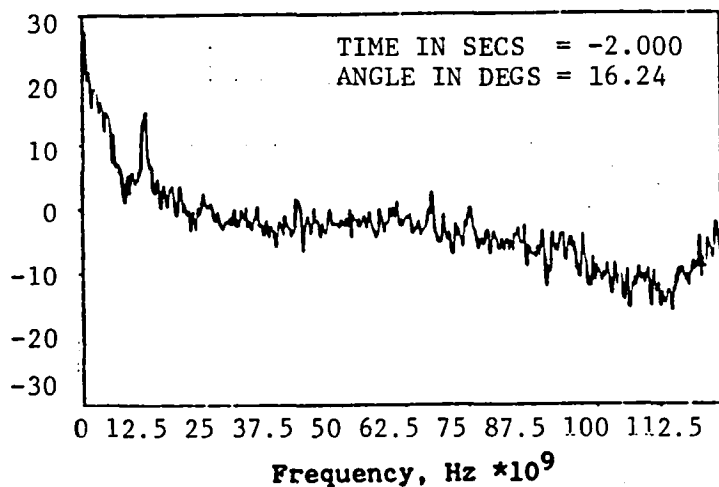Projected to Flight 1471

Figure 5-11. Spectral Difference Time History for Run LRC 7.0 /
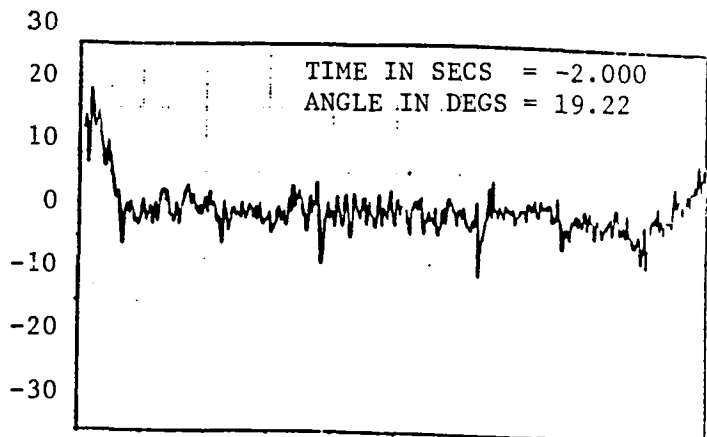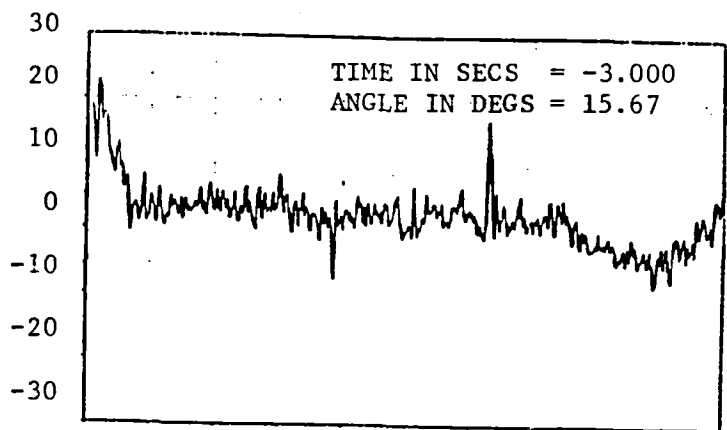Projected to Flight 1471

Figures 5-12 through 5-14. The comparisons generally indicate a much stronger MPT contribution to the projected flight data compared to the actual flight data. This is especially true for the wind tunnel data. Conversely, the flight BPF is much broader in flight and contains a significantly larger amount of acoustic energy. In many cases near overhead the flight BPF exceeds the projection by more than 10 dB, whereas the projected MPT's are 10 dB greater than the flight data.

5.2   ONE-THIRD OCTAVE BAND DATA ANALYSIS

One-third octave results for times of 3.0, 2.0, 1.0, and 0.0 seconds prior to the time the aircraft is overhead for Langley Flights 1461, 1471, and 1481 are compared to the flight projected values in Tables 5-1 through 5-3. The results quantify in one-third form the spectral differences indicated in the previous subsections. Principally, the broadband energy differences at subsonic and transonic fan tip speeds lead to projected levels which are higher than the flight measured data. In the supersonic case, Table 5-3, the MPT differences lead to much higher flight projected values than flight measured at frequencies below the fan BPF; however, the one-third octave band containing the BPF is higher in the flight case as was also indicated in narrowband results of Subsection 5.1.

Comparative plots of the PNLT directivities for each flight case are presented in Figures 5-15 to 5-17. Then PNLT directivities mirror the broadband discrepancies observed in Subsection 5.1. The flight projected levels are on the order of 2 to 3 dB high at subsonic and transonic conditions and as much as 6 dB high at the supersonic speed point due to MPT differences. The differences in PNLT are translated into the EPNL differences computed in Table 5-4 where a forward quadrant EPNL calculation was accomplished for each test projection.
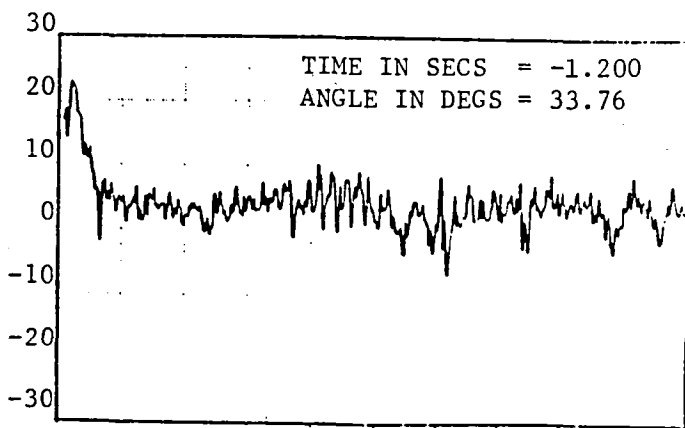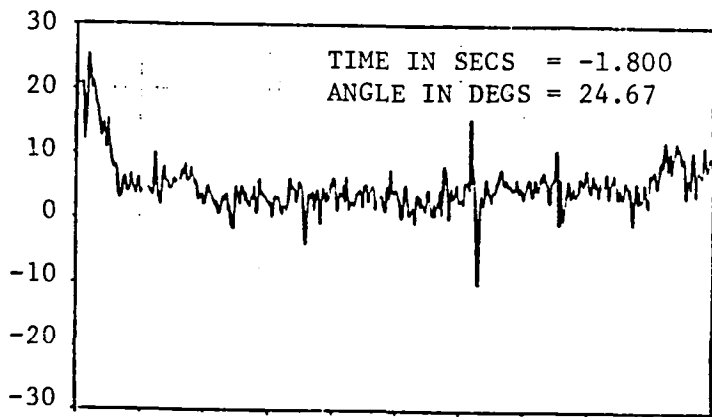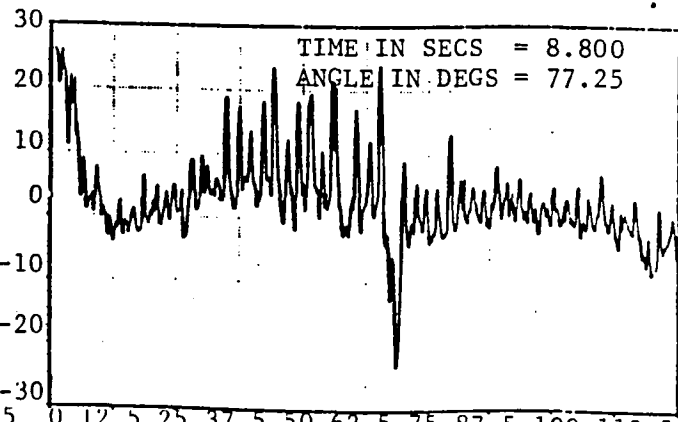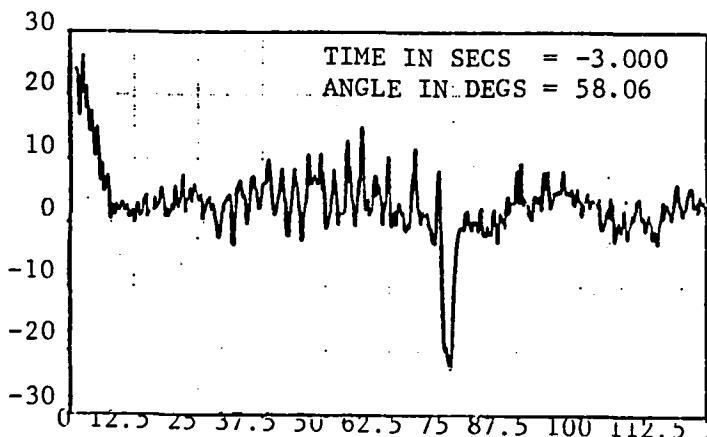
Figure 5-12. Spectral Difference Time History for Run GE.1.03
Projected to Flight 1461
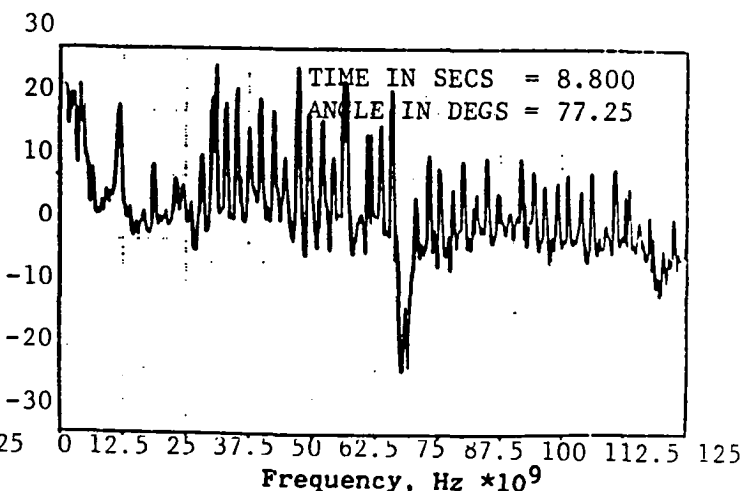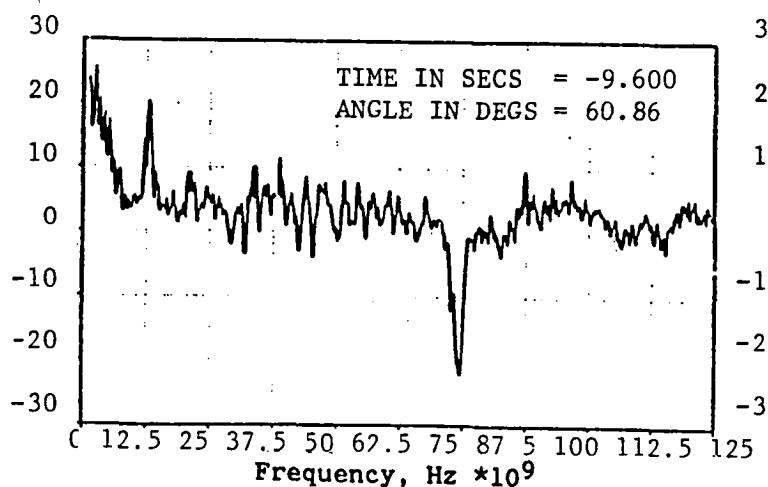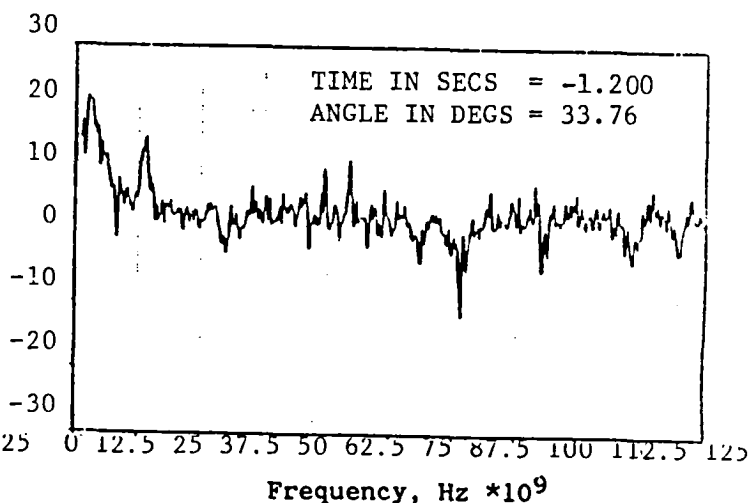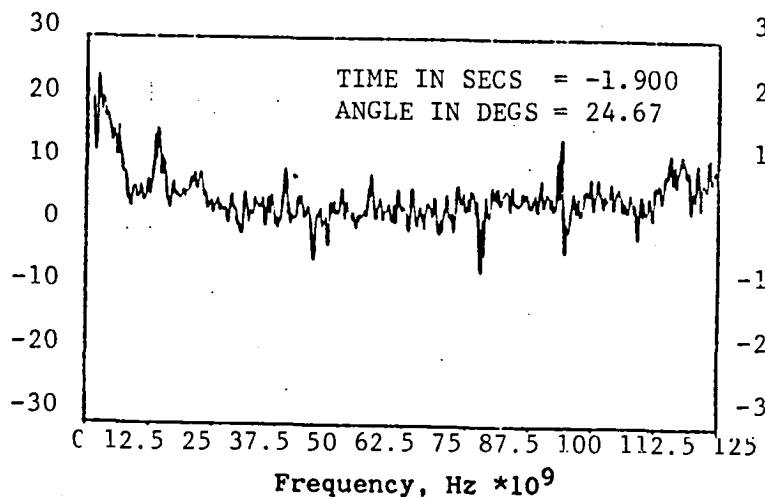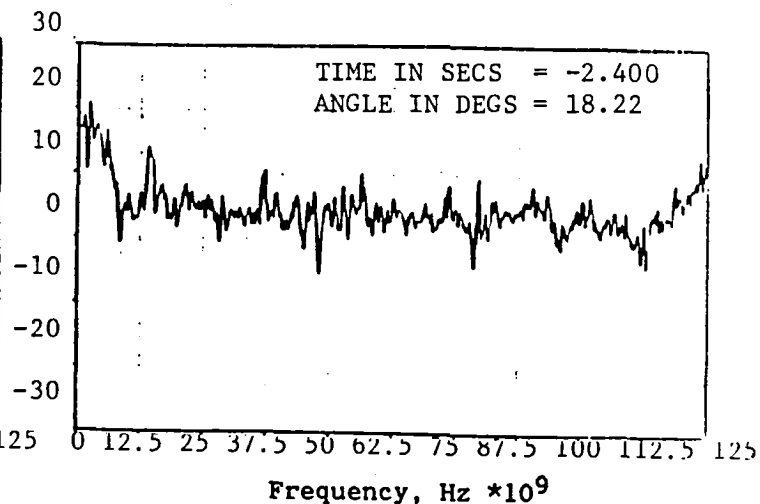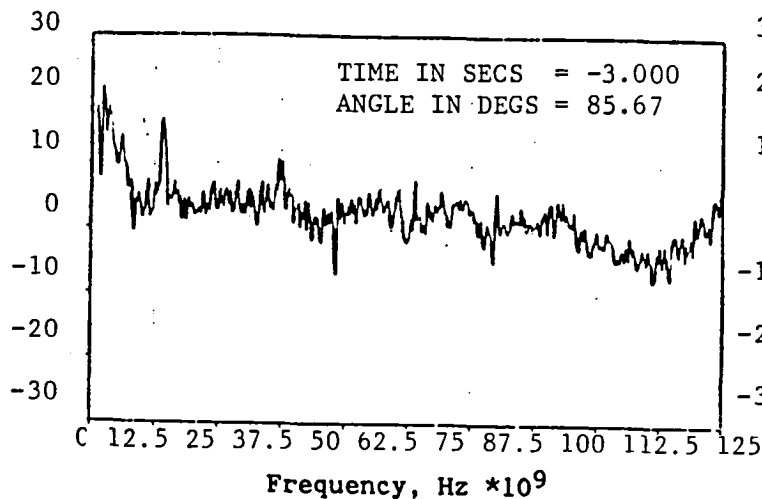
Figure 5-13. Spectral Difference Time History for Run GE.3.03
Projected to Flight 1461

81
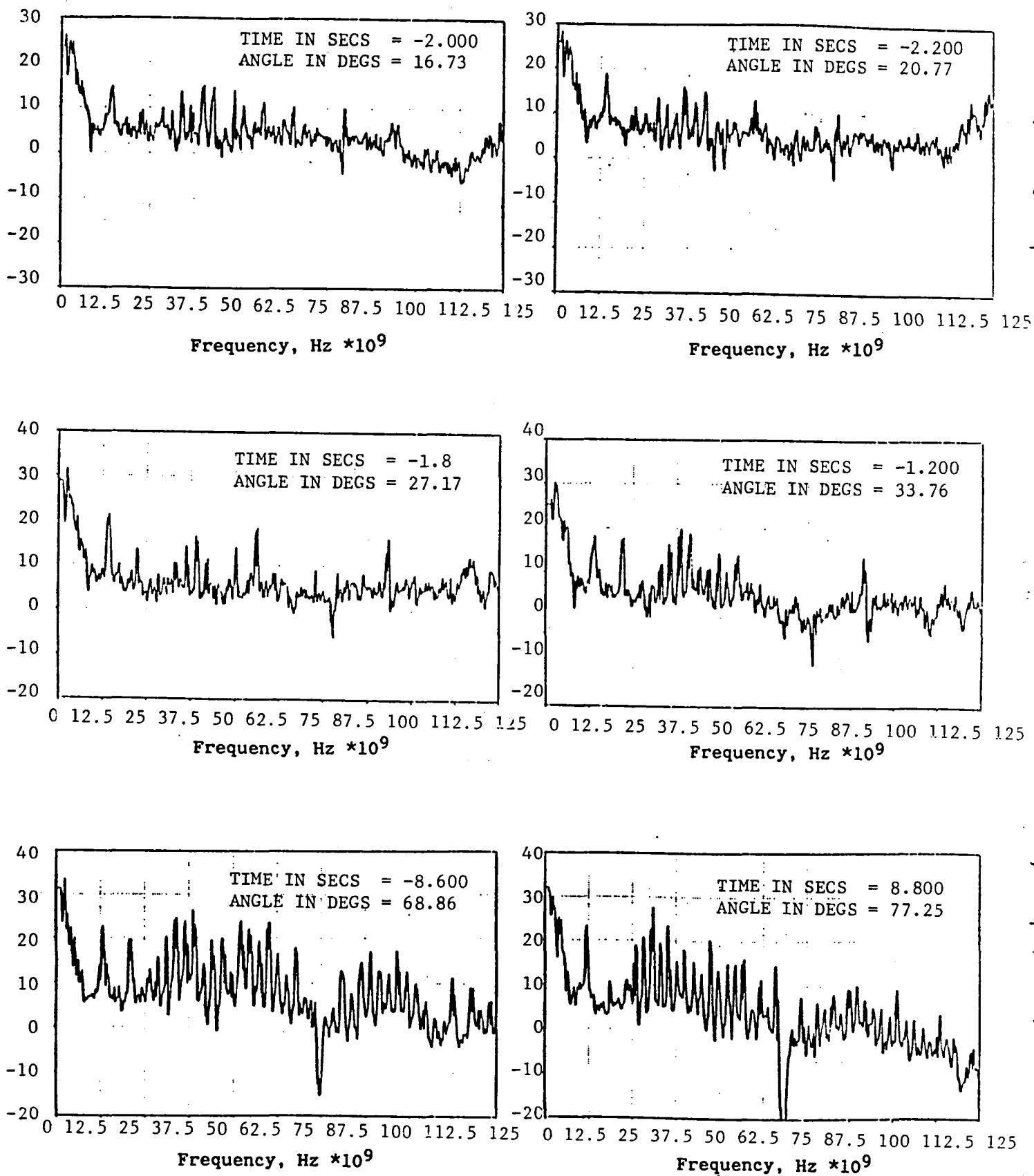
Figure 5-14.   Spectral Difference Time History for Run GE.ε.10
Projected to Flight 1461.

TABLE 5-1

SUPERSONIC ONE-THIRD OCTAVE RESULTS

JT15D FLIGHT TEST/FLT 1461

TIME IN SECONDS = -3.0

THIRD OCTAVE OUTPUT PAGE

| BAND NO.	CENTER FREQ	LEVEL DB	GE 1.03 LEVEL DB	GE 3.03 LEVEL DB	GE 8.10 LEVEL DB
17	50.00	35.6	35.6	35.6	35.6
18	63.00	36.0	36.0	36.0	36.0
19	80.00	36.1	36.1	36.1	36.1
20	100.00	31.4	31.4		
21	125.00	33.0	33.0	33.0	33.0
22	160.00	40.4	40.4	40.4	40.4
23	200.00	40.8	40.8	40.8	40.8
24	250.00	34.7	34.7	34.7	34.7
25	315.00	39.6	39.6	39.6	39.6
26	400.00	40.9	40.9	40.9	40.9
27	500.00	46.5	46.5	46.5	46.5
28	630.00	47.4	47.4	47.4	47.4
29	800.00	56.2	56.2	56.2	56.2
30	1000.00	57.9	57.9	57.9	57.9
31	1250.00	59.3	58.2	68.5	59.3
32	1600.00	60.1	59.7	67.5	68.5
33	2000.00	60.4	61.2	60.6	62.5
34	2500.00	60.0	60.5	61.3	63.1
35	3150.00	59.4	59.5	61.1	63.6
36	4000.00	60.4	62.4	64.1	69.0
37	5000.00	59.0	58.4	58.9	69.0
38	6300.00	55.1	55.8	56.6	58.9
39	8000.00	50.3	55.7	50.3	52.6
40	10000.00	44.8	41.4	41.6	42.1
	OASPL =	75.1	75.6	75.6	73.1
	PNL =	88.5	88.9	88.6	87.5
	PNLT =	89.1	89.3	89.1	89.6

TABLE 5-1 (Continued)

SUPERSONIC ONE-THIRD OCTAVE RESULTS

JT15D NASA LARC OV-1 TEST/FLT 1461

TIME IN SECONDS = -2.0

	THIRD OCTAVE OUTPUT PAGE		GE 1.03	GE 3.03	GE 8.10
BAND NO.	CENTER FREQ	LEVEL DB	LEVEL DB	LEVEL DB	LEVEL DB
17	50.00	35.7	35.7	35.7	35.7
18	63.00	36.3	36.3	36.3	36.3
19	80.00	36.8	36.8	36.8	36.8
20	100.00	33.1	33.1	33.1	33.1
21	125.00	35.0	35.0	35.0	35.0
22	160.00	39.8	39.8	39.8	39.8
23	200.00	40.8	40.8	40.8	40.8
24	250.00	36.9	36.9	36.9	36.9
25	315.00	40.6	40.6	40.6	40.6
26	400.00	42.4	42.4	42.4	42.4
27	500.00	47.9	47.9	47.9	47.9
28	630.00	50.5	50.5	50.5	50.5
29	800.00	58.4	58.4	58.4	58.4
30	1000.00	59.1	59.1	59.1	59.1
31	1250.00	62.1	61.7	69.2	62.1
32	1600.00	63.1	63.0	69.9	71.6
33	2000.00	63.2	65.5	65.3	67.3
34	2500.00	64.4	65.8	66.1	67.6
35	3150.00	64.9	65.5	65.0	68.9
36	4000.00	64.7	67.5	68.5	73.1
37	5000.00	64.6	65.9	65.1	68.1
38	6300.00	62.7	63.3	63.6	65.7
39	8000.00	60.1	64.2	62.2	60.2
40	10000.00	52.3	53.9	53.9	52.7
	OASPL =	72.1	70.7	70.8	77.7
	PNL =	85.1	83.9	84.0	92.0
	PNLT =	85.7	84.5	84.7	93.5

TABLE 5-1 (Continued)

SUPERSONIC ONE-THIRD OCTAVE RESULTS

JT15D NASA LARC OV-1 TEST/FLT 1461

TIME IN SECONDS = -1.0

THIRD OCTAVE OUTPUT PAGE			GE 1.03	GE 3.03	GE 8.10
BAND NO.	CENTER FREQ	LEVEL DB	LEVEL DB	LEVEL DB	LEVEL DB
17	50.00	37.1	37.1	37.1	37.1
18	63.00	37.1	37.1	37.1	37.1
19	80.00	36.7	36.7	36.7	36.7
20	100.00	34.0	34.0	34.0	34.0
21	125.00	35.6	35.6	35.6	35.6
22	160.00	40.5	40.5	40.5	40.5
23	200.00	41.2	41.2	41.2	41.2
24	250.00	37.8	37.8	37.8	37.8
25	315.00	40.6	40.6	40.6	40.6
26	400.00	44.8	44.8	48.8	44.8
27	500.00	50.2	50.2	50.2	50.2
28	630.00	55.4	55.4	55.4	55.4
29	800.00	62.1	62.1	62.1	62.1
30	1000.00	63.2	63.2	63.2	63.2
31	1250.00	64.8	64.5	76.4	64.8
32	1600.00	66.1	66.5	69.9	73.8
33	2000.00	66.8	68.3	68.9	78.3
34	2500.00	67.8	69.3	70.1	73.5
35	3150.00	69.9	71.1	71.0	80.9
36	4000.00	69.1	72.4	72.4	82.9
37	5000.00	68.5	71.8	72.8	80.5
38	6300.00	68.0	70.1	69.7	73.3
39	8000.00	74.9	68.1	68.9	70.7
40	10000.00	62.8	63.3	63.8	63.7
	OASPL =	77.5	79.0	79.7	87.6
	PNL =	90.0	91.8	92.2	101.2
	PNLT =	90.7	92.5	92.8	103.2

TABLE 5-1 (Concluded)

SUPERSONIC ONE-THIRD OCTAVE RESULTS

JT15D-1 NASA LARC OV-1 TEST/FLT 1461

TIME IN SECONDS = 0.0

THIRD OCTAVE OUTPUT PAGE

BAND NO.	CENTER FREQ.	LEVEL DB	GE 1.03 LEVEL DB	GE 3.03 LEVEL DB	GE 8.10 LEVEL DB
17	50.00	35.8	35.8	35.8	35.8
18	63.00	37.0	37.0	37.0	37.0
19	80.00	37.9	37.9	37.9	37.9
20	100.00	35.6	35.6	35.6	35.6
21	125.00	36.9	36.9	36.9	36.9
22	160.00	40.6	40.6	40.6	40.6
23	200.00	42.3	42.3	42.3	42.3
24	250.00	42.4	42.4	42.4	42.4
25	315.00	48.2	48.2	48.2	48.2
26	400.00	49.7	49.7	49.7	49.7
27	500.00	57.2	57.2	57.2	57.2
28	630.00	60.3	60.3	60.3	60.3
29	800.00	64.7	64.7	64.7	64.7
30	1000.00	66.2	66.2	66.2	66.2
31	1250.00	69.1	68.2	73.5	69.1
32	1600.00	70.4	68.6	72.2	74.6
33	2000.00	70.1	71.1	75.5	76.3
34	2500.00	69.9	71.8	75.1	81.6
35	3150.00	70.1	78.3	86.0	85.9
36	4000.00	69.3	80.8	80.6	78.9
37	5000.00	71.2	83.9	85.0	79.8
38	6300.00	83.7	84.3	85.1	78.2
39	8000.00	70.3	72.1	75.6	71.9
40	10000.00	66.8	67.8	70.5	67.3
	OASPL =	77.5	79.0	79.7	89.8
	PNL =	90.0	91.8	92.2	103.8
	PNLT =	90.7	92.5	92.8	105.7

TABLE 5-2

TRANSONIC ONE-THIRD OCTAVE RESULTS

JT15D-1 NASA LARC OV-1 TEST/FLT 1471

TIME IN SECONDS = -2.8

THIRD OCTAVE OUTPUT PAGE			GE 1.07	GE 3.07	GE 8.16	LRC 7.07
BAND NO.	CENTER FREQ.	LEVEL DB	LEVEL DB	LEVEL DB	LEVEL DB	LEVEL DB
17	50.00	35.0	35.0	35.0	35.0	35.0
18	63.00	35.5	35.5	35.5	35.5	35.5
19	80.00	35.8	35.8	35.8	35.8	35.8
20	100.00	35.1	35.1	35.1	35.1	35.1
21	125.00	36.9	36.9	36.9	36.9	36.9
22	160.00	39.2	39.2	39.2	39.2	39.2
23	200.00	40.0	40.0	40.0	40.0	40.0
24	250.00	40.4	40.4	40.4	40.4	40.4
25	315.00	42.0	42.0	42.0	42.0	42.0
26	400.00	42.6	42.6	42.6	42.6	42.6
27	500.00	46.2	46.2	46.2	46.2	46.2
28	630.00	50.2	50.2	50.2	50.2	50.2
29	800.00	56.8	56.8	56.8	56.8	56.8
30	1000.00	58.1	58.1	58.1	58.1	58.1
31	1250.00	60.8	59.2	61.9	64.5	64.5
32	1600.00	62.8	62.3	62.4	61.5	61.1
33	2000.00	65.6	63.4	62.8	61.9	62.6
34	2500.00	67.1	64.1	63.3	65.0	64.4
35	3150.00	66.9	65.3	62.4	64.8	63.7
36	4000.00	67.4	64.3	63.6	65.2	63.9
37	5000.00	65.0	61.7	60.3	62.7	62.2
38	6300.00	61.2	59.0	58.4	59.1	57.9
39	8000.00	57.2	52.8	52.2	52.7	52.0
40	10000.00	55.5	45.3	43.5	45.7	44.2
	OASPL =	74.6	72.5	71.7	72.9	72.4
	PNL =	88.0	85.8	84.7	86.0	85.1
	PNLT =	88.9	86.7	85.6	87.5	86.7

TABLE 5-2 (Continued)

TRANSONIC ONE-THIRD OCTAVE RESULTS

JT15D-1 NASA LARC OV-1 TEST/FLT 1471

TIME IN SECONDS = -2.0

THIRD OCTAVE OUTPUT PAGE			GE 1.07	GE 3.07	GE 8.16	LRC 7.07
BAND NO.	CENTER FREQ.	LEVEL DB	LEVEL DB	LEVEL DB	LEVEL DB	LEVEL DB
17	50.00	33.4	33.4	33.4	33.4	33.4
18	63.00	34.4	34.4	34.4	34.4	34.4
19	80.00	35.3	35.3	35.3	35.3	35.3
20	100.00	36.0	36.0	36.0	36.0	36.0
21	125.00	37.7	37.7	37.7	37.7	37.7
22	160.00	40.7	40.7	40.7	40.7	40.7
23	200.00	40.9	40.9	40.9	40.9	40.9
24	250.00	40.8	40.8	40.8	40.8	40.8
25	315.00	43.0	43.0	43.0	43.0	43.0
26	400.00	44.9	44.9	44.9	44.9	44.9
27	500.00	48.6	48.6	48.6	48.6	48.6
28	630.00	51.8	51.8	51.8	51.8	51.8
29	800.00	59.3	59.3	59.3	59.3	59.3
30	1000.00	61.7	61.7	61.7	61.7	61.7
31	1250.00	63.3	61.9	66.2	71.2	68.7
32	1600.00	66.8	66.0	64.9	64.2	64.1
33	2000.00	67.7	67.7	65.9	65.2	65.2
34	2500.00	70.7	68.0	66.9	67.7	67.3
35	3150.00	70.6	68.7	67.2	67.6	67.1
36	4000.00	71.6	68.8	67.7	66.8	67.6
37	5000.00	69.9	66.7	65.2	66.0	66.9
38	6300.00	68.4	66.7	63.2	63.8	64.2
39	8000.00	63.8	61.3	60.4	60.0	59.8
40	10000.00	62.0	55.3	53.7	53.6	52.9
	OASPL =	78.7	76.7	75.6	76.6	76.1
	PNL =	92.1	89.8	88.8	89.0	88.9
	PNLT =	92.9	90.6	89.6	91.7	90.8

TABLE 5-2 (Continued)

TRANSONIC ONE-THIRD OCTAVE RESULTS

JT15D-1 NASA LARC OV-1 TEST/FLT 1471

TIME IN SECONDS = -1.0

THIRD OCTAVE OUTPUT PAGE

BAND NO.	CENTER FREQ.	LEVEL DB	GE 1.07 LEVEL DB	GE 3.07 LEVEL DB	GE 8.16 LEVEL DB	LRC 7.07 LEVEL DB
17	50.00	36.6	36.6	36.6	36.6	36.6
18	63.00	37.5	37.5	37.5	37.5	37.5
19	80.00	38.2	38.2	38.2	38.2	38.2
20	100.00	38.0	38.0	38.0	38.0	38.0
21	125.00	38.9	38.9	38.9	38.9	38.9
22	160.00	41.6	41.6	41.6	41.6	41.6
23	200.00	43.1	43.1	43.1	43.1	43.1
24	250.00	40.4	40.4	40.4	40.4	40.4
25	315.00	43.4	43.4	43.4	43.4	43.4
26	400.00	44.9	44.9	44.9	44.9	44.9
27	500.00	49.6	49.6	49.6	49.6	49.6
28	630.00	53.0	53.0	53.0	53.0	53.0
29	800.00	61.8	61.8	61.8	61.8	61.8
30	1000.00	63.9	63.9	63.9	63.9	63.9
31	1250.00	66.8	65.7	66.8	69.4	68.0
32	1600.00	67.7	68.5	66.8	67.6	69.5
33	2000.00	68.6	70.4	68.8	68.4	71.7
34	2500.00	71.2	72.6	71.3	71.2	71.7
35	3150.00	70.5	73.6	71.9	70.7	71.7
36	4000.00	69.7	74.7	72.7	70.3	71.9
37	5000.00	69.4	73.3	72.0	68.9	69.8
38	6300.00	69.9	74.2	70.3	68.5	67.2
39	8000.00	68.5	70.2	67.9	66.0	64.7
40	10000.00	67.2	66.5	65.3	63.8	64.7
	OASPL =	79.4	82.0	80.2	79.2	80.3
	PNL =	92.3	95.4	93.6	92.2	93.2
	PNLT =	93.0	96.1	94.3	93.4	94.3

TABLE 5-2 (Concluded)

TRANSONIC ONE-THIRD OCTAVE RESULTS

JT15D-1 NASA LARC OV-1 TEST/FLT 1471

TIME IN SECONDS = 0.0

THIRD OCTAVE OUTPUT PAGE			GE 1.07	GE 3.07	GE 8.16	LRC 7.07
BAND NO.	CENTER FREQ.	LEVEL DB	LEVEL DB	LEVEL DB	LEVEL DB	LEVEL DB
17	50.00	33.6	33.6	33.6	33.6	33.6
18	63.00	34.8	34.8	34.8	34.8	34.8
19	80.00	36.0	36.0	36.0	36.0	36.0
20	100.00	37.9	37.9	37.9	37.9	37.9
21	125.00	38.7	38.7	38.7	38.7	38.7
22	160.00	40.5	40.5	40.5	40.5	40.5
23	200.00	41.2	41.2	41.2	41.2	41.2
24	250.00	40.6	40.6	40.6	40.6	40.6
25	315.00	44.5	44.5	44.5	44.5	44.5
26	400.00	47.8	47.8	47.8	47.8	47.8
27	500.00	52.0	52.0	52.0	52.0	52.0
28	630.00	56.3	56.3	56.3	56.3	56.3
29	800.00	61.5	61.5	61.5	61.5	61.5
30	1000.00	66.1	66.1	66.1	66.1	66.1
31	1250.00	67.7	66.8	67.8	69.9	68.9
32	1600.00	69.4	68.4	68.8	70.6	69.2
33	2000.00	68.6	70.9	71.9	73.1	71.7
34	2500.00	67.7	72.4	71.3	72.1	70.3
35	3150.00	68.5	73.0	71.3	71.6	70.0
36	4000.00	68.0	73.0	71.3	70.6	68.9
37	5000.00	68.8	73.2	71.1	69.5	67.9
38	6300.00	69.7	73.5	74.0	67.6	67.4
39	8000.00	68.9	72.4	70.1	64.9	65.8
40	10000.00	70.4	70.2	68.2	60.6	63.6
	OASPL =	79.2	82.0	81.2	80.4	79.2
	PNL =	91.2	94.7	93.8	93.0	91.8
	PNLT =	91.6	95.1	94.2	93.4	92.3

TABLE 5-3

SUBSONIC ONE-THIRD OCTAVE RESULTS

NASA OV-1 @WALLOPS/FLT 1481

TIME IN SECONDS = -3.0

THIRD OCTAVE OUTPUT PAGE

BAND NO.	CENTER FREQ.	GE 1.11 LEVEL DB	GE 3.11 LEVEL DB	GE 8.22 LEVEL DB	LRC 7.08 LEVEL DB	LEVEL DB
17	50.00	35.3	35.3	35.3	35.3	35.3
18	63.00	36.0	36.0	36.0	36.0	36.0
19	80.00	36.5	36.5	36.5	36.5	36.5
20	100.00	34.9	34.9	34.9	34.9	34.9
21	125.00	34.6	34.6	34.6	34.6	34.6
22	160.00	39.0	39.0	39.0	39.0	39.0
23	200.00	39.7	39.7	39.7	39.7	39.7
24	250.00	37.5	37.5	37.5	37.5	37.5
25	315.00	37.5	37.5	37.5	37.5	37.5
26	400.00	39.0	39.0	39.0	39.0	39.0
27	500.00	43.7	43.7	43.7	43.7	43.7
28	630.00	47.4	47.4	47.4	47.4	47.4
29	800.00	53.9	53.9	53.9	53.9	53.9
30	1000.00	56.7	56.7	56.7	56.7	56.7
31	1250.00	59.8	57.4	58.1	58.8	58.4
32	1600.00	60.5	58.8	59.9	59.2	58.0
33	2000.00	63.3	62.4	62.7	61.2	62.1
34	2500.00	65.4	63.2	61.7	63.0	63.3
35	3150.00	64.3	62.9	63.4	63.6	62.4
36	4000.00	64.6	63.2	62.6	63.9	63.4
37	5000.00	61.1	60.7	59.9	61.2	61.1
38	6300.00	57.3	57.4	60.2	58.2	57.1
39	8000.00	52.3	51.9	52.4	52.2	51.1
40	10000.00	45.5	42.7	43.4	43.5	42.2
OASPL =		72.1	70.7	70.8	71.0	70.7
PNL =		85.1	83.9	84.0	84.4	83.9
PNLT =		85.7	84.5	84.7	85.0	84.5

TABLE 5-3 (Continued)

SUBSONIC ONE-THIRD OCTAVE RESULTS

NASA OV-1 @WALLOPS/FLT 1481

TIME IN SECONDS = -2.0

THIRD OCTAVE OUTPUT PAGE			GE 1.11	GE 3.11	GE 8.22	LRC 7.08
BAND NO.	CENTER FREQ.	LEVEL DB	LEVEL DB	LEVEL DB	LEVEL DB	LEVEL DB
17	50.00	33.9	33.9	33.9	33.9	33.9
18	63.00	34.6	34.6	34.6	34.6	34.6
19	80.00	35.2	35.2	35.2	35.2	35.2
20	100.00	34.9	34.9	34.9	34.9	34.9
21	125.00	36.2	36.2	36.2	36.2	36.2
22	160.00	39.5	39.5	39.5	39.5	39.5
23	200.00	39.2	39.2	39.2	39.2	39.2
24	250.00	37.0	37.0	37.0	37.0	37.0
25	315.00	38.8	38.8	38.8	38.8	38.8
26	400.00	40.3	40.3	40.3	40.3	40.3
27	500.00	45.4	45.4	45.4	45.4	45.4
28	630.00	50.9	50.9	50.9	50.9	50.9
29	800.00	57.2	57.2	57.2	57.2	57.2
30	1000.00	60.3	60.3	60.3	60.3	60.3
31	1250.00	62.5	61.0	61.6	62.1	61.8
32	1600.00	62.9	63.2	63.2	63.7	62.3
33	2000.00	65.3	66.6	66.9	65.9	65.5
34	2500.00	68.2	67.3	67.7	67.3	66.8
35	3150.00	67.6	68.2	67.7	69.0	68.1
36	4000.00	68.2	67.3	67.7	70.5	68.9
37	5000.00	63.7	66.8	66.5	66.8	66.5
38	6300.00	61.8	64.9	63.8	64.5	63.7
39	8000.00	58.7	59.8	60.2	59.9	59.8
40	10000.00	53.2	54.3	54.6	55.1	53.2
	OASPL =	75.1	75.6	75.6	76.4	75.5
	PNL =	88.5	88.9	88.6	90.2	89.1
	PNLT =	89.1	89.3	89.1	90.8	89.5

TABLE 5-3 (Continued)

SUBSONIC ONE-THIRD OCTAVE RESULTS

NASA OV-1 @WALLOPS/FLT 1481

TIME IN SECONDS = -1.0

THIRD OCTAVE OUTPUT PAGE			GE 1.11	GE 3.11	GE 8.22	LRC 7.08
BAND NO.	CENTER FREQ.	LEVEL DB	LEVEL DB	LEVEL DB	LEVEL DB	LEVEL DB
17	50.00	34.0	34.0	34.0	34.0	34.0
18	63.00	35.2	35.2	35.2	35.2	35.2
19	80.00	36.2	36.2	36.2	36.2	36.2
20	100.00	36.7	36.7	36.7	36.7	36.7
21	125.00	36.6	36.6	36.6	36.6	36.6
22	160.00	38.9	38.9	38.9	38.9	38.9
23	200.00	41.0	41.0	41.0	41.0	41.0
24	250.00	40.6	40.6	40.6	40.6	40.6
25	315.00	43.2	43.2	43.2	43.2	43.2
26	400.00	44.7	44.7	44.7	44.7	44.7
27	500.00	49.5	49.5	49.5	49.5	49.5
28	630.00	52.9	52.9	52.9	52.9	52.9
29	800.00	59.2	59.2	59.2	59.2	59.2
30	1000.00	62.0	62.0	62.0	62.0	62.0
31	1250.00	64.5	63.9	64.3	64.8	64.3
32	1600.00	65.8	67.3	66.3	66.9	66.6
33	2000.00	68.8	69.0	69.0	70.1	69.2
34	2500.00	71.5	70.9	70.3	71.3	70.9
35	3150.00	70.2	72.2	71.8	71.2	71.8
36	4000.00	69.4	73.5	73.6	70.1	69.4
37	5000.00	67.5	72.2	71.9	69.6	68.2
38	6300.00	66.6	71.0	70.9	68.8	68.2
39	8000.00	65.9	68.8	71.0	67.2	67.4
40	10000.00	63.4	65.8	65.6	64.2	64.3
	OASPL =	78.2	80.4	80.4	79.2	78.8
	PNL =	91.4	93.9	93.9	92.3	92.3
	PNLT =	92.0	94.5	94.5	92.9	92.9

TABLE 5-3 (Concluded)

SUBSONIC ONE-THIRD OCTAVE RESULTS

NASA OV-1 @WALLOPS/FLT 1481

TIME IN SECONDS = -0.0

THIRD OCTAVE OUTPUT PAGE			GE 1.11	GE 3.11	GE 8.22	LRC 7.08
BAND NO.	CENTER FREQ.	LEVEL DB	LEVEL DB	LEVEL DB	LEVEL DB	LEVEL DB
17	50.00	35.7	35.7	35.7	35.7	35.7
18	63.00	36.2	36.2	36.2	36.2	36.2
19	80.00	36.5	36.5	36.5	36.5	36.5
20	100.00	35.6	35.6	35.6	35.6	35.6
21	125.00	37.0	37.0	37.0	37.0	37.0
22	160.00	39.7	39.7	39.7	39.7	39.7
23	200.00	40.7	40.7	40.7	40.7	40.7
24	250.00	41.3	41.3	41.3	41.3	41.3
25	315.00	44.4	44.4	44.4	44.4	44.4
26	400.00	48.2	48.2	48.2	48.2	48.2
27	500.00	51.5	51.5	51.5	51.5	51.5
28	630.00	57.9	57.9	57.9	57.9	57.9
29	800.00	60.3	60.3	60.3	60.3	60.3
30	1000.00	64.6	64.6	64.6	64.6	64.6
31	1250.00	64.6	64.6	64.6	64.6	64.6
32	1600.00	67.1	66.7	68.3	67.0	67.8
33	2000.00	67.9	68.5	68.9	68.4	67.1
34	2500.00	68.0	70.0	70.3	68.1	67.5
35	3150.00	67.6	69.9	69.7	66.4	65.8
36	4000.00	66.8	69.4	69.9	65.5	64.7
37	5000.00	66.4	69.4	70.2	65.4	64.6
38	6300.00	65.4	70.0	70.7	62.7	62.4
39	8000.00	66.2	68.7	70.0	61.7	61.7
40	10000.00	67.6	67.3	68.8	57.9	59.3
	OASPL =	77.5	79.0	79.7	76.2	75.9
	PNL =	90.0	91.8	92.2	89.0	88.6
	PNLT =	90.7	92.7	92.8	89.6	89.2
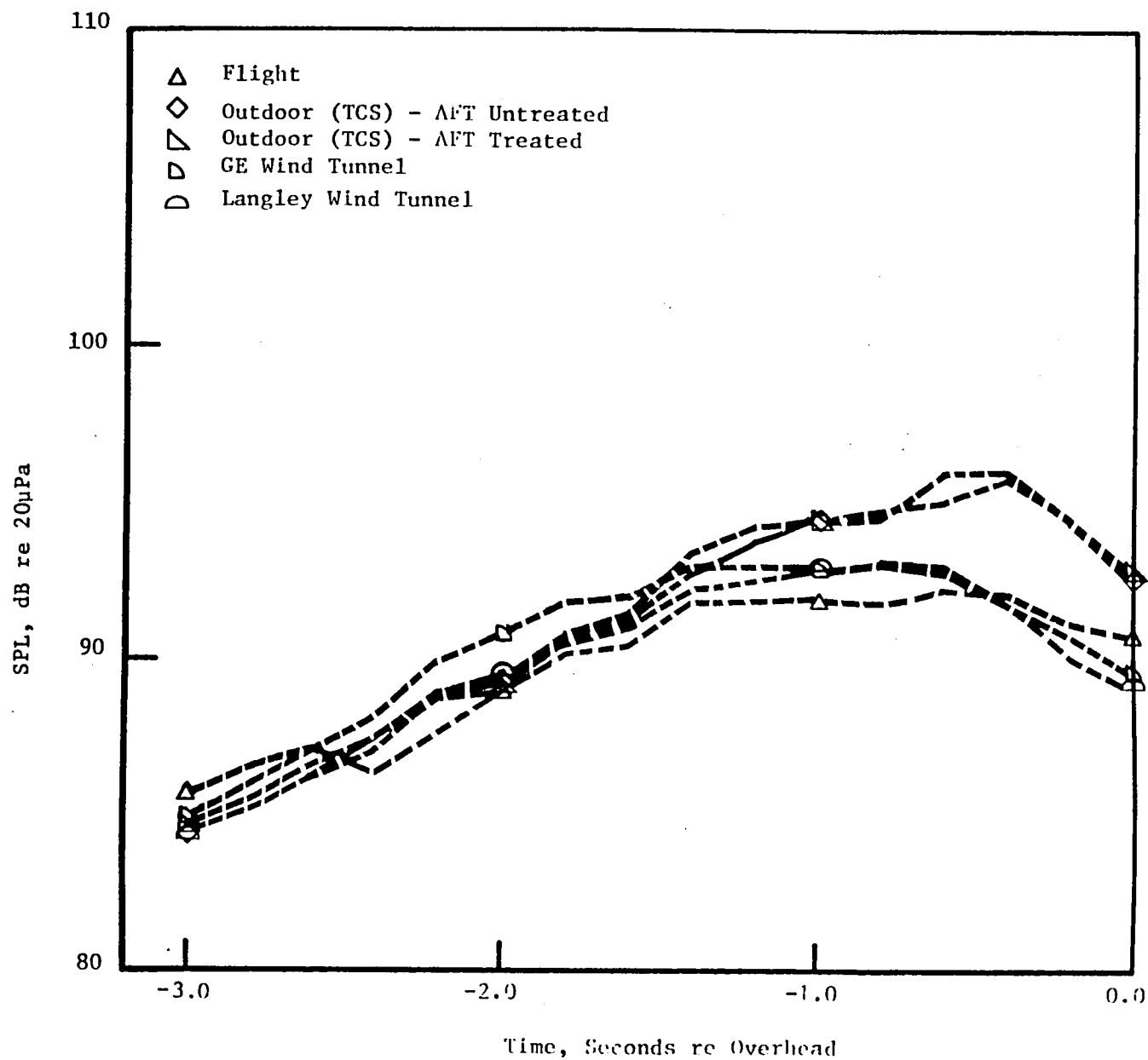
Figure 5-15. PNLT Time Histories of Flight and Flight Projected Results (Engine Speed = 10,500 RPM).
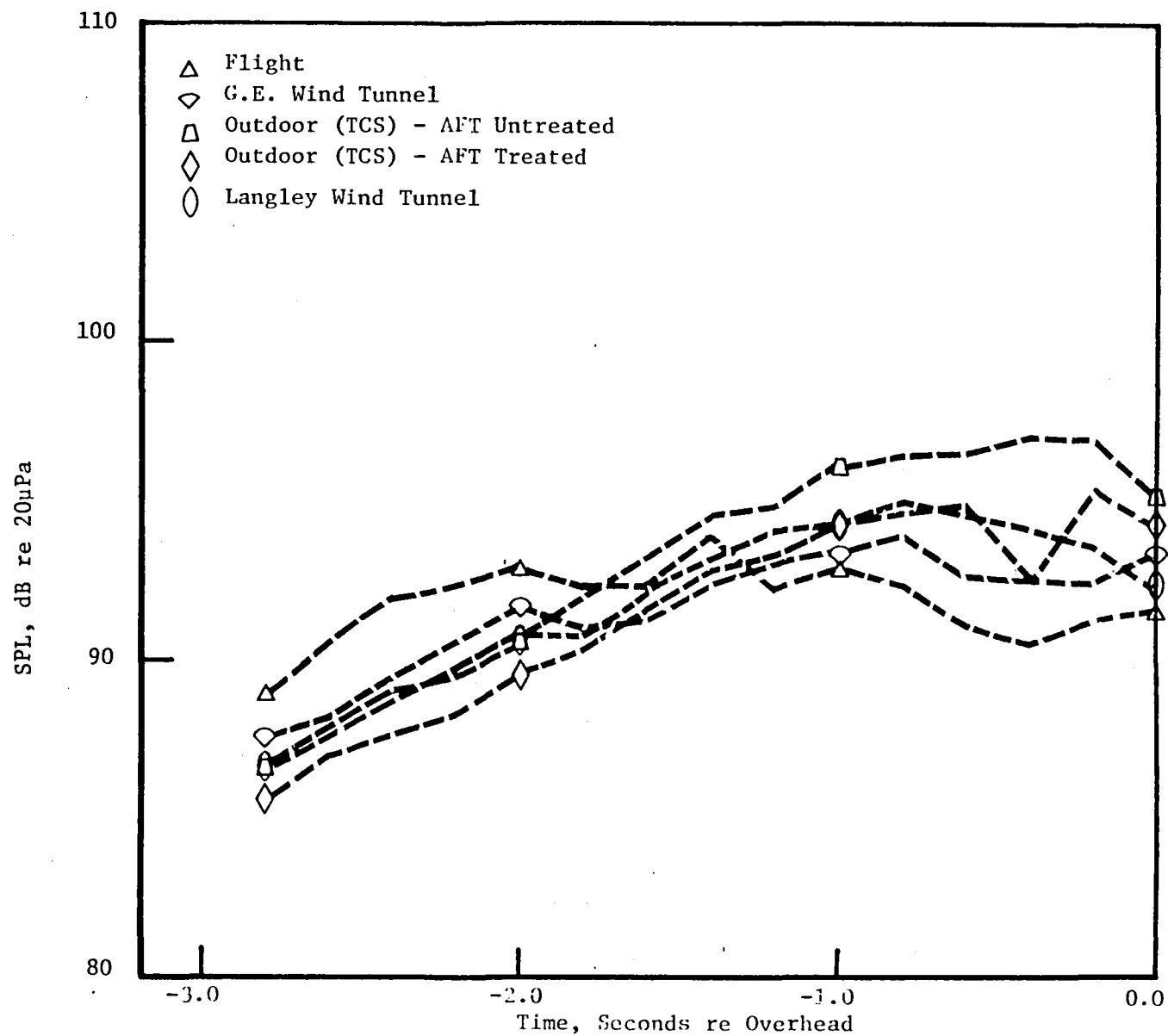
Figure 5-16. PNLT Time Histories of Flight and Flight Projected Results (Engine Speed ≈ 11,800 RPM).
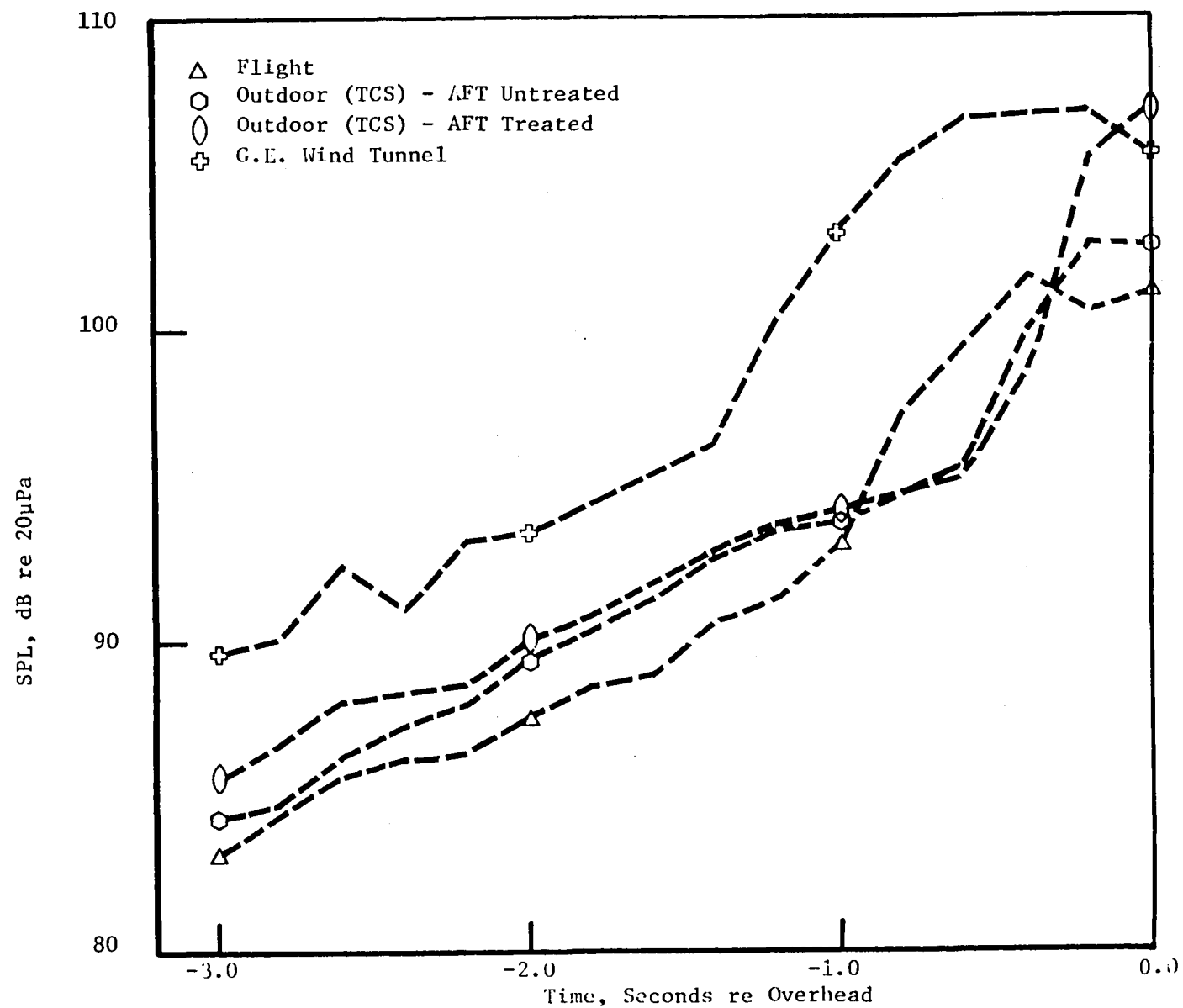
Figure 5-17. PNLT Time Histories of Flight and Flight Projected Results
(Engine Speed ≈ 13,500 RPM).

TABLE 5-4

EPNL PROJECTED

	Approximate Engine Speed		
	10,500	11,800	13,500
Flight	102.4	103.8	108.0
OD/TCS (Treated Aft)	104.1	104.2	110.6
OD/TCS (Untreated Aft)	104.6	106.0	108.4
GE Wind Tunnel	104.1	103.7	113.7
Langley Wind Tunnel	102.2	104.3	—

5.3   TONAL COMPARISONS

The time histories of the BPF tone, compressor tone, and twice BPF tone are compared between flight-measured and flight-projected from simulated flight test data in this subsection. The results for the simulated flight non-supersonic tip speed BPF situation display considerable variability in pattern shape but relative agreement in level. The subsonic and transonic tip speed flight results (Figures 5-18 and 5-21) are somewhat different than the modal type patterns observed for the projections. This tendency suggests that refractive effects may cause smoothing of the directivities of those acoustic sources contributing to the flight measurement. At supersonic tip speeds, Figures 5-24(a-c) and 5-25, the pattern shapes between flight and flight projected results are in better agreement since the patterns in both situations contain a broad hump of concentrated acoustic energy rather than many smaller humps of acoustic energy at the lower engine speed points.

Specific comparisons suggest that similar projected time histories patterns exist for Figures 5-18(b) and 5-18(d). These figures compare the flight BPF to projected BPF at 10,500 RPM, hence indicating relatively good agreement between two different simulated flight results. A similar situation exists for Figures 5-19(a) and 5-19(b) where compressor tones for outdoor situations with and without a treated aft region indicate excellent agreement. The agreement between simulated flight results in these situations is better than the agreement with the actual flight measured data.

Figure 5-20 displays a comparison of the twice BPF projected from outdoor TCS test versus the flight measured result pattern and level similarity is achieved. In the transonic tip speed case, Figure series 5-21 and 5-22, the fine structure of the projected results is not matched; however, satisfactory overall agreement is achieved. This overall relative agreement is demonstrated in Figure 5-23 where the outdoor TCS BPF time history is compared to 0.2 second narrowband flight results (as measured in Section 5.1). It is noted from this figure that good overall agreement is achieved.

Figure 5-24(a) yields very good tone pattern agreement between the untreated aft outdoor TCS projected results and flight measurement. It is noted that this aft configuration is actually closer to the flight
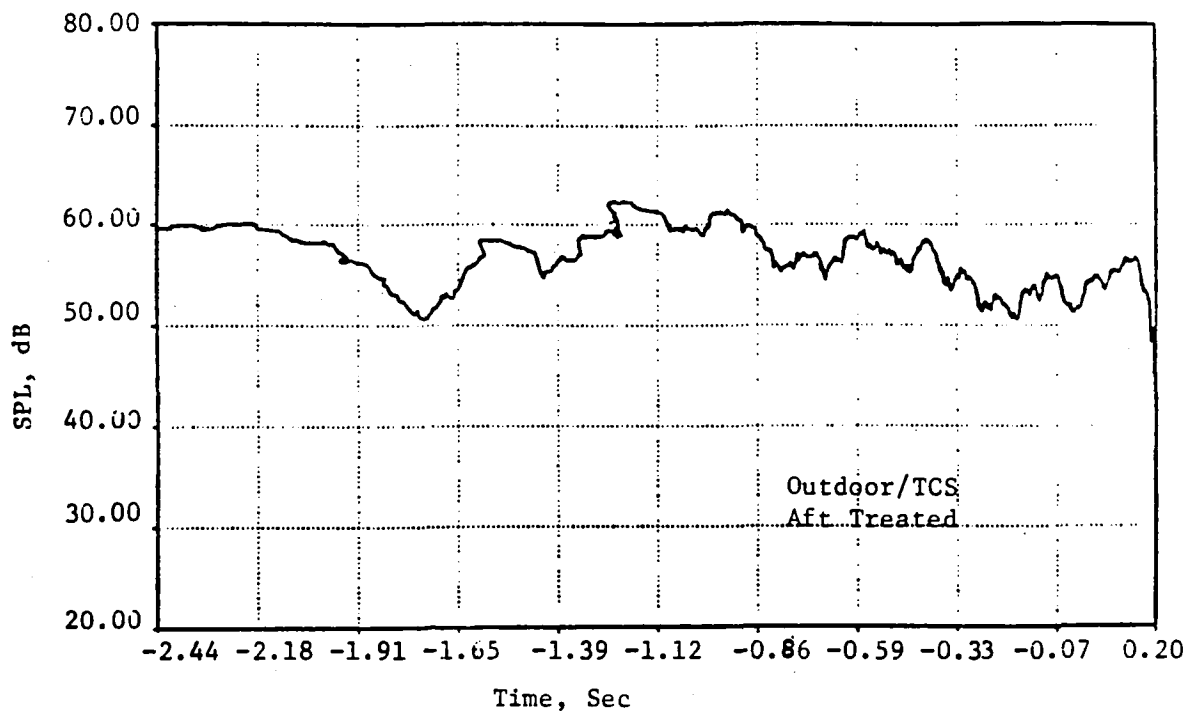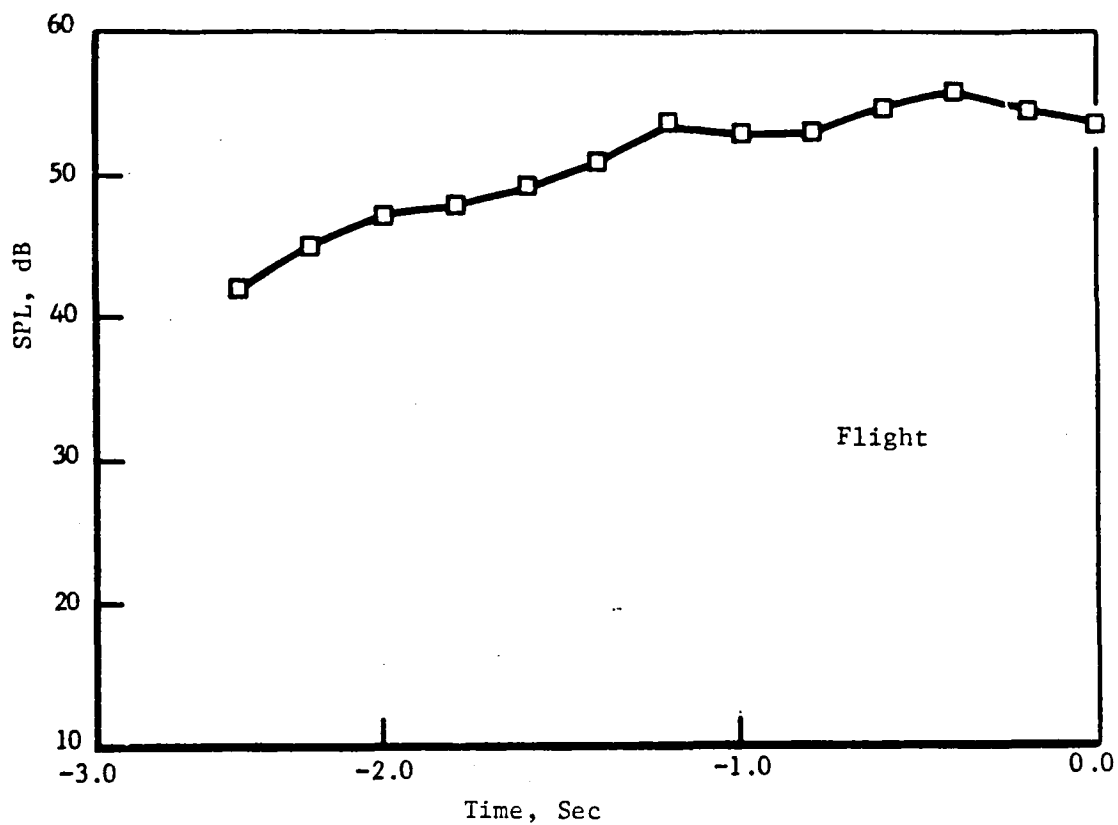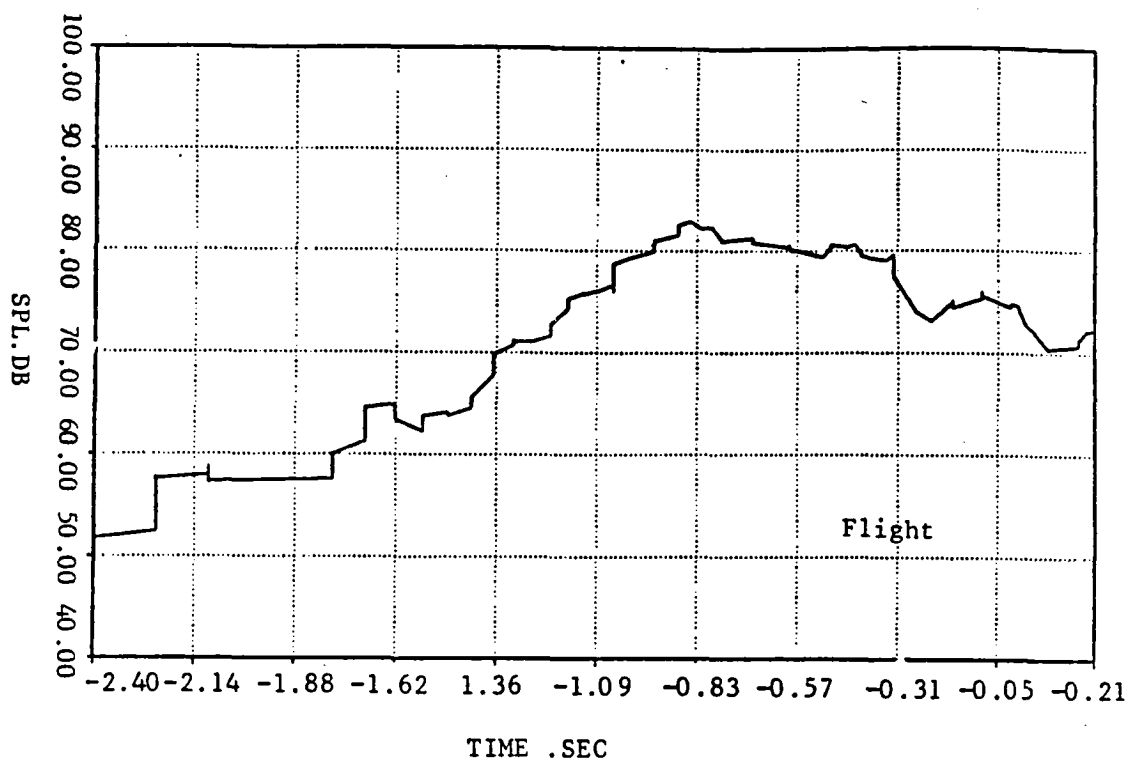
Figure 5-18a. Comparison of Flight and Flight Projected BPF Time
Histories at 10,500 RPM Engine Speed.
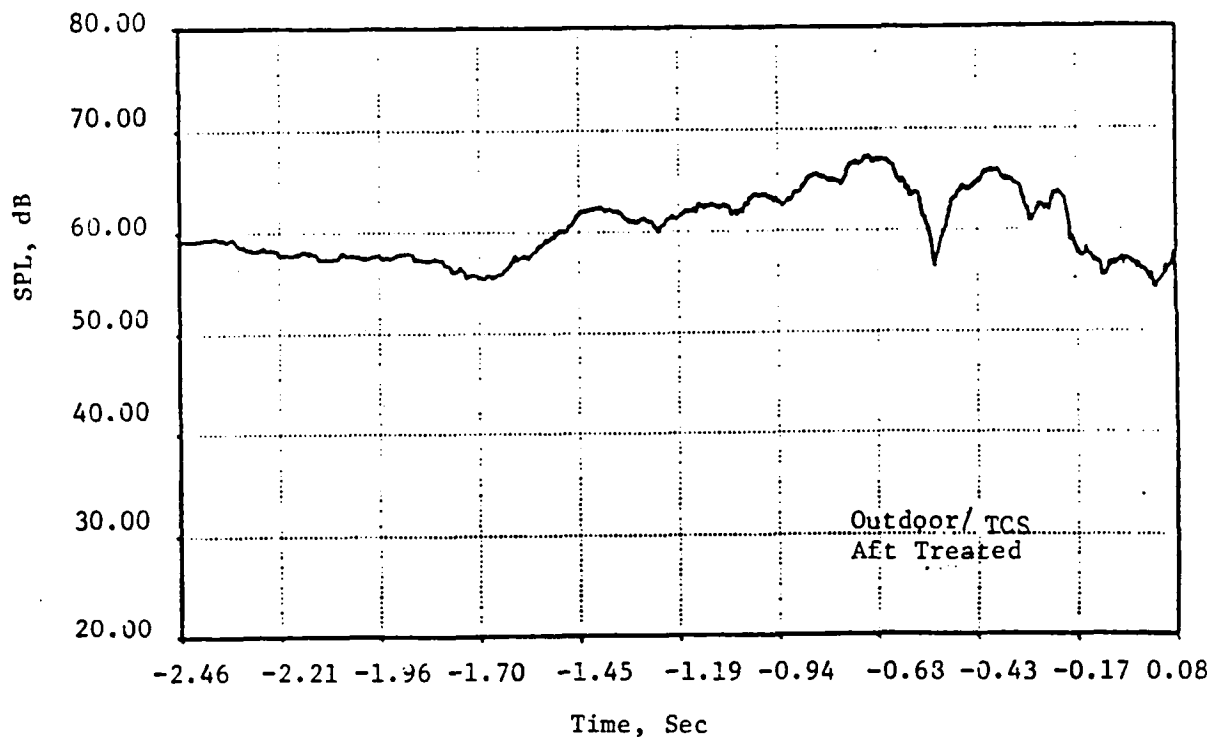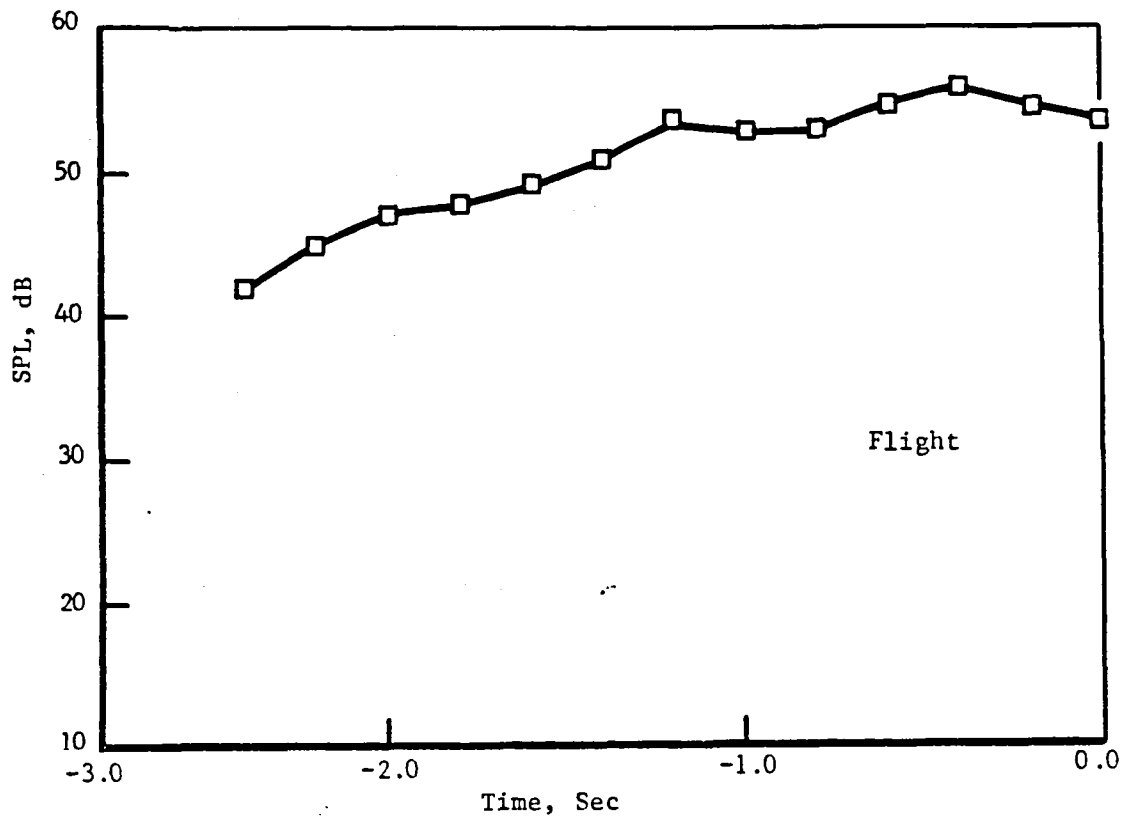
Figure 5-18b. Comparison of Flight and Flight Projected BPF Time Histories at 10,500 RPM Engine Speed.
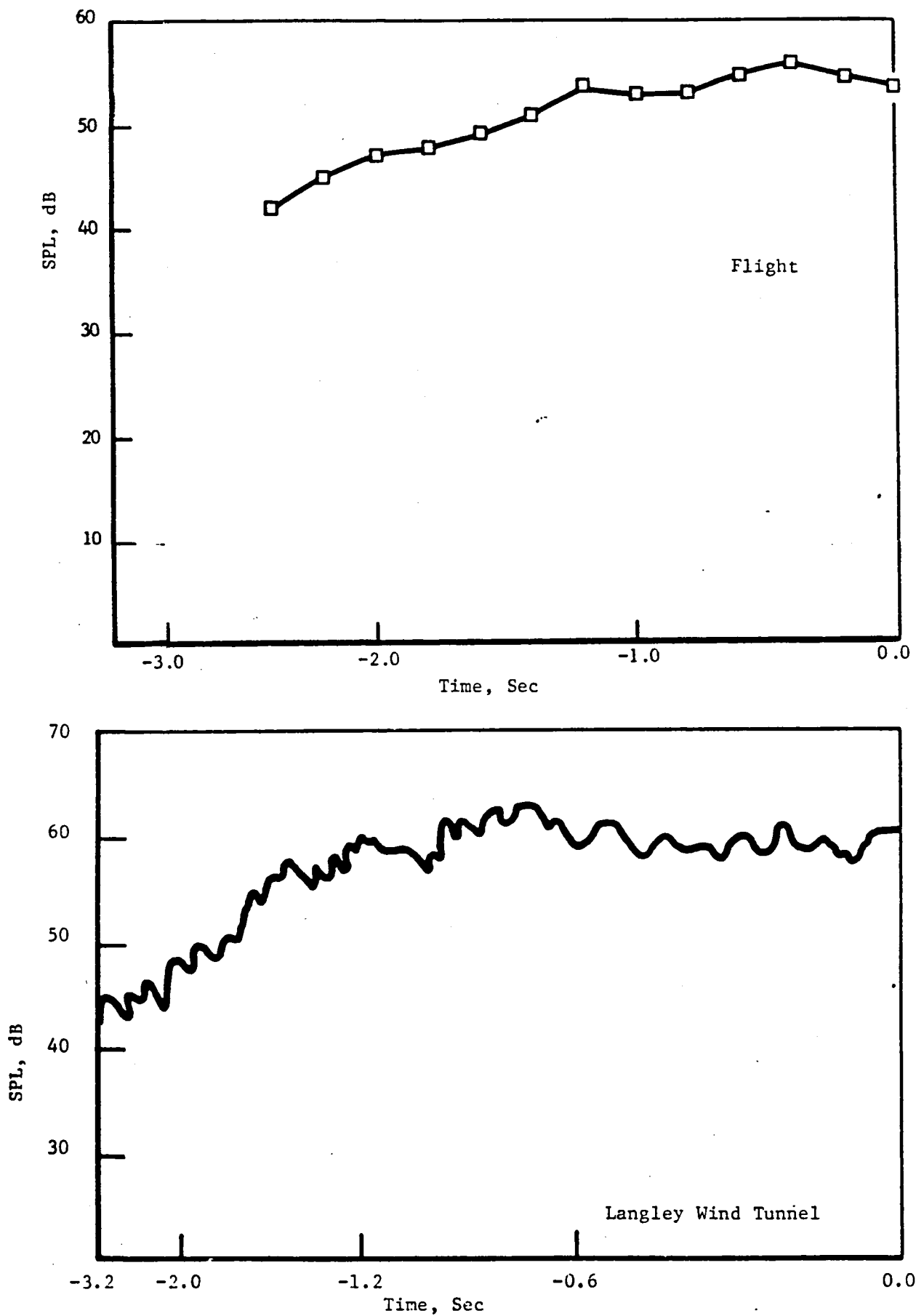
Figure 5-18c. Comparison of Flight and Flight Projected BPF Time
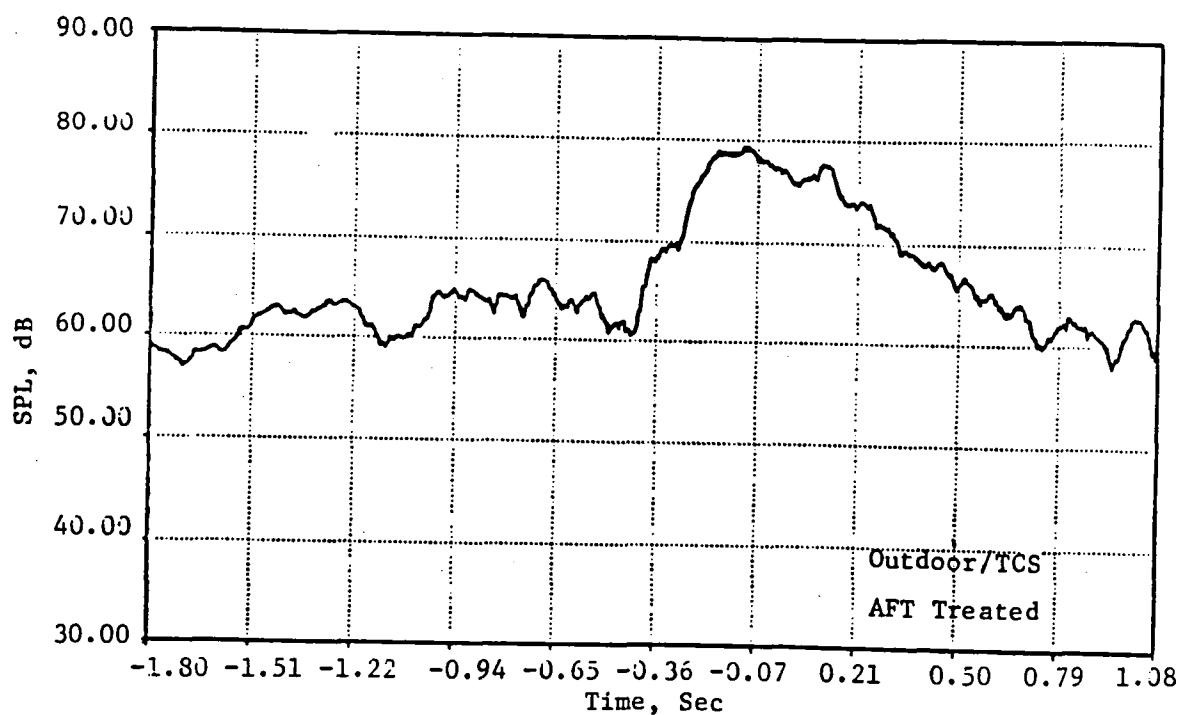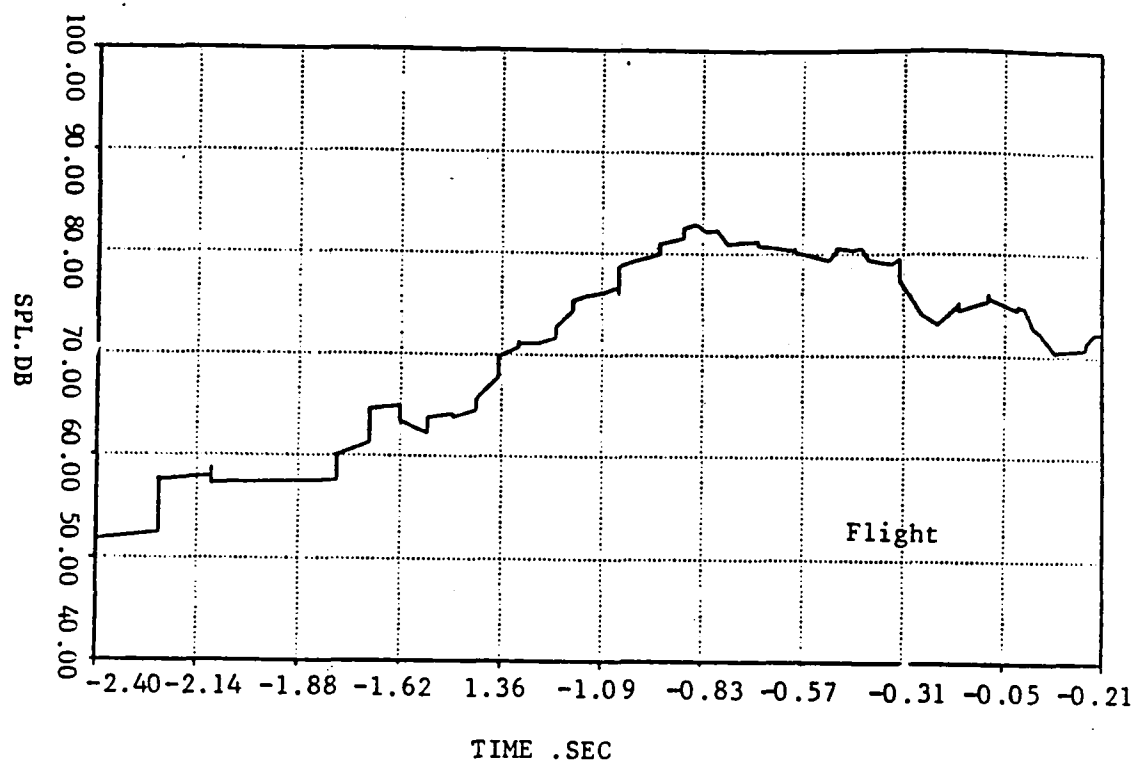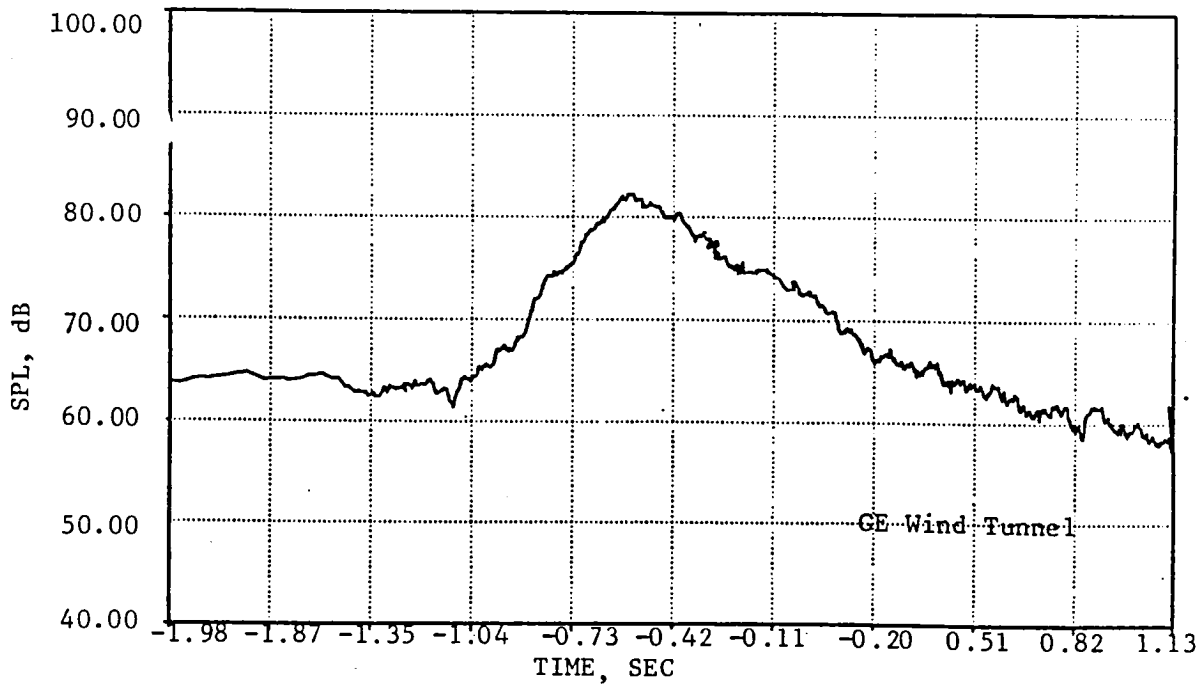Histories at 10,500 RPM Engine Speed.
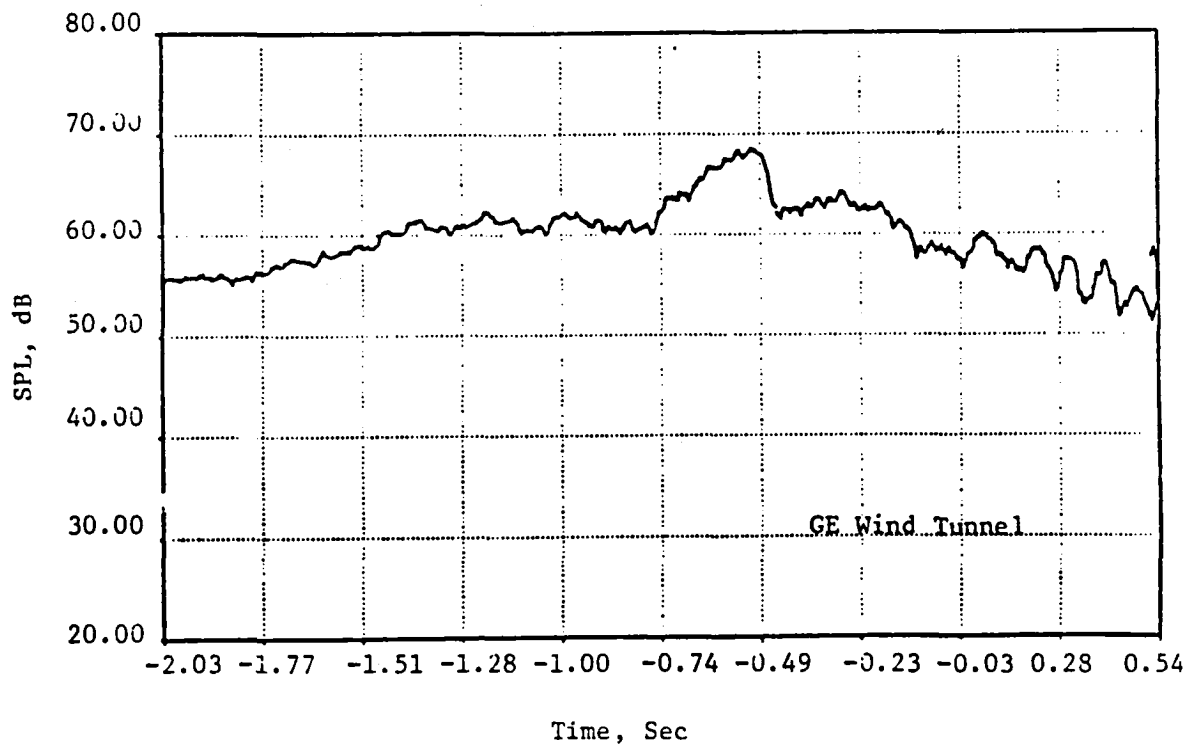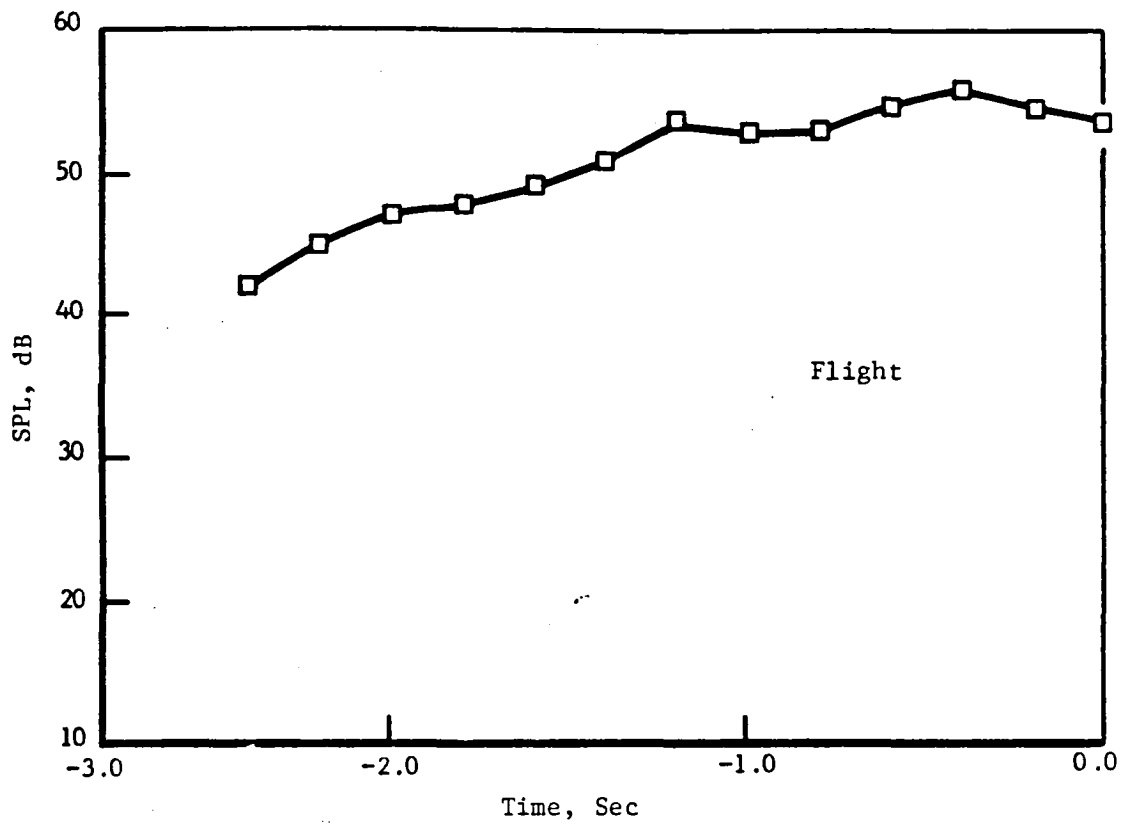
Figure 5-18d.   Comparison of Flight and Flight Projected BPF Time
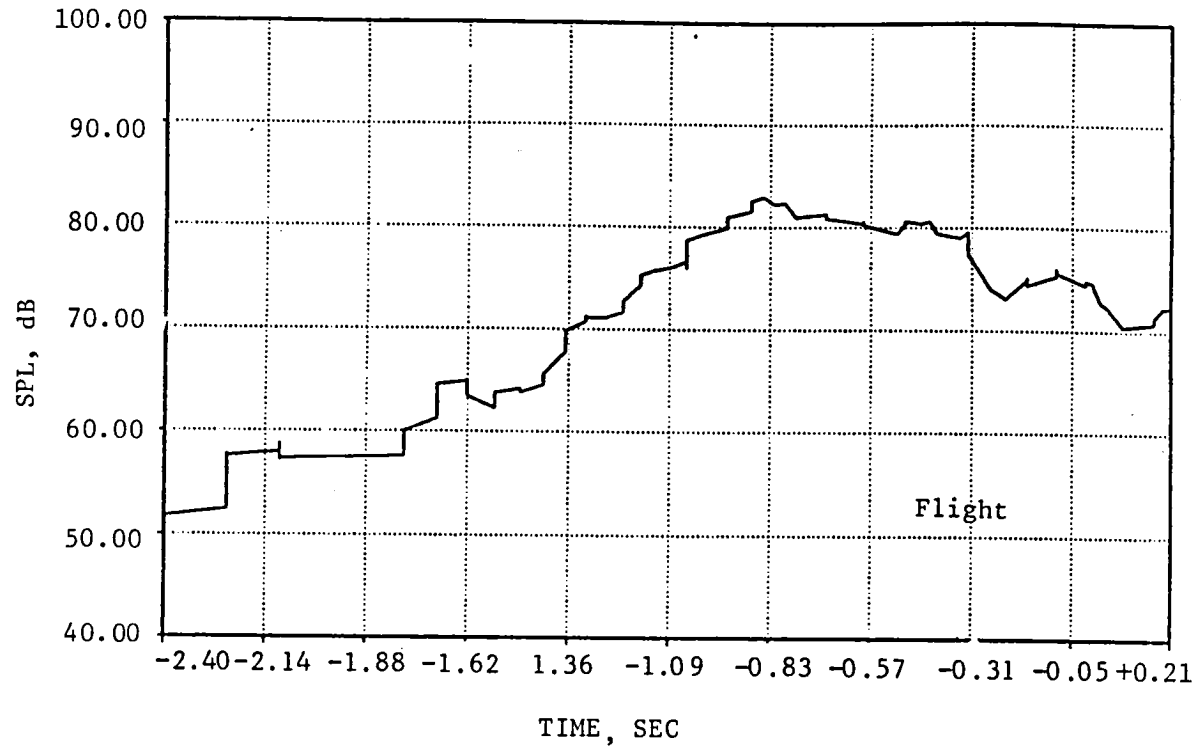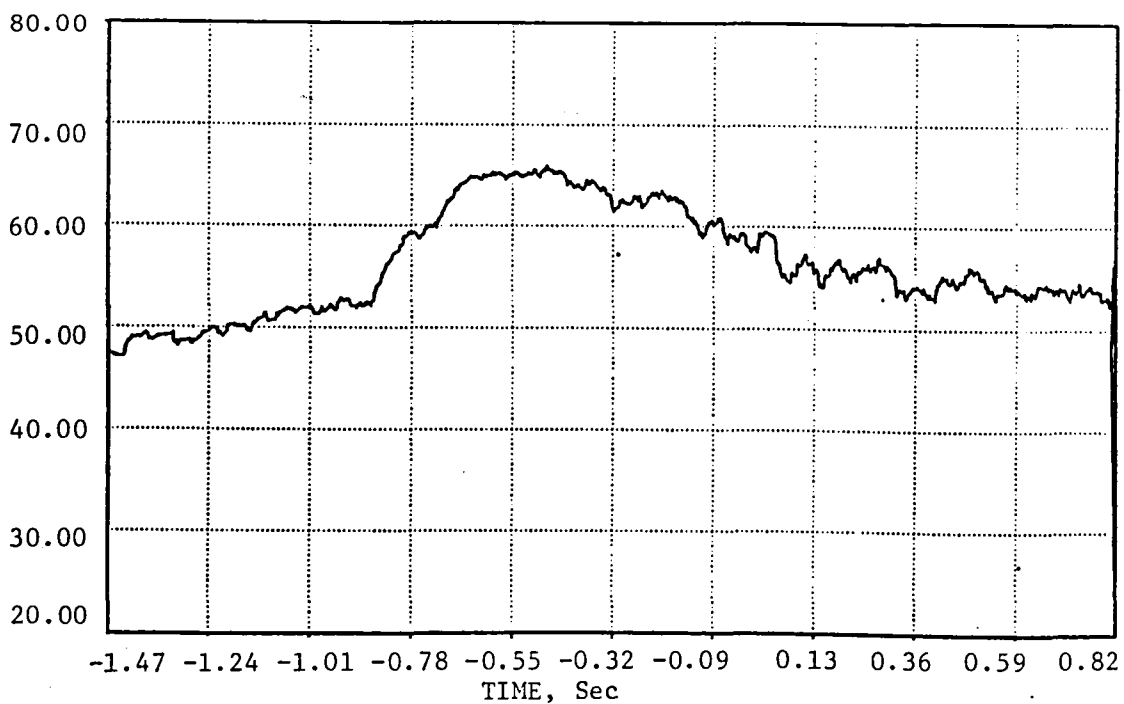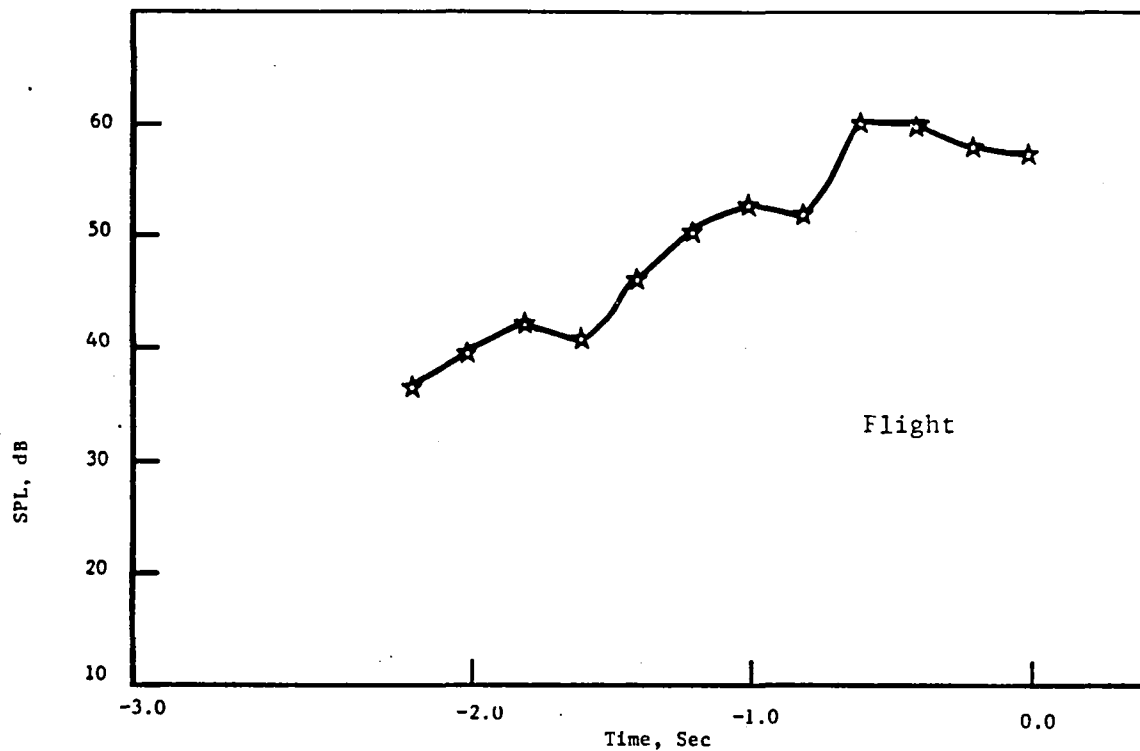Histories for Engine Speed of 10,500 RPM.
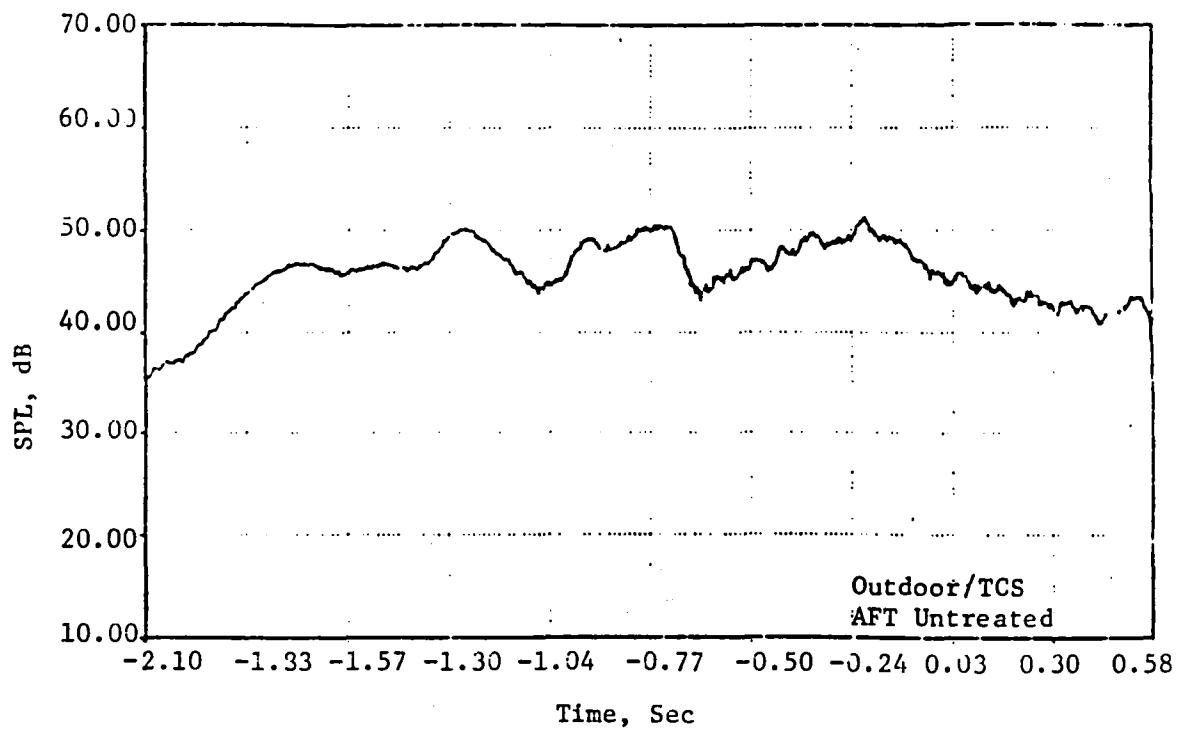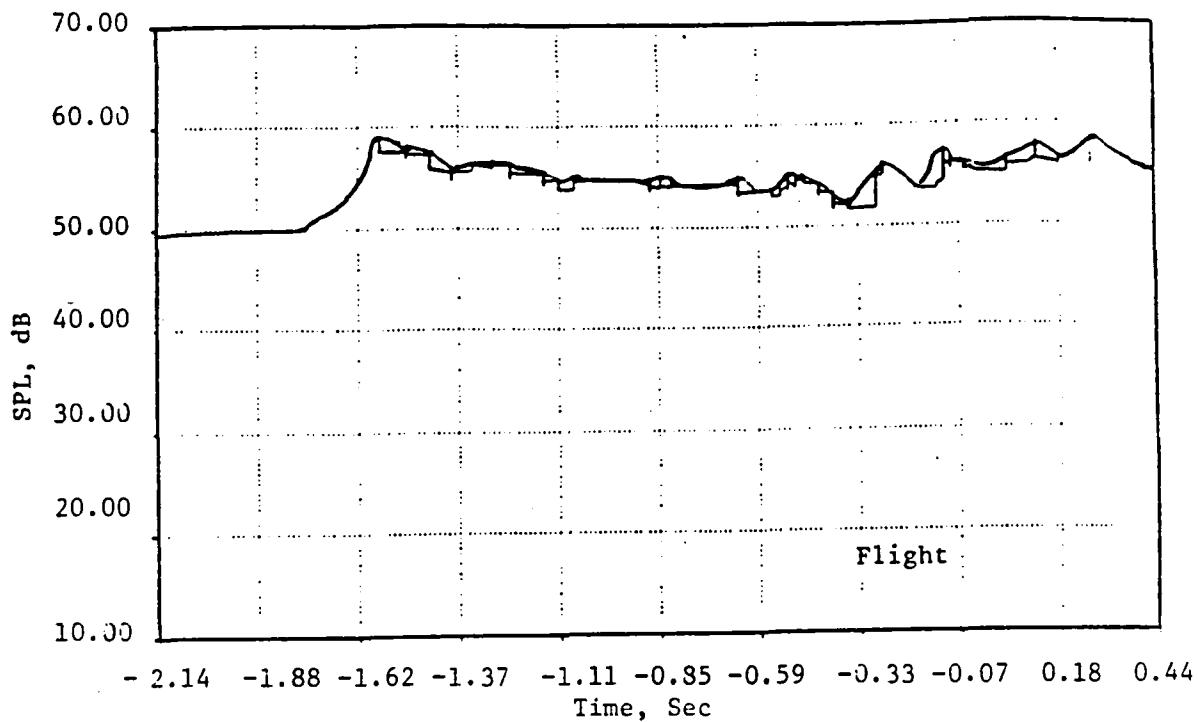
Figure 5-19a. Comparison of Flight and Flight Projected Compressor Tone
Time Histories for Engine Speed of 10,500 RPM.

104
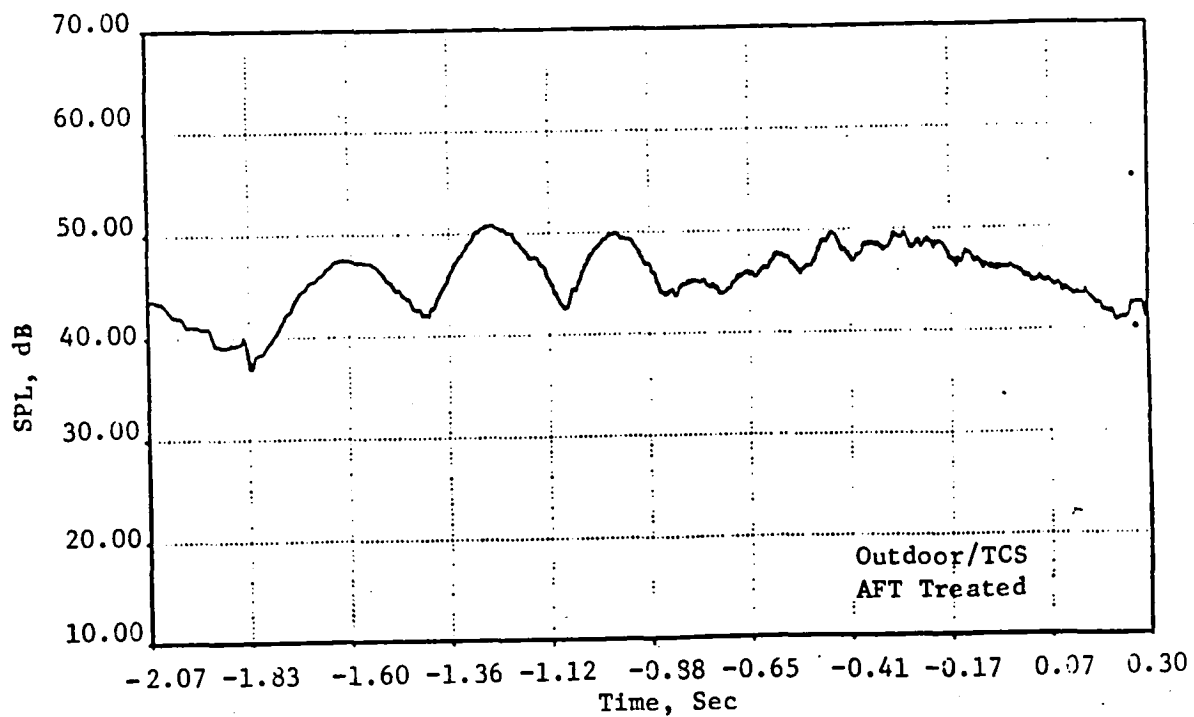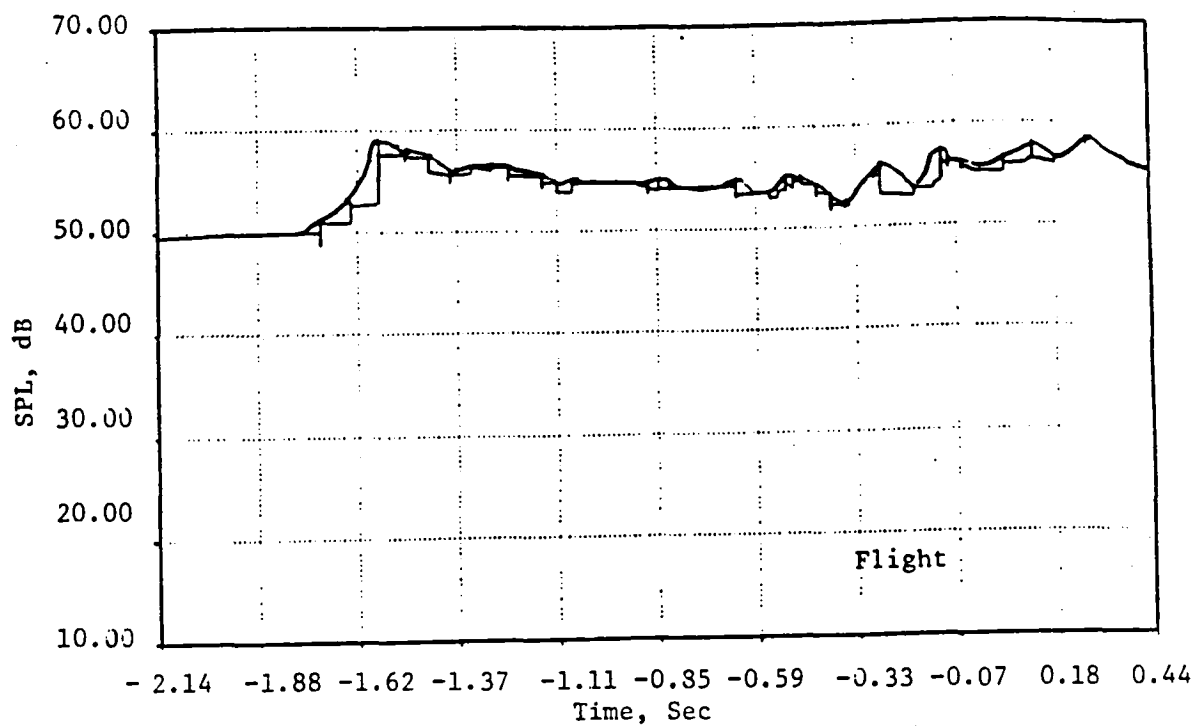
Figure 5-19b. Comparison of Flight and Flight Projected Compressor Tone Time Histories at Engine Speed of 10,500 RPM.

105
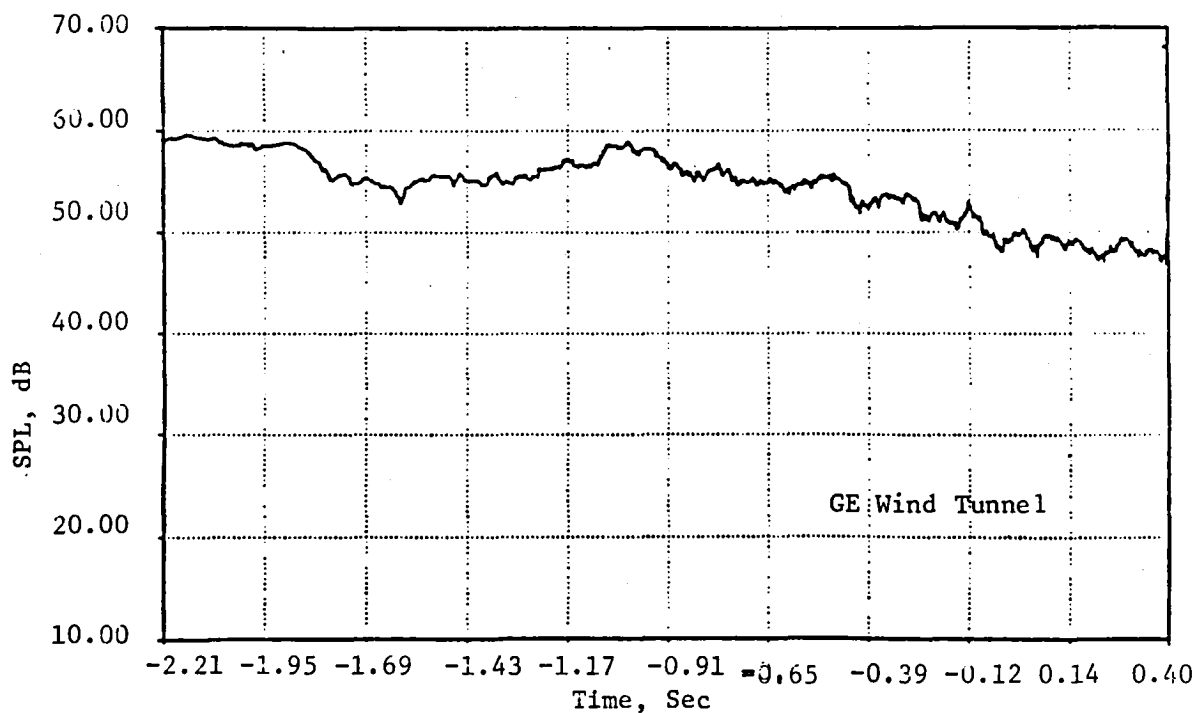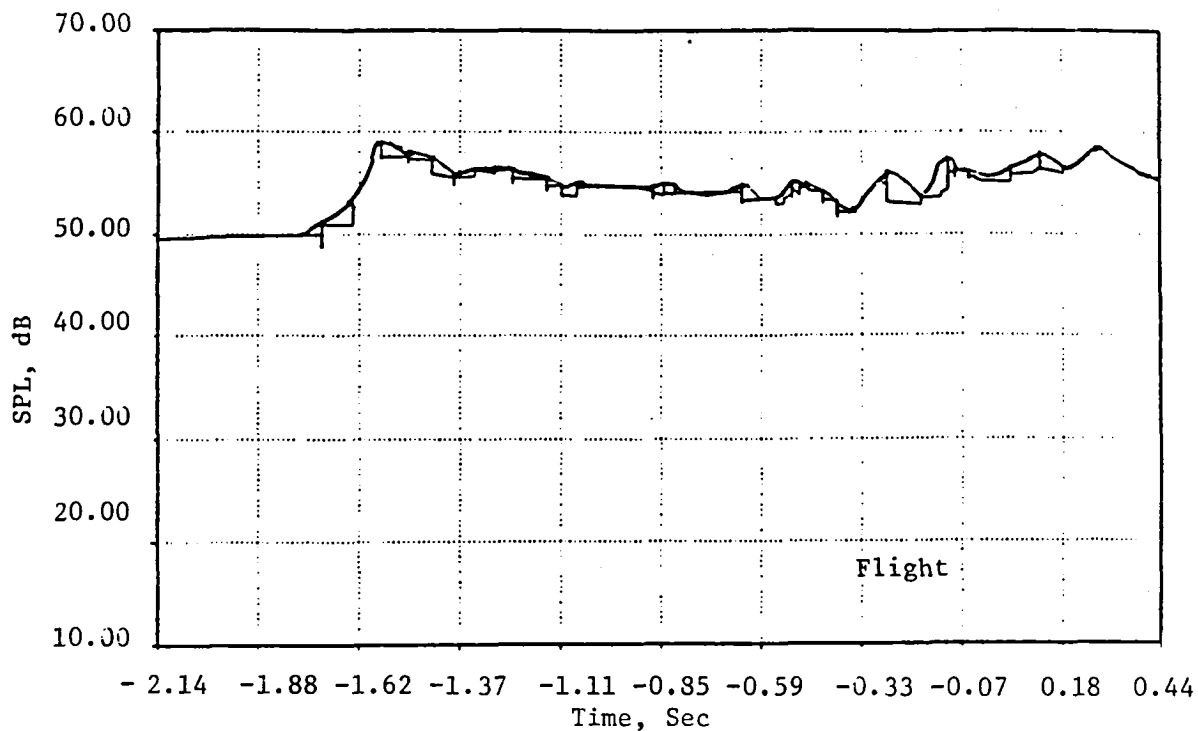
Figure 5-19c. Comparison of Flight and Flight Projected Compressor Tone
Time Histories at Engine Speed of 10,500 RPM.
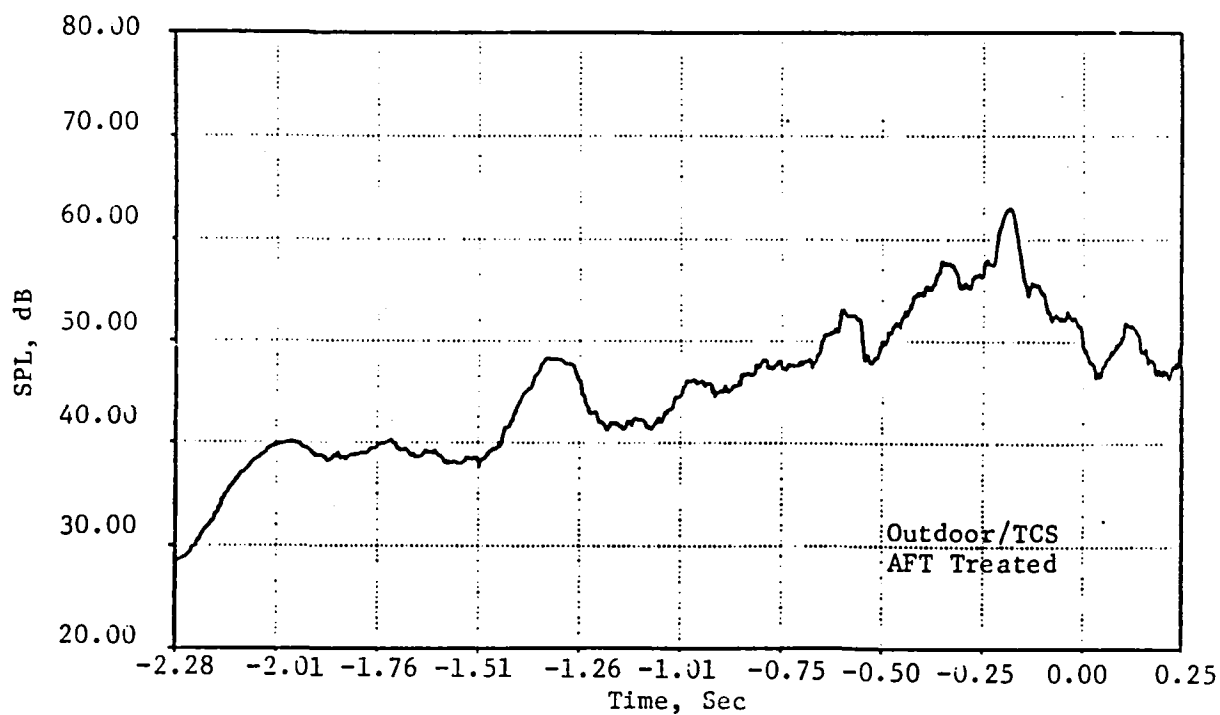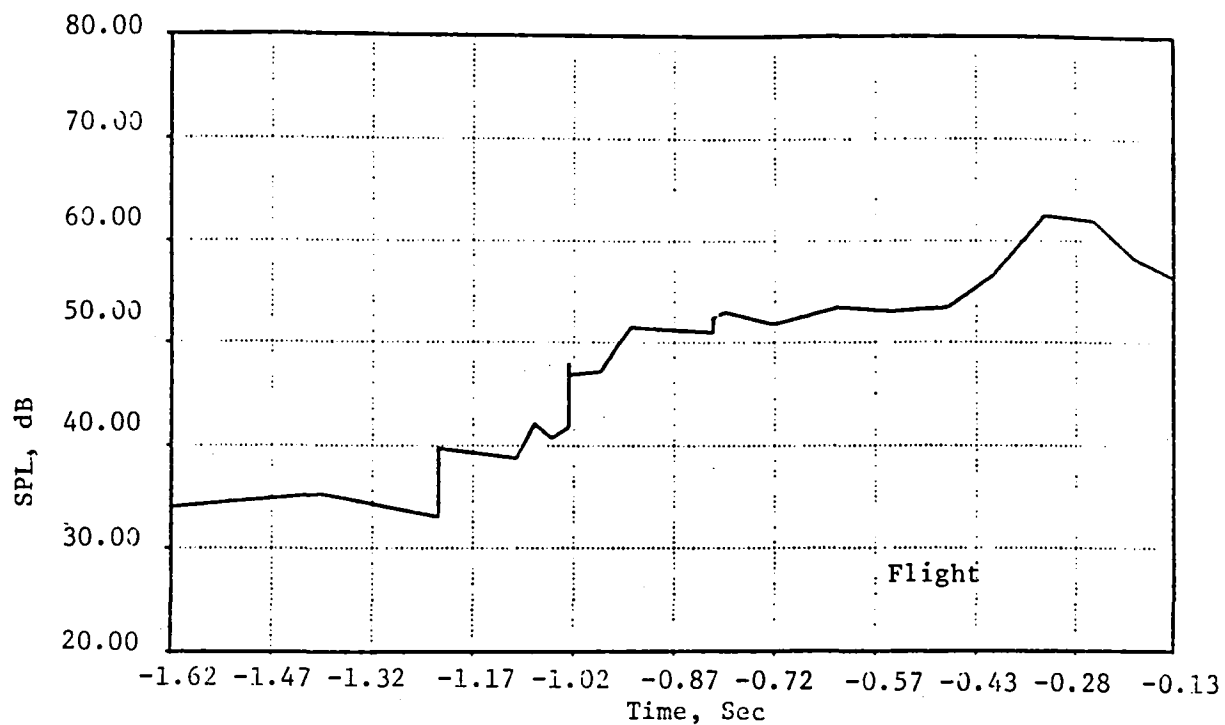
Figure 5-20. Comparison of Flight and Flight Projected Twice BPF Time
Histories at Engine Speed of 10,500 RPM.
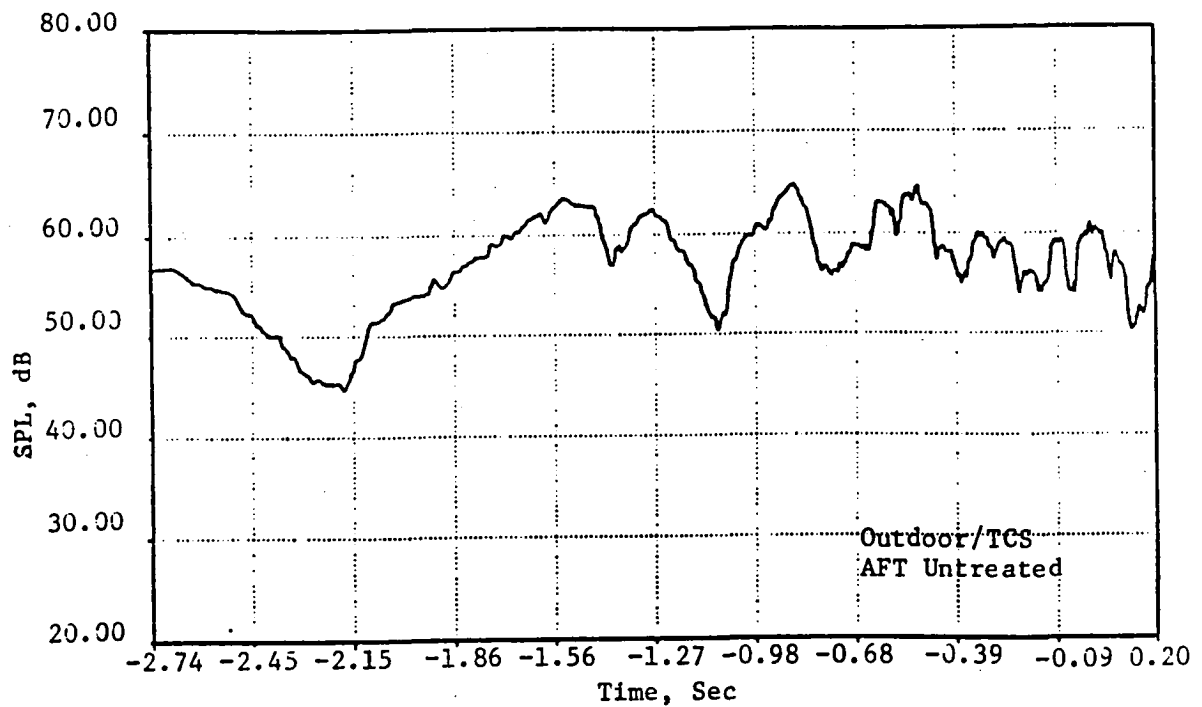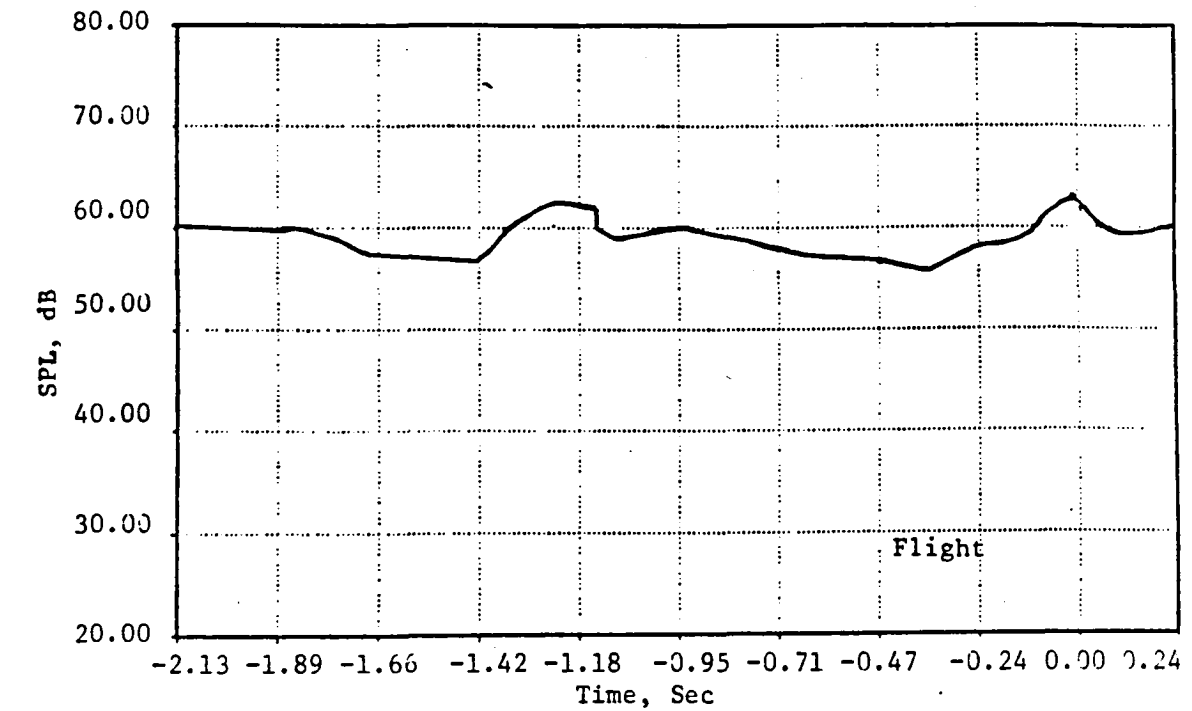
Figure 5-21a. Comparison of Flight and Flight Projected BPF Time
Histories at Engine Speed of 11,800 RPM
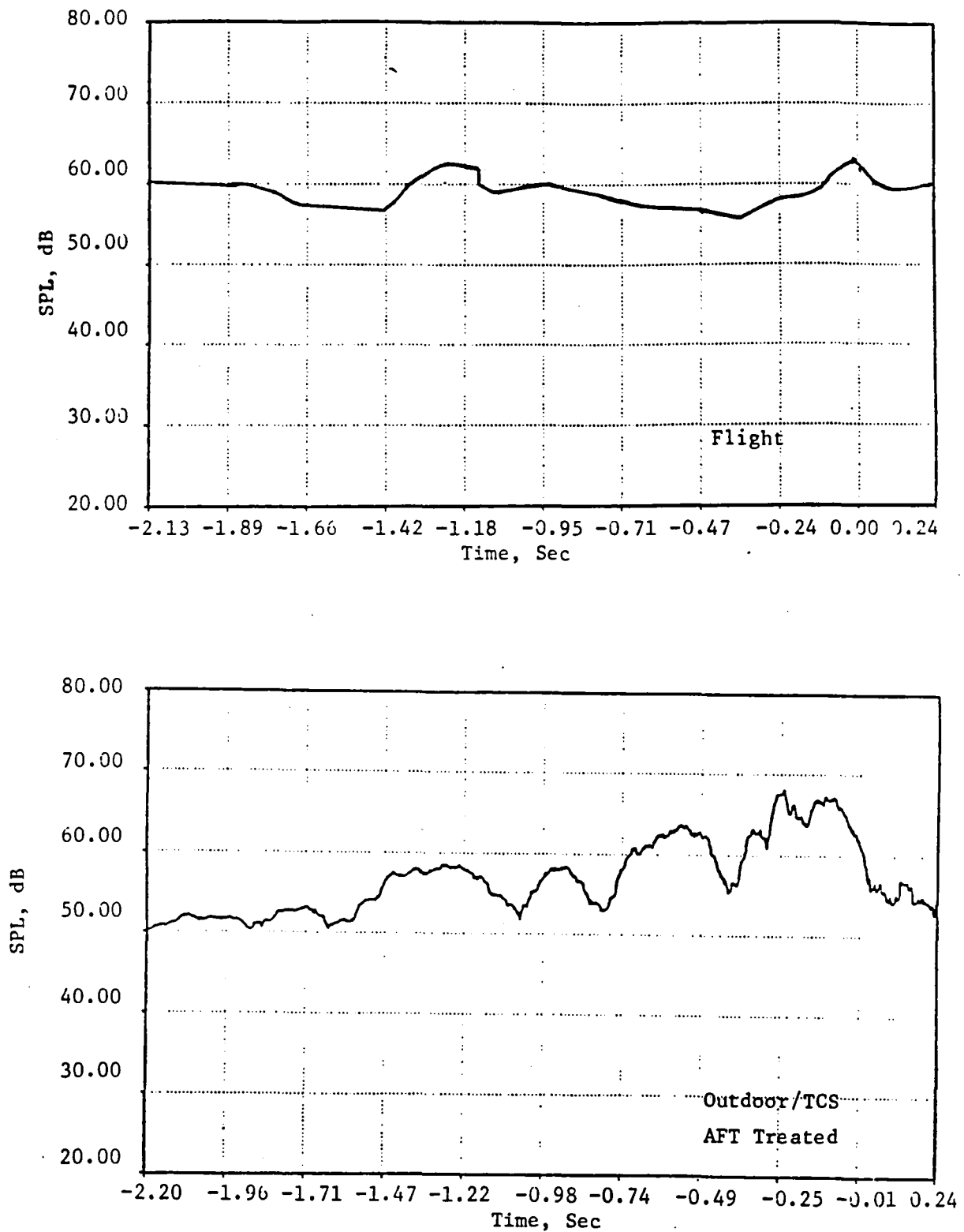
Figure 5-21b.   Comparison of Flight and Flight Projected BPF
Time Histories at Engine Speed of 11,300 RPM.
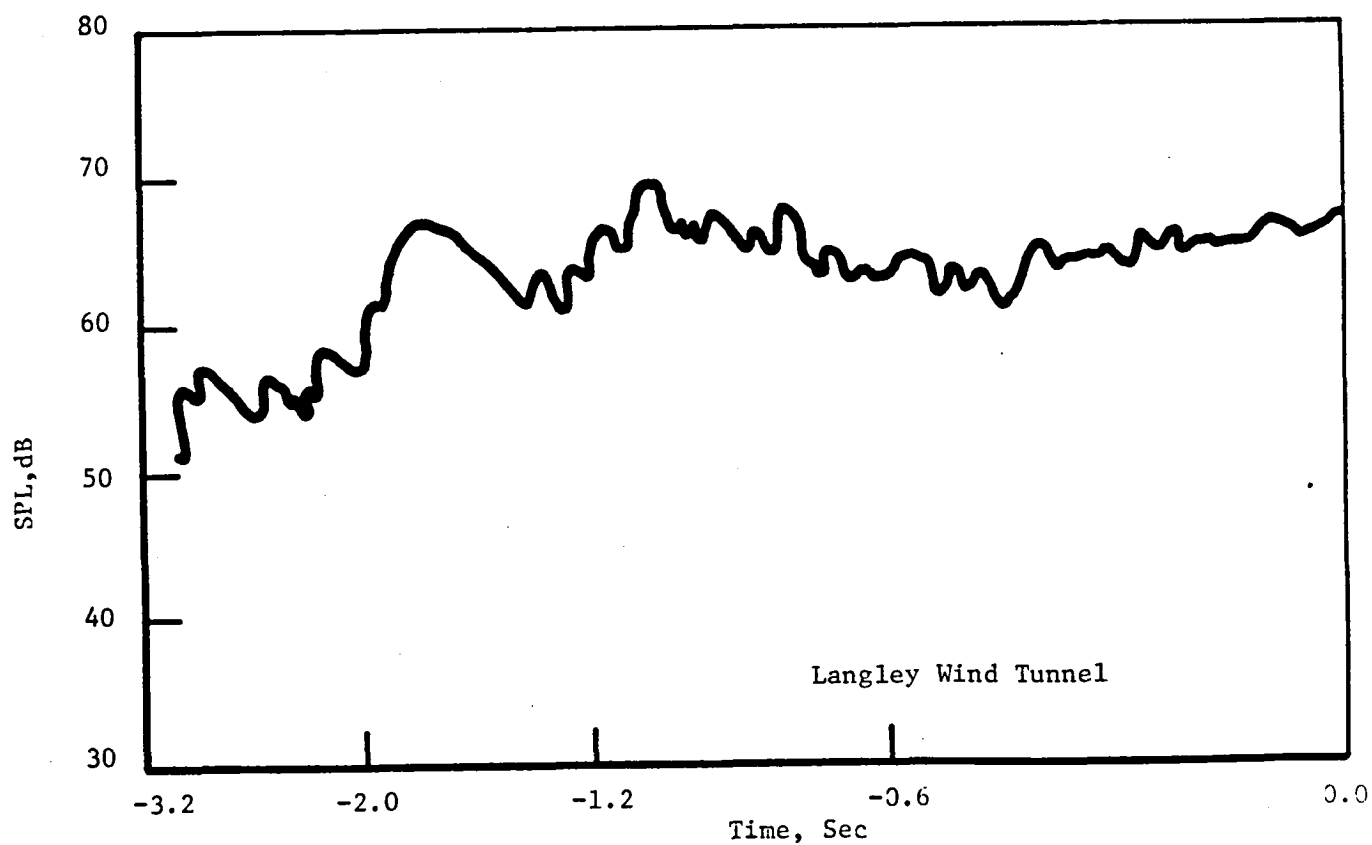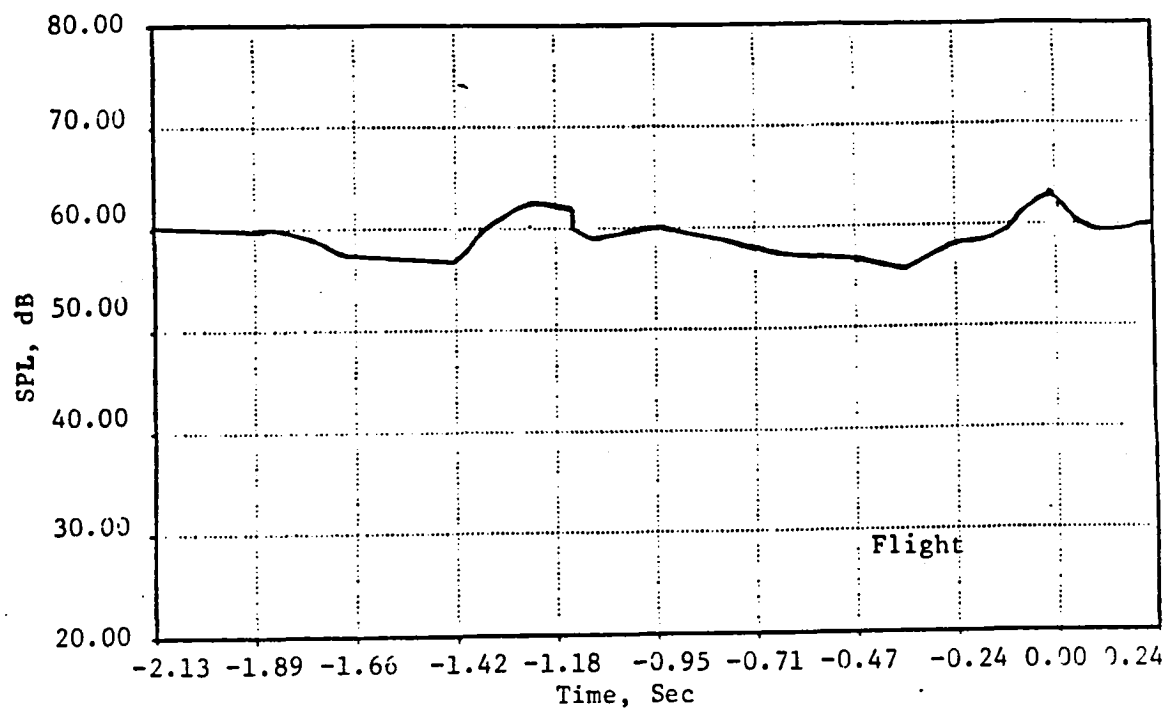
Figure 5-21c. Comparison of Flight and Flight Projected BPF Time
Histories at Engine Speed oif 11,800 RPM.
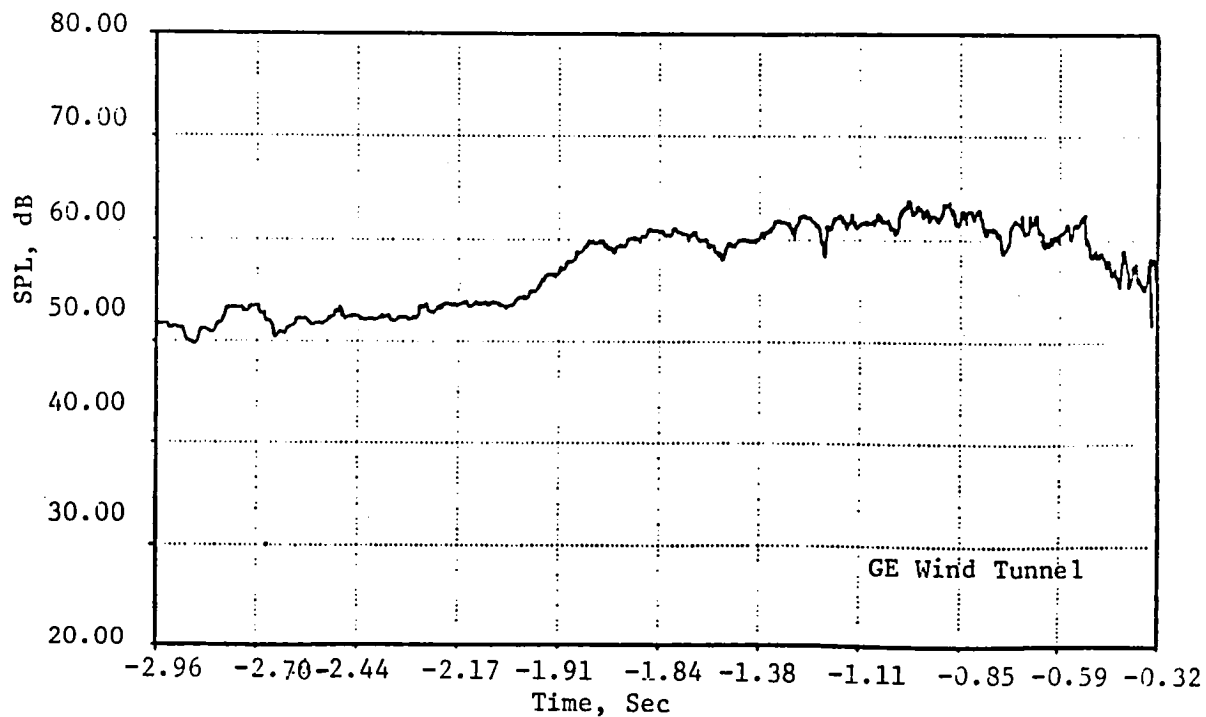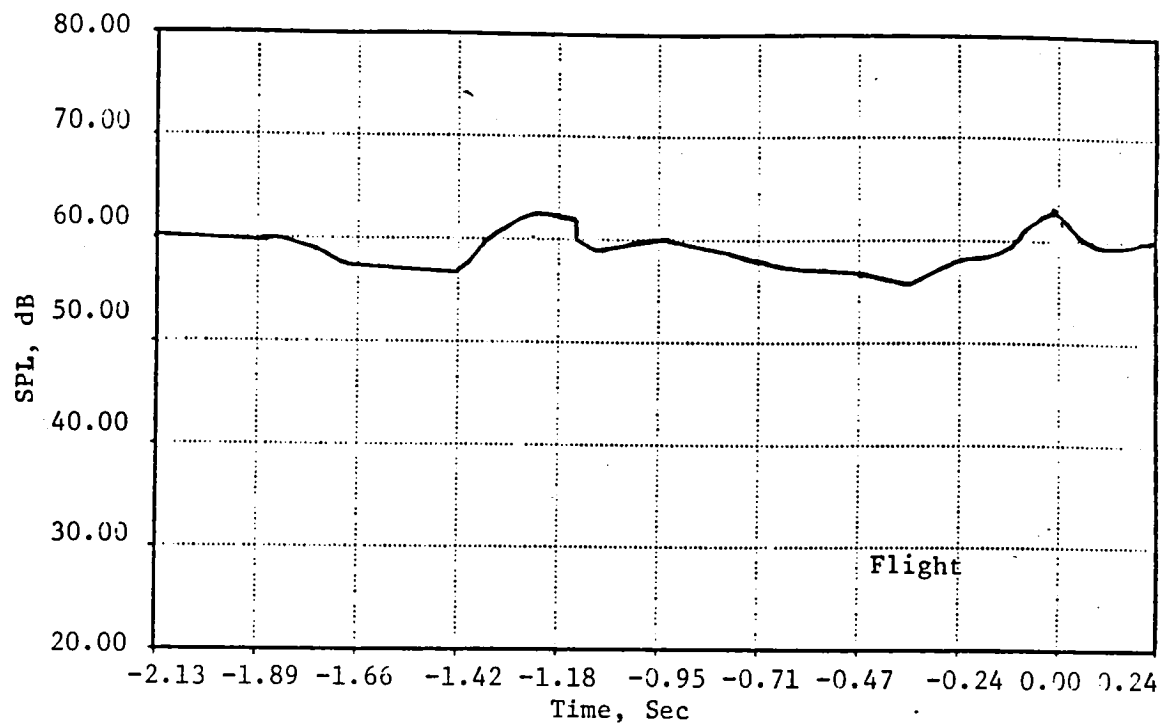
Figure 5-21d.   Comparison of Flight and Flight Projected BPF Time
Histories at Engine Speed of 11,300 RPM.
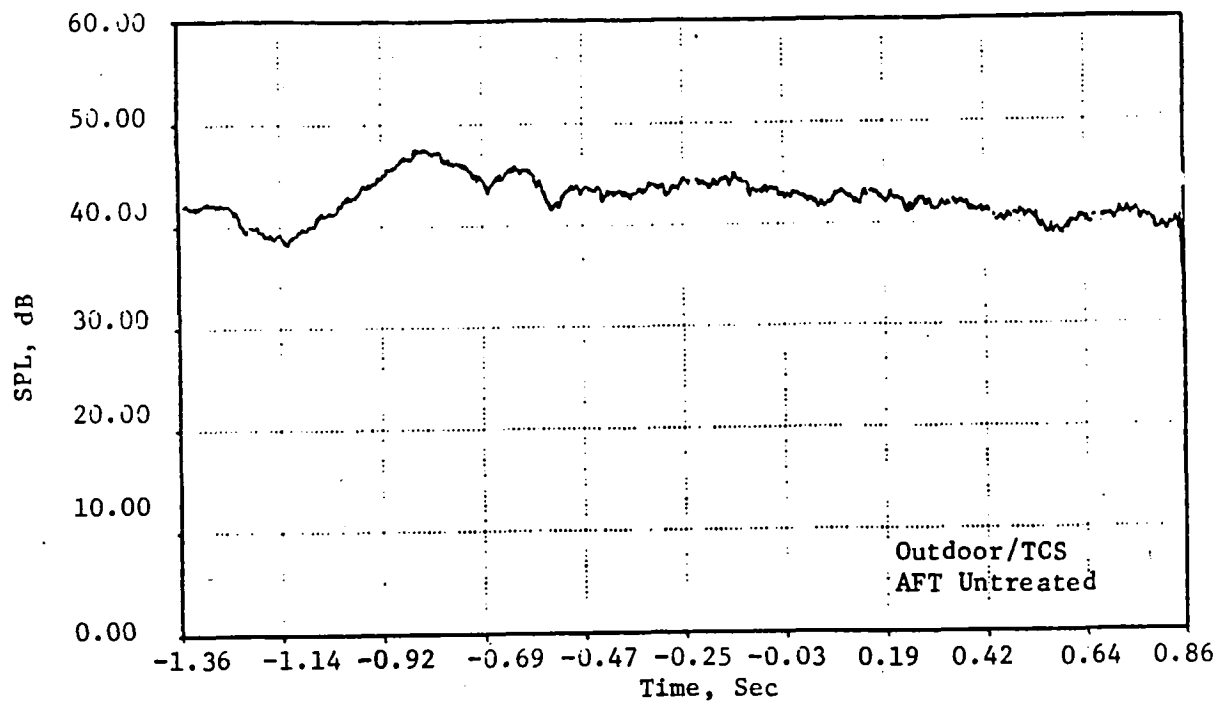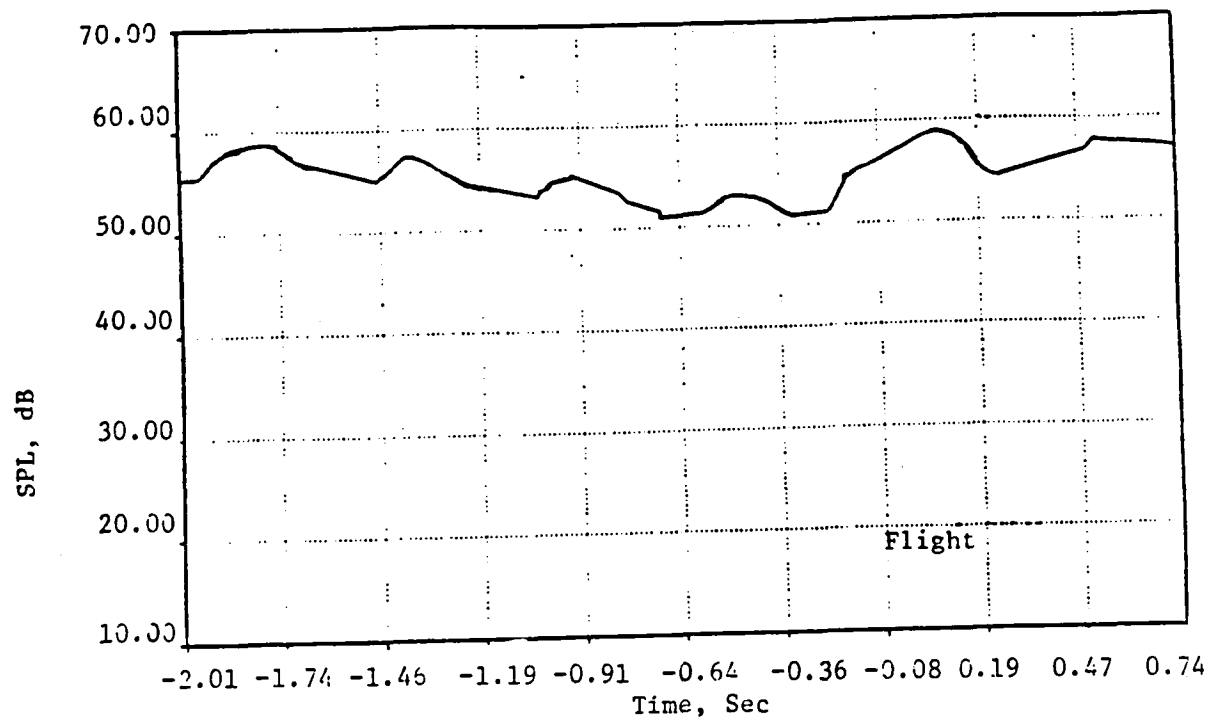
Figure 5-22a.. Comparison of Flight and Flight Projected Compressor Tone
Time Histories of Engine Speed 11,800 RPM.

112
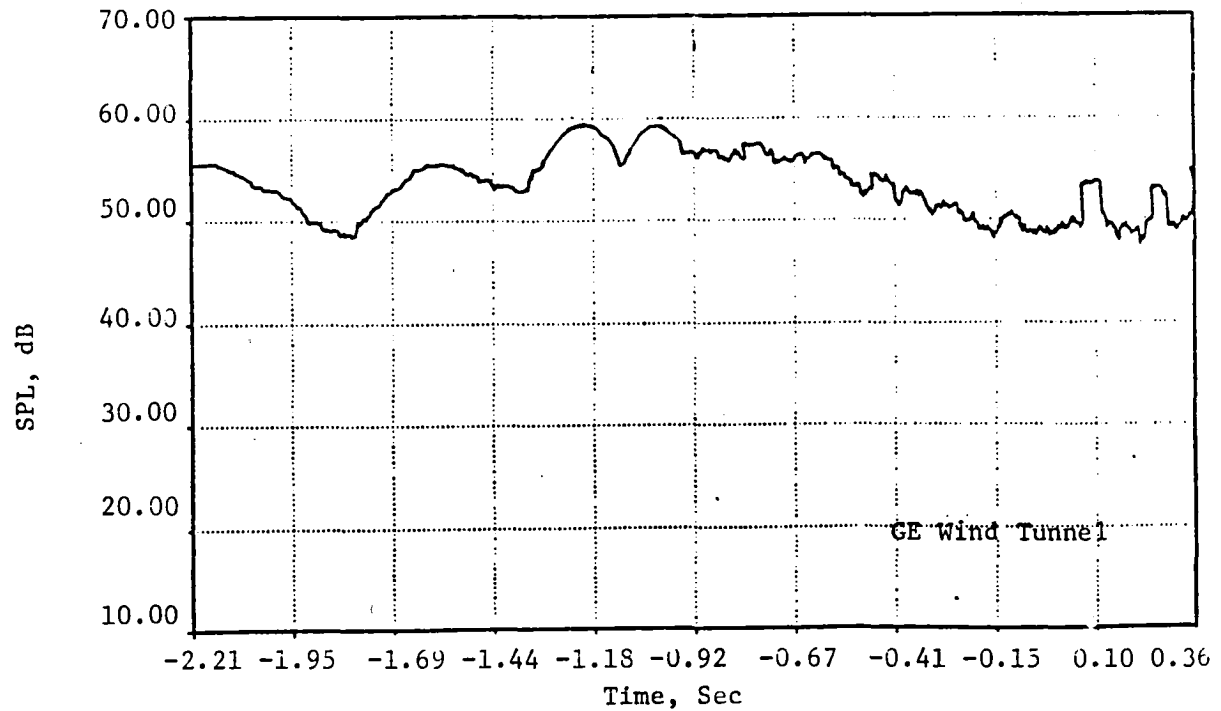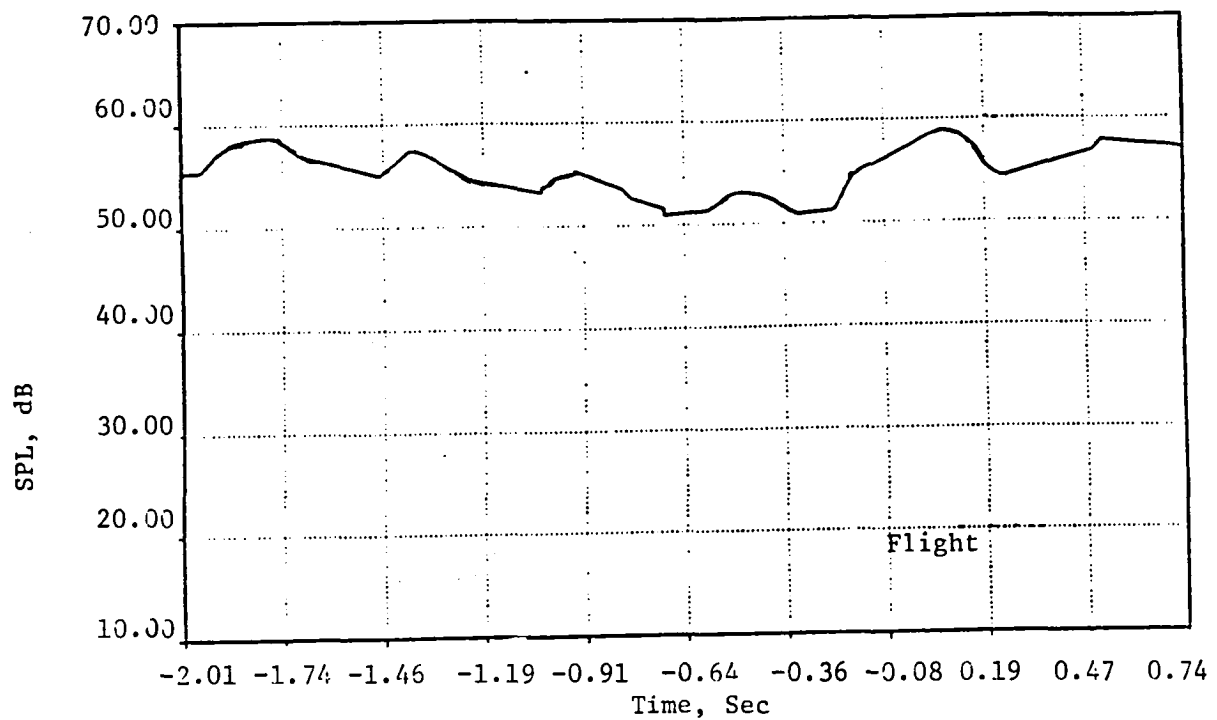
Figure 5-22b. Comparison of Flight and Flight Projected Compressor Tone Time Histories at Engine Speed of 11,800 RPM.
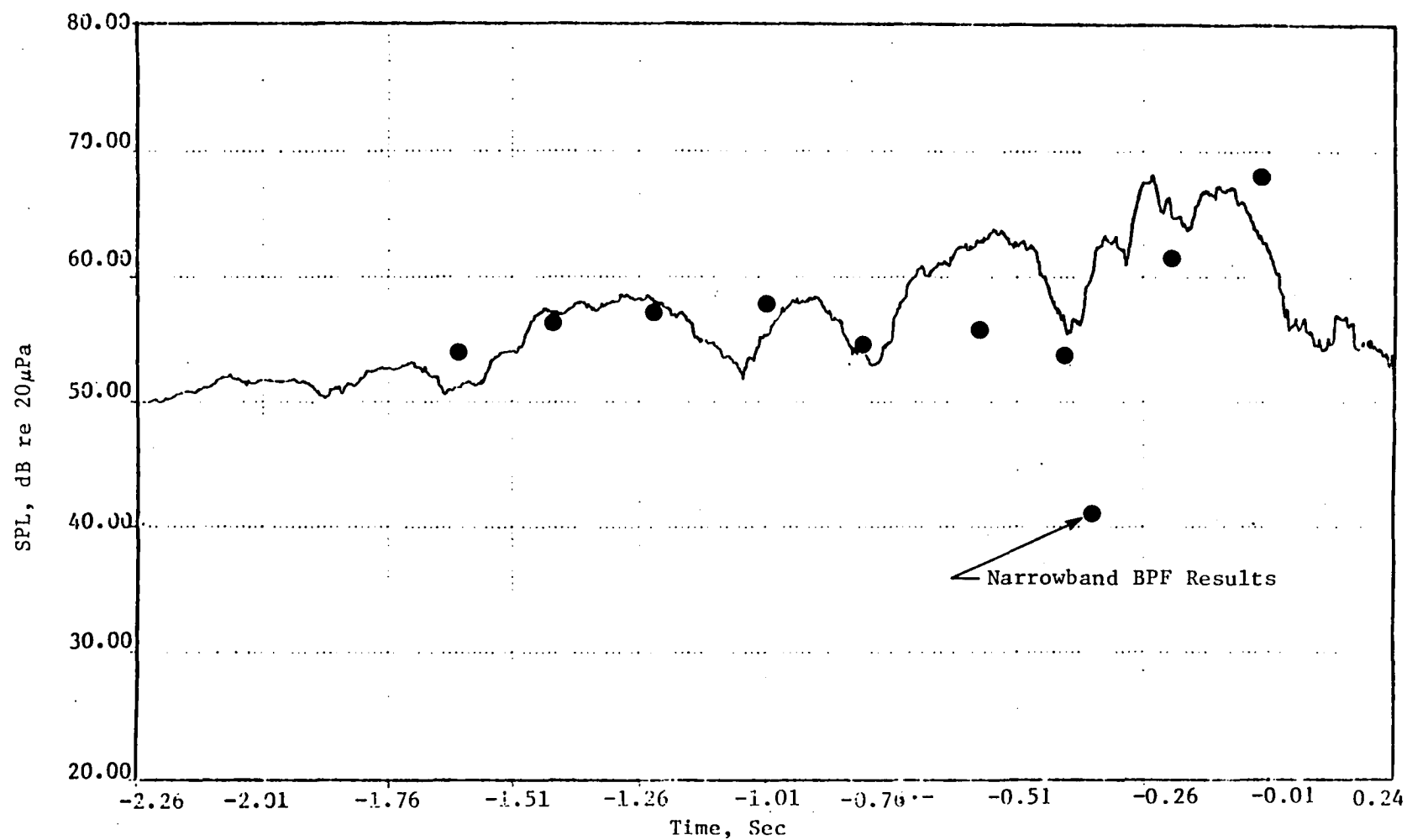
Figure 5-23. Comparison of Flight Narrowband BPF Results with Outdoor TCS Flight Projected Time History.
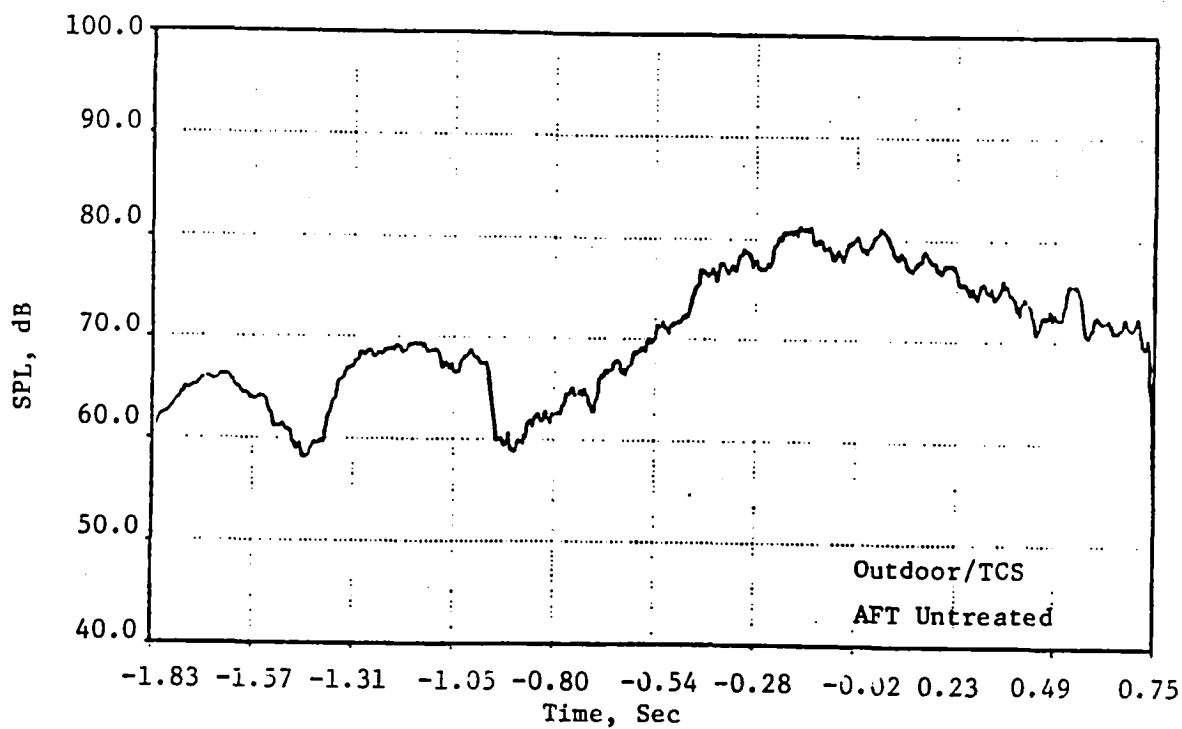
Figure 5-24a. Comparison of Flight and Flight Projected BPF
Time Histories at Engine Speed of 13,500 RPM.

115

Figure 5-24b. Comparison of Flight and Flight Projected BPF Time
Histories at Engine Speed of 13,500 RPM.

116

Figure 5-24c.   Comparison of Flight and Flight Projected Time Histories
at Engine Speed of 13,500 RPM

Figure 5-25. Comparison of Flight and Flight Projected Compressor Tone Time Histories at Engine Speed of 13,500 RPM

118

test/configuration than the treated aft configuration. Again the projected
results in Figures 5-24(b) and 5-24(c) display good agreement between
simulated flight results but not as good agreement to the actual flight data.
Figure 5-25 shows the comparison of the flight projected and flight measured
compressor tone at the supersonic fan speed condition. The projected tone
displays a broad concentrated acoustic energy hump at 0.5 seconds to overhead
location, while the flight measured results peaks at a slightly different
location on the time scale.

5.4   BLADE MOUNTED TRANSDUCER ANALYSIS

The rotor blade mounted transducers were analyzed using a variety of
methods to obtain detailed information regarding their signatures.
Traditional methods of obtaining the averaged waveform and standard deviation
for 500 Averages, i.e., 500 revolutions, were accomplished (References 5-1 and
5-2). In addition, the enhanced spectrum, averaged spectrum, and the random
spectrum of various transducers were determined. The enhanced spectrum is the
Fourier transform of the averaged waveform, whereas the averaged spectrum is
the Fourier transform of individual data samples which are then averaged in
the Frequency domain. The random spectrum is obtained by removing the
averaged waveform from each individual data sample then processing as if an
averaged spectrum were being determined.

A summary of the rotor blade mounted results for the differential of
(H-K) are displayed in Figures 5-26 through 5-37. The differential pressure
(H-K) is displayed since in the succeeding sections this information is
utilized to make predictions of the farfield tone directivity. The most
dominant feature in many of the figures is the existence of a strong six per
revolution component. This component is most obvious in the waveforms,
attributable to the existence of six engine support struts, and has been
investigated as an acoustic source in References 5-2, 5-3 and 5-4. Another
prevalent feature in the (H-K) BMT waveforms and spectra is the existence of a
sixty-six per revolution component which is observed in Figures 5-27, 5-28 and
5-33. The sixty-six per revolution component is due to the sixty-six stator
blades behind the rotor. Other harmonic components which are present in the
spectrum are not as deterministic in origin and thus must be attributable to
unknown sources, with the possible exception of the one per revolution which

AVERAGED SPECTRUM

BMT 'H-K'

JT15D-1 FLIGHT TEST #2

WALLOPS ISLAND. OV-1B

DATE: 12-JUN-81.

FAN SPEED = 10,435 RPM

SPL, dB

160
150
140
130
120
110
100

0 20 40 60 80 100 120 140 160 180 200

Frequency, Hz *10^9

ENHANCED SPECTRUM

SPL, dB

150
140
130
120
110
100
90

0 20 40 60 80 100 120 140 160 180 200

Frequency, Hz *10^9

RANDOM SPECTRUM

SPL, dB

160
150
140
130
120
110
100

0 20 40 60 80 100 120 140 160 180 200

Frequency, Hz *10^9

WAVEFORM

Amplitude, psi

0.30
0.20
0.10
0.00
-0.10
-0.20
-0.30

360°

STANDARD DEVIATION

Amplitude, psi

0.70
0.60
0.50
0.40
0.30
0.20
0.10

360°
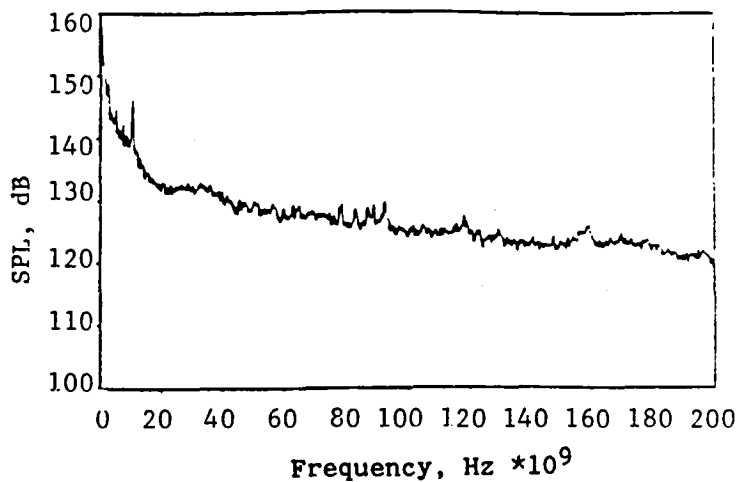
Figure 5-26. BMT Results for JT15D Flight Test at Engine Speed 10,435 RPM.

120

AVERAGED SPECTRUM

BMT 'H-K'

JT15D-1 LANGLEY/AMES TUNNEL
TEST

RUN # 551-7.   VO = 60 KTS

DATE: 15-MAR-80.

FAN SPEED = 10,500 RPM

ENHANCED SPECTRUM

RANDOM SPECTRUM

WAVEFORM

STANDARD DEVIATION
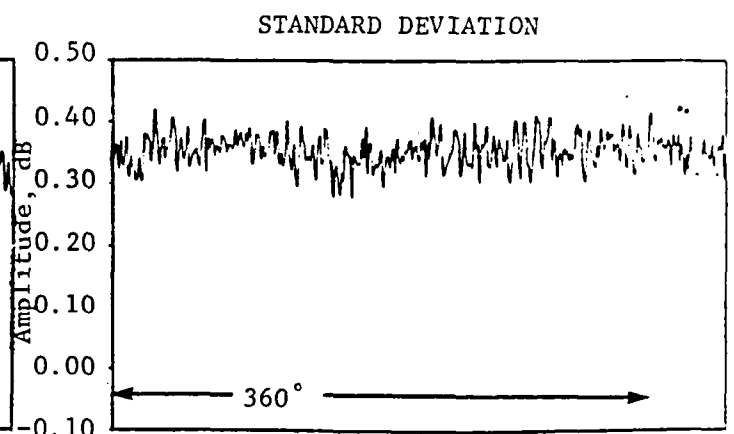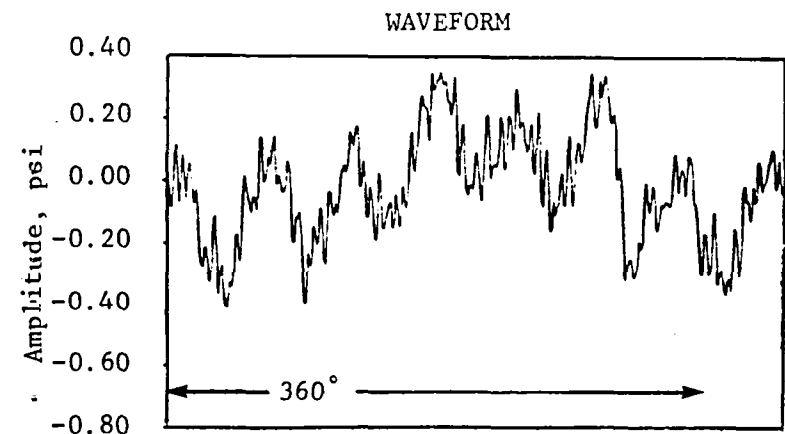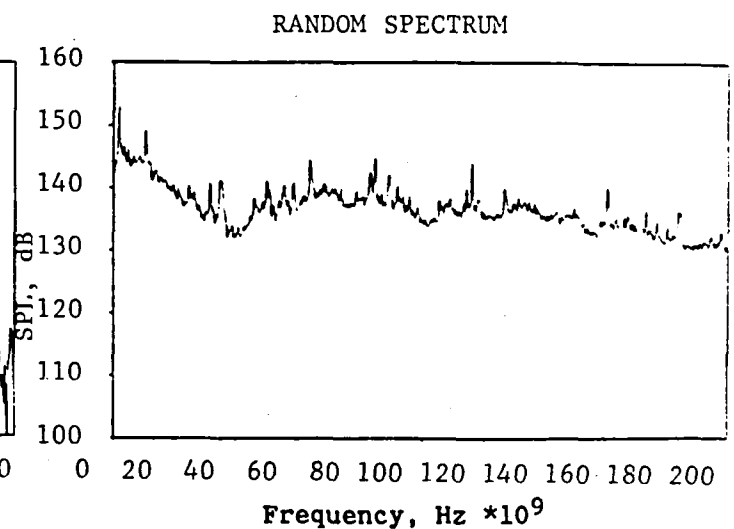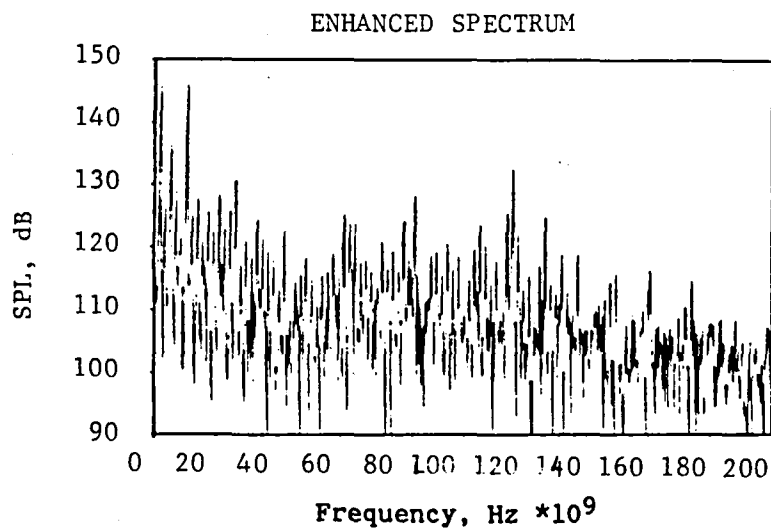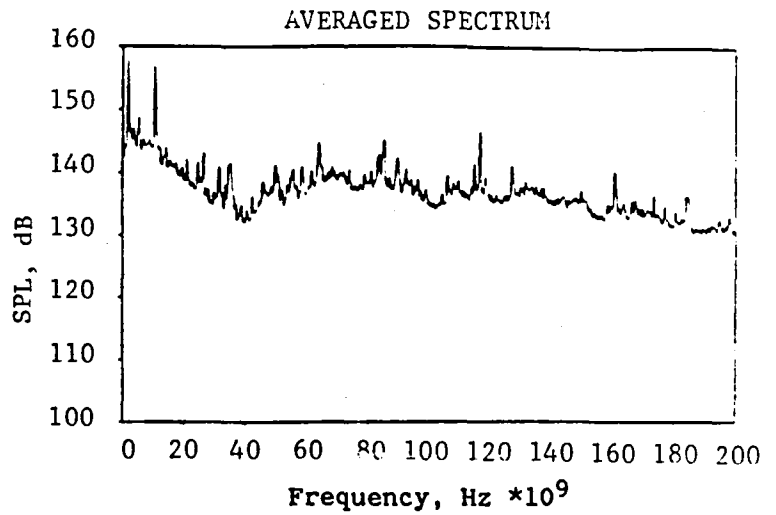
Figure 5-27.   BMT Results for JT15D Wind Tunnel Test at Engine Speed of 10,500 RPM.
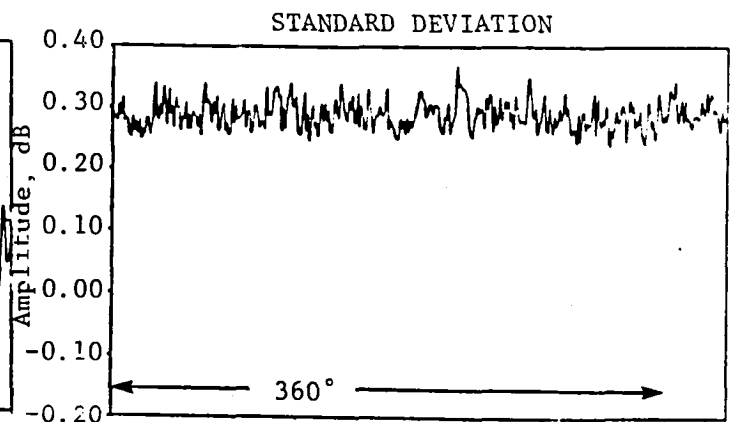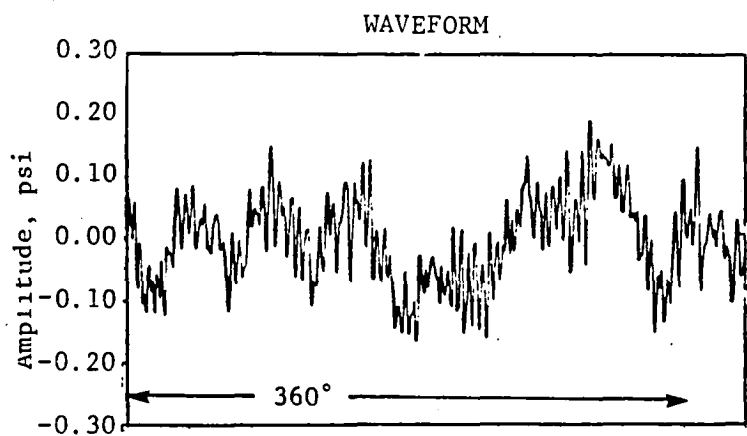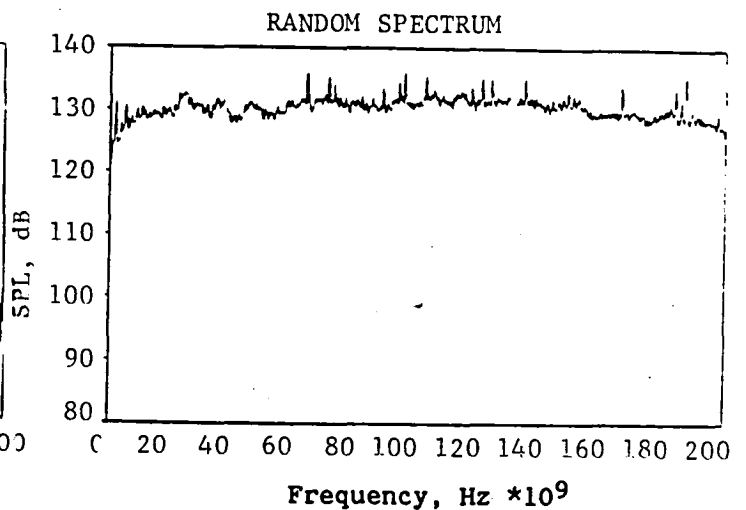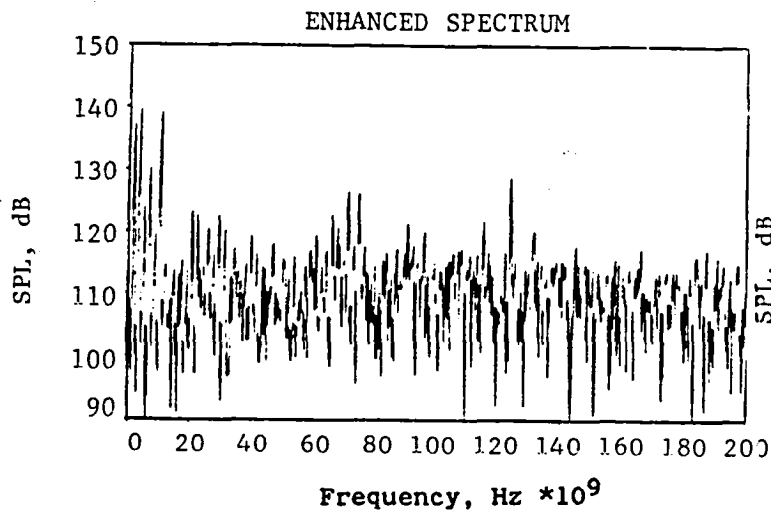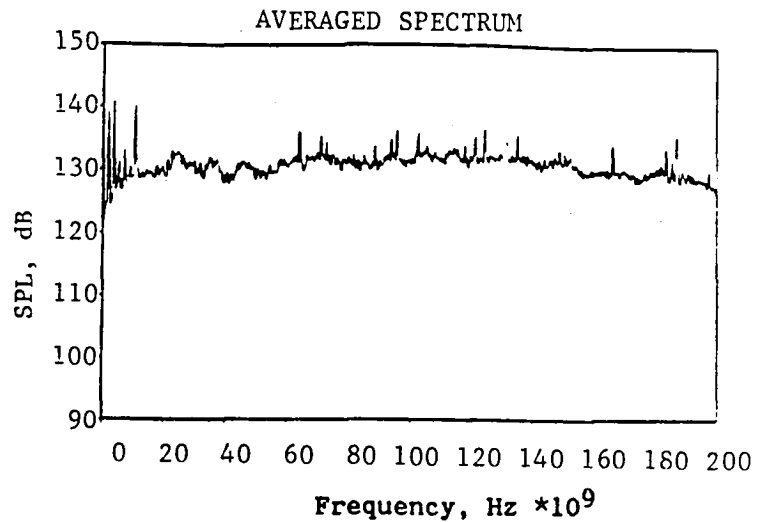
Figure 5-28.   BMT Results for JT15D Outdoor Test (no ICS) at Engine Speed
of 10,500 RPM.

AVERAGED SPECTRUM

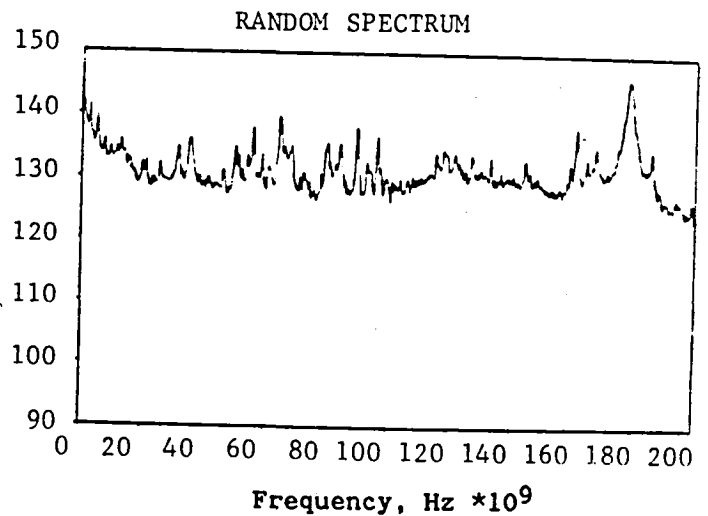BMT 'H-K'
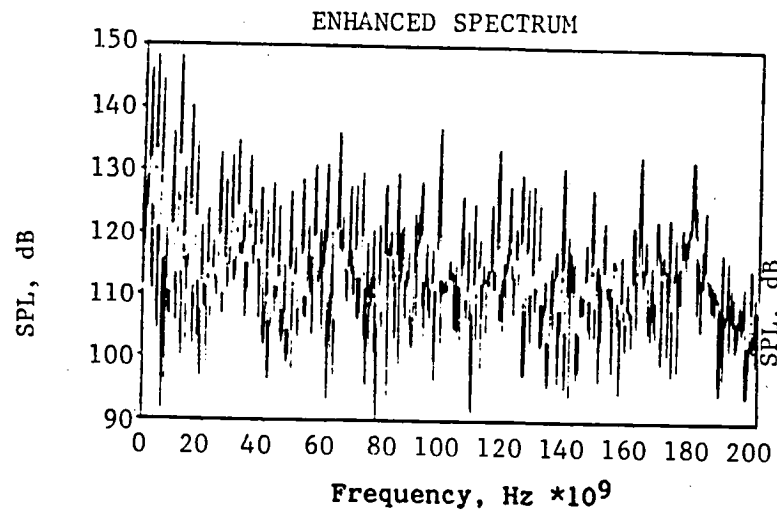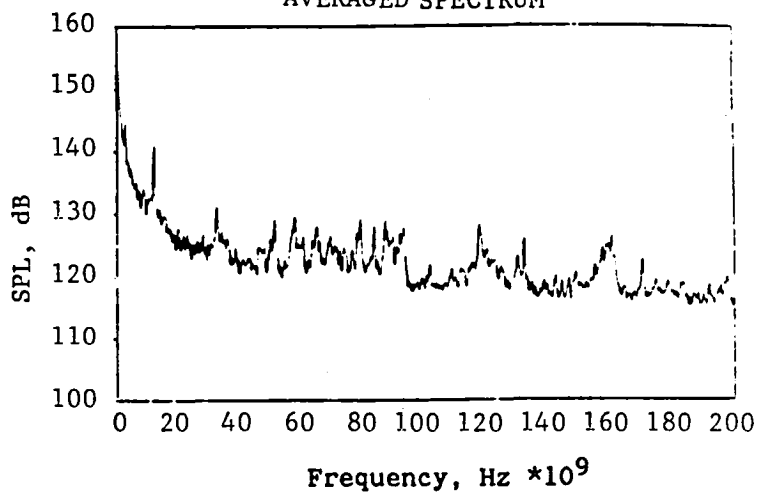JT15D-1 AMES OUTDOOR TEST
DATE: 24-APR-80.
FAN SPEED = 10,500 RPM

Frequency, Hz *10⁹

ENHANCED SPECTRUM

Frequency, Hz *10⁹

RANDOM SPECTRUM

Frequency, Hz *10⁹

WAVEFORM

360°

STANDARD DEVIATION

360°
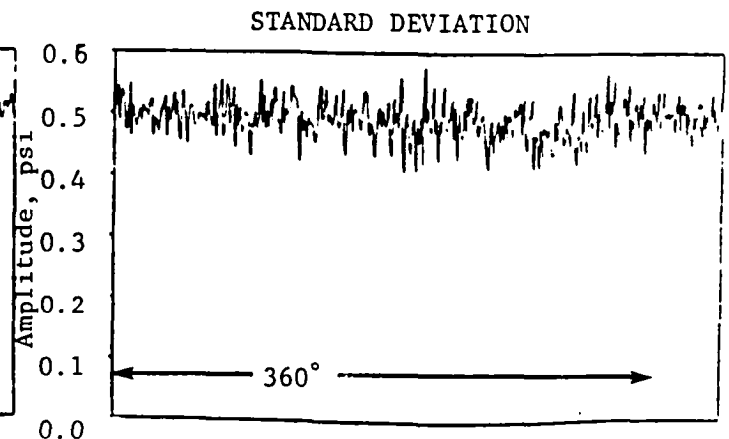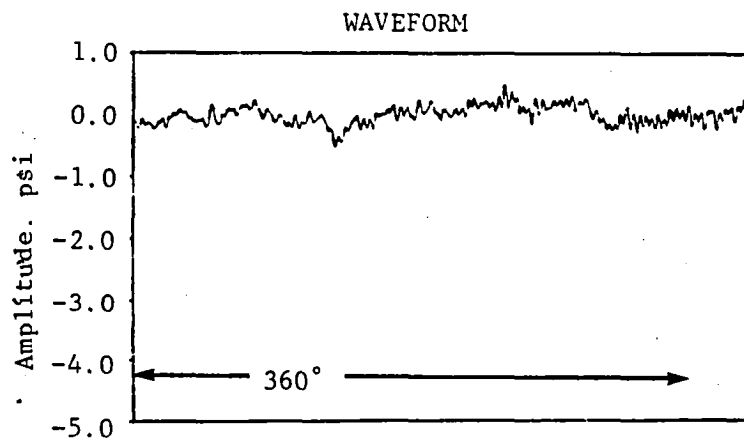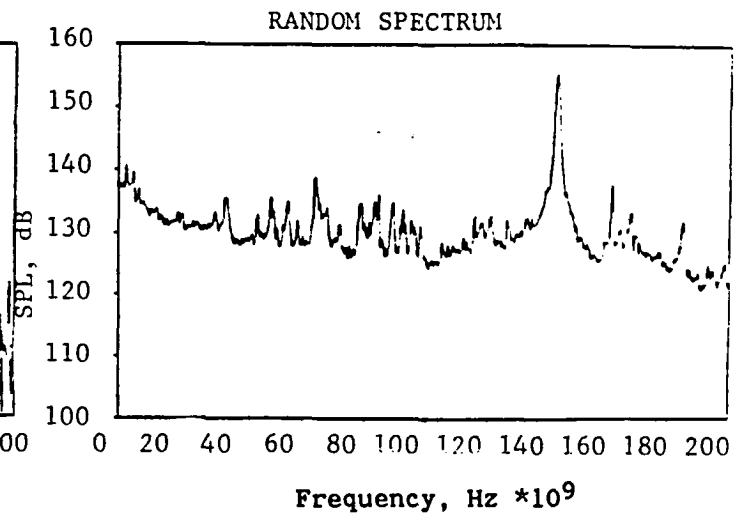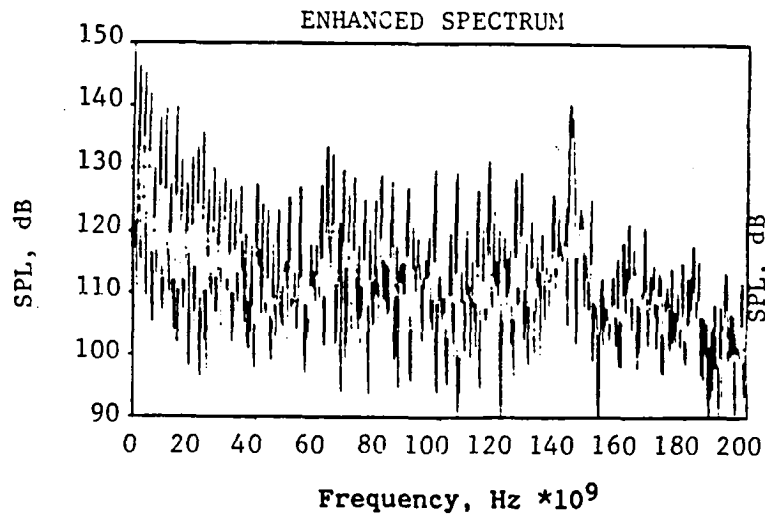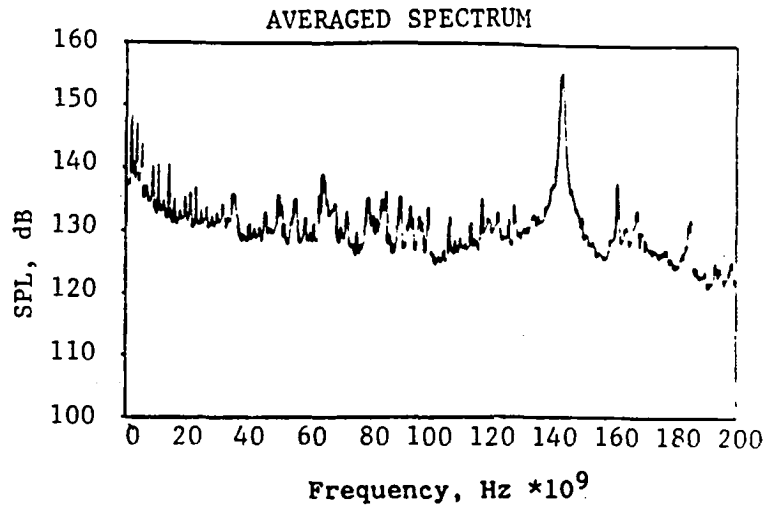
Figure 5-29.   BMT Results for JT15D Outdoor Test (TCS) at Engine Speed
of 10,500 RPM.

123

AVERAGED SPECTRUM

BMT 'H-K'
JT15D-1 AMES OUTDOOR TEST
DATE: 23-APR-80.
FAN SPEED = 11,500 RPM

ENHANCED SPECTRUM

RANDOM SPECTRUM

WAVEFORM

STANDARD DEVIATION
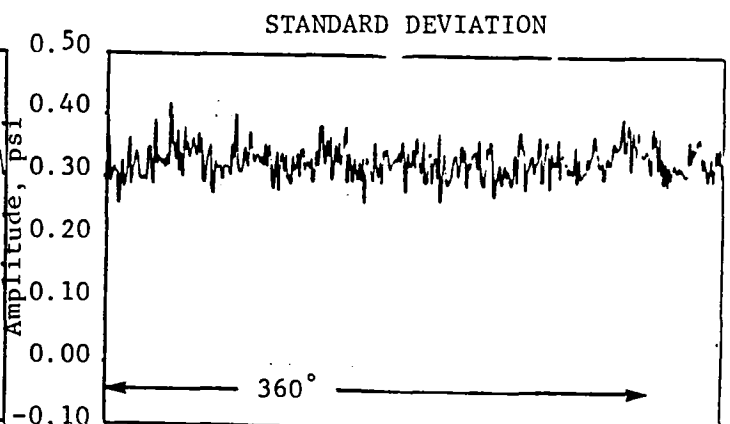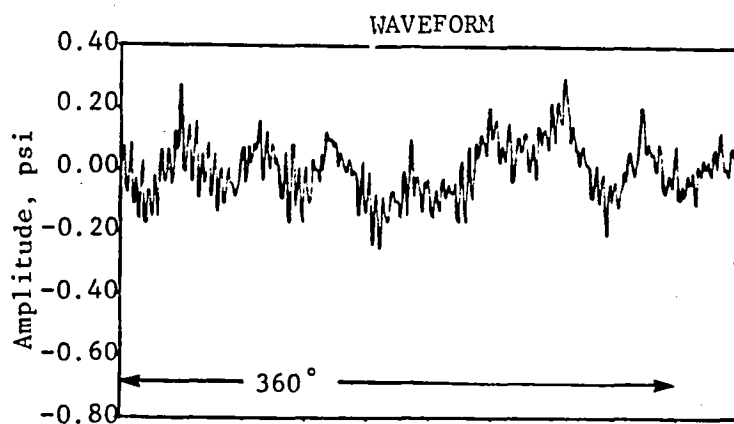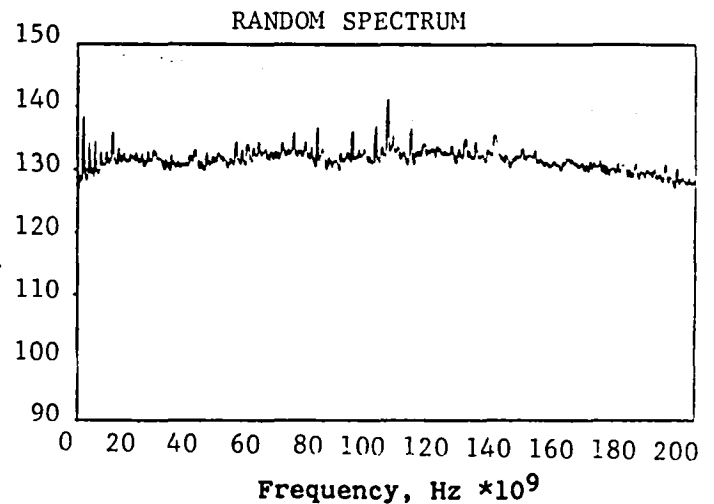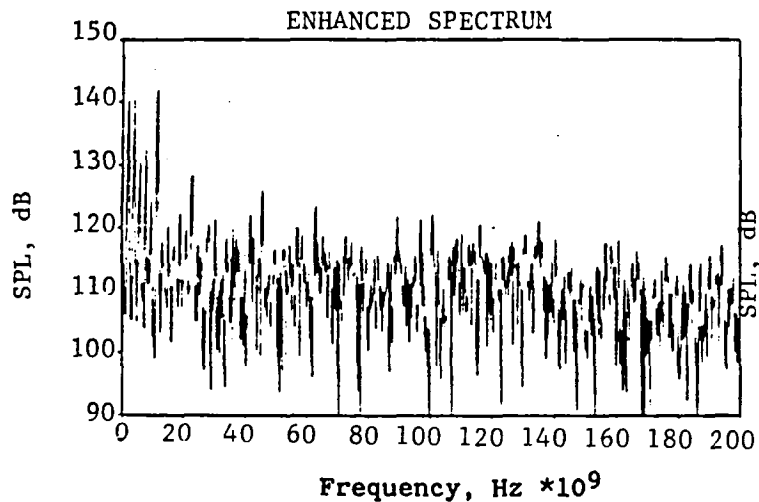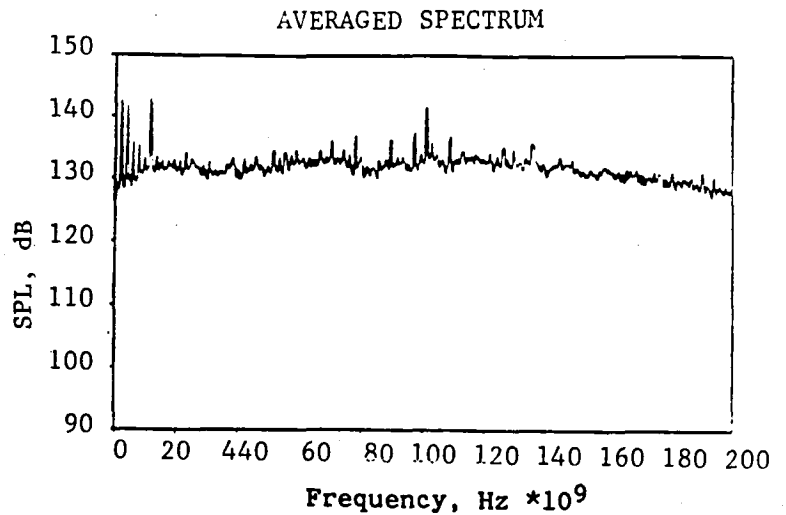
Figure 5-30. BMT Results for JT15D Outdoor Test (No TCS) at Engine Speed of 11,500 RPM.

AVERAGED SPECTRUM

BMT 'H-K'

JT15D-1 AMES OUTDOOR TEST

DATE: 24-APR-80.

FAN SPEED = 11,500 RPM
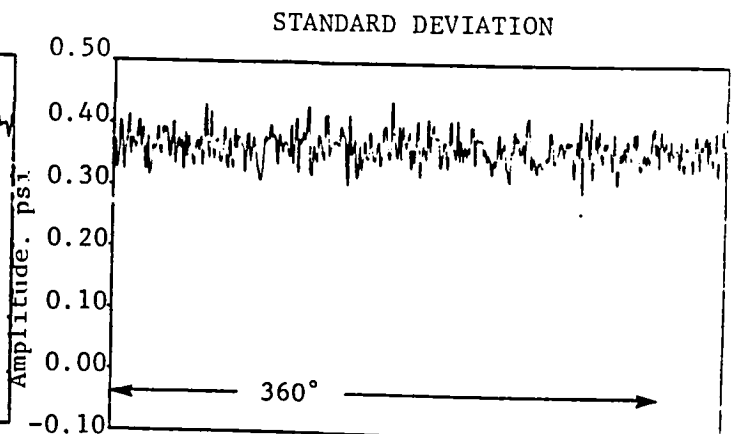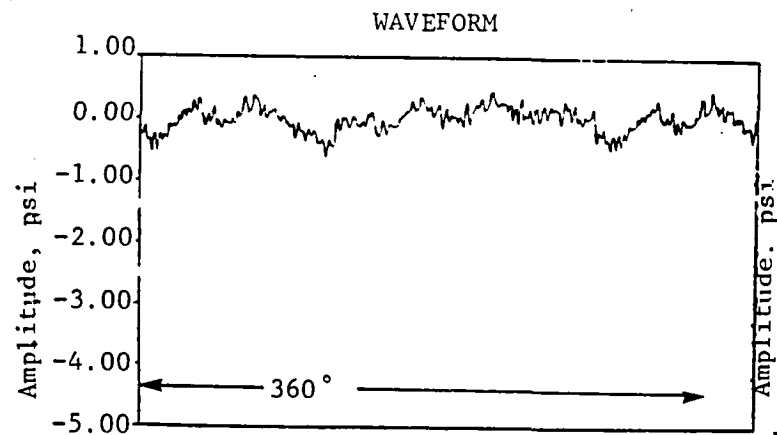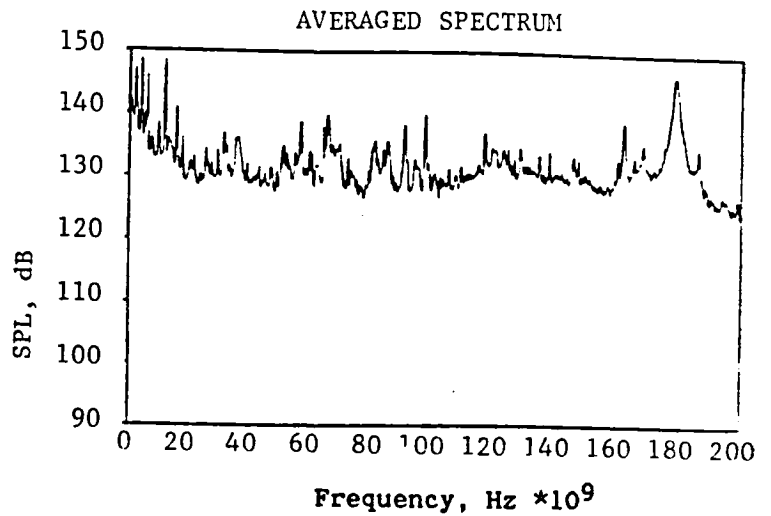
ENHANCED SPECTRUM

RANDOM SPECTRUM

WAVEFORM

STANDARD DEVIATION

Figure 5-31. BMT Results for JT15D Outdoor Test (TCS) at Engine Speed of 11,500 RPM.

AVERAGED SPECTRUM

ENHANCED SPECTRUM

RANDOM SPECTRUM

WAVEFORM

STANDARD DEVIATION

BMT 'H-K'

JT15D-1 FLIGHT TEST #2

WALLOPS ISLAND. OV-1B

DATE: 12-JUN-81.
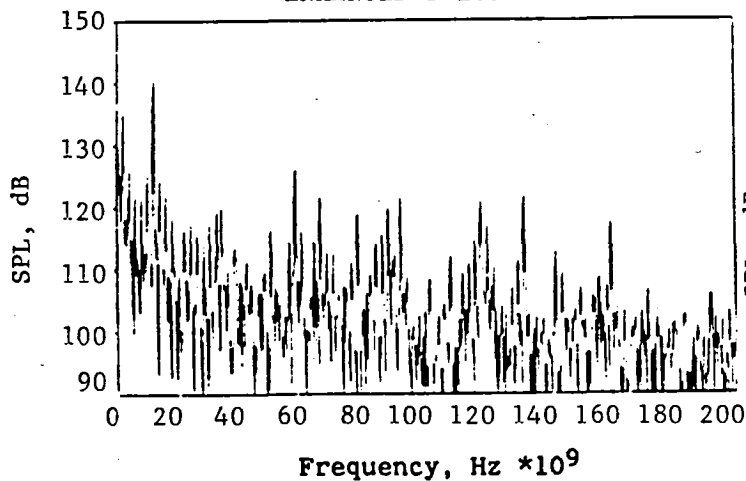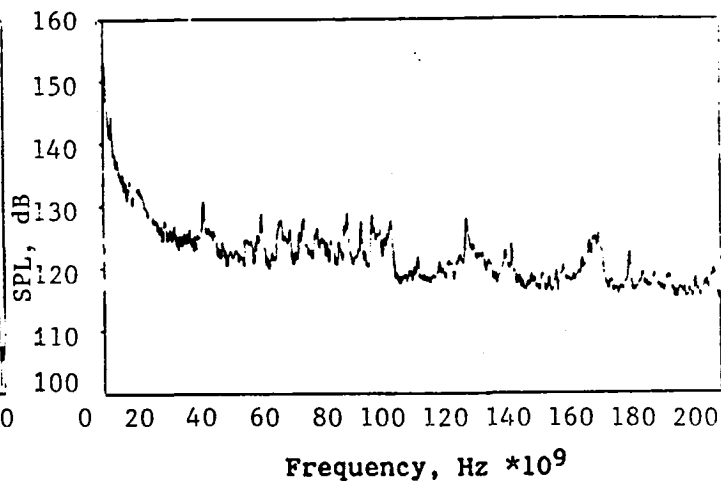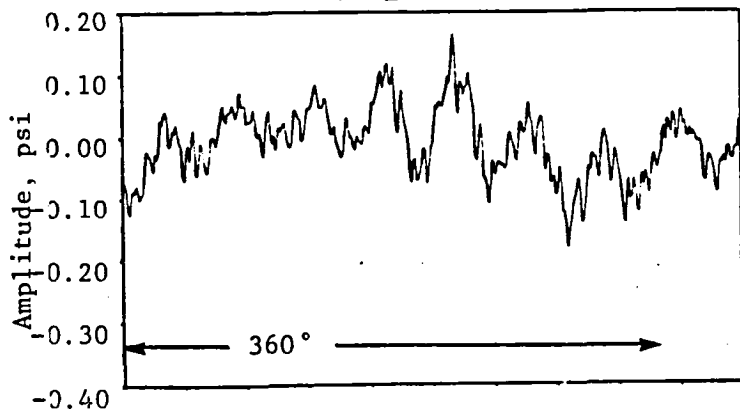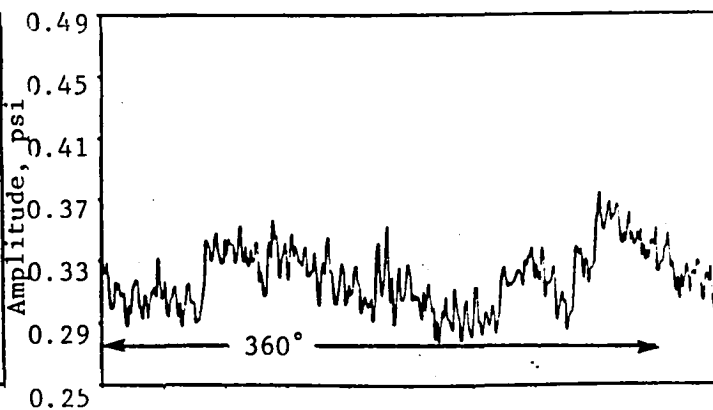
FAN SPEED = 11,924 RPM

Figure 5-32. BMT Results for JT15D Flight Test at Engine Speed 11,924 RPM.

AVERAGED SPECTRUM

BMT 'H-K'

JT15D-1 LANGLEY/AMES TUNNEL
TEST

RUN 551-7. VO = 60 KTS
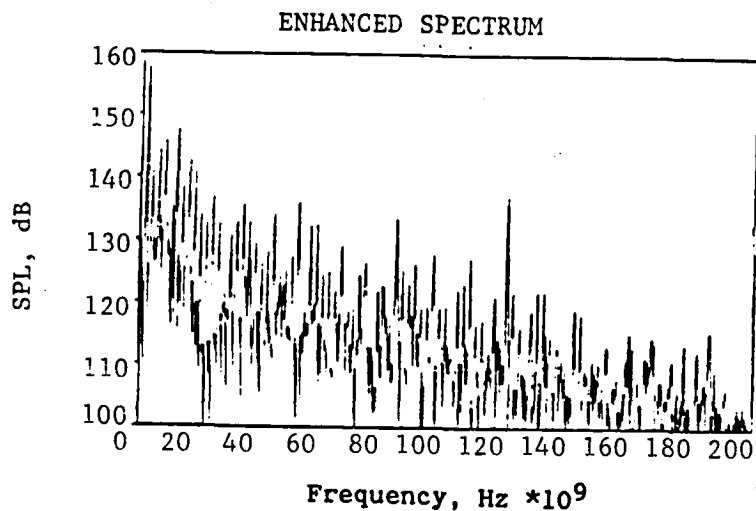
DATE: 15-MAR-80.

FAN SPEED = 12,000 RPM

ENHANCED SPECTRUM

RANDOM SPECTRUM

WAVEFORM

STANDARD DEVIATION
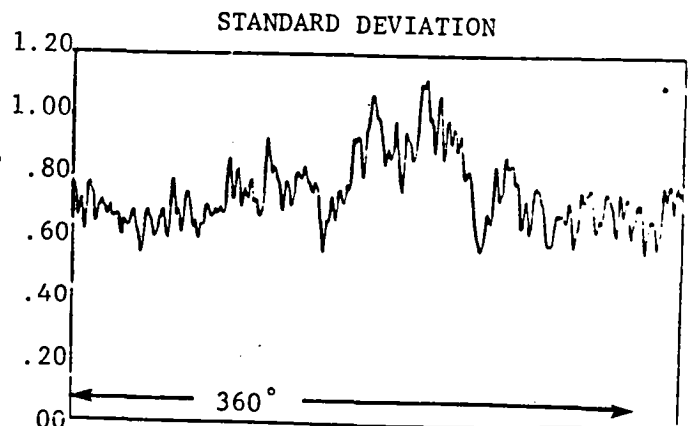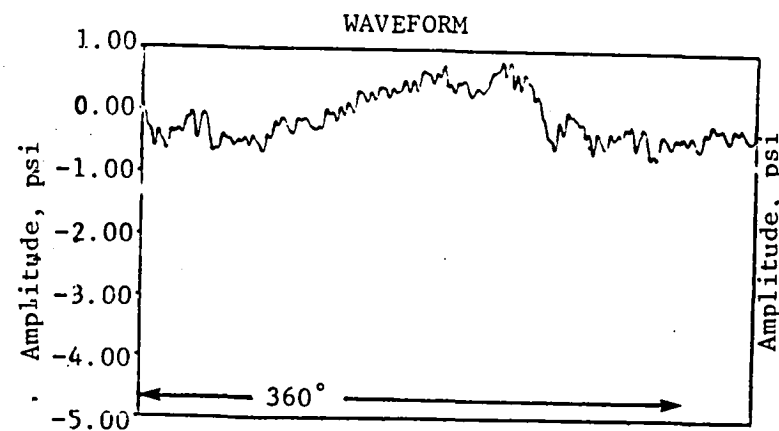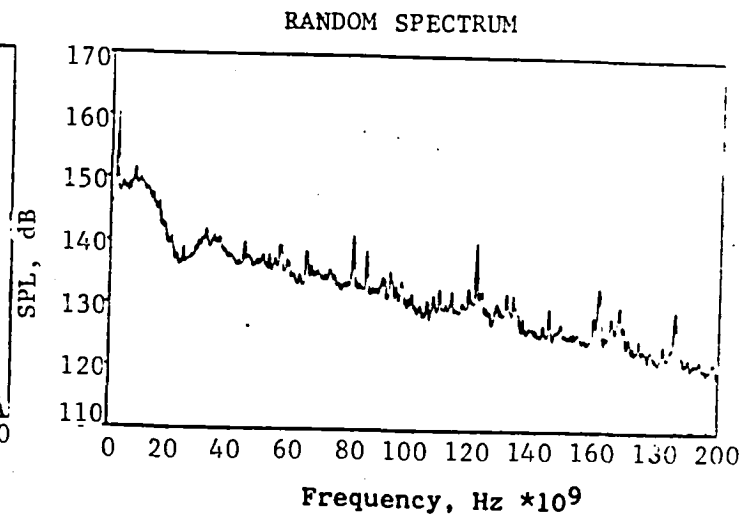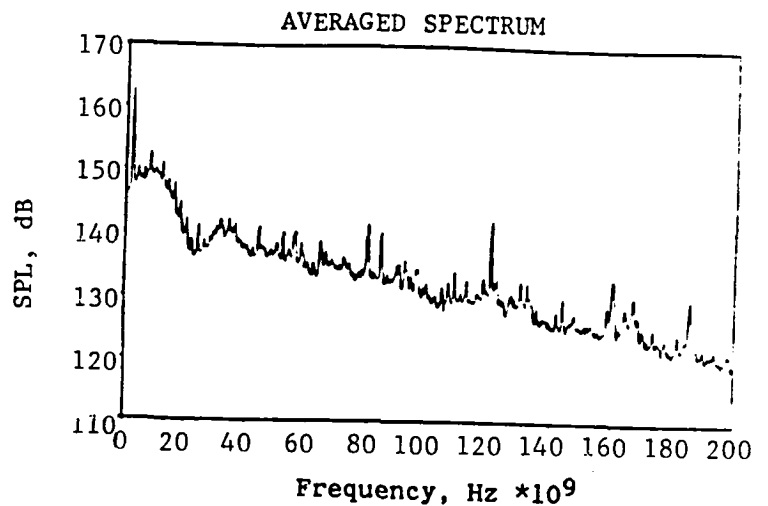
Figure 5-33.   BMT Results for JT15D Wind Tunnel Test at Engine Speed of
12,000 RPM.

AVERAGED SPECTRUM

BMT 'H-K'

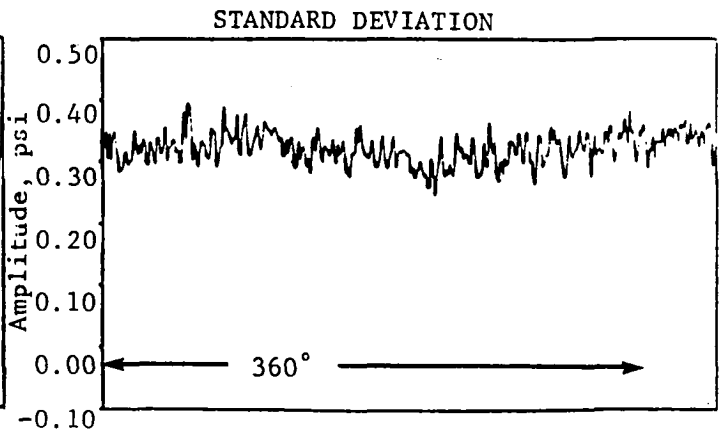JT15D-1 AMES OUTDOOR TEST

DATE: 23-APR-80.

FAN SPEED = 12,000 RPM

ENHANCED SPECTRUM

RANDOM SPECTRUM

WAVEFORM

STANDARD DEVIATION
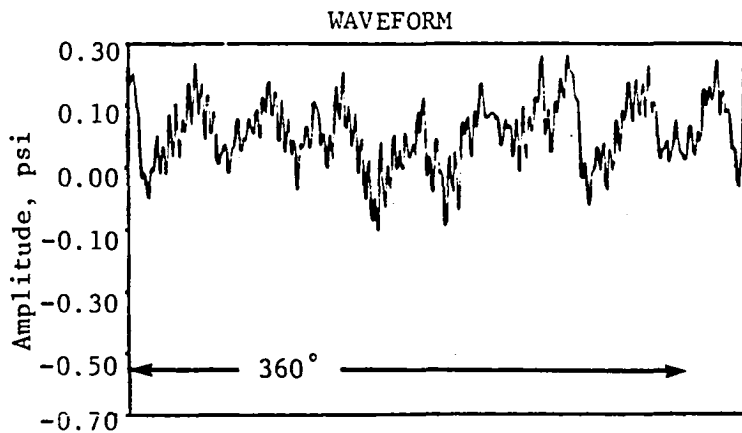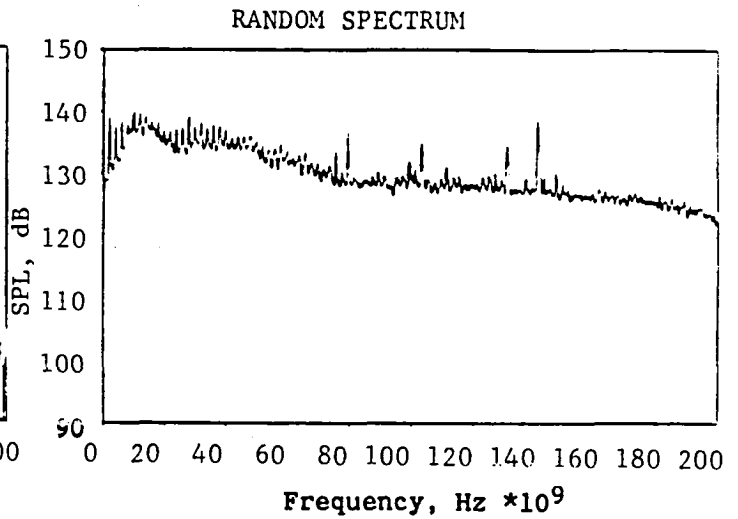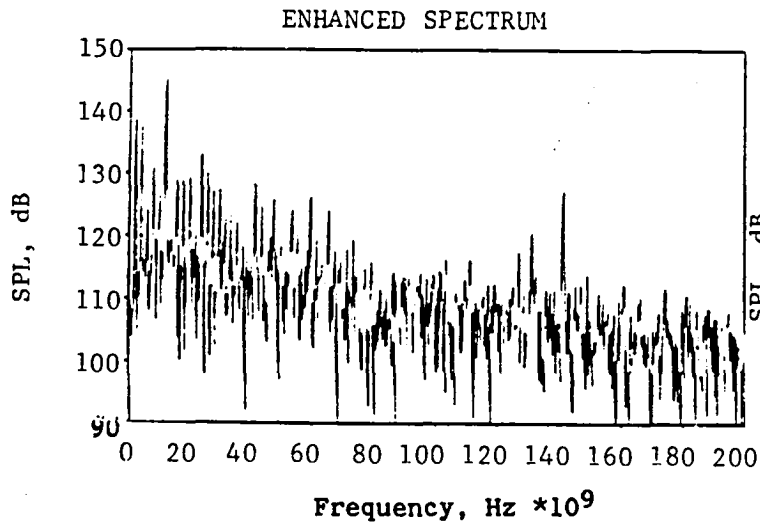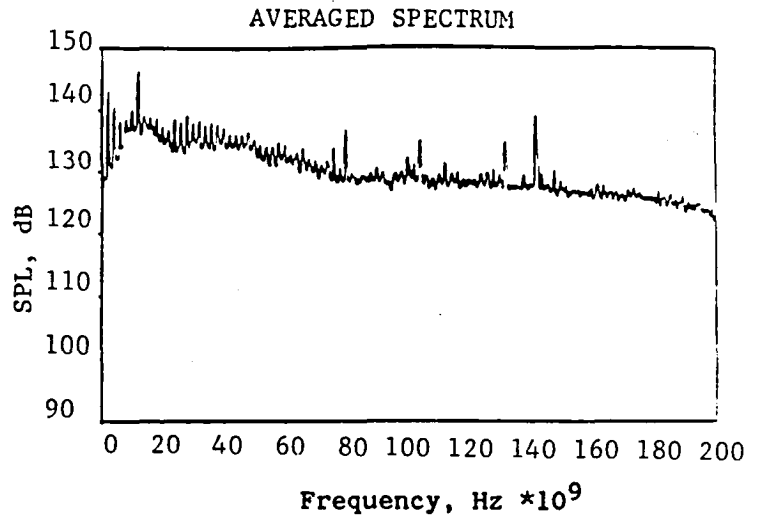
Figure 5-34. BMT Results for JT15D Outdoor Test (no TCS) at Engine Speed of 12,000 RPM.
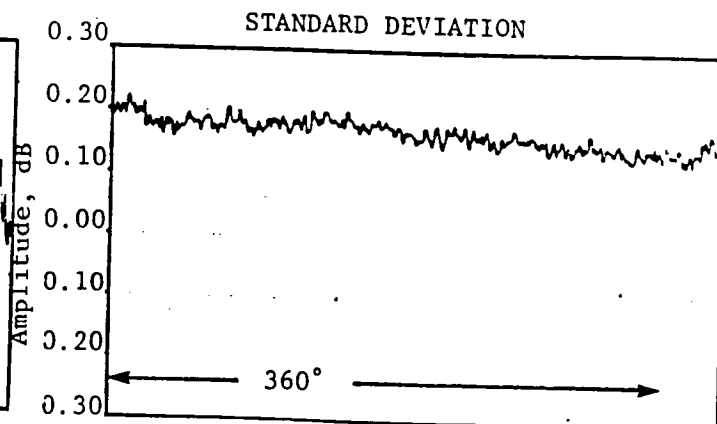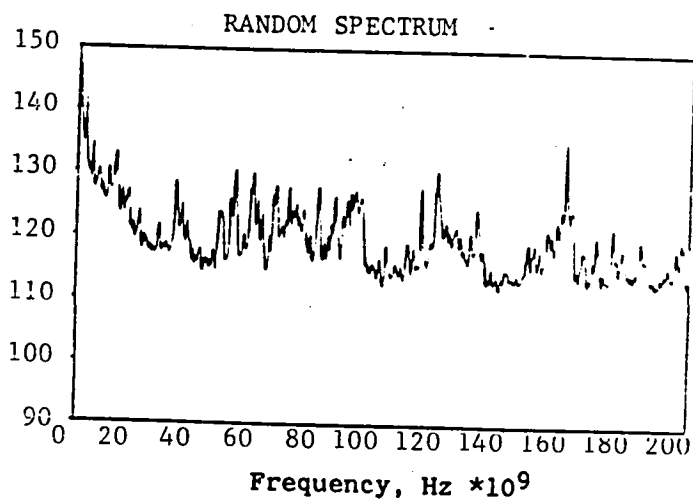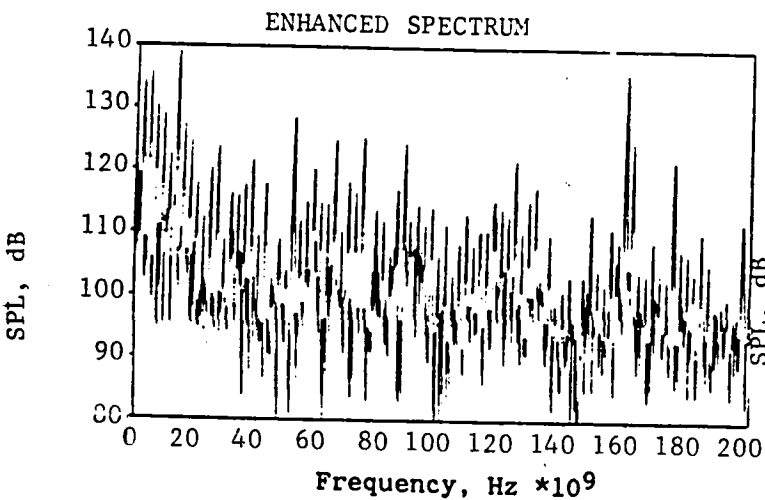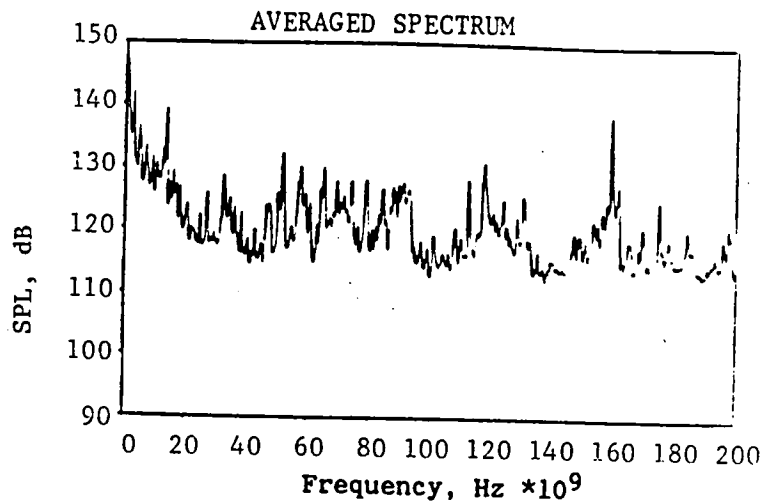
Figure 5-35. BMT Results for JT15D Flight Test at Engine Speed of 13,403 RPM.

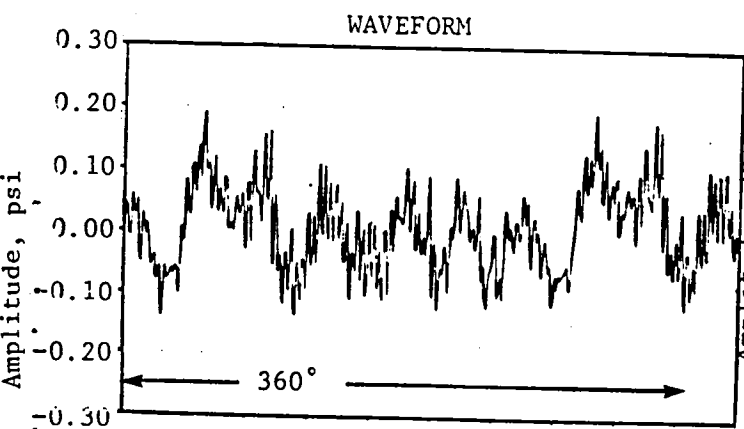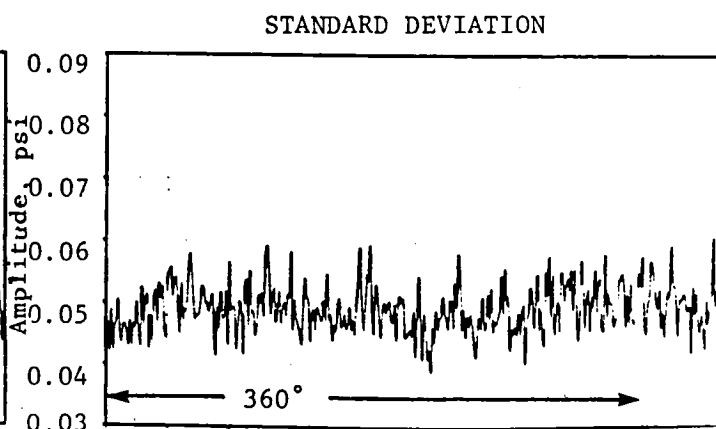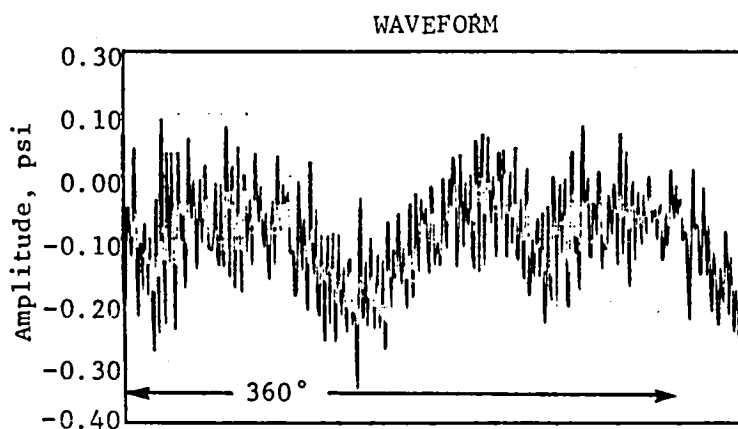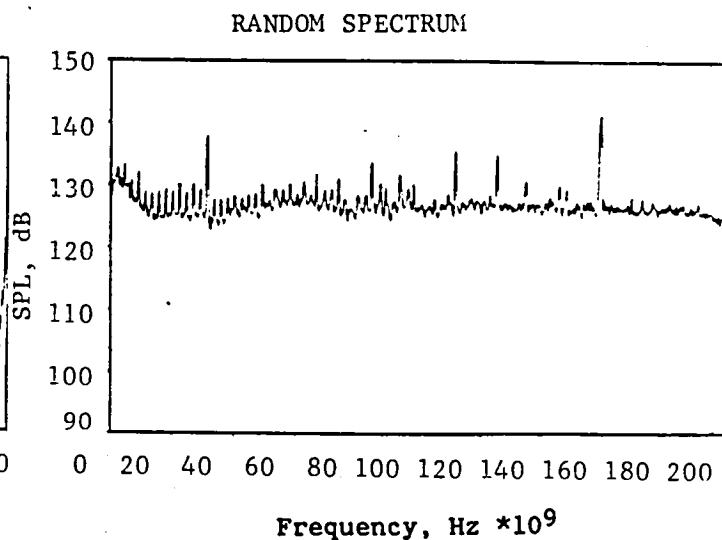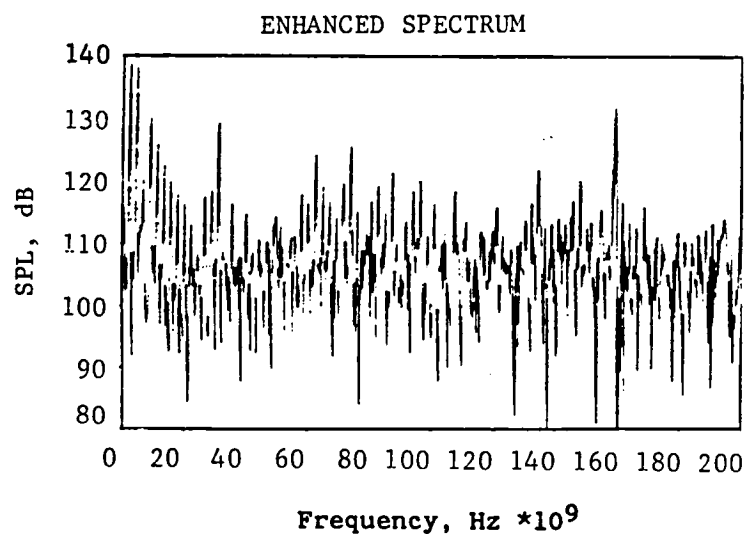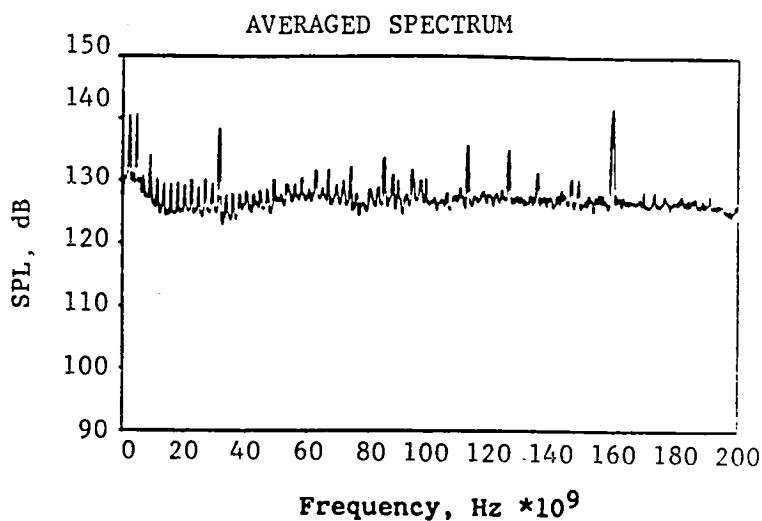Figure 5-36. BMT Results for JT15D Outdoor Test (no TCS) at Engine Speed of 13,500 RPM.
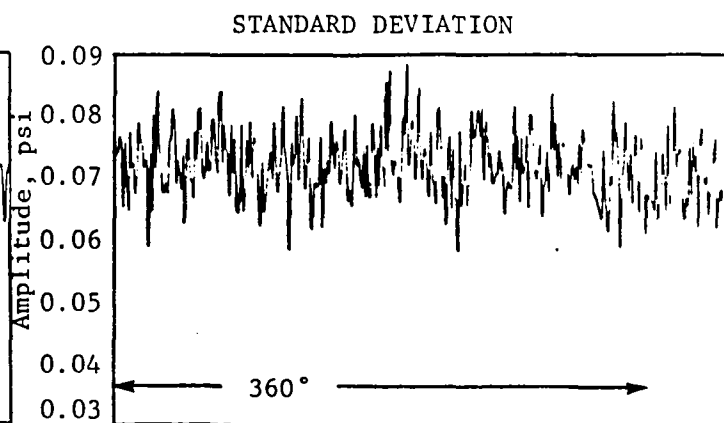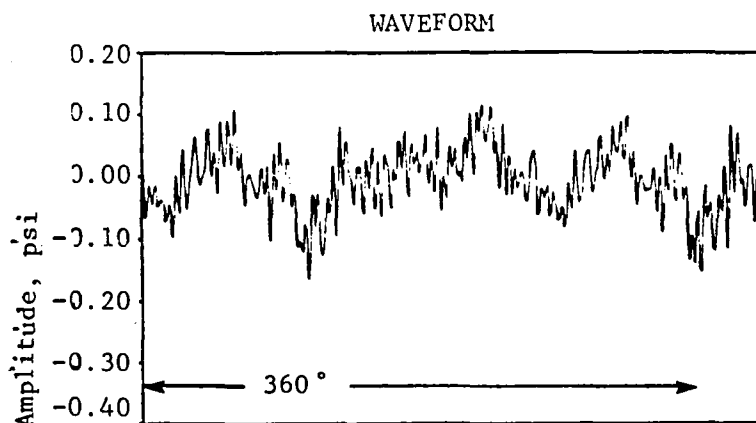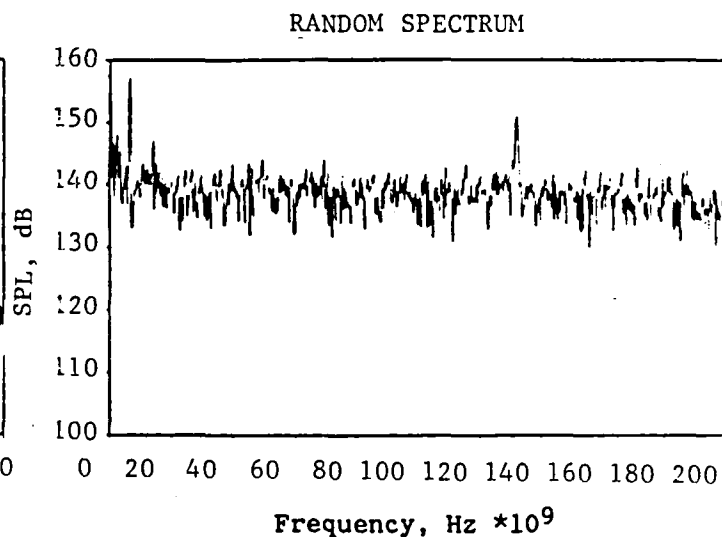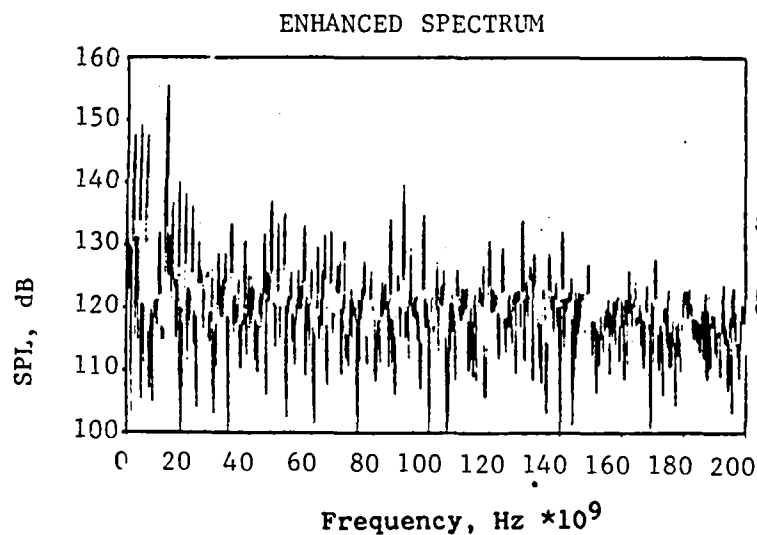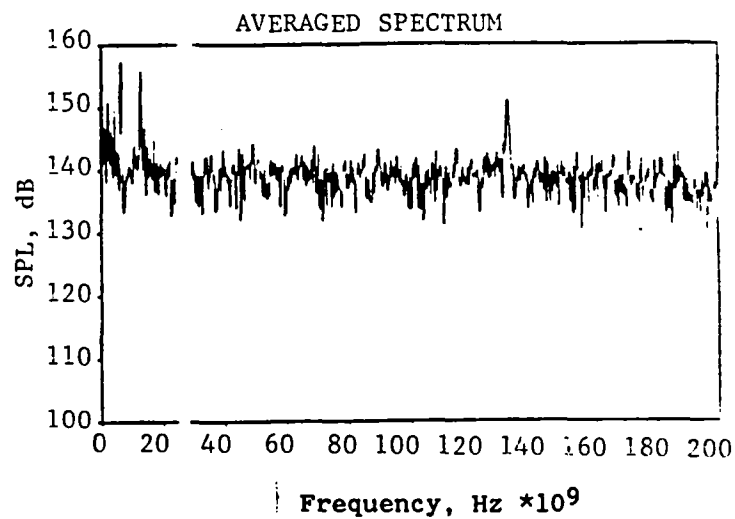
Figure 5-37. BMT Results for JT15D Outdoor Test (TCS) at Engine Speed of 13,500 RPM.

131

in some instances has been related to non-uniform flow conditions
(Reference 5-5). However, for the particular data sets being analyzed,
non-uniform flow conditions were monitored closely and did not exist during
any of the tests.

An interesting feature noted from the BMT results, Figure 5-27, is the
existence of relatively strong frequency components corresponding to the one
per revolution and six per revolution values in the random spectrum. This
feature indicates that the periodic components observed in the enhanced
spectrum are not purely sinusoidal at this speed condition. Thus, at subsonic
speeds a portion of the acoustic radiated energy may be modulated in strength
due to its non-periodic nature. A more detailed discussion of BMT results for
individual transducers is contained in Reference 5-6.

Another interesting feature of the BMT results is comparing the
waveforms and standard deviations for Figures 5-30 and 5-31 where TCS and
non-TCS cases are presented respectively for an engine speed of 11,500 RPM.
Significantly higher standard deviations for the non-TCS case compared to the
TCS case are noted. The enhanced spectrum for the TCS case also displayed
much more high frequency periodic activity than the enhanced spectrum for the
non-TCS case. These effects influence the projected tone energy from the BMT
results as shall be shown in Section 7.0.

SECTION 6.0

TONAL PREDICTION METHODS AND PROCEDURES

6.0 TONAL PREDICTION METHODS AND PROCEDURES

In the generation and radiation of tones with frequencies proportional to the fundamental and harmonics of blade passing fequencies, the noise sources are usually the unsteady aerodynamics fields induced on the rotating blades and vanes. Several mechanisms contribute to such unsteady forces depending on fan geometry. From a noise control point of view, it is relevant to know which mechanism is dominant. The aerodynamic field over a blade or vane becomes unsteady when the angle of incidence is unsteady.

For a rotor blade, a time dependent angle of incidence can be due to

- circumferential non-uniformity of the mean flow and

- presence of turbulence in the inlet flow field including turbulence in the boundary layer.

Inlet mean flow distortion can be caused by inlet droop, suction of large scale vortex structure (for static tests without inflow control structures), the potential flow fields of stator vanes, struts and pylons, and wakes of intrusive elements in the inlet.

For a stator vane, a time dependent angle of incidence is associated with the rotating wakes of the rotor blades and associated turbulence. The angle of incidence variation usually has a periodic and a random component.

The efficiency of acoustic radiation by the unsteady aerodynamic forces is not only a function of the amplitude but also of the relative phase from blade to blade (or vane to vane) and of the coherence (chordwise and spanwise) for each blade or vane. The unsteady aerodynamic forces excite spinning and radial duct modes whose amplitude and relative phase distribution is dependent on the above mentioned phase and coherence distributions. The level and directivity of the noise radiated to the farfield depend on the propagation and radiation properties of the modes and their relative amplitude and relative phase distributions.

6.1   PERIODIC ACOUSTIC SOURCE EVALUATION

In the generation and radiation of tones proportional to blade passing frequencies, several mechanisms are known to exist within the fan and compressor. Some of these are:

1.   rotor/turbulence interaction,

2.   rotor/inflow distortion interaction,

3.   rotor/casing boundary layer interaction,

4.   rotor wake/stator interaction,

5.   rotor interaction with potential field of downstream vane rows, struts and pylons,

6.   rotor-alone source including the phenomenon of multiple pure tone (MPT), and

7.   scattering by a rotating blade row of acoustic fields generated downstream of rotating blade row.

Except for item 7, each one of the above noise sources has its origin in the unsteady aerodynamic force induced on the blades or on the vanes, due to modification in the angle of the incident flow field. Of this unsteady aerodynamic pressure fluctuation, only a fraction is emitted upstream and downstream as acoustic waves. This fraction is what is commonly known as aeroacoustic efficiency; it is a function of not only the amplitude and phase distribution of the aerodynamic fluctuating field but also of the aeroacoustic properties of duct modes.

A blade mounted transducer responds to the unsteady pressure field which comprises not only the local unsteady aerodynamic field (of which only a fraction corresponds to the acoustic field of the local source) but also to acoustic fields emitted from other sources. However, it may be expected that contribution of the local unsteady aerodynamic field would be dominant.

134

In the analytical modelling of noise emission from unsteady aerodynamic fields, it is the unsteady lift (that is, the differential pressure between the suction and pressure side of the blade) that is relevant. Such unsteady lift is usually decomposed into unsteady thrust and unsteady torque components. Each component couples somewhat differently to the acoustic fields.

The specific objective of this section is to describe the methodology for fan tone noise source identification and decomposition of the farfield, by on-Rotor Blade and Stator Vane Mounted Instrumentation Data Analysis and Application of Theoretical Modelling Concepts. The approach adopted is the following:

- Develop Blade Mounted Transducer (BMT) data analysis techniques to provide input parameters for existing fan source noise mechanism models

- Predict farfield noise radiation pattern and compare with farfield acoustic measurement

- Evaluate hypotheses and assumptions made to achieve prediction.

The fundamental areas addressed in the succeeding subsections shall be for periodic acoustic source mechanisms, turbulent (random) acoustic source mechanisms, rotor-stator interaction noise, and radiation modelling.

The fundamental hypothesis used to achieve predictions of the periodic portion of the acoustic source is that the differential pressure (ΔP) measured on the blade is equal but opposite to the fluctuating force per unit area applied to the fluid at this location. Thus, the thrust and torque components can be directly obtained by multiplying the measured pressure (ΔP) by the local blade stagger angle components at the measurement location. The total pressure applied to the fluid becomes an integral over the blade surface as is indicated in Reference 6-3. This integral is approximated by obtaining spanwise and chordwise correlation lengths using a coherence function technqiue. The signals from two blade mounted transducers

135

on opposite sides of a rotor blade (H and K) are directly differenced in the time domain. This signal is then digitized and stored for processing using the enhancement procedure described in Subsection 5.4.

The coherence between individual transducers (H-J), (H-I), and (H-G) are used to estimate correlation lengths as follows:

$$\text{Spanwise Correlation Length} = d_{H-I} * C_{H-I} + d_{H-G} C_{H-G}$$
$$\text{Chordwise Correlation Length} = d_{H-J} * C_{H-J}$$

where the d refers to the distance between transducers and the C refers to the coherence value determined via analysis of the signals. The physical locations of the transducers H, I, J and G is shown schematically in Figure 3-24. These lengths are multiplied by the H-K enhanced pressure levels to yield the sound power level at the source.

The measurement of the spanwise and chordwise distributions of the actual unsteady pressure field is desirable and requires several blade mounted transducers on the pressure and suction sides. However, due to the limited number of permissible transducers, it was judged that location represented a reasonable compromise being neither in the outer wall boundary layer nor too close to the hub.

The phase between transducers H and J is illustrated in Figure 6-1 where the slope at high frequencies indicated an acoustic wave whereas at lower frequencies the lower slope corresponds to aerodynamic time delays hence the assumptions made are believed to be adequate for these predictions.

This procedure yields the harmonic BMT power level components from which circumferential mode power level components are computed. The assumption is made that only the lowest order radial mode is present which is a reasonable approximation for high circumferential modes close to cut-on. In general, much of the circumferential mode energy is transported via these higher order circumferential modes.
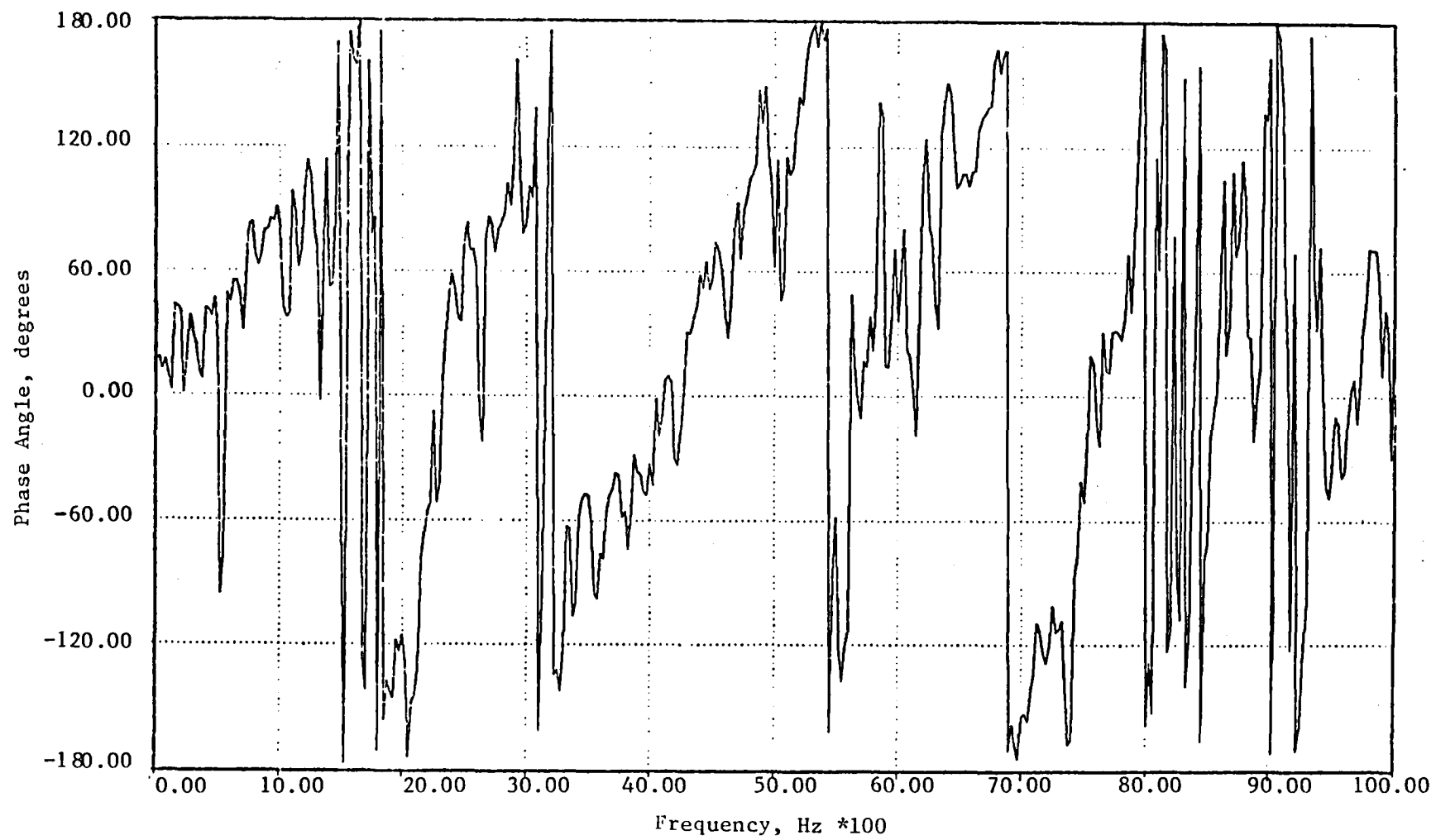
Figure 6-1.   Phase Angle Plot between BMT "H" and BMT "J".

6.2   TURBULENT (RANDOM) ACOUSTIC SOURCE EVALUATION

The interaction of the fluid turbulence with the rotating blade also produces noise. The analytical models appropriate to this problem are documented in References 6-2 and 6-3 where the random turbulence components required for input to the analytical models are those based on pitch line quantities. It was felt that the measurements obtained on Blade Mounted Transducer G (BMT G) were most representative of the required input.

The inputs required to these models (refer to Figure 6-2) are the turbulent axial length scale (ℓ_a) and transverse length scale (1_t) and the axial and transverse turbulent intensity (u'_a and u'_t). In addition, details of fan geometry and flow condition are necessary. The methodology utilized to estimate these quantities was as follows:

- Estimate ℓ_a from correlation of BMT G in the axial direction.

- Estimate ℓ_t from previous experience as a function of the ratio of ℓ_a / ℓ_t.

- Estimate u'_a from a correlation to hot wire measurements of u'_a versus BMT G standard deviation ($\bar{\sigma}$) psi.

- Estimate u'_t from previous experience as a function of a ratio of u'_t / u'_a.

The results of these parametric derivations are presented in Figures 6-3 to 6-5. The values of u'_a / u_a are correlated versus $\bar{\sigma}$ psi in Figure 6-3 with the resultant values of $\bar{\sigma}$ shown for the other test cases. A sample determination of the length scales is shown in Figure 6-4(a) and 6-4(b) where the correlation length of BMT G for the outdoor TCS case and the Hot Wire non-TCS case are displayed. The BMT G length (ℓ_x is assumed to be representative of the hotwire length (ℓ_a) for these calculations. This equivalence was generally found to be acceptable when the BMT G signal was filtered to remove higher frequencies (>100 Hz). This finding is consistent with the phase plot shown in Figure 6-1 which illustrated that at low frequencies propagation was principally aerodynamic.
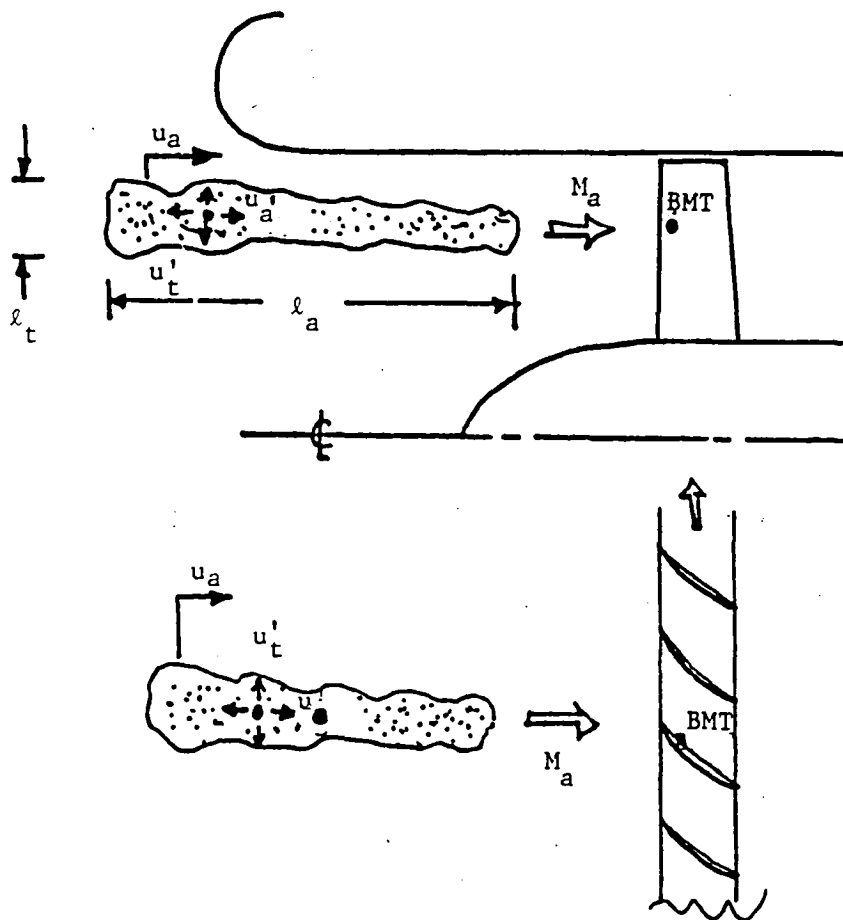
138

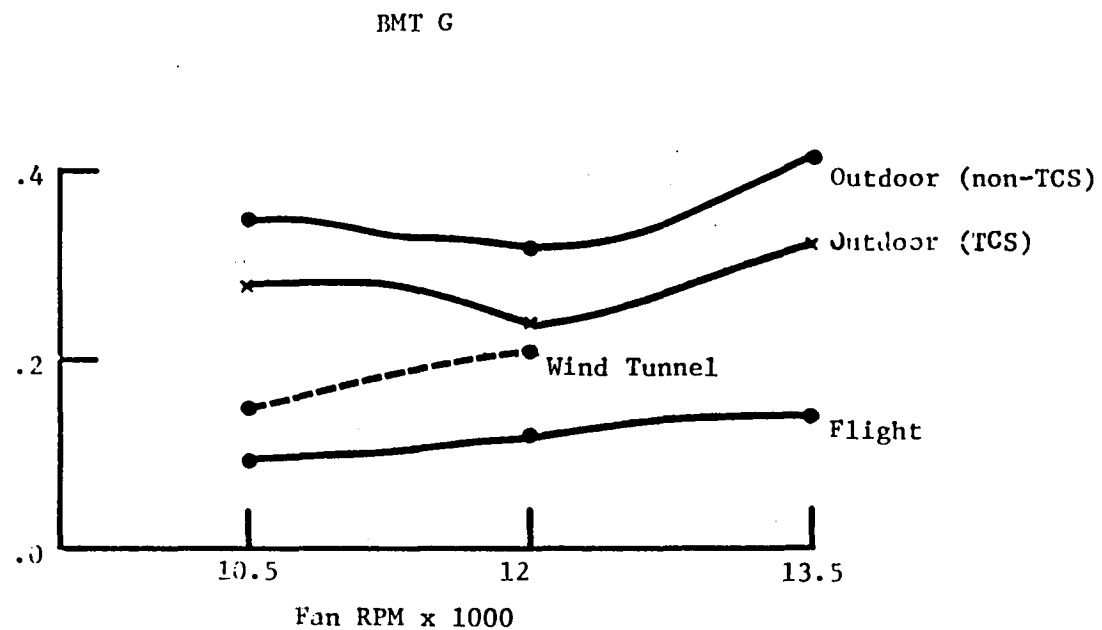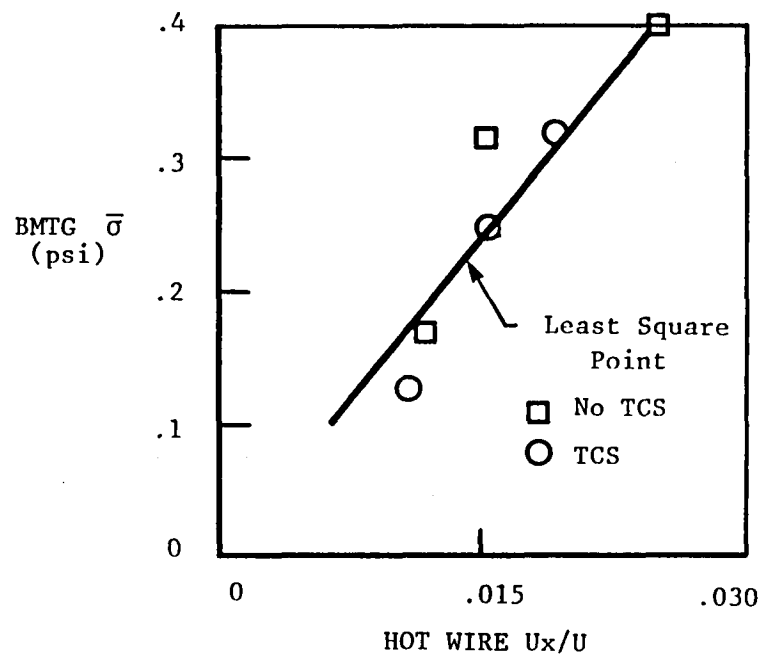Figure 6-2. Illustration of Parameters Required for Random Acoustic Source Evaluation.

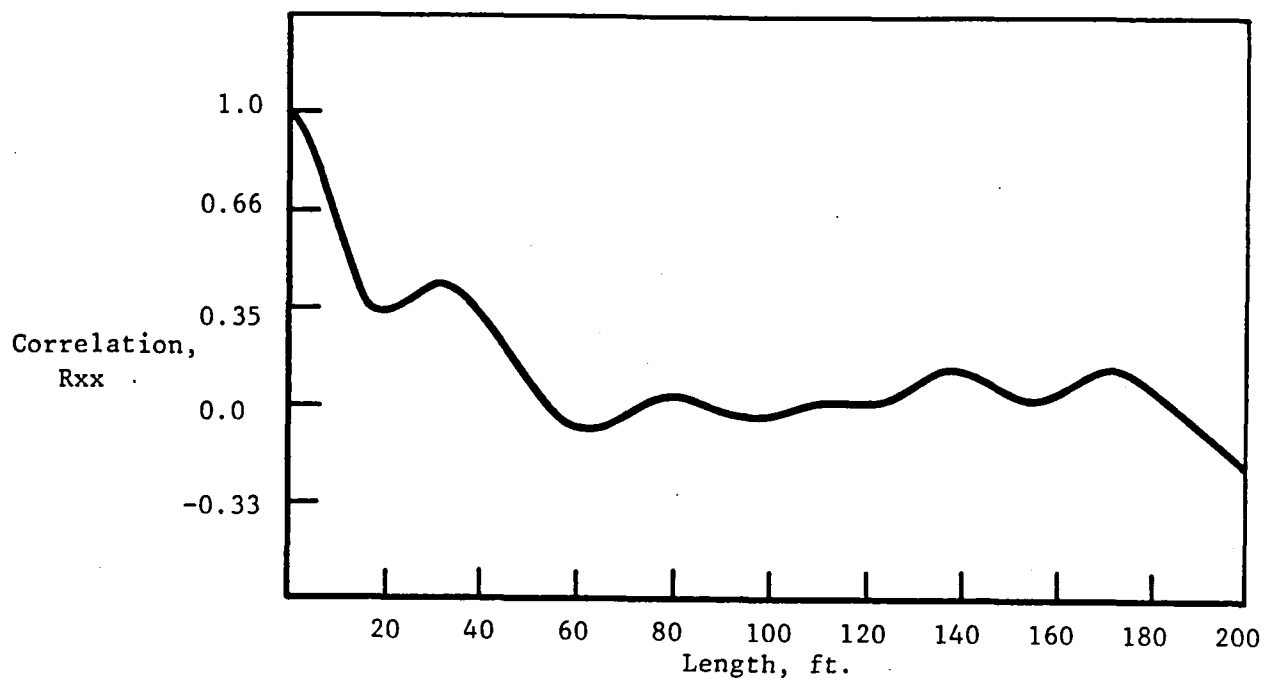Figure 6-3. BMT G $\overline{\sigma}$(psi) resulting with Correlation to Hot Wire U_a'/U_a.

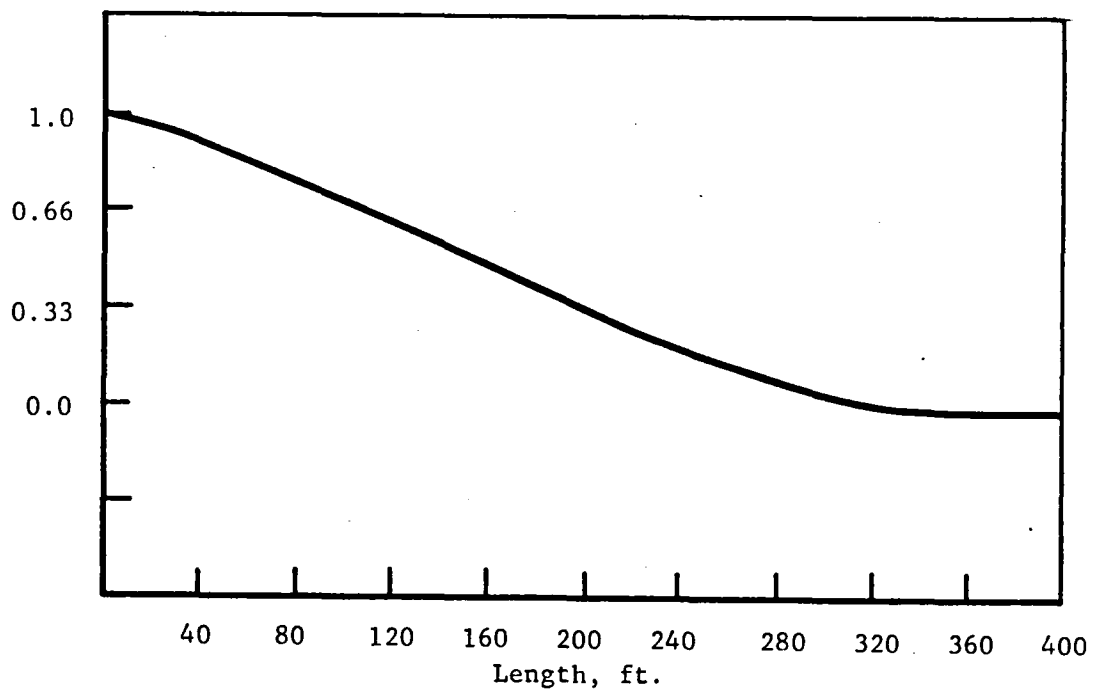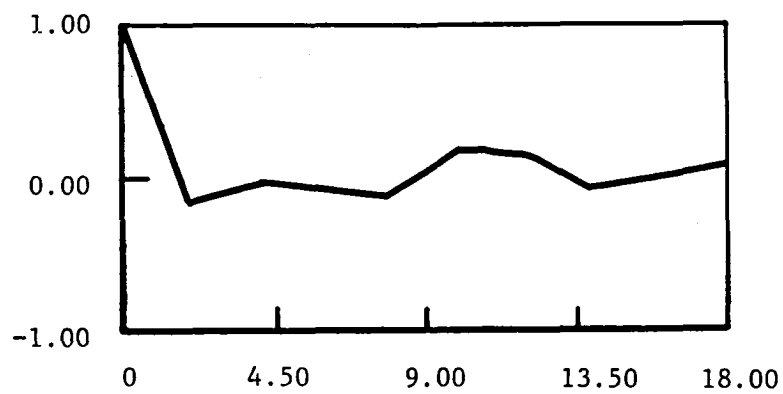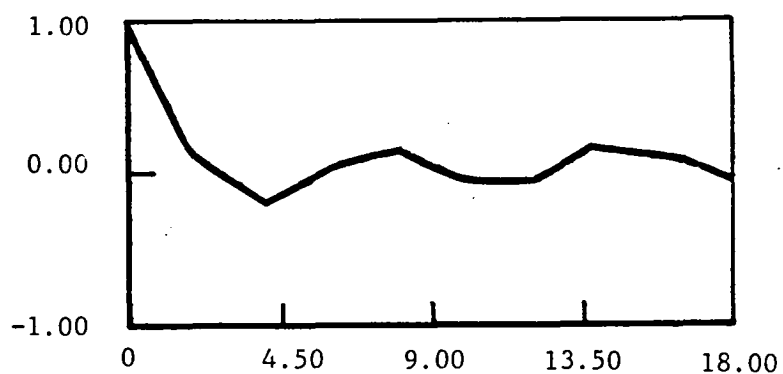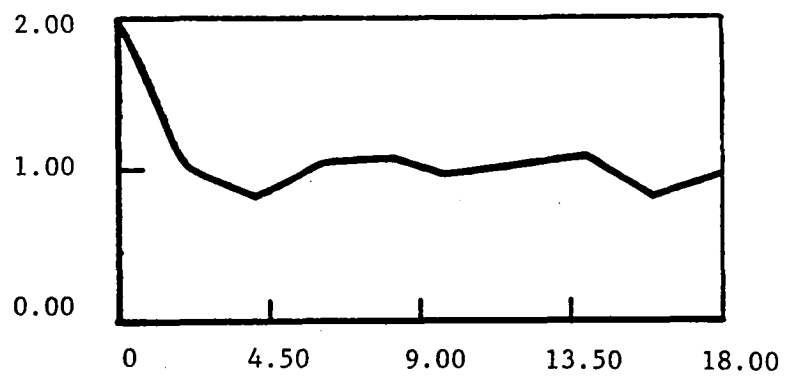Figure 6-4a.   BMT G Correlation for Engine Speed of 11,800 RPM.

Figure 6-4b.   Hot Wire Correlation for Engine Speed of 10,500 RPM.

(a) 10,500 RPM

(b) 12,000 RPM

(c) 13,500 RPM

Figure 6-5. BMT G Correlation Results for Various Engine Speeds.

The lengths scales utilized in the acoustic determinations to follow were assumed to be independent of speed based on results of correlations. In Figure 6-5, the correlation for BMT G for 3 speeds illustrate that this assumption has merit. It was found that considerable variation in length scale would occur circumferentially and many correlations were performed to select the largest length scale. An illustration of this variation is shown in Figures 6-6(a), (b), and (c) where carpet plots of the pressure variation of BMT G are displayed. These figures also generally show the difference in $\bar{\sigma}$ with various environment. Note that considerable masking of length scales is imposed because the data has not been filtered at 100 Hz. A summary of the length scale parameters used for the acoustic determinations is presented in Table 6-1.

TABLE 6-1

Environment	$\ell_x \sim \ell_a$	ℓ_x/ℓ_t
Flight	16'	200
Wind Tunnel	24'	300
Outdoor (TCS)	36'	300
Outdoor (No TCS)	180'	300

6.3   ROTOR-STATOR INTERACTION SOURCE EVALUATION

The evaluation of the acoustic source on the stator vane is accomplished in a manner similar to that on the blade. The differential pressure on the stator is determined from transducers F and D as indicated in Figure 6-7. The coherence between D and C and D and E is then used to determine a blade loading area to make a power estimate of the rotor-stator duct mode. In the JT15D case the 28 blades and 66 vanes introduce a 10th order circumferential duct mode. The stator data is displayed in Figure 6-8 with the prediction of the 2nd harmonic farfield directivity in Figure 6-9. The relative phase between the various locations on the stator are shown in Figure 6-10(a, b and c). These figures also show the variability of the waveform as the tip of the blade is approached. These influences can affect the farfield radiated directivity as shown in Reference 6-4.
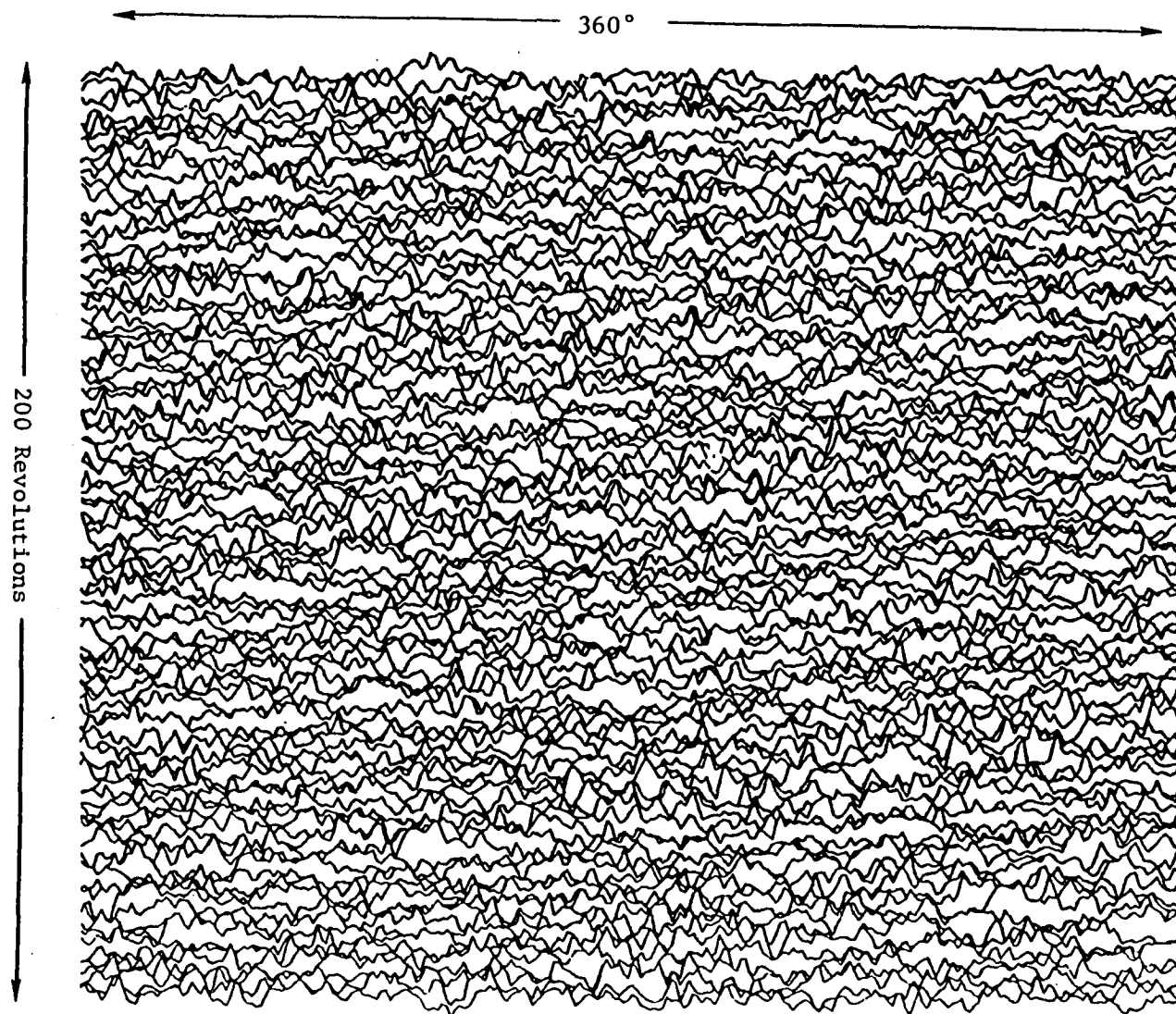
143

360°

200 Revolutions

144

Figure 6-6a. Outdoor BMT "G" (no TCS) at 12,000 RPM
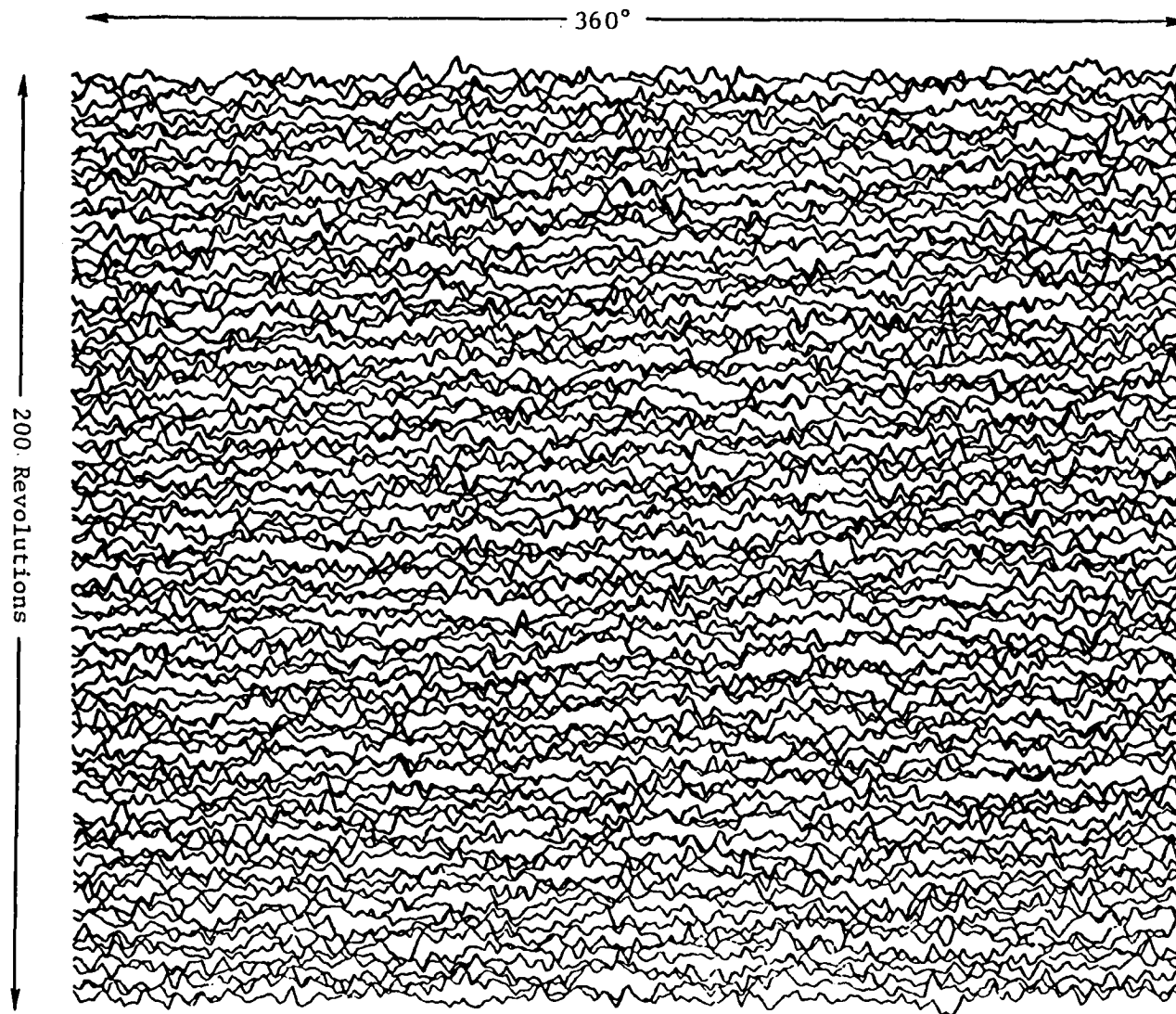
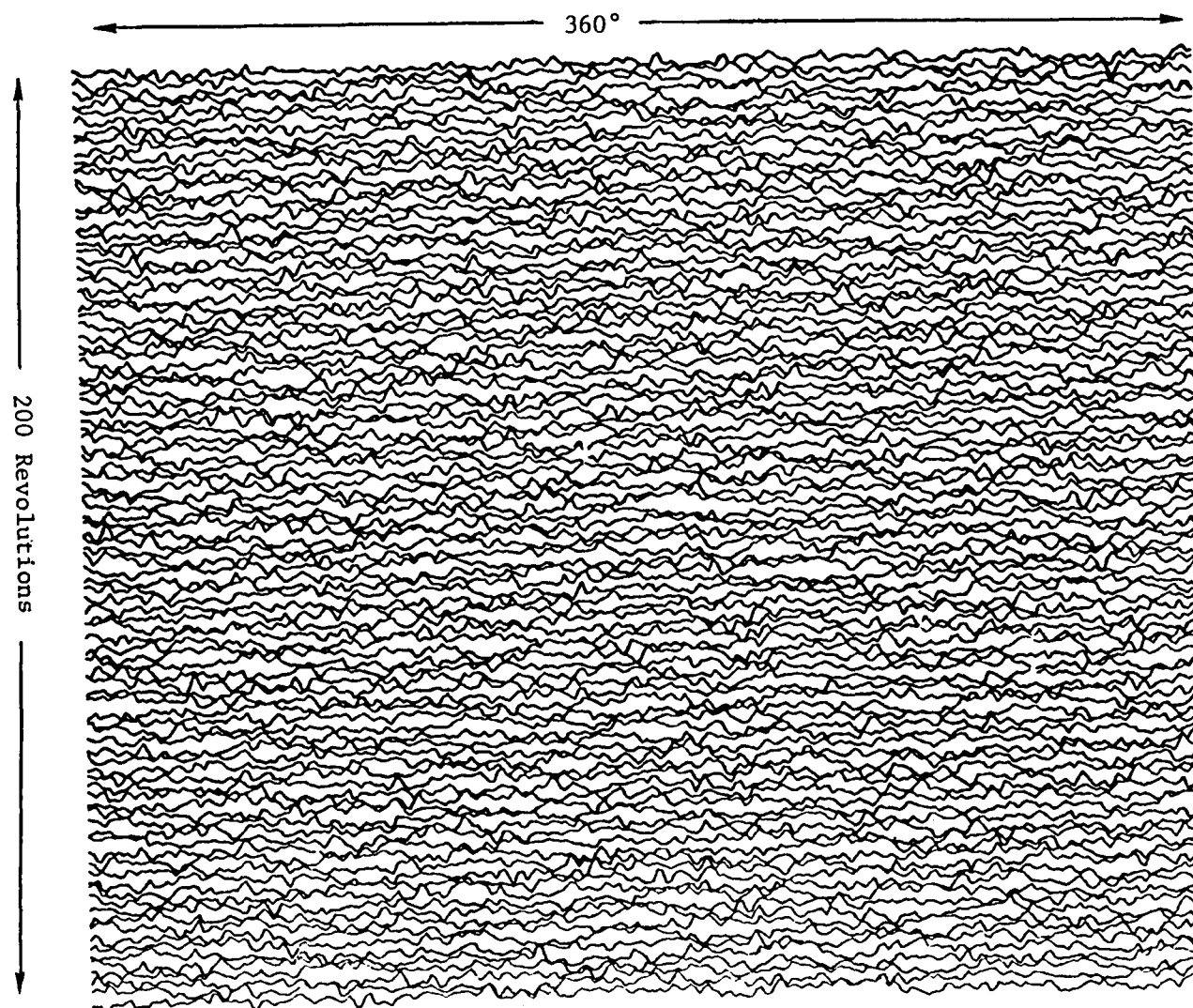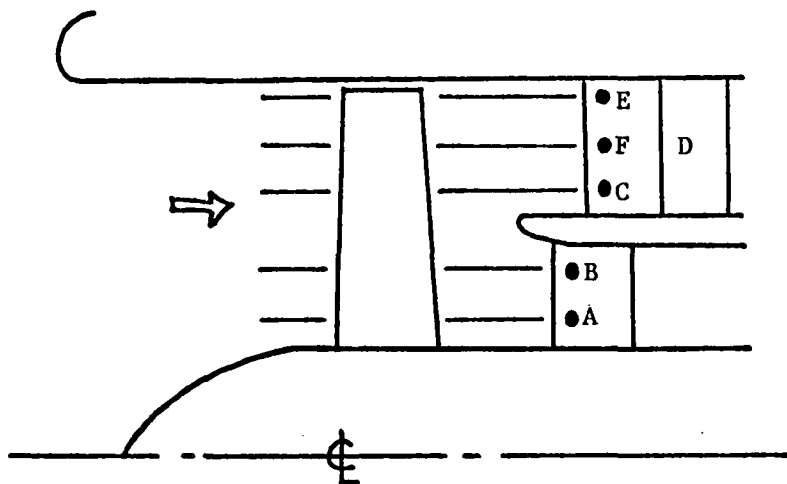Figure 6-6b. Outdoor BMT "G" (TCS) at 12,000 RPM

360°

200 Revolutions

146

Figure 6-6c.   Langley Wind Tunnel BMT "G" at 12,000 RPM

PREDICT TONE PWL CIRCUMFER.
MODE CONTENT FROM FSNAP3

PREDICT TONE DIRECTIVITY FROM
SPLDIPAC

- USING ALL STATOR VANE BMT's PREDICT (ESTIMATE) UNSTEADY LIFT:
$$F' = \Delta P_{F-D} x A_c$$

- USING ONE-SIDED BMT SIGNAL SPECTRUM AND UNSTEADY AIRFOIL THEORY (E.G., AMIET) PREDICT UNSTEADY LIFT.

- INTERPRET $P'(t)$ SIGNAL AS WAKE WAVE FORM:
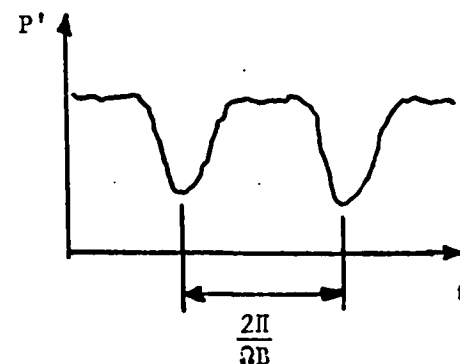
- USE PROGRAM DIRECTLY WITHOUT BMT INPUT (NEED ROTOR C_D)
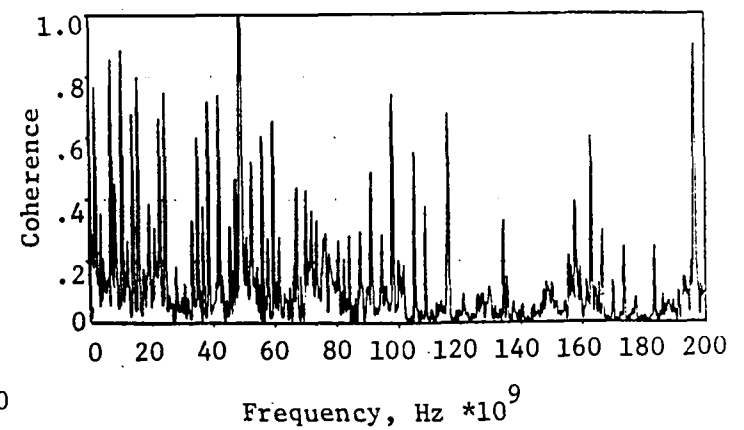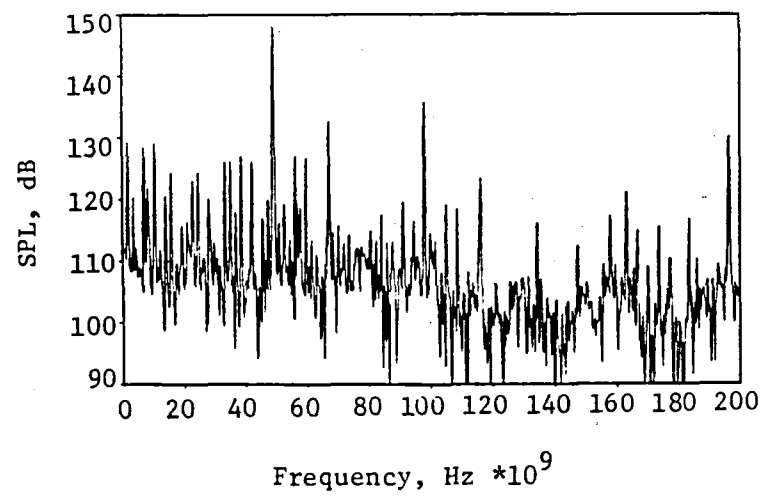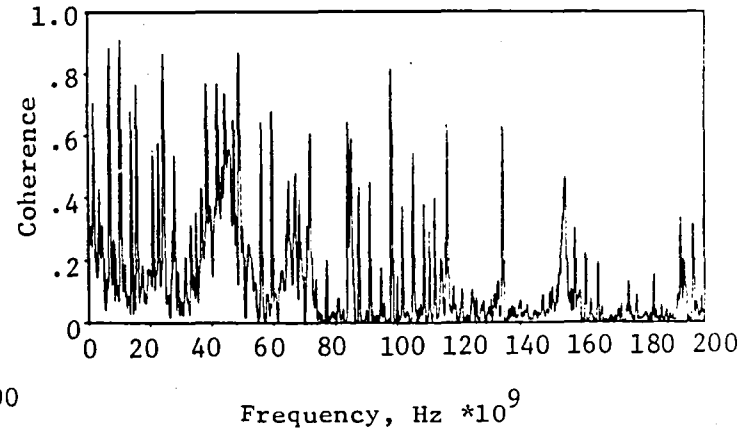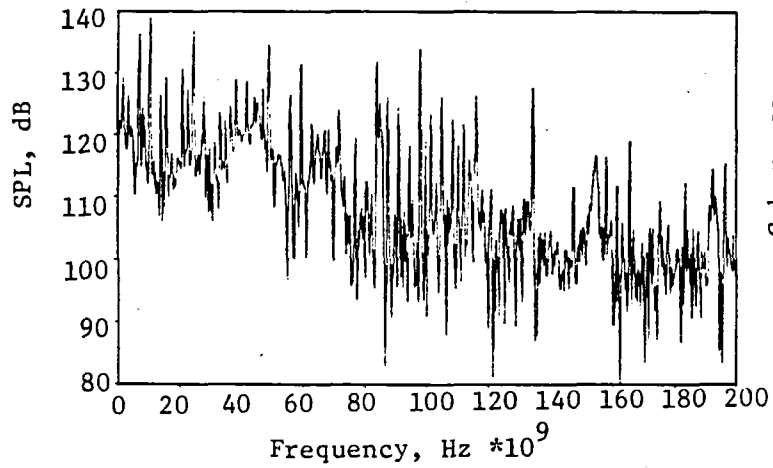
Figure 6-7. Schematic of Stator BMT Locations.

COHERENT OUTPUT SPECTRUM

COHERENCE PLOT
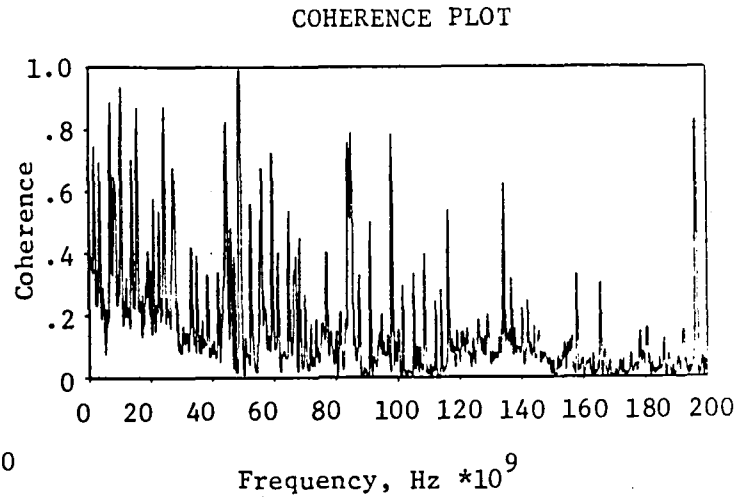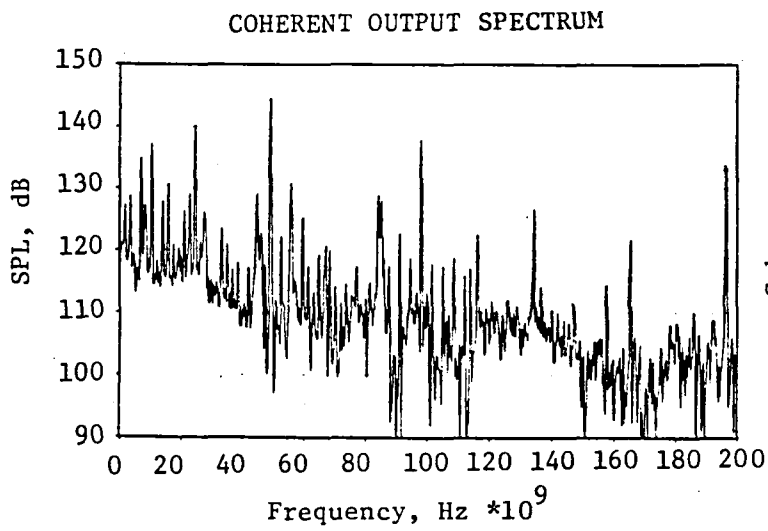
Figure 6-8. Display of Stator Data

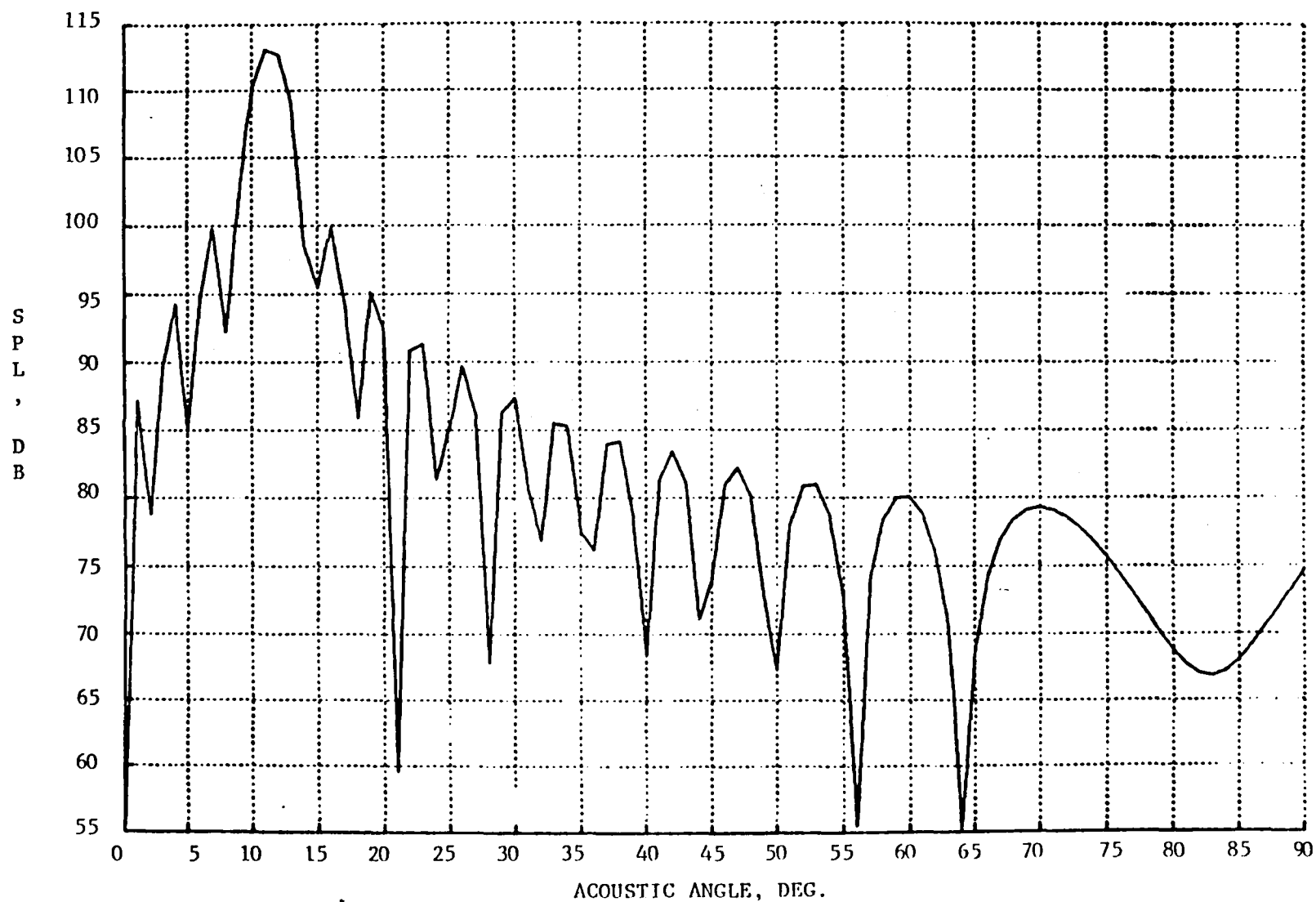| Harmonic No. | = 2 | Circum. Mode No. | = 10 |
| Blade No. | = 28 | Radial Mode No. | = 0 |
| Frequency | = 10628 Hz | PWL, dB | = 123.3 |

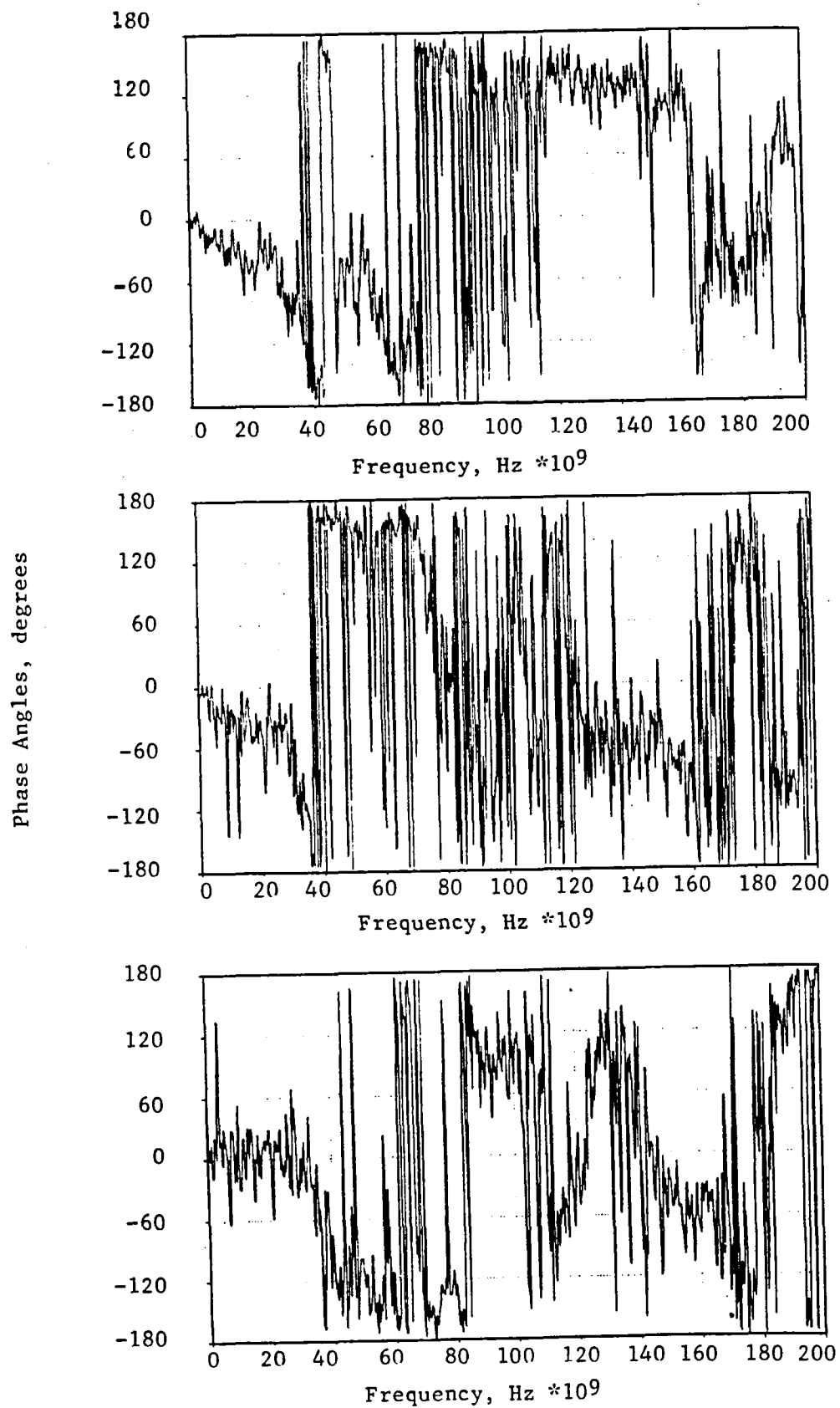Figure 6-9.   Lossless SPL's For Fan Source Noise

Figure 6-10. Relative Phase Between the Various Locations on the Stator

150

6.4   ACOUSTIC RADIATION MODELLING

The determination of the acoustic source modal levels is the initial step in the prediction procedure whose end result is the estimated farfield tone directivity. Once the mode level at the source has been computed, the propagation down the duct and the radiation of sound from the inlet face need to be evaluated. A relatively simple model to perform these computations is presented in Reference 6-5. This model was utilized to make the computations presented in the following section. The model does not take into account the phasing effects between modes such as in the more sophisticated approach of Reference 6-6; however, it does an adequate job when a single mode is present or when a large number of modes are present. In the situation where only two modes are present, then the phasing between the modes can greatly influence the farfield directivity as illustrated in Figure 6-11 whose results were computed using the latter model.

To show the sensitivity of farfield directivity on relative phasing, one case has been computed using analysis based on Reference 6-6.

The results of Figure 6-11 were derived for two circumferential modes of equal power but with different phase angles between them. Note that when modes propagate in a duct, the phase angle between various modes changes continuously such that the inlet length becomes a governing criteria for phasing effects. In the calculations performed during the course of this program, these phases were computed; however, due to the large number of modes which contribute energy to the farfield, the use of the more sophisticated model was not warranted.
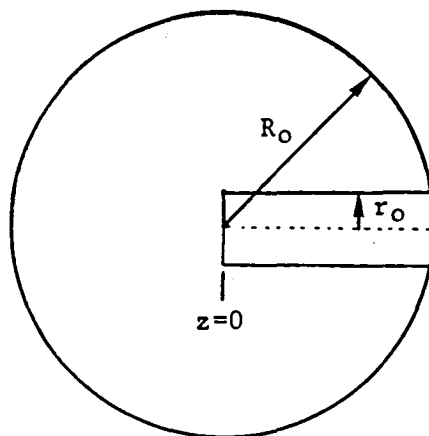
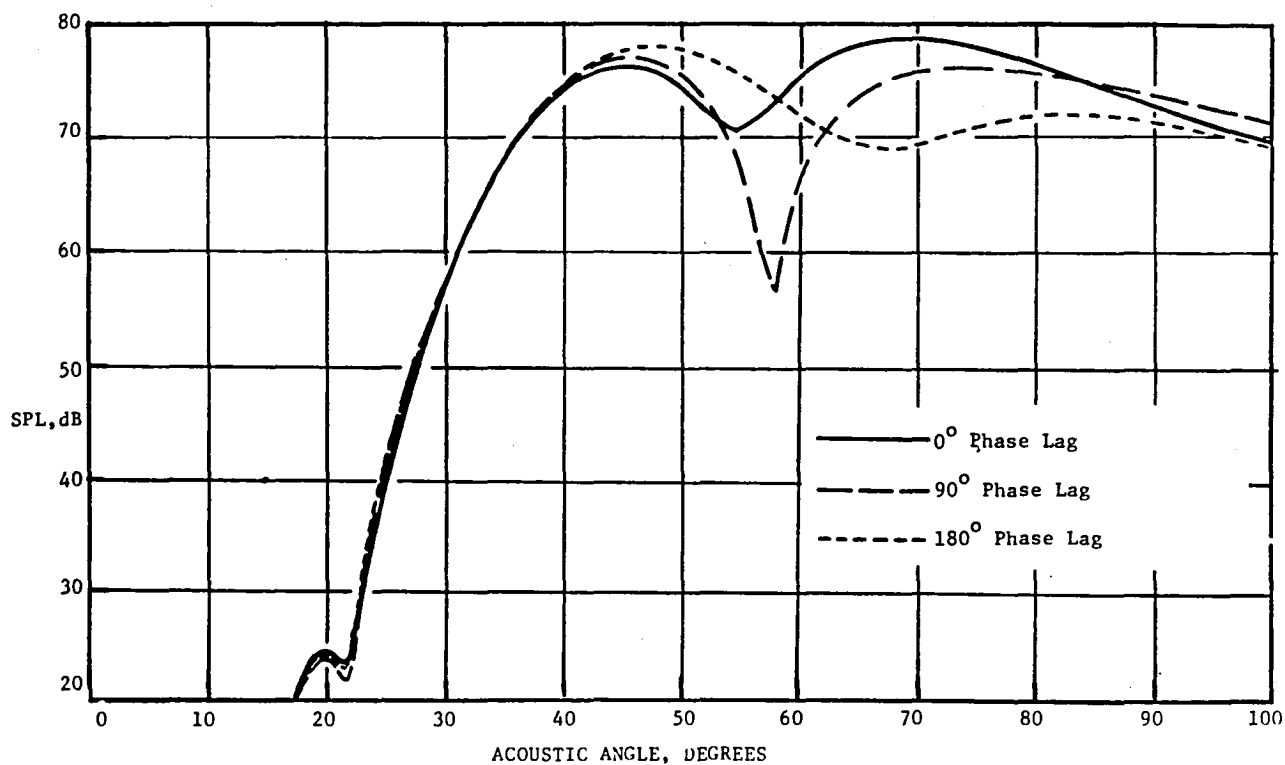Figure 6-11. Radiation Model Schematic.

Figure 6-12. Far-Field Directivity for Spinning Modes (16, 0) and (22, 0)
with Equal Amplitudes and Various Phase Differences.

152

SECTION 7.0

TONAL PREDICTION EVALUATION

7.0   TONAL PREDICTION EVALUATION

The methods delineated in Section 6.0 are applied to the Blade and Vane mounted transducer results to derive predictions of the tonal directivity at one and two times the Blade Passage Frequency at the nominal 10,500 RPM engine speed. Four test environments are utilized in this assessment to encompass a wide variety of conditions for which the tone directivities are evaluated. The data sets are all predicted at a 3.66 m, (12 ft) radius from the fan such that inlet length effects are accounted for in the predicted tone directivities.

The four test environments for which the tone predictions are accomplished are combined into the next three subsections. Subsection 7.1 deals with the prediction of tones in the wind tunnel measurement environment. Subsection 7.2 deals with the outdoor measurement environment where testing was performed with and without a turbulence control device installed on the front of the engine. Subsection 7.3 pertains to the prediction of tones using internal engine data as measured during flight tests. For each environment three engine speeds are used which categorically can be labelled subsonic, transonic and supersonic fan tip speed cases.

7.1   WIND TUNNEL TONE PREDICTIONS

The prediction of wind tunnel tones was accomplished using the BMT results presented in Figures 7-1 and 7-2. The largest harmonic values contributing to the spinning duct mode energies are tabulated in Table 7-1. The methodology utilized to make the tone predictions was discussed in Section 6.0. The BMT results shown in Figure 7-1 and 7-2 generally have surprisingly high coherence values along the blade leading edge implying the possiblity of existing correlated radial modes. Due to the limited number of spanwise transducers, no attempt has been made to resolve the spinning modal contributions into their respective radial modal contents. The chordwise coherence [Figure 7-1(d) and 7-2(d)] is low except for isolated harmonics. This implies a compact line of acoustic strength along the blade leading edge and lends support to actuator disk modelling of blade unsteady aerodynamic forces.
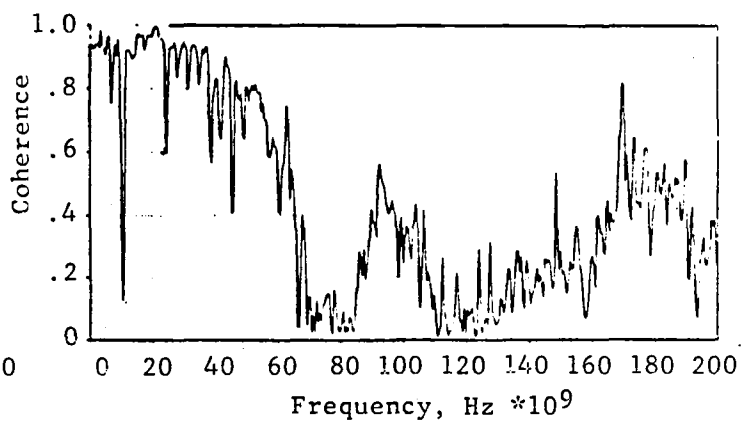
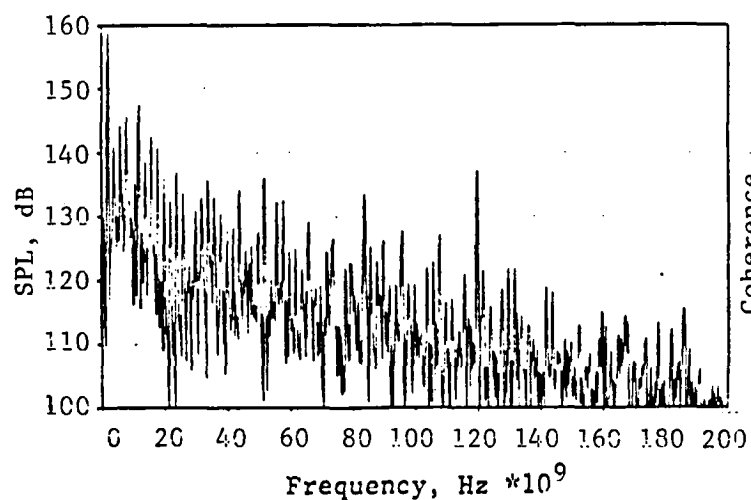153
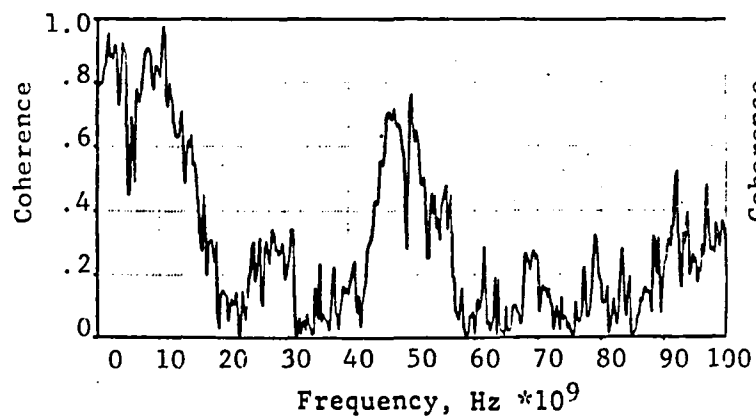
c. Coherence of H and G
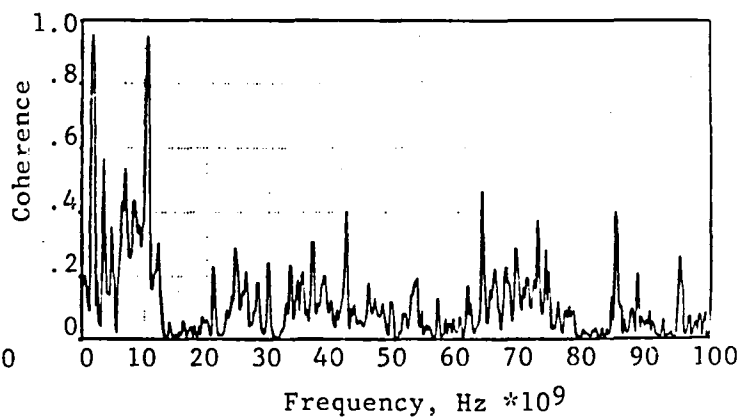
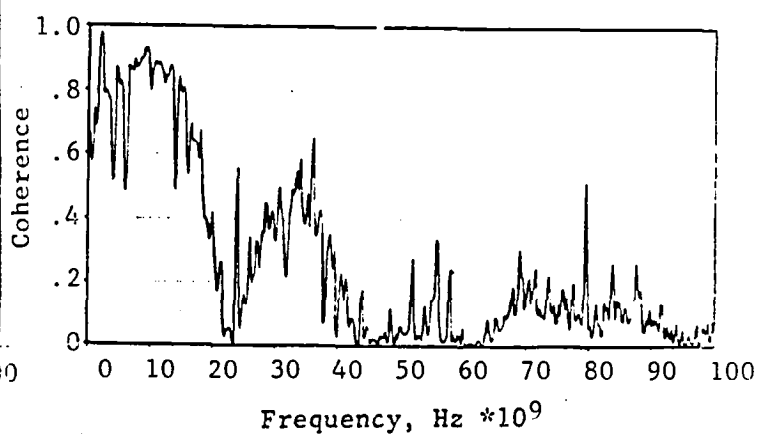d. Coherence of H and J
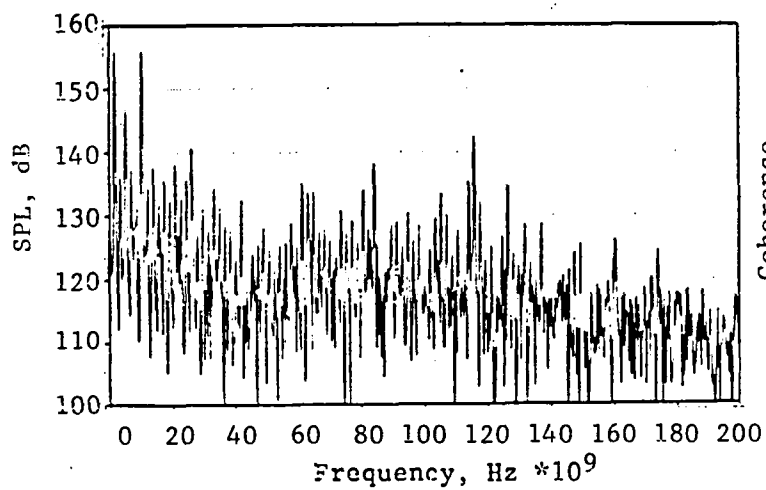
a. "H-K" Enhanced Spectrum

b. Coherence of H and I

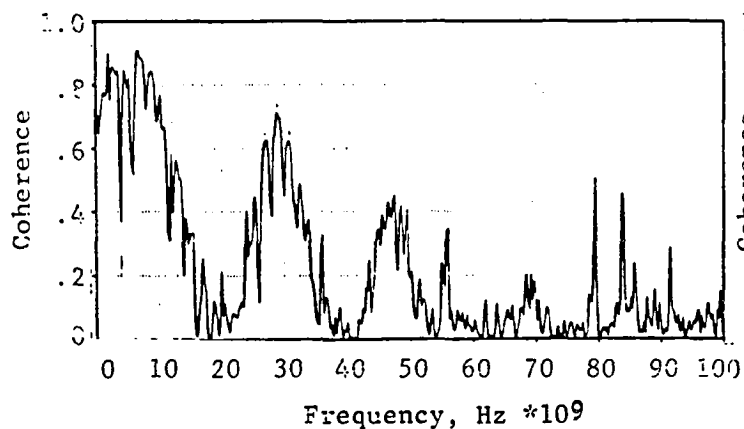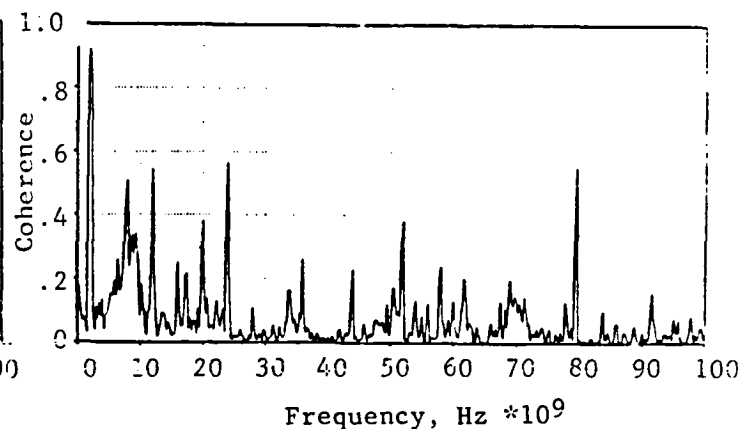Figure 7-1. BMT Results for Wind Tunnel Test at 10,500 RPM.

154

a.   "H-K" Enhanced Spectrum

b.   Coherence of H and I

c.   Coherence of H and G

d.   Coherence of H and J

Figure 7-2.   BMT Results for Wind Tunnel Test at 12,000 RPM.

TABLE 7-1

PRINCIPAL MODES AND POWER LEVELS FOR TONE PREDICTIONS

Approximate Engine Speed(RPM)	(Mode, PWL)			
X1000	LWT	TCS	No-TCS	FLT
		16,118.0	22,110.7	18,106.2
		20,116.6	3,93.3	8,101.7
10.5 (BPF)	20,135.6	17,109.1	7,89.4	15,100.4
	13,126.7	9,108.1	11,93.4	10,98.1
		9,107.7	15,96.4	
			18,88.6	
10.5 (2 BPF)	8,107.8	10,116.4	10,100.9	10,98.7
	10,121.3	16,111.6	16,102.9	
	16,117.5			
11.5 (BPF)	N/A	22,119.0	24,133.5	N/A
		5,117.4	22,113.3	
			7,115.2	
			16,93.9	
11.8 (BPF)	N/A	N/A	N/A	22,123.0
				14,111.9
				11,109.9
				12,92.5
12.0 (BPF)	22,137,8	N/A	N/A	N/A
	10,130.0			
	2,117.6			
	16,116.4			
13.5 (BPF)	N/A	28,127.3	28,129.1	26,125.7
		27,109.4	27,109.8	27,119.4
		24,112.6	22,104.0	22,116.8
		22,110.1	12,100.3	16,112.0

7.1.1 SUBSONIC WIND TUNNEL EVALUATION

The prediction of the Wind Tunnel BPF and twice BPF for an engine speed of 10,500 RPM are displayed in Figures 7-3 and 7-4. These figures compare the measured tonal directivities to the predicted directivities using discrete (periodic) and random blade leading components. The predictions generally overestimate the random portion of the tonal energy while the periodic predictions demonstrate relative agreement in terms of level. The shape of the directivity pattern for this speed condition is very non-descript, thus indicating the contributions of many modes of similar amplitudes as is also implied by the BMT evaluation.

In this respect, the BMT's were useful. The second harmonic determination is slightly better as the rotor-stator interaction modes are present and show up in the directivity. The mode numbers associated with the core stator interaction is 15 whereas the bypass stator interaction noise produces a mode number of 10. Both modes spin counter to the rotor; however, in the analysis utilized this is not a distinguishable feature. A plot of the BPF directivity for the GE Wind Tunnel configuration is presented in Figure 7-5 which shows that a directivity hump in the 55° area not observed in the Langley data which is compared in this figure. The spinning mode number which would produce this effect would be 16; however, BMT data is not available to evaluate this observation. It is noted that the Langley BMT data at this speed point does not produce a significant 12/rev component which would give rise to the 16th order mode.

Comparison of measured and predicted directivities at 12,000 RPM are shown in Figure 7-6. At angles $\theta < 70°$ the predicted levels for both the periodic and the random components are 10 to 15 dB too high.

7.1.2 SUPERSONIC WIND TUNNEL EVALUATION

The dominant feature of the supersonic speed condition is the rotor-alone field. Other modal amplitudes contribute to a lesser degree to the predicted tone directivity at this speed point. Reasonably good agreement between the predicted and measured tone directivity is obtained by considering
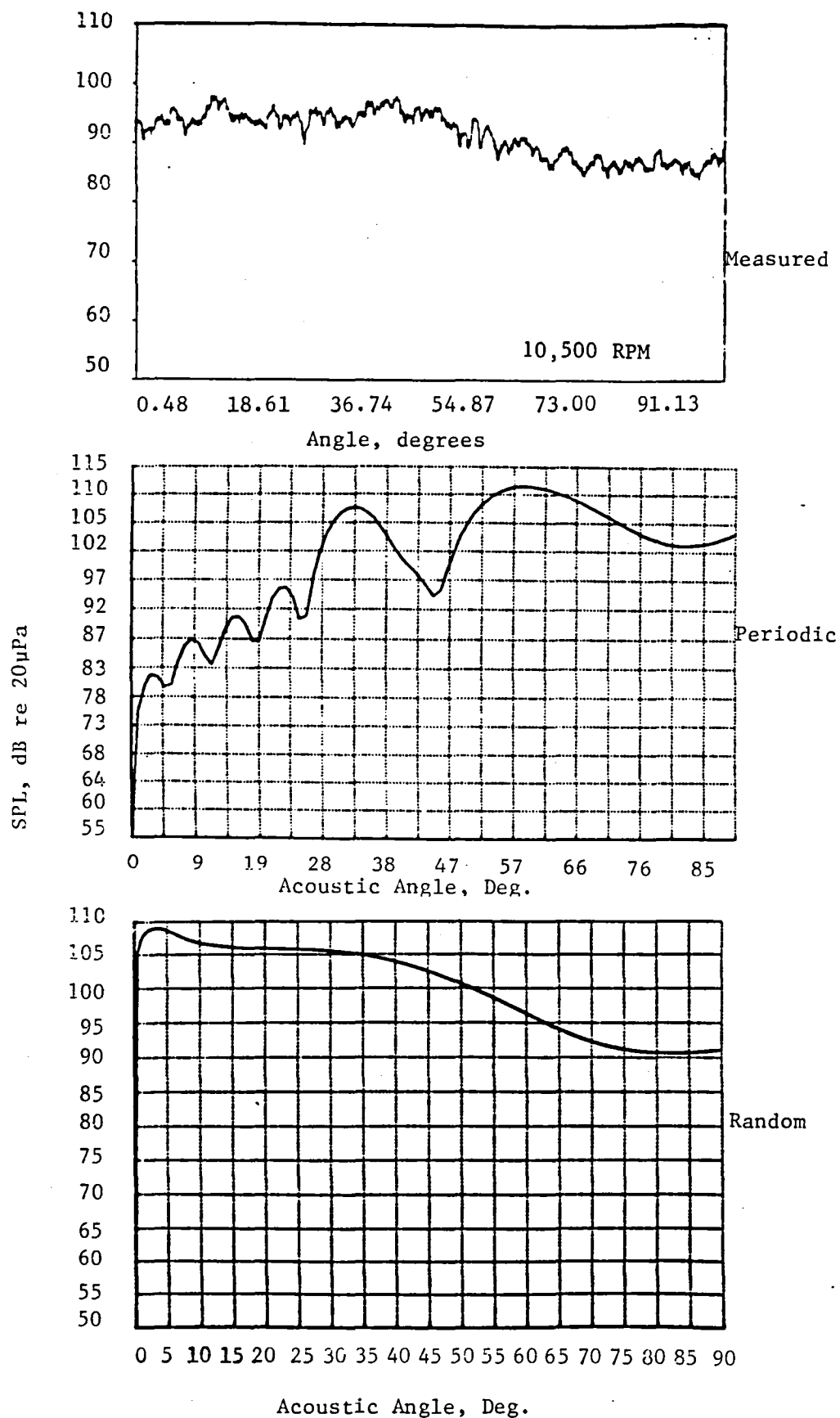
Figure 7-3. Comparison of Measured Wind Tunnel BPF Tone Directivity with BPF Predictions of Periodic and Random Acoustic Sources.
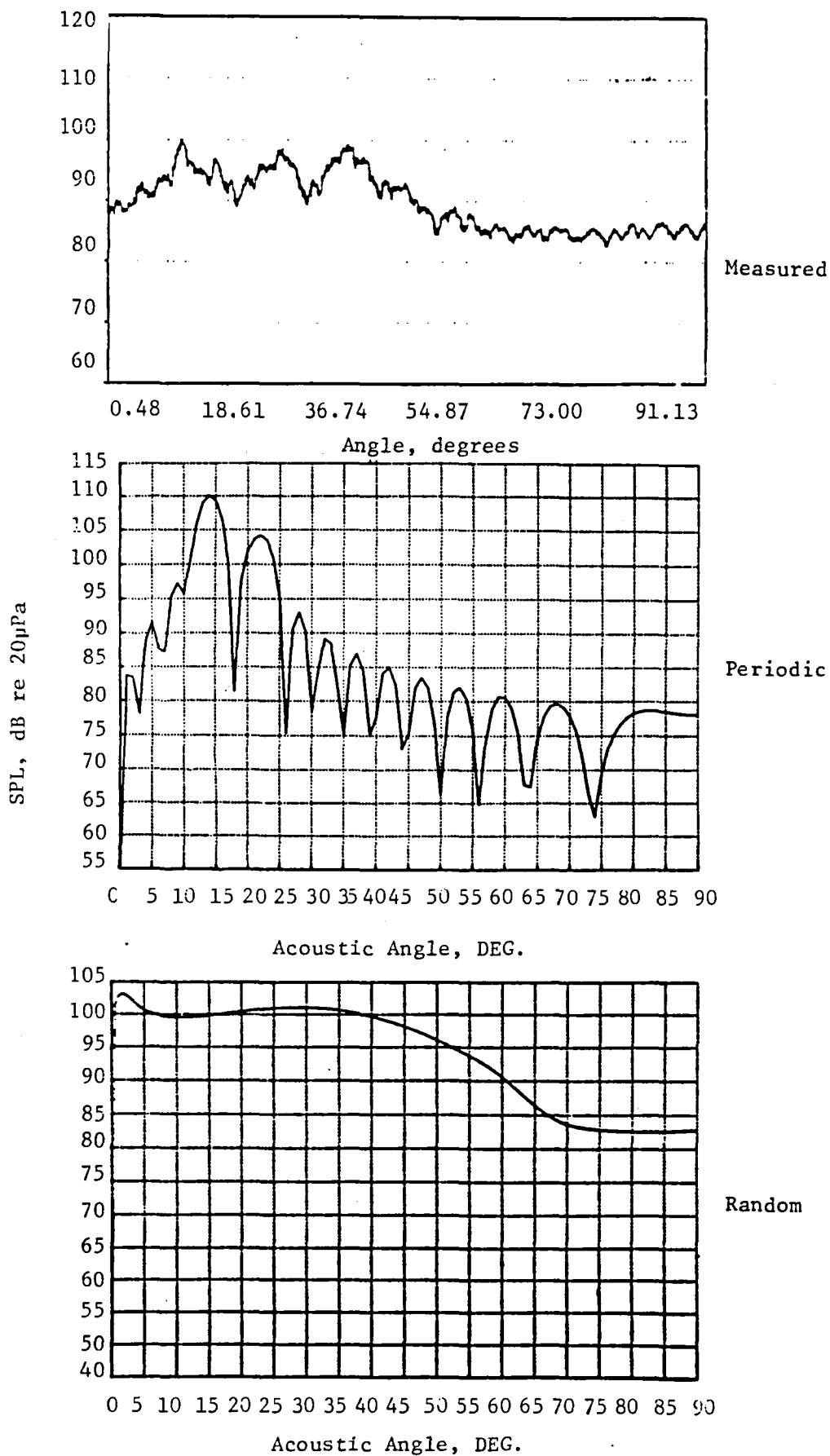
158

Figure 7-4. Comparison of Measured Wind Tunnel Directivity at 2 X BPF with Corresponding Predictions for Periodic and Random Acoustic Sources.
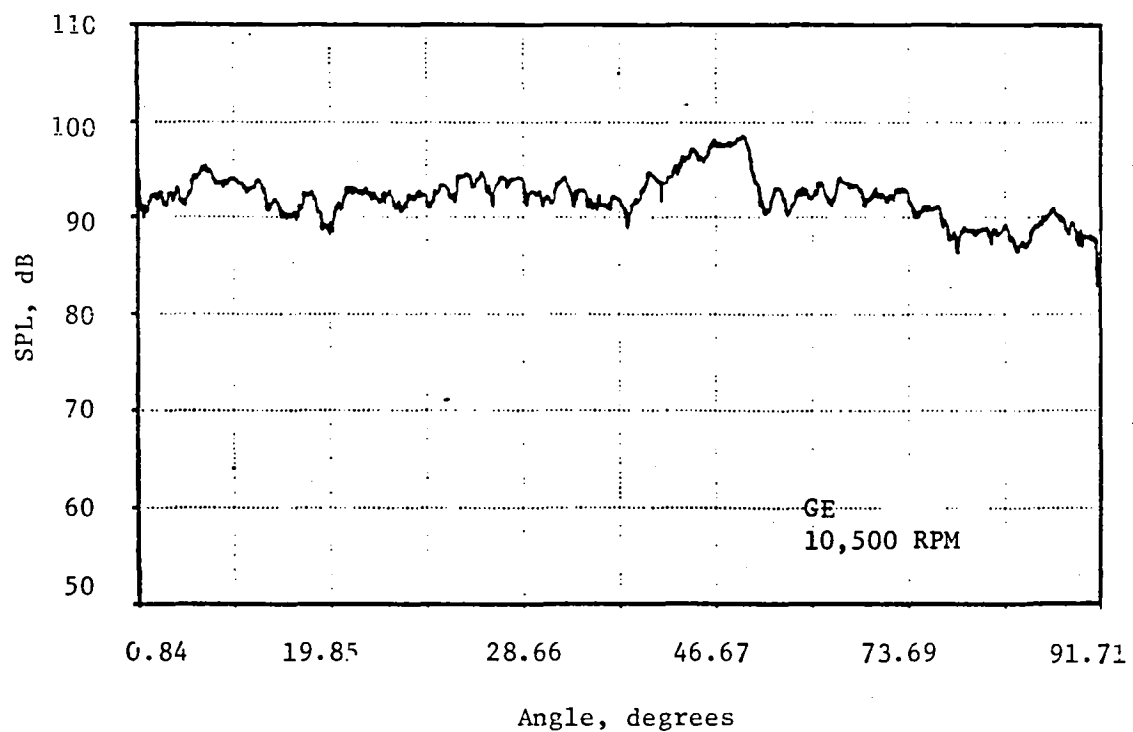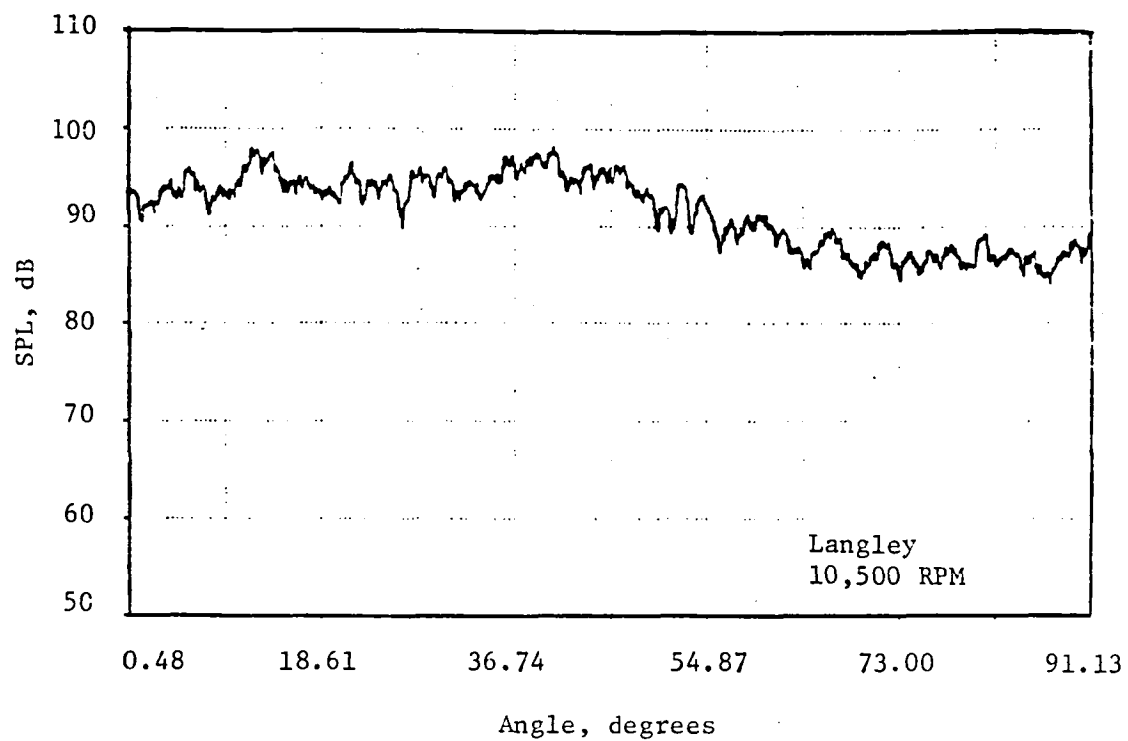
Figure 7-5. Comp.rison of Measured BPF Tone Directivity for Langley and GE Wind Tunn. 1 Configurations.
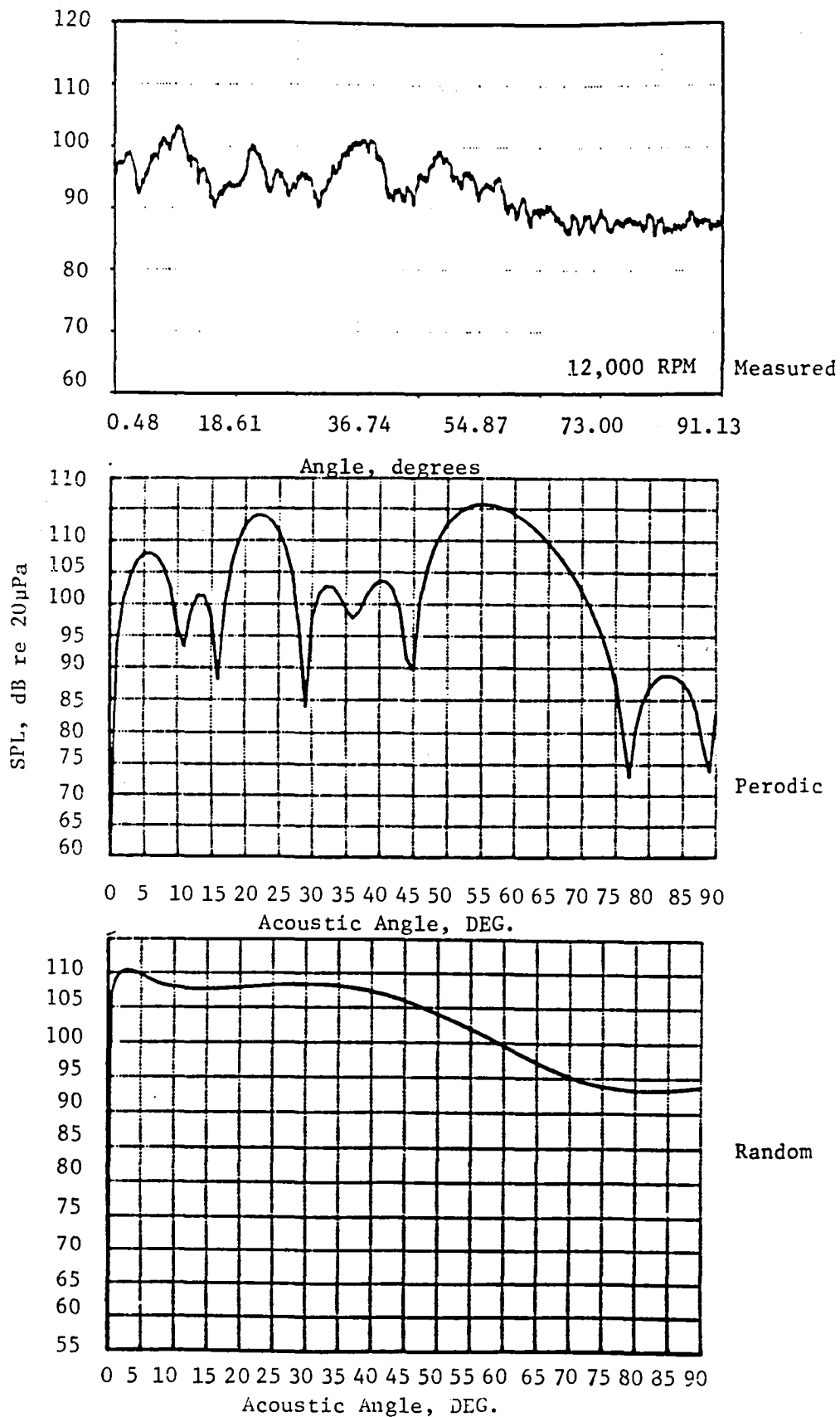
160

Figure 7-6. Comparison of Measured Wind Tunnel BPF Tone Directivity with BPF Predictions of Periodic and Random Acoustic Sources.

the rotor-alone field, since no Langley Wind Tunnel directivity is available at this speed point. The GE wind tunnel BPF tone directivity is presented in Figure 7-7.

7.2   OUTDOOR STATIC EVALUATION

The outdoor static test tone evaluations are presented for turbulence controlled and non-turbulence controlled conditions in this subsection. The Blade Mounted Transducer results utilized to perform the tone predictions are displayed in Figures 7-8 through 7-13. Generally, it is noted that the coherence values for the non-turbulence controlled situation are significantly lower as compared to the turbulence controlled environment. Also, when the turbulence controlled BMT results are compared to their wind tunnel counterparts in Subsection 7.1, it is noted that much less low frequency spanwise coherence is present and only selected harmonics (principally 1 and 6) produce high coherence values over the entire blade surface.

7.2.1 TURBULENCE CONTROLLED AND NON-TURBULENCE CONTROLLED SUBSONIC FAN SPEED

Measured and predicted tonal directivities for the BPF and twice BPF of the JT15D fan are presented in Figures 7-14 through 7-17 for turbulence controlled and non-turbulence controlled outdoor static tests. Relatively good agreement for the turbulence controlled case (Figures 7-15 and 7-17) is achieved. Significant differences between the angular distribution of energy remains; however, some structural similarities are noted for the turbulence controlled environment. Again the predictions based on random sources (rotor-turbulence interaction) overestimate the measured acoustic farfield strength. It is interesting to note, however, that the relative difference between the non-turbulence controlled random prediction and the turbulence controlled random prediction are of the same relative differential as that measured. This observation is based on the assessment that the periodic sources in the non-turbulence controlled situation are very incoherent and thus the measured directivity is a good measure of the random source contribution. The conclusion that the periodic sources are incoherent is borne out by the BMT results of the previous subsection and lead to the low acoustic strengths for the non-turbulence controlled predictions in Figures 7-14 and 7-16.
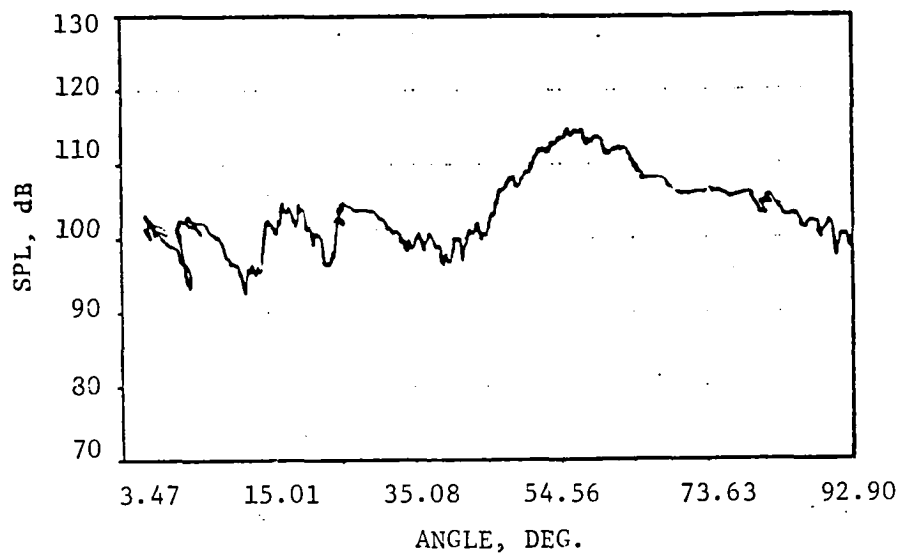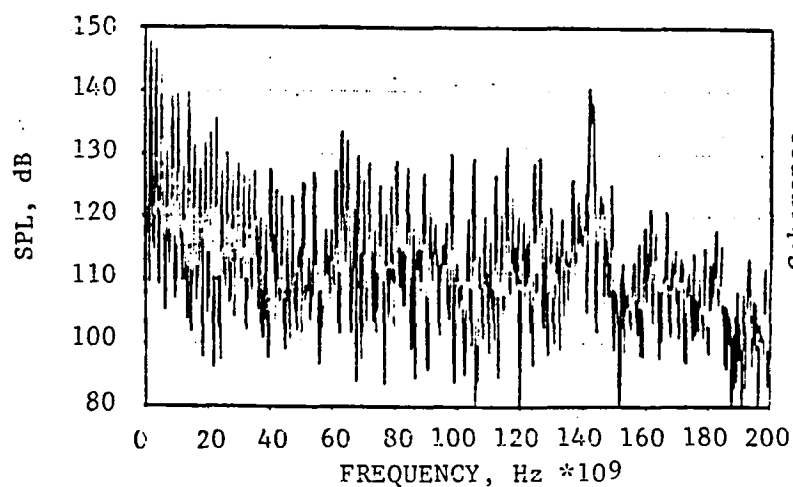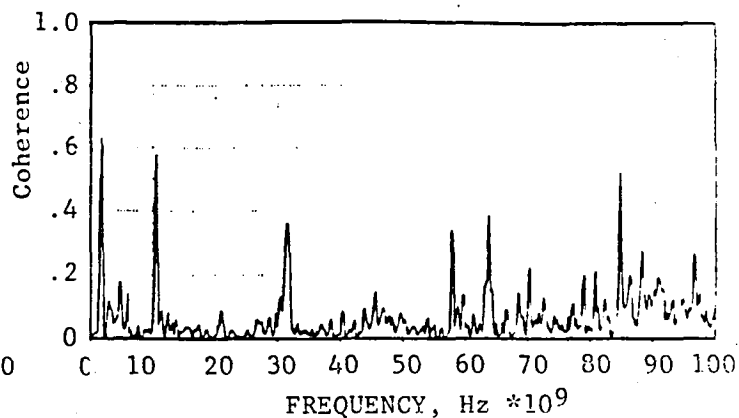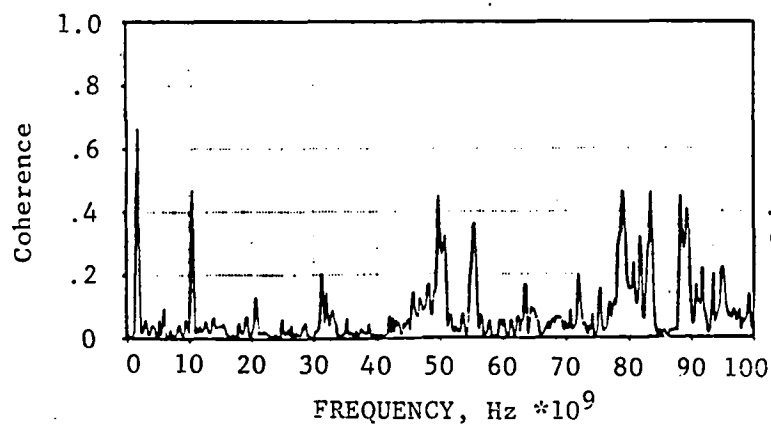
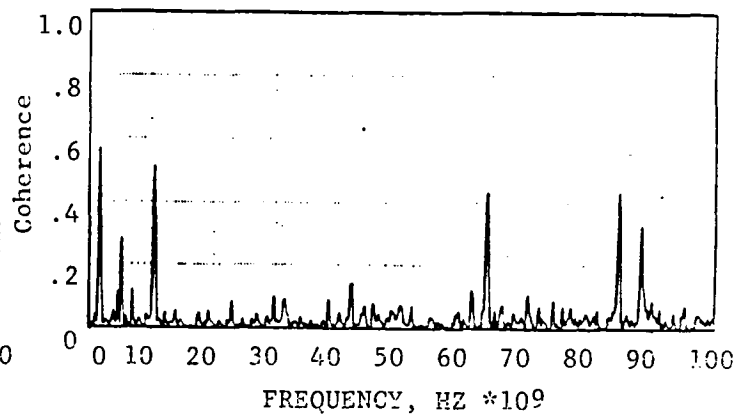Figure 7-7.   GE Wind Tunnel BPF Directivity for Supersonic Tip Speed.

a. "H-K" Enhanced Spectrum

SPL, dB — 150, 140, 130, 120, 110, 100, 80

FREQUENCY, Hz *109 — 0 20 40 60 80 100 120 140 160 180 200

b. Coherence H and I

Coherence — 1.0, .8, .6, .4, .2, 0

FREQUENCY, Hz *10^9 — C 10 20 30 40 50 60 70 80 90 100

c. Coherence of H and G

Coherence — 1.0, .8, .6, .4, .2, 0

FREQUENCY, Hz *10^9 — 0 10 20 30 40 50 60 70 80 90 100

d. Coherence of H and J

Coherence — 1.0, .8, .6, .4, .2, 0

FREQUENCY, HZ *10^9 — 0 10 20 30 40 50 60 70 80 90 100

Figure 7-8. BMT Results for Turbulence Controlled Outdoor Static
Tests at 10,500 RPM.

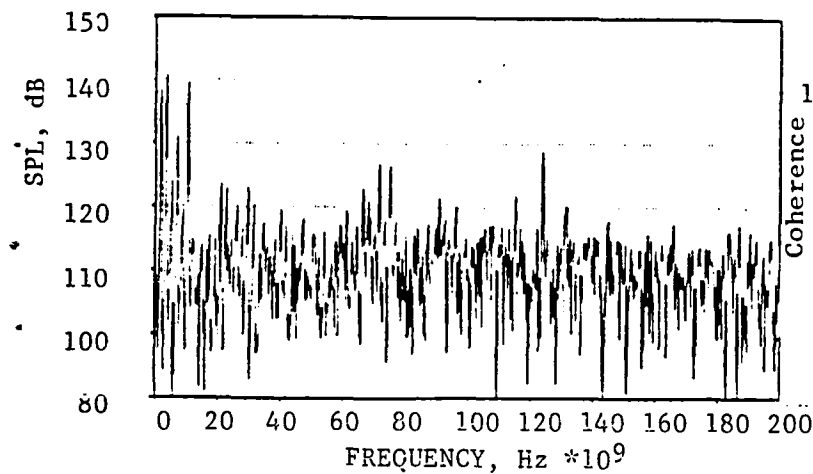a. "H-K" Enhanced Spectrum

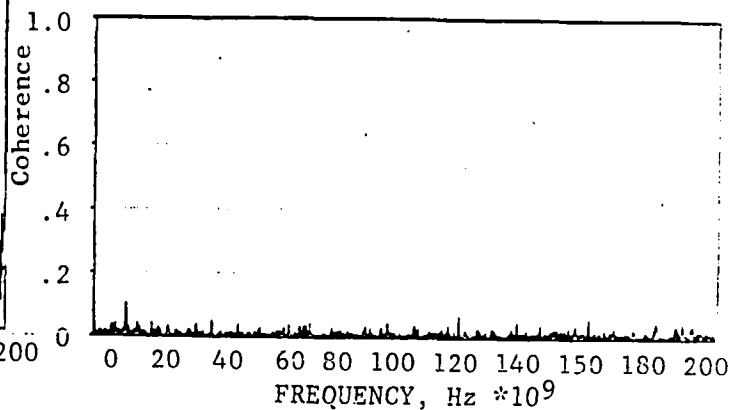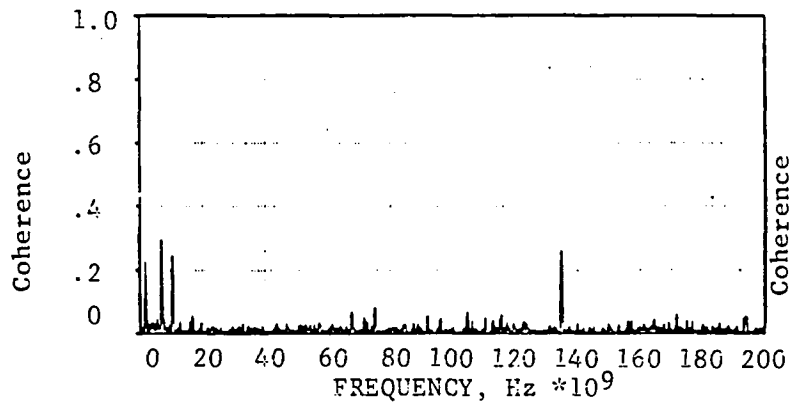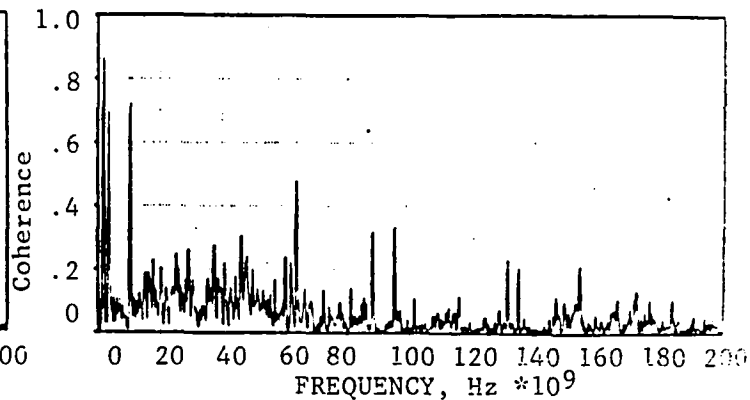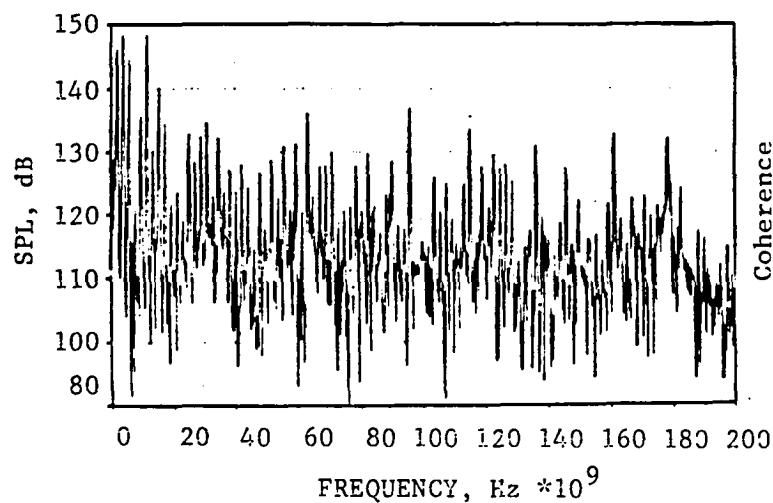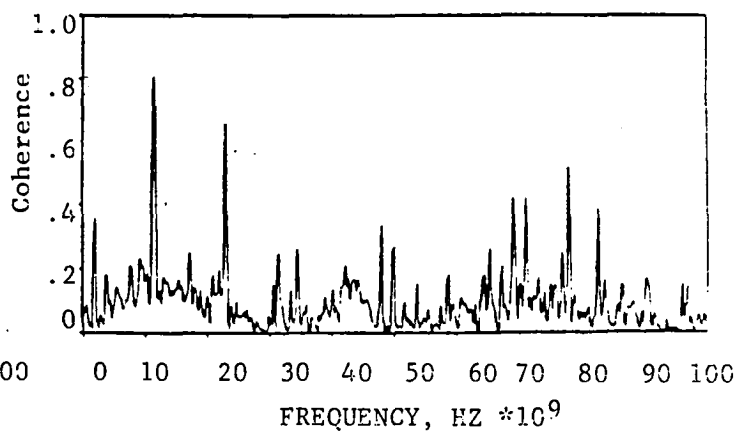b. Coherence of H and I

c. Coherence of H and G

d. Coherence of H and J

Figure 7-9. BMT Results for Non-Turbulence Controlled Outdoor Static
Tests at 10,500 RPM.

a. "H-K" Enhanced Spectrum

b. Coherence of H and I

c. Coherence of H and G

d. Coherence of H and J

Figure 7-10. BMT Results for Turbulence Controlled Outdoor Static
Tests at 11,500 RPM.

166

a. "H-K" Enhanced Spectrum

b. Coherence of H and I

c. Coherence of H and G

d. Coherence of H and J

Figure 7-11.   BMT Results for Non-Turbulence Controlled Outdcor Static
Tests at 11,500 RPM.
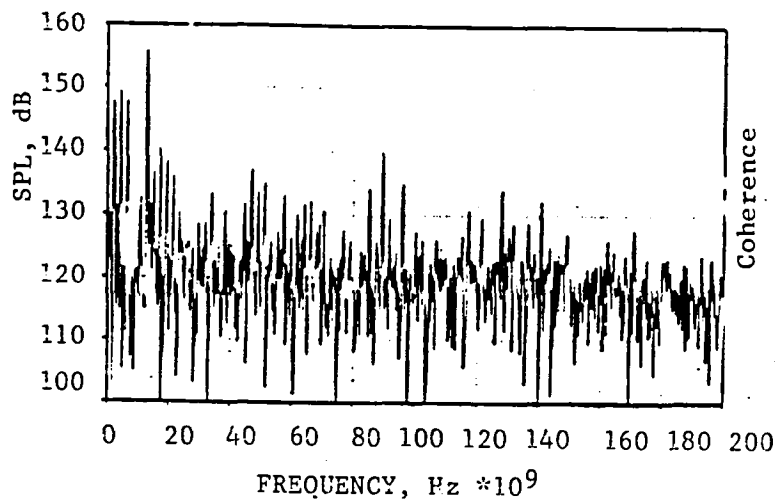
167

a. "H-K" Enhanced Spectrum
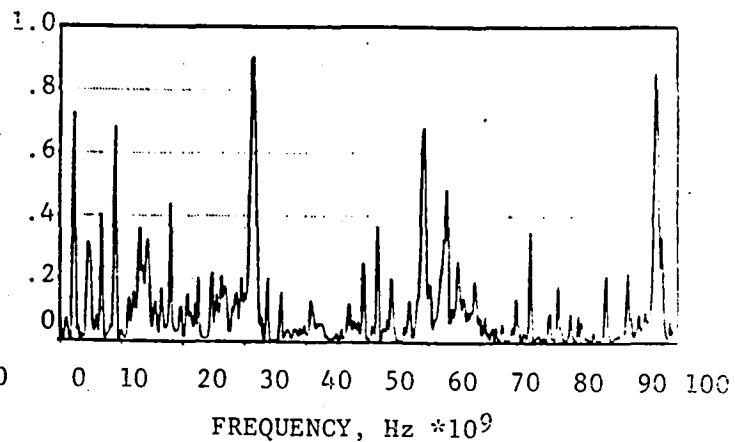
b. Coherence of H and I
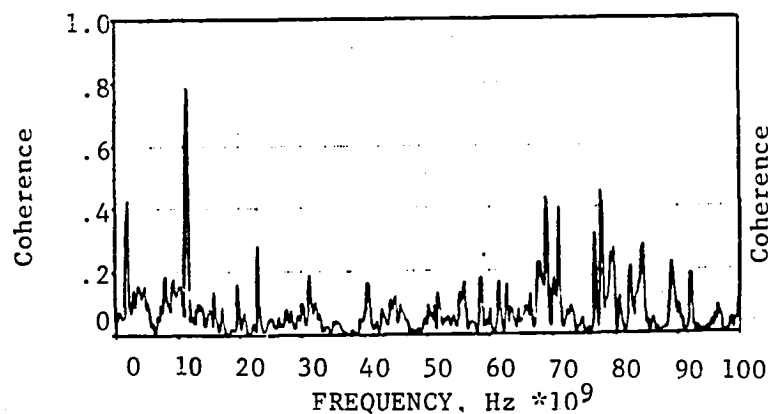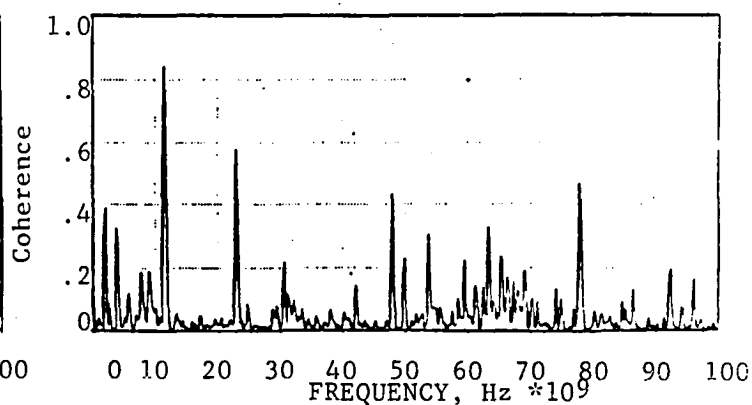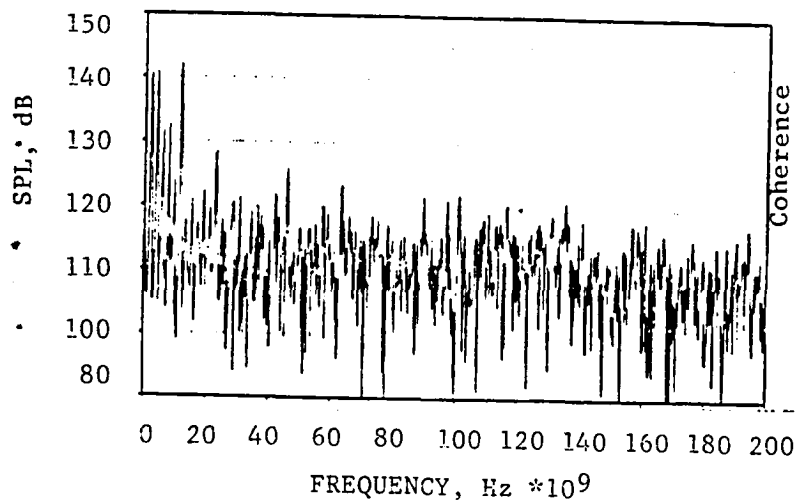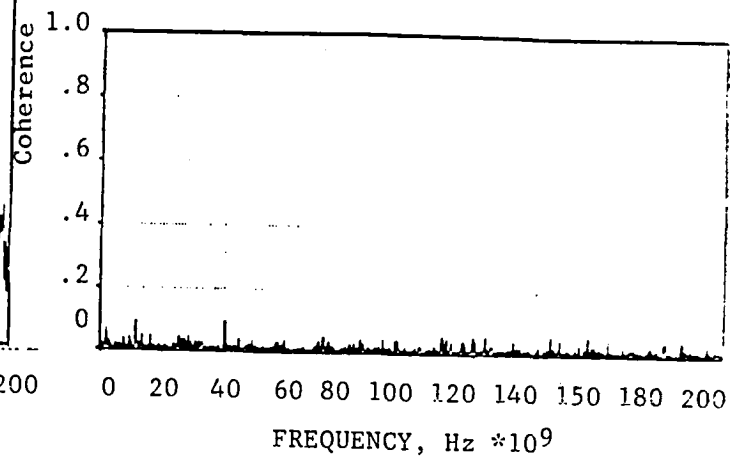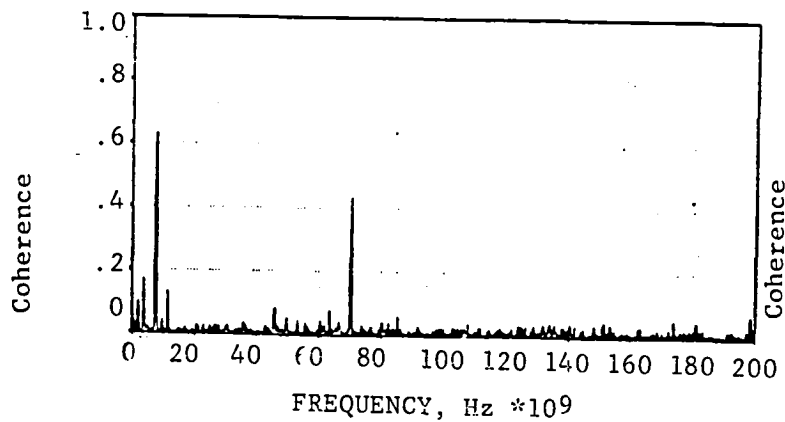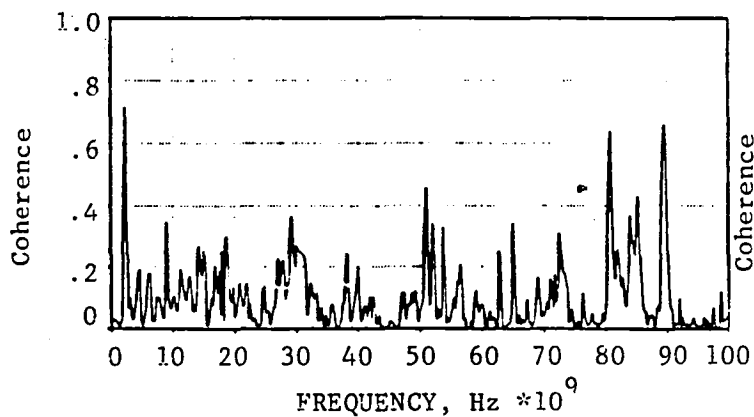
c. Coherence of H and G
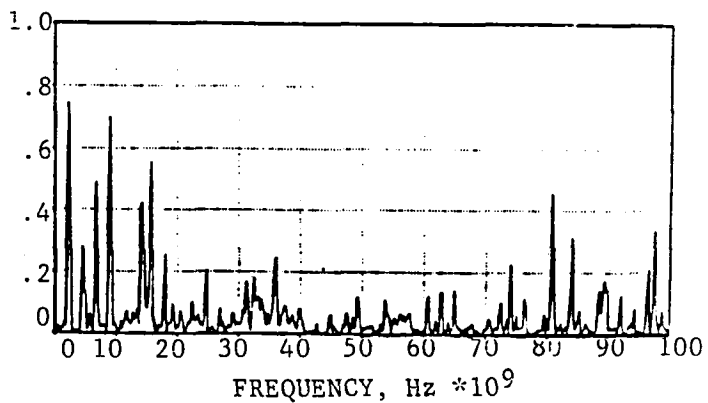
d. Coherence of H and J

Figure 7-12. BMT Results for Turbulence Controlled Outdoor Static
Tests at 13,500 RPM.
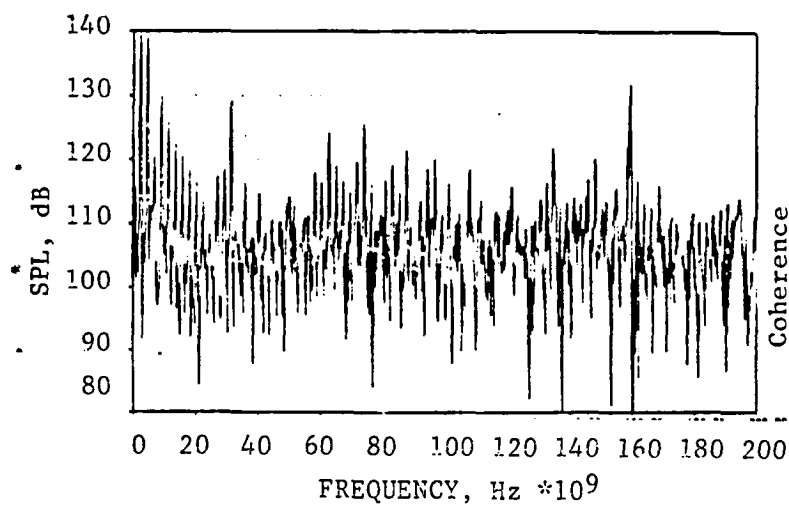
a. "H-K" Enhanced Spectrum
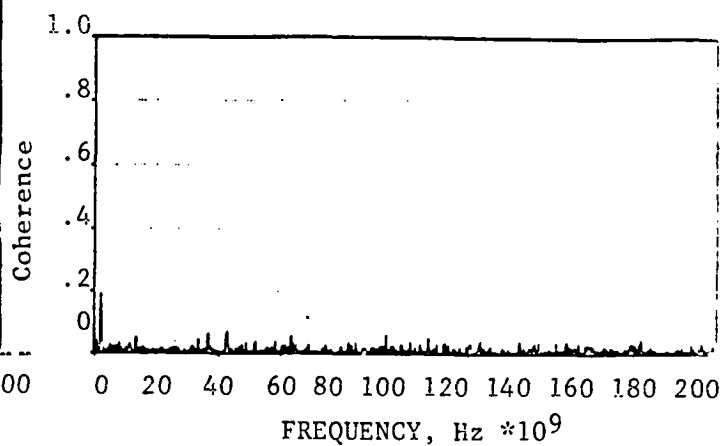
b. Coherence of H and I
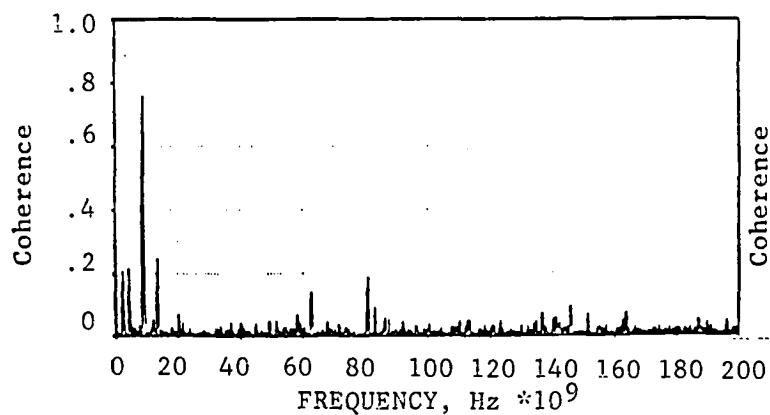
c. Coherence of H and G
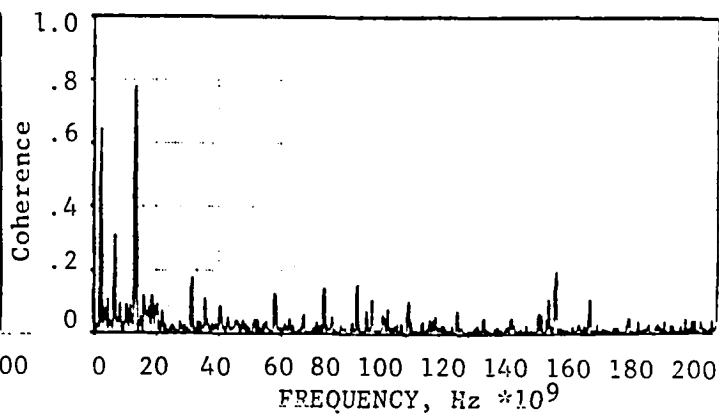
d. Coherence of H and J

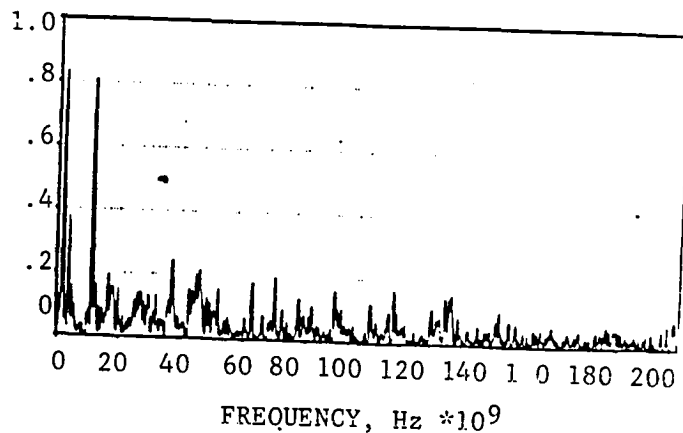Figure 7-13. BMT Results for Non-Turbulence Controlled Outdoor Static
Tests at 13,500 RPM.

Figure 7-14. Comparison of Measured Outdoor Static (no TCS) BPF Tone Directivity with BPF Predictions of Periodic and Random Acoustic Sources (10,500 RPM).

Figure 7-15. Comparison of Measured Outdoor Static (TCS) BPF Tone Directivity with BPF Predictions of Periodic and Random Acoustic Sources (10,500 RPM).

Figure 7-16. Comparison of Measured Outdoor Static (no TCS) Twice BPF Tone Directivity with Twice BPF Prediction of Periodic and Random Acoustic Sources (10,500 RPM).

Figure 7-17. Comparison of Measured Outdoor Static (TCS) Twice BPF Tone Directivity with Twice BPF Predictions of Periodic and Random Acoustic Sources (10,500 RPM).

7.2.2 (TCS AND NON-TCS) TRANSONIC TIP SPEED

Distinctive differences between the turbulence controlled (TCS) and non-turbulence controlled (non-TCS) BPF directivities are apparent in the near transonic speed regime. The non-TCS directivity pattern appears to be turbulence dominated while the TCS case is very lobular. The directivity patterns are predicted at 11,500 RPM since BMT data for the TCS case was not available at 11,800 or 12,000 RPM where very unique BPF directivity patterns were observed (Figures 7-18 and 7-19). The agreement between predicted and measured patterns for a fan speed of 11,500 RPM is shown in Figures 7-20 and 7-21. The TCS case appears to be distortion dominated as the prediction also indicates, whereas the non-TCS pattern appears to be turbulence dominated again as suggested by the predicted results. The turbulence predicted level is again high which may in part be the result of the modal powers being non-additive in the sense that phasing effects between various modes may diminish their radiation efficiency as discussed in Subsection 6.4.

The unique directivity patterns (Figure 7-19) observed for the TCS case at 11,800 and 12,000 RPM strongly suggest the existence of the 22nd order mode in combination with a 16th order mode and thus the discussion in Subsection 6.3 is very relevant to these directivity patterns. Unfortunately, the necessary BMT information at these speeds to perform predictions was not available, and thus a check of the procedures used for periodic acoustic source evaluation could not be made.

7.2.3 (TCS AND NON-TCS) SUPERSONIC TIP SPEED

The supersonic tip speed case is again dominated by the rotor-alone field, i.e., 28th order mode. The other distortion related modal energies contribute and provide reasonably good predictions of the tone directivities for both the TCS and non-TCS situations as shown in Figures 7-22 and 7-23, respectively. At this speed point the turbulence predictions overestimate the measured level by a large margin; however, the turbulence related directivity shape is peaked more toward the central angles as opposed to the shallow angle peaked directivities at subsonic tip speeds.
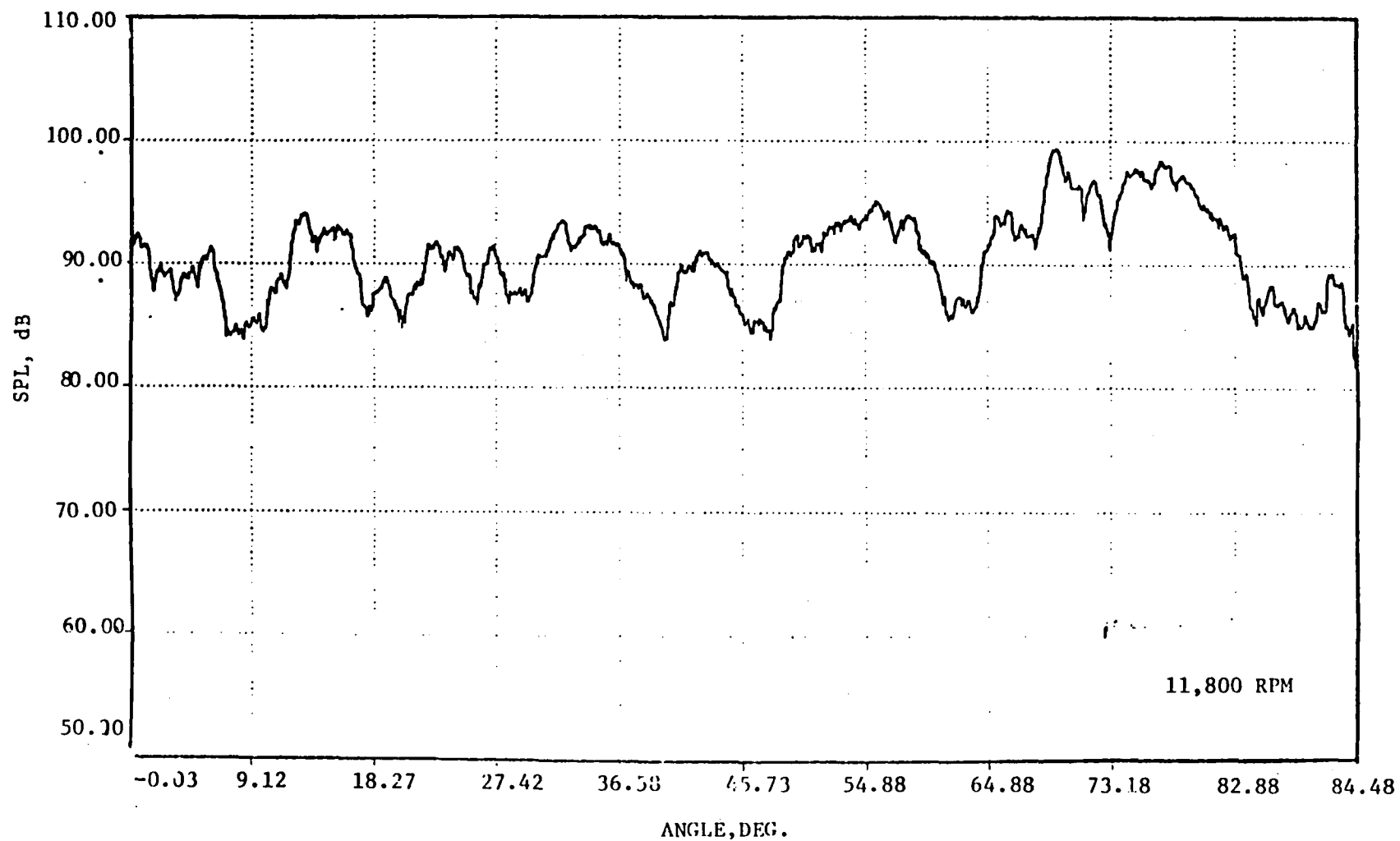
Figure 7-18. BPF Directivity for Outdoor TCS (AFT Treated) Test at Engine Speeds of 11,800 RPM.
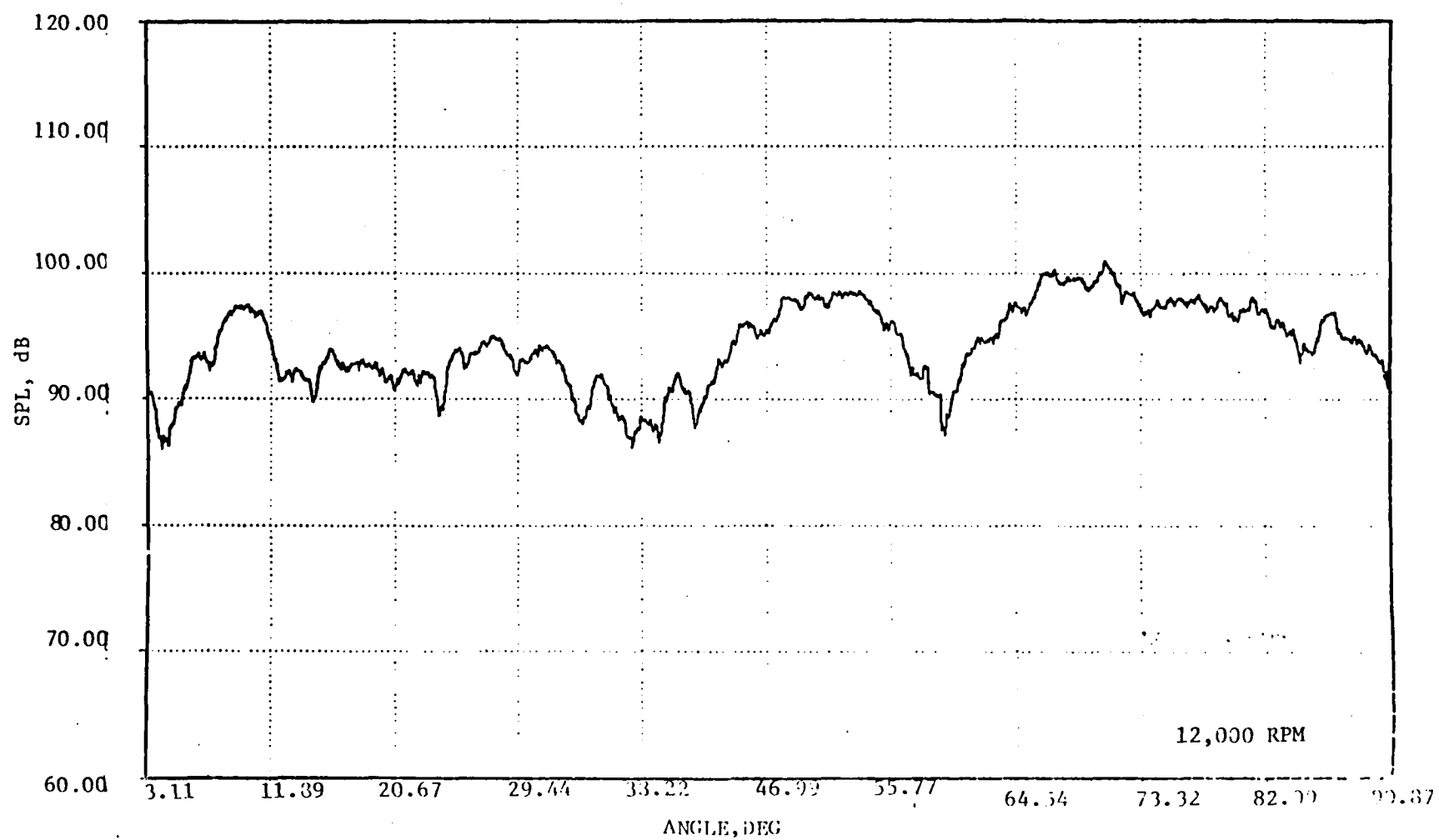
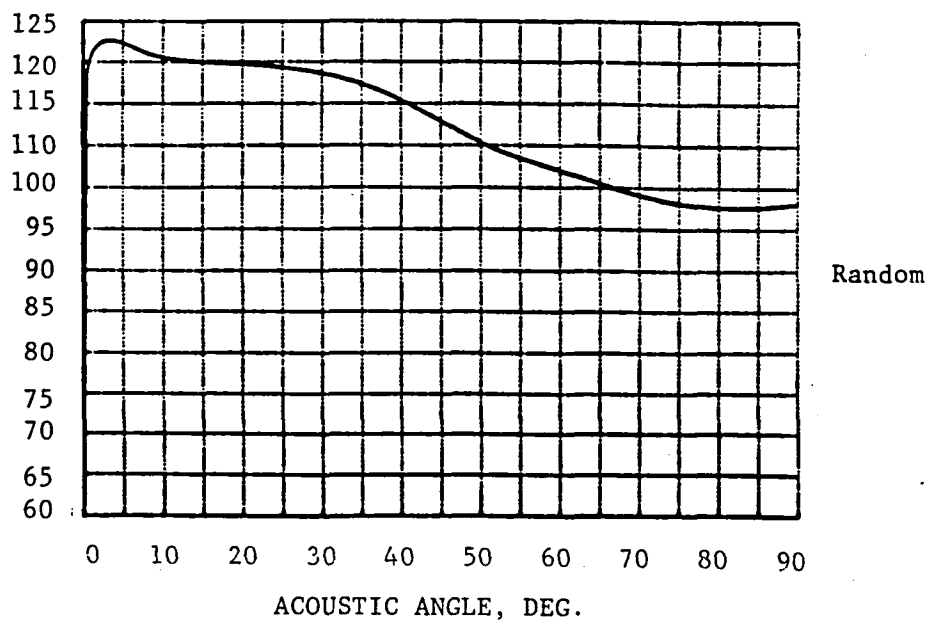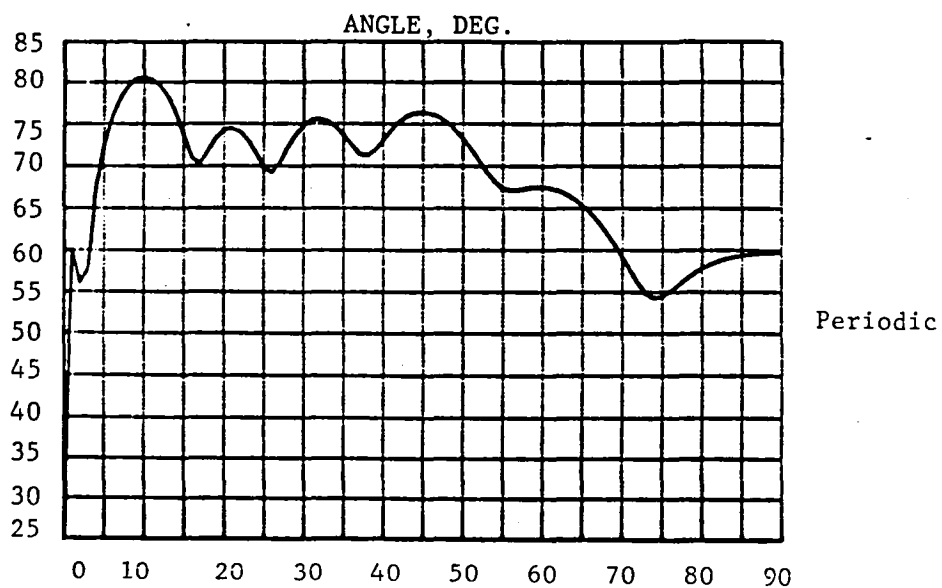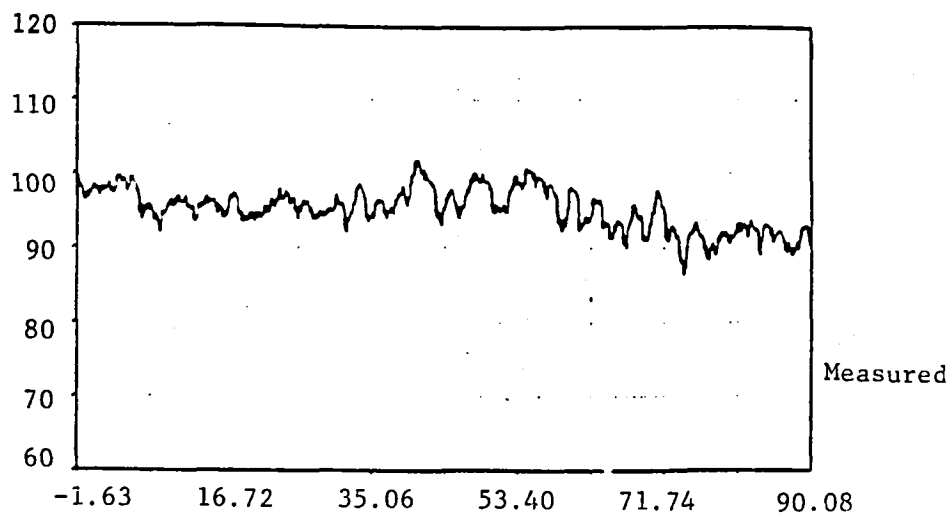Figure 7-19. BPF Directivity for Outdoor TCS (AFT Treated) Test at Engine Speeds of 12,000 RPM.
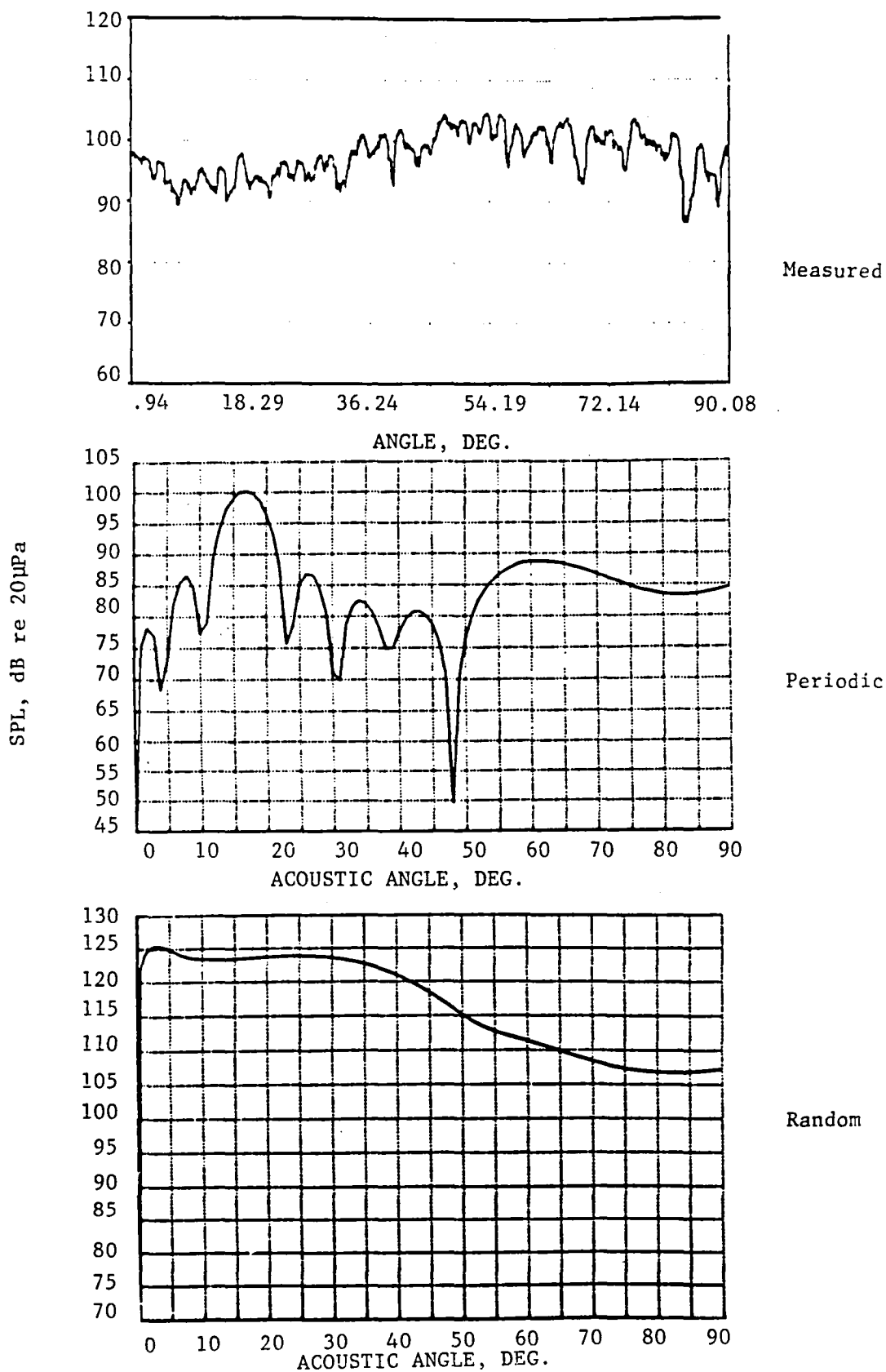
Figure 7-20. Comparison of Measured Outdoor Static (no TCS) BPF Tone Directivity with BPF Predictions of Periodic and Random Acoustic Sources (11,500 RPM).
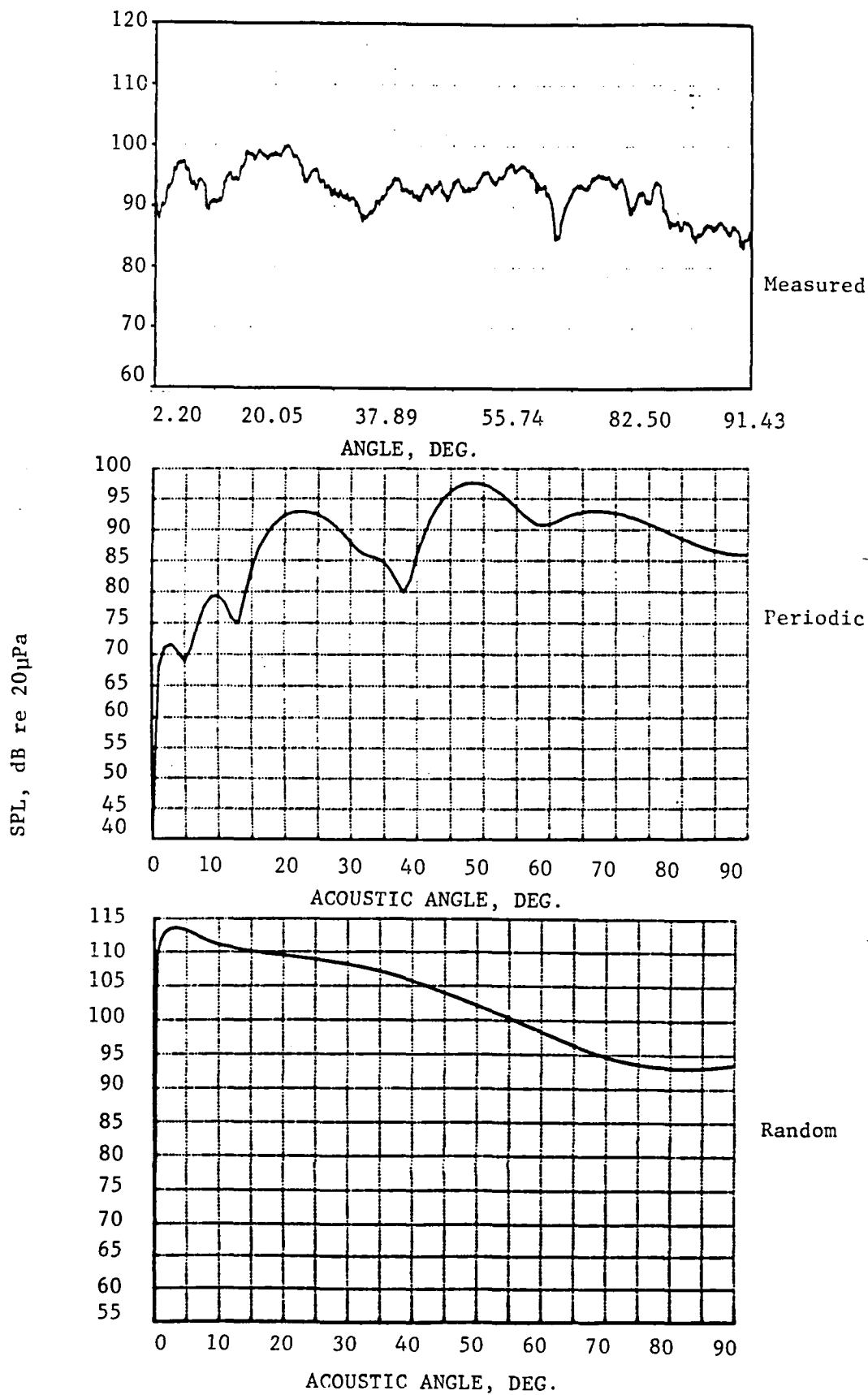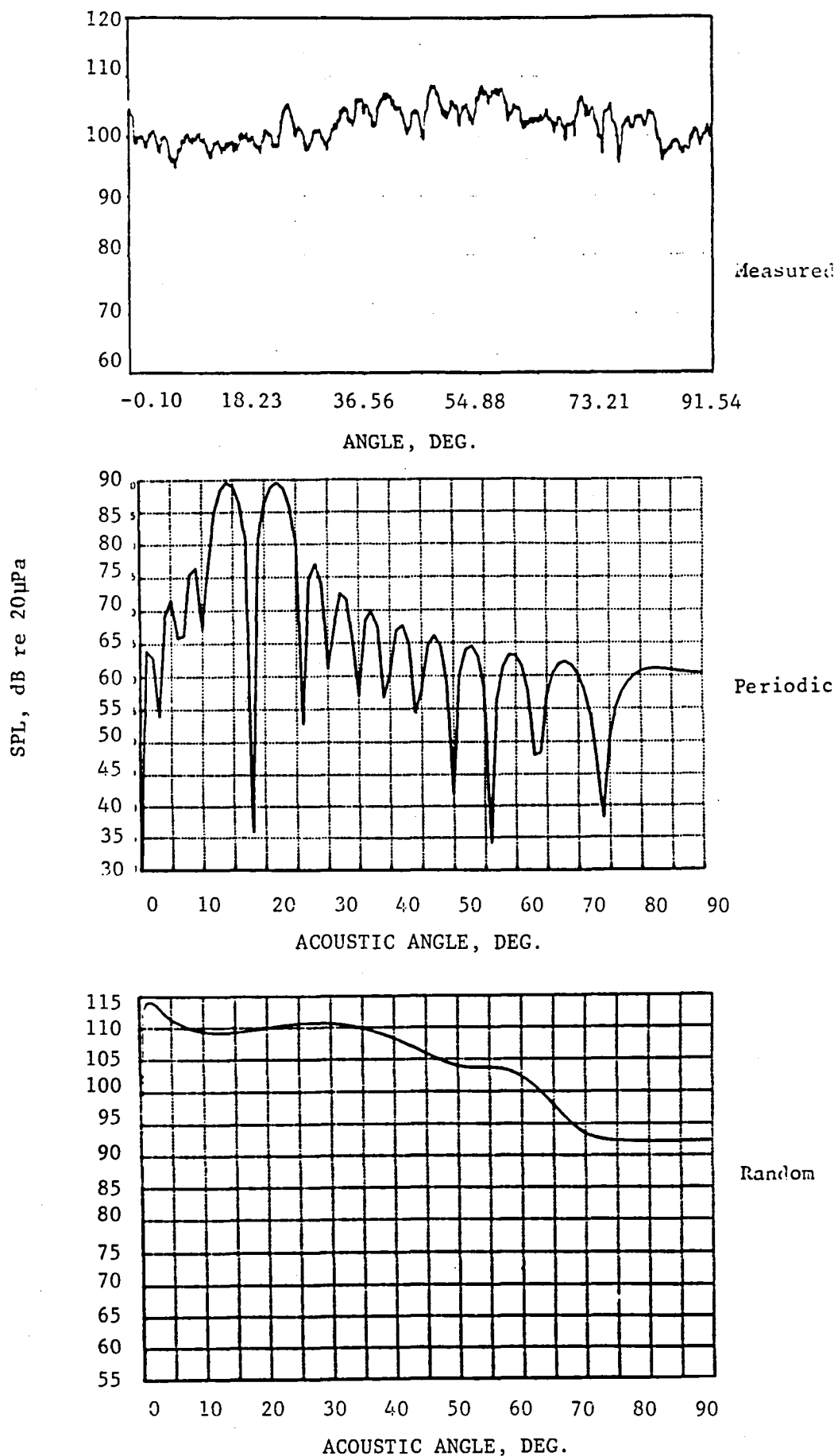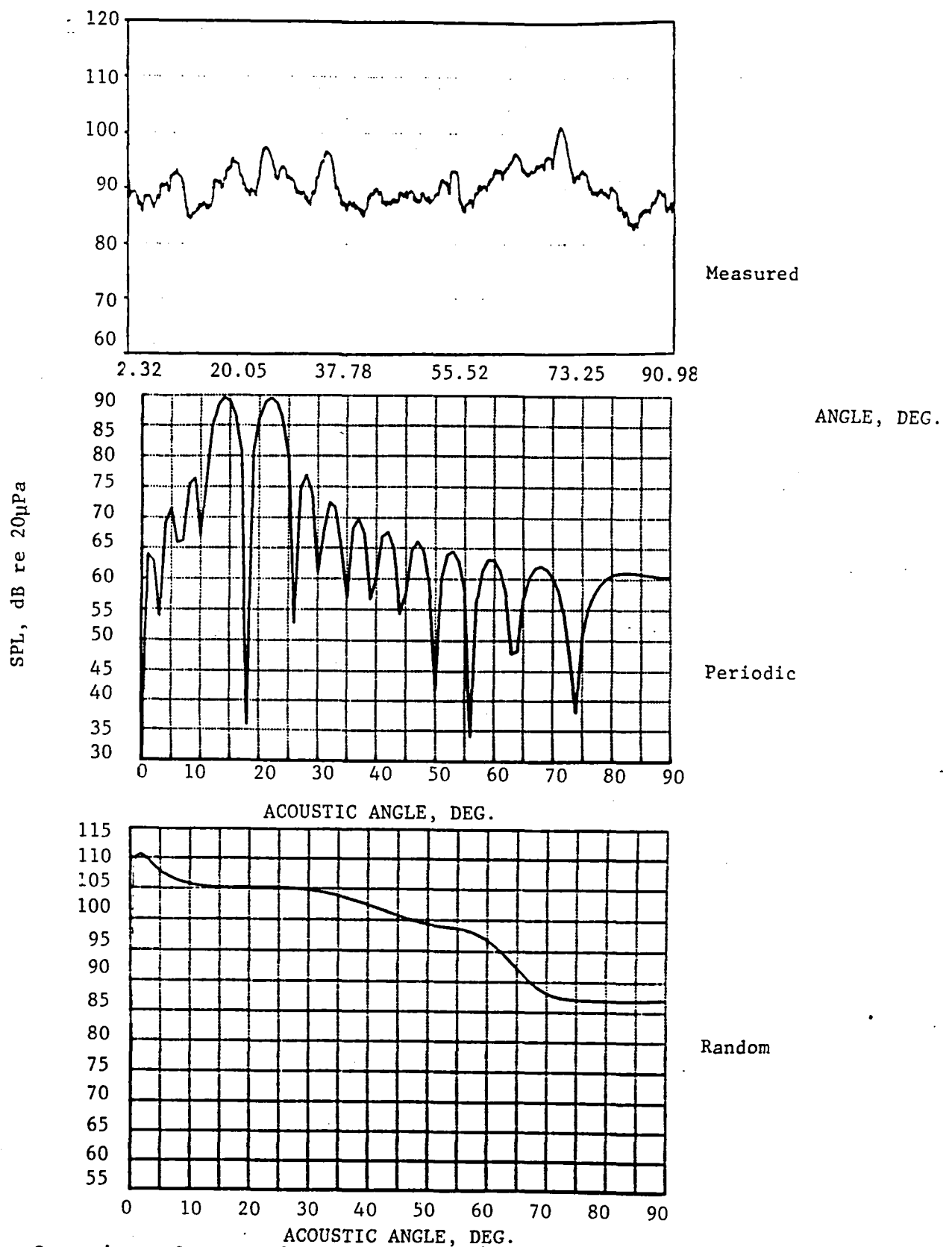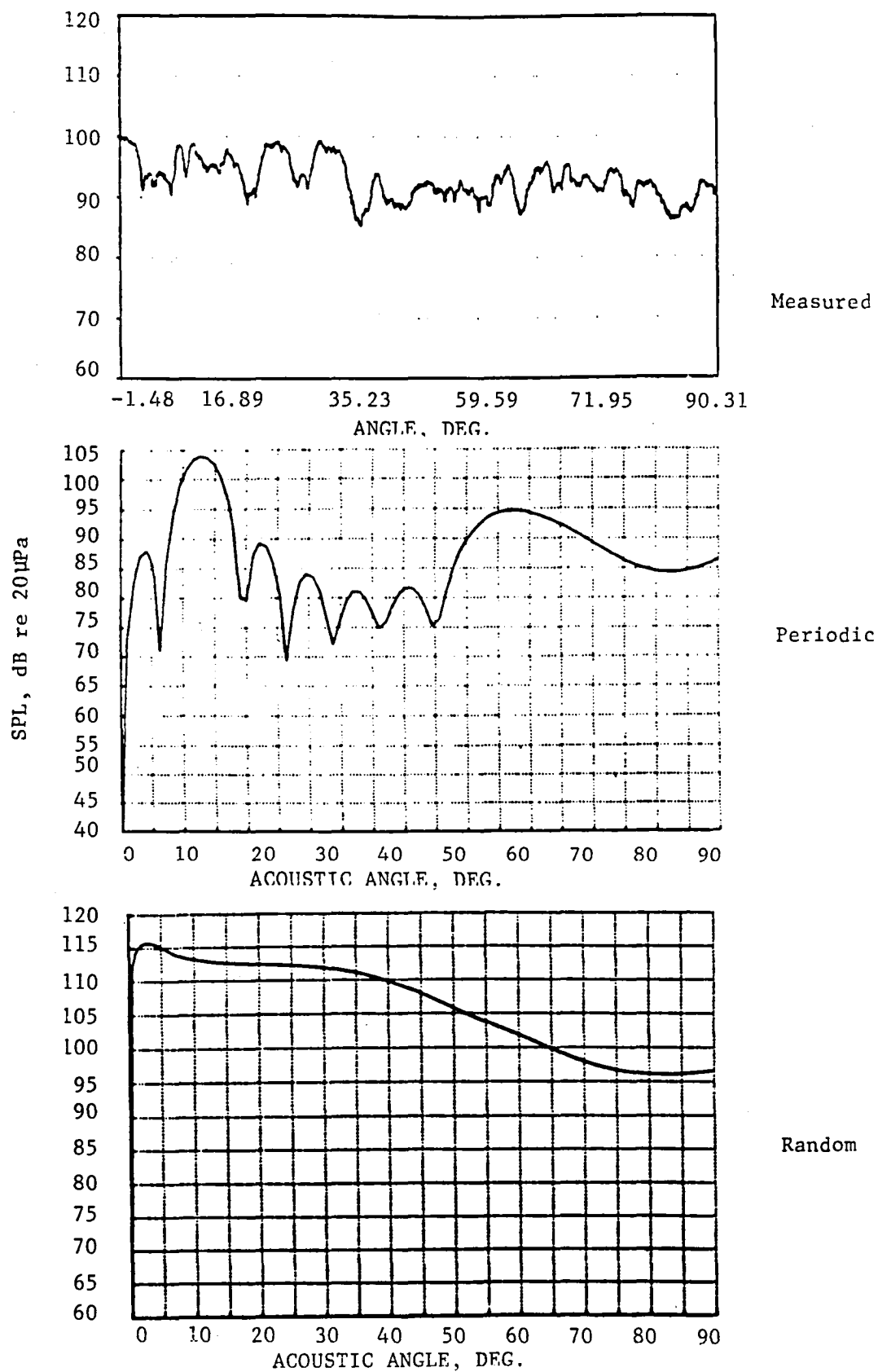
Figure 7-21. Comparison of Measured Outdoor Static (TCS) BPF Tone Directivity with BPF Predictions of Periodic and Random Acoustic Sources (11,500 RPM).
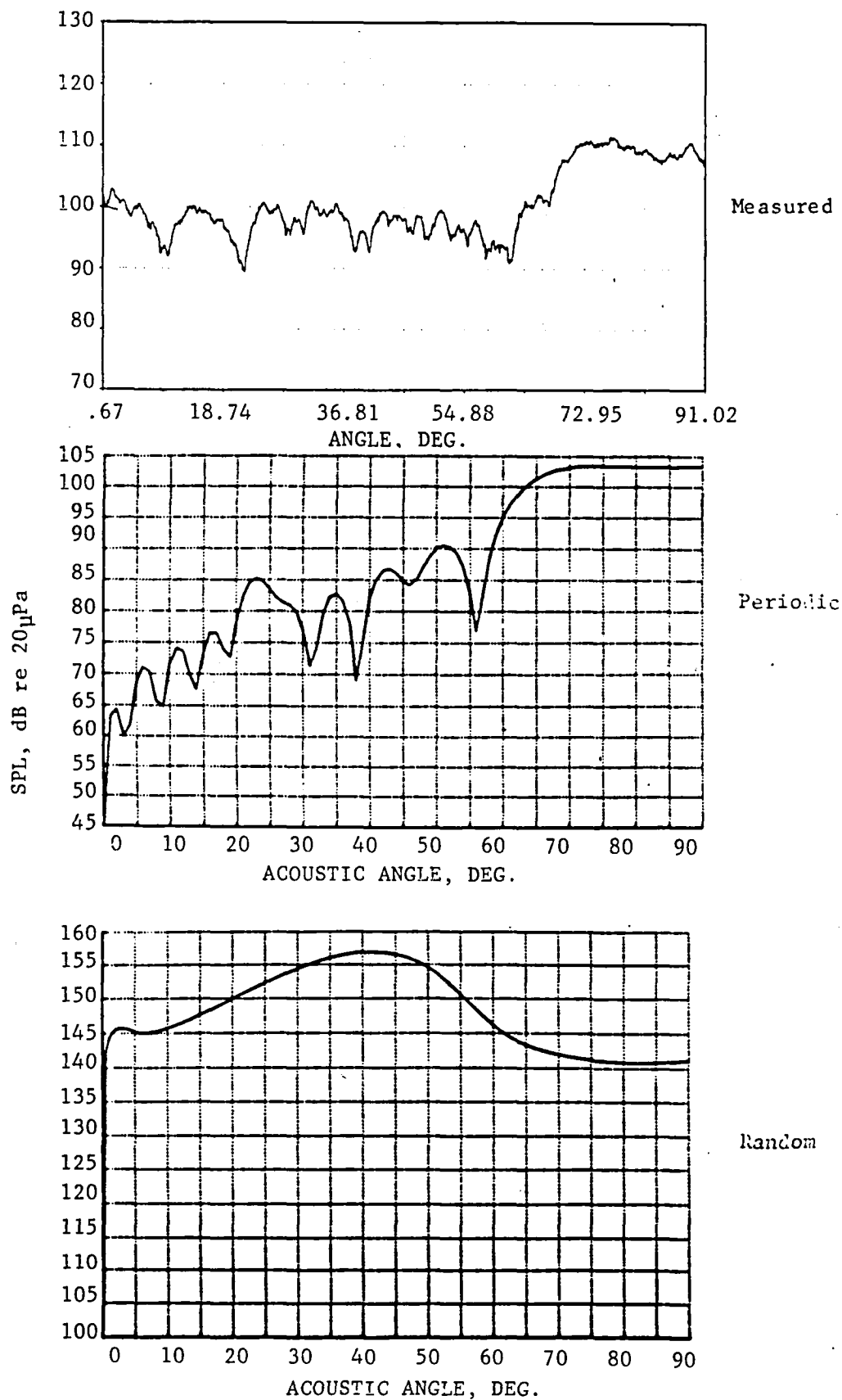
Figure 7-22.   Comparison of Measured Outdoor Static (TCS) BPF Tone Directivity with BPF
Predictions of Peridoic and Random Acoustic Source (13,500 RPM).

179
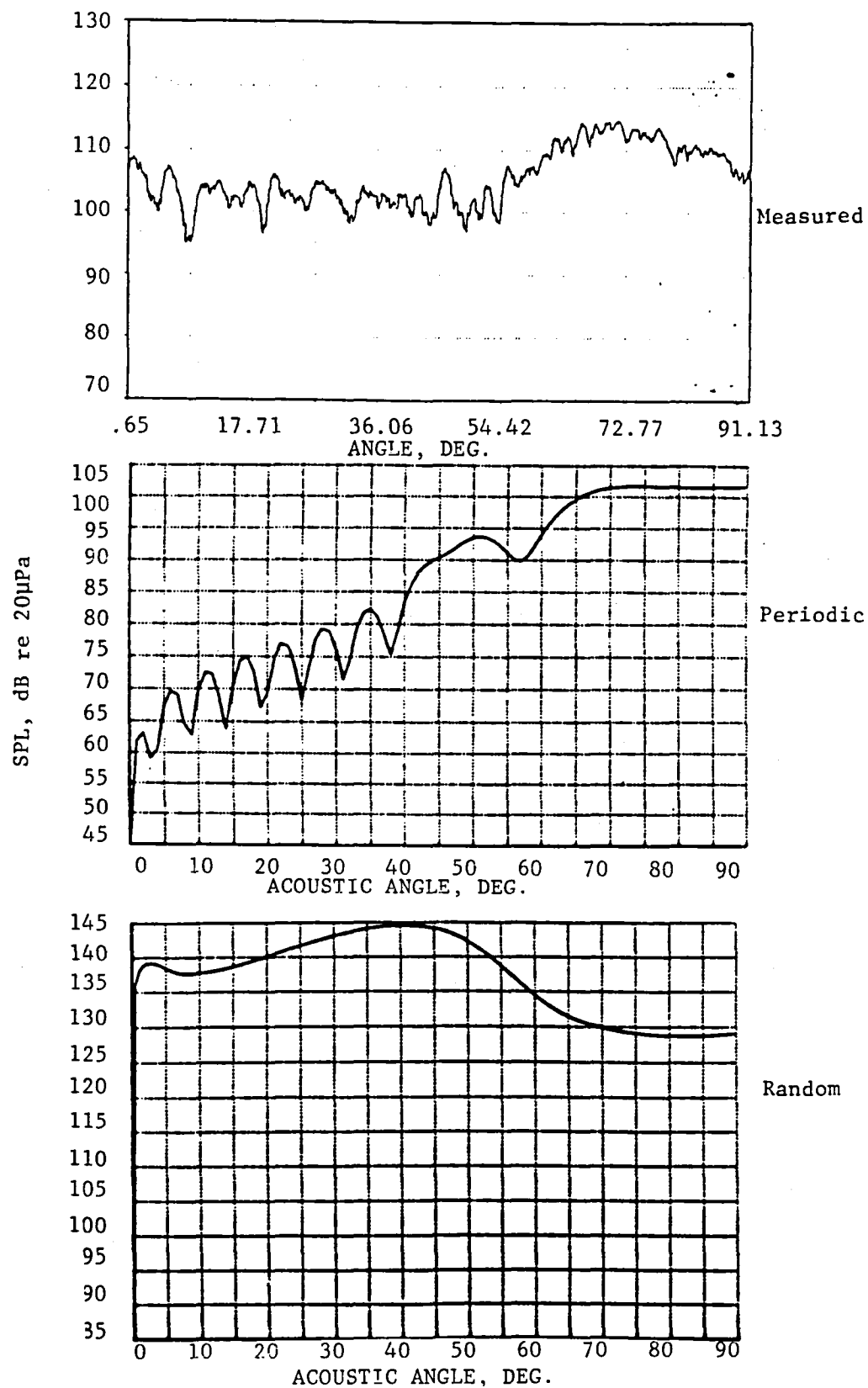
Figure 7-23. Comparison of Measured Outdoor Static (no-TCS) BPF Tone Directivity with BPF Predictions of Perodic and Random Acoustic Sources (13,500 RPM).

7.3   FLIGHT EVALUATION

The BMT results used to predict flight tonal directivities are presented in Figures 7-24 to 7-26. The directivities are computed on a 3.66 m (12 ft) arc for consistency to the other data sets. The measured flight tone time history is then converted back to an equivalent 3.66 m (12 ft) arc condition for these comparisons. The flight BMT results display coherence near the tip region as the H and I values indicate. Strong coherence is also displayed for the six and sixty-six components associated with struts and stators respectively at the 10,435 and 11,924 RPM fan speeds.

7.3.1   SUBSONIC TIP SPEED

The flight subsonic tone is barely visible in the narrowband spectra as was shown in Subsection 5.1; hence, it is interesting to observe that the BMT distortion related tone directivity is also very low (Figure 7-27). In this sense, relative agreement between the BMT predicted result and the flight measurement is achieved.

The twice BPF results are presented in Figure 7-28 where the hump of energy near 90° is not predicted and the high frequency absorption masks any measurable directivity at shallow angles, i.e., less than 20°.

7.3.2   TRANSONIC TIP SPEED

The BMT projected BPF tone directivity (Figure 7-29) is dominated by the 6/rev component; however, the flight measured tone directivity is not nearly as distinct indicating that propagation effects may play an important role in smoothing out of the tone directivity patterns. The general level between the projected and measured results is in satisfactory agreement.

7.3.3   SUPERSONIC TIP SPEED

The flight supersonic tip speed case, Figure 7-30, again reflects the large energy hump attributable to the rotor-alone field which energizes the 28th order acoustic mode and dominates the tonal directivity. Reasonably good prediction is achieved from the periodic portion of the BMT data; however, turbulence related tone noise is again overpredicted by a significant amount.
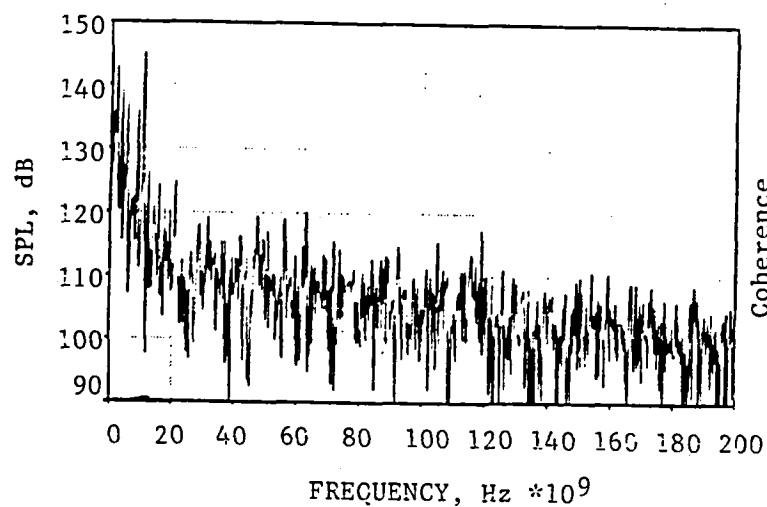
a. "H-K" Enhanced Spectrum
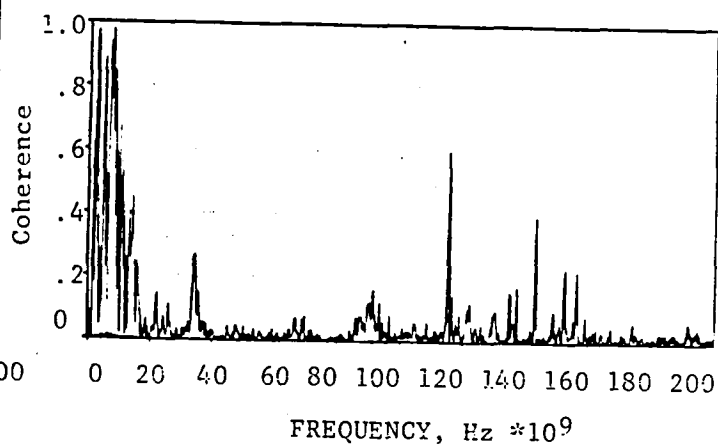
b. Coherence of H and I
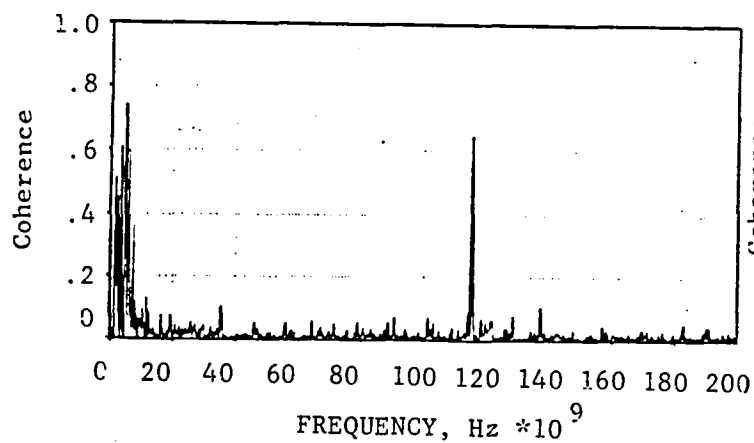
c. Coherence of H and G
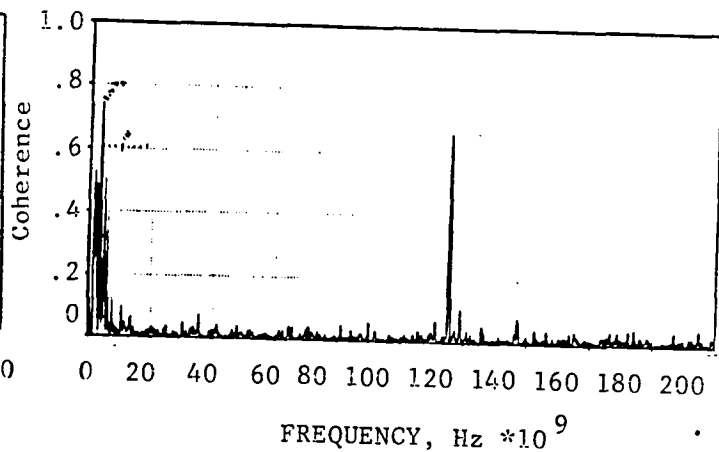
d. Coherence of H and J

Figure 7-24. BMT Results for Flight Test 10,435 RPM.

a. "H-K" Enhanced Spectrum

b. Coherence of H and I

c. Coherence of H and G

d. Coherence of H and J
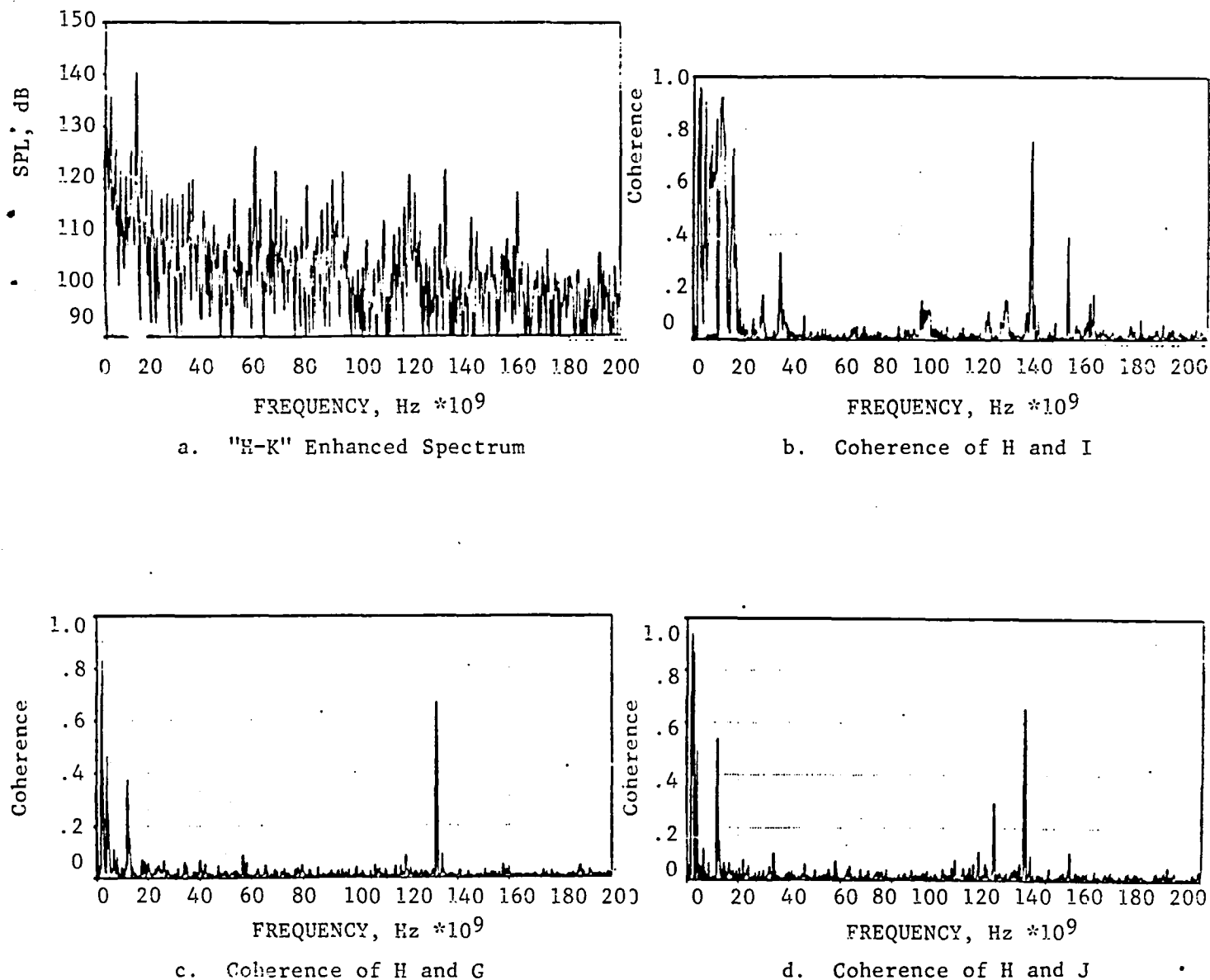
Figure 7-25. BMT Results for Flight Test at 11,924 RPM.
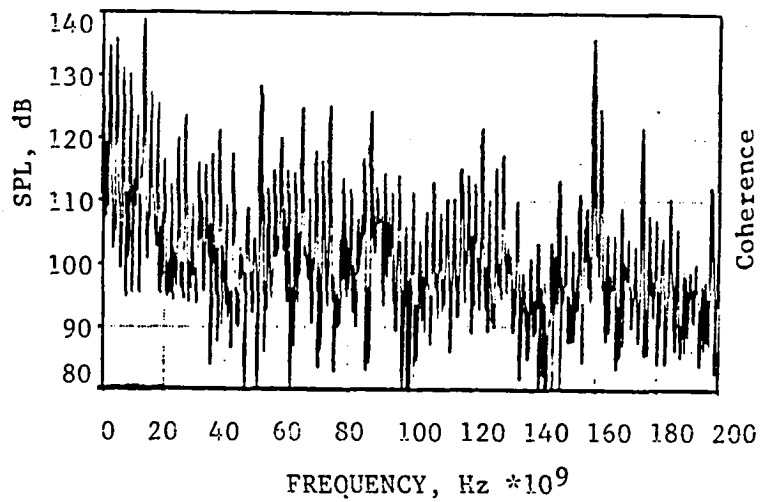
183

a. "H-K" Enhanced Spectrum
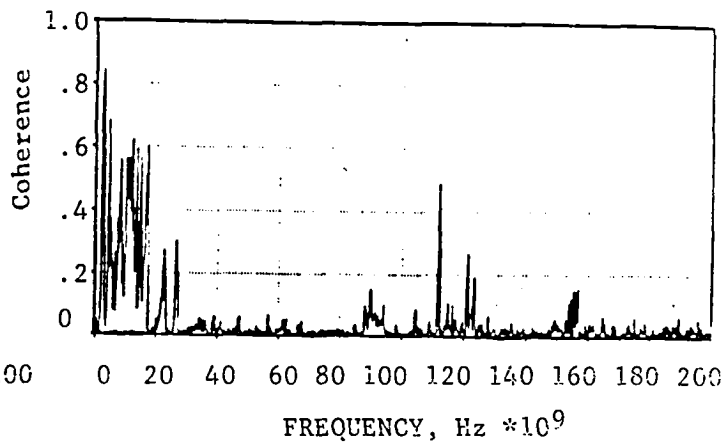
b. Coherence of H and I
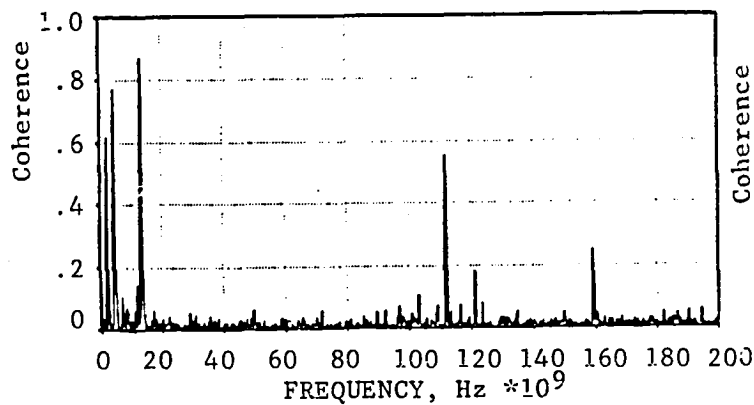
c. Coherence of H and G
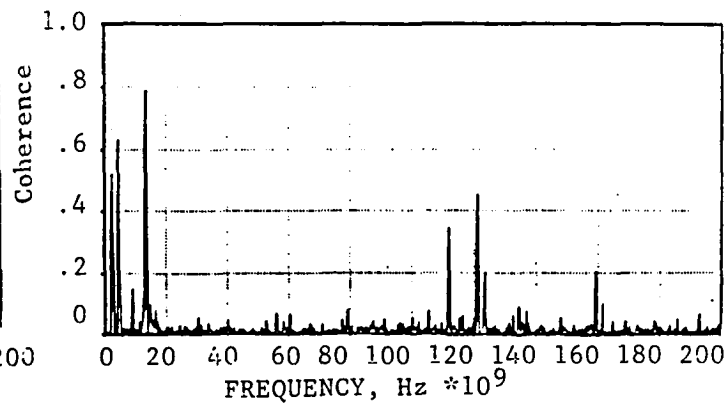
d. Coherence of H and J

Figure 7-26. BMT Results for Flight Test at 13,403 RPM.
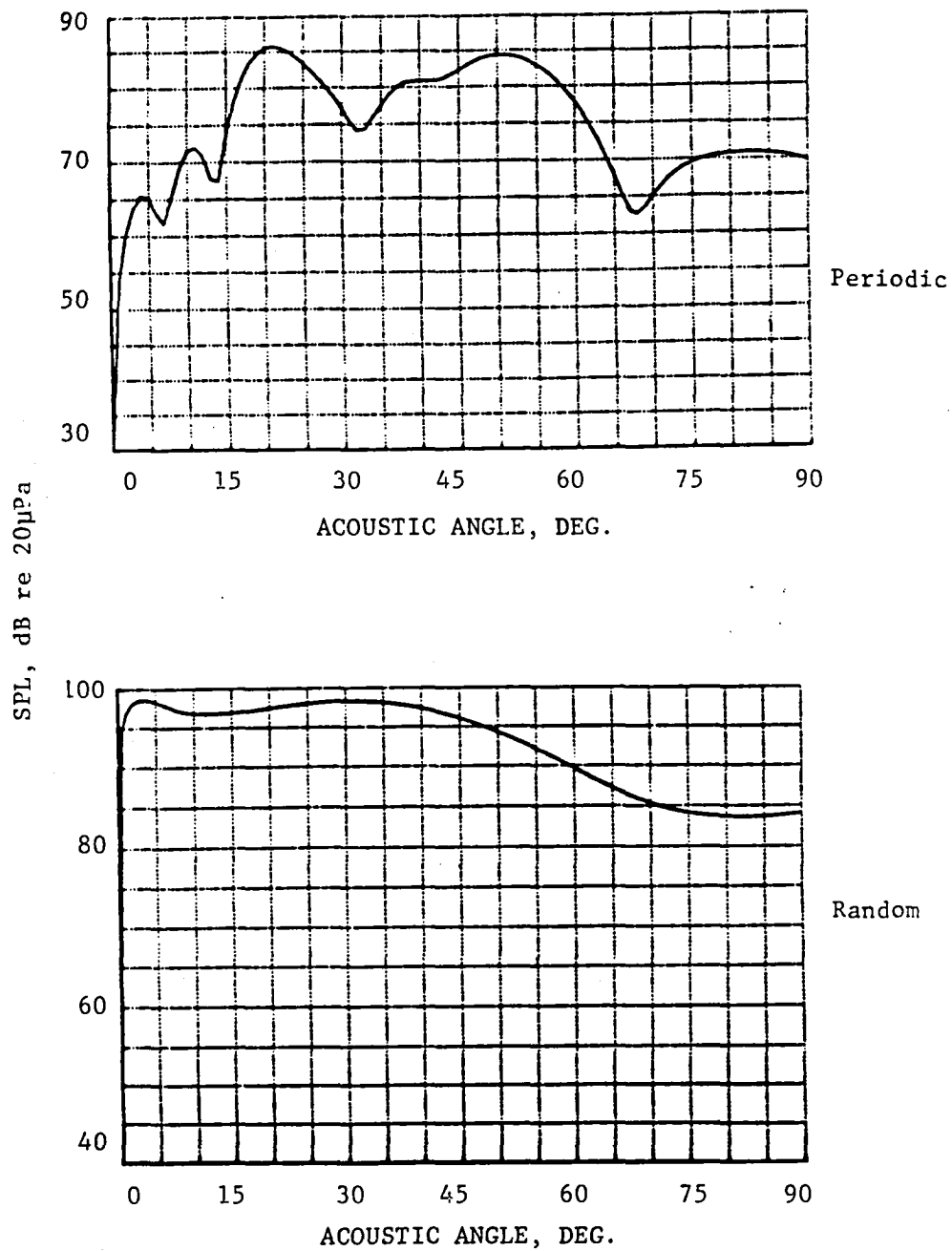
Figure 7-27. Comparison of Determined Flight BPF Tone Directivity with BPF
Perdictions of Periodic and Randome Acoustic Sources (10,435 RPM).

185
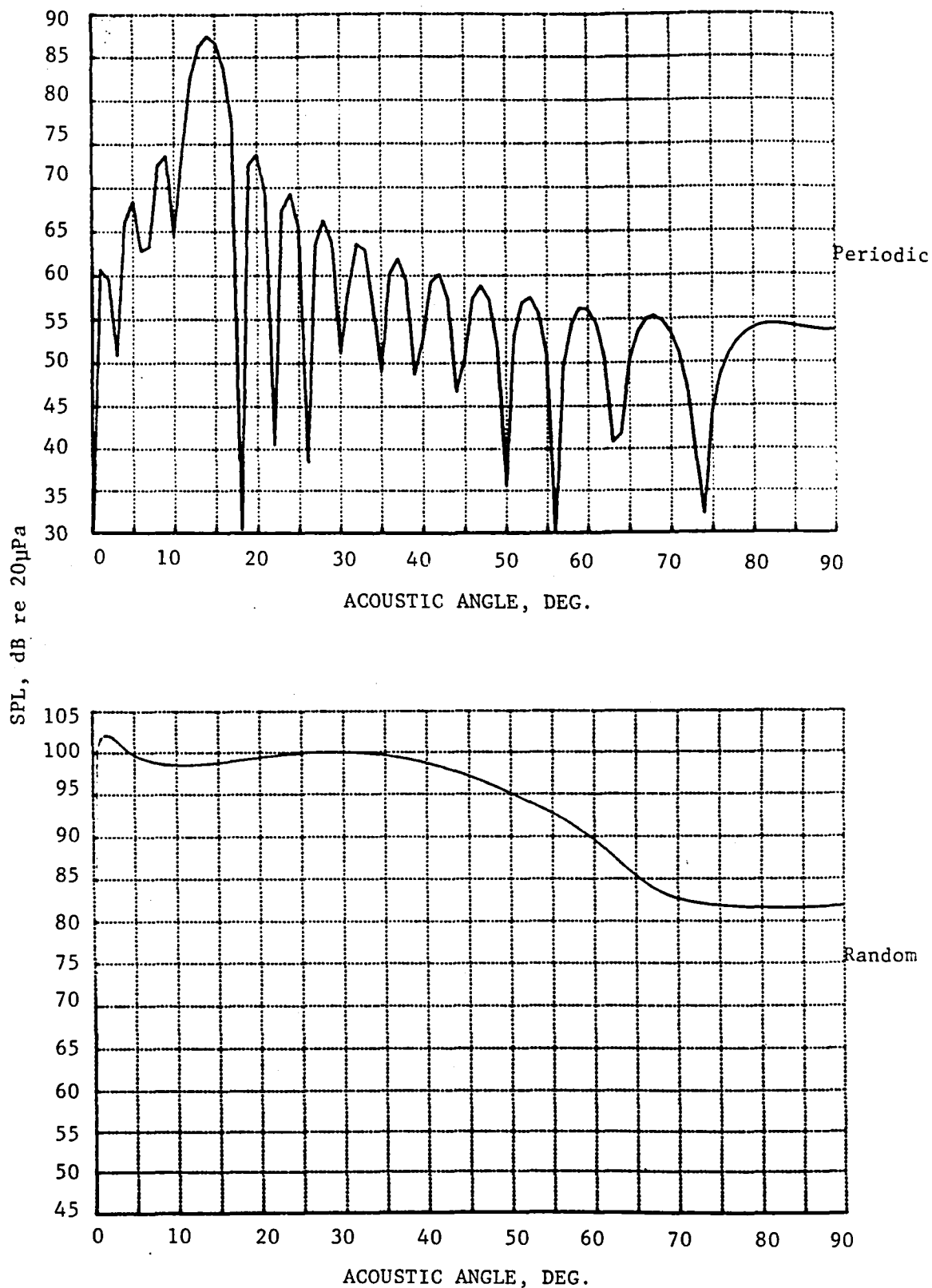
Figure 7-28. Comparison of Determined Flight Twice BPF Tone Directivity with BPF Predictions of Periodic and Random Acoustic Sources (10,534 RPM).
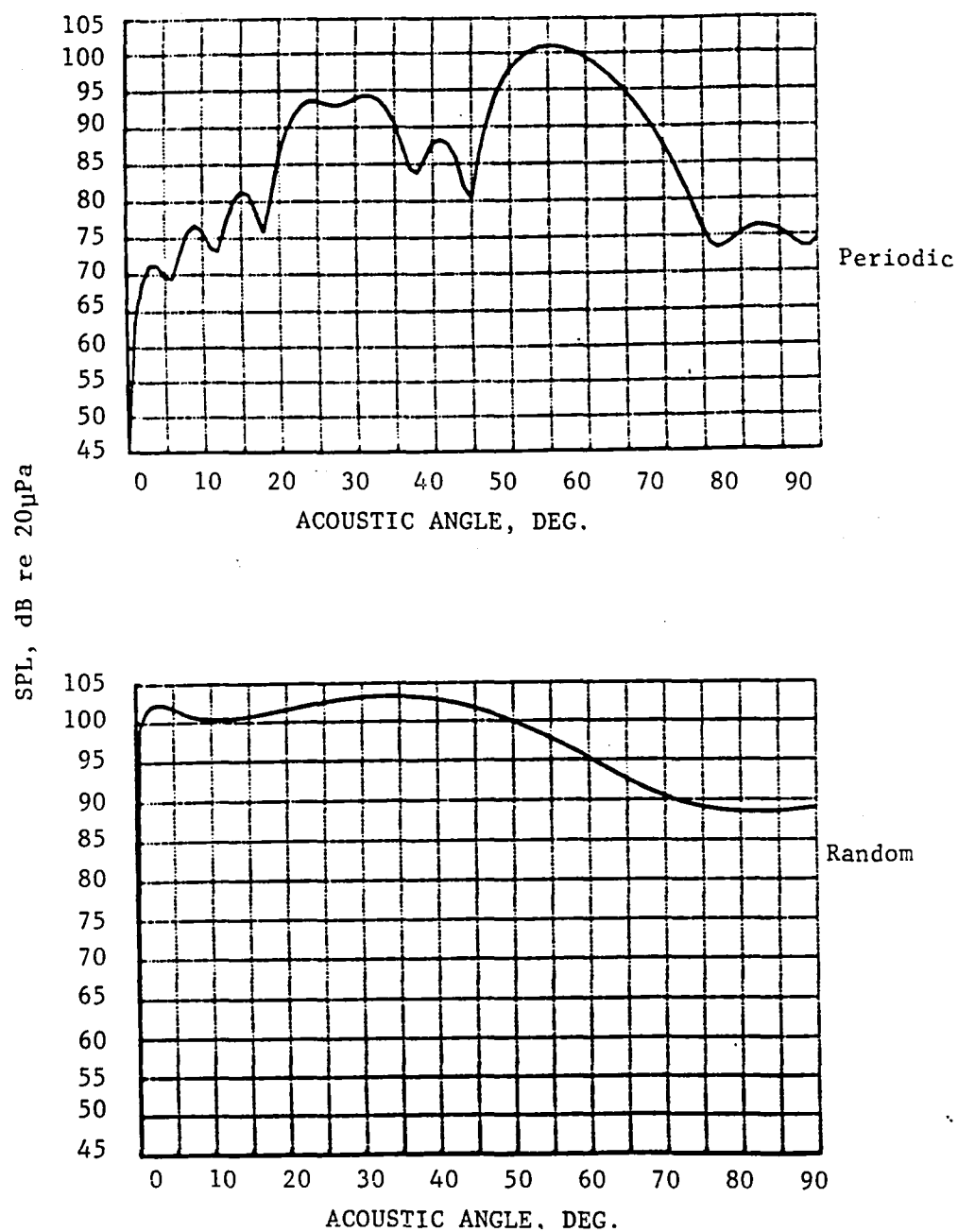
Figure 7-29. Comparison of Determined Flight BPF with BPF Predictions of Periodic And Random Acoustic Sources (11,924 RPM).
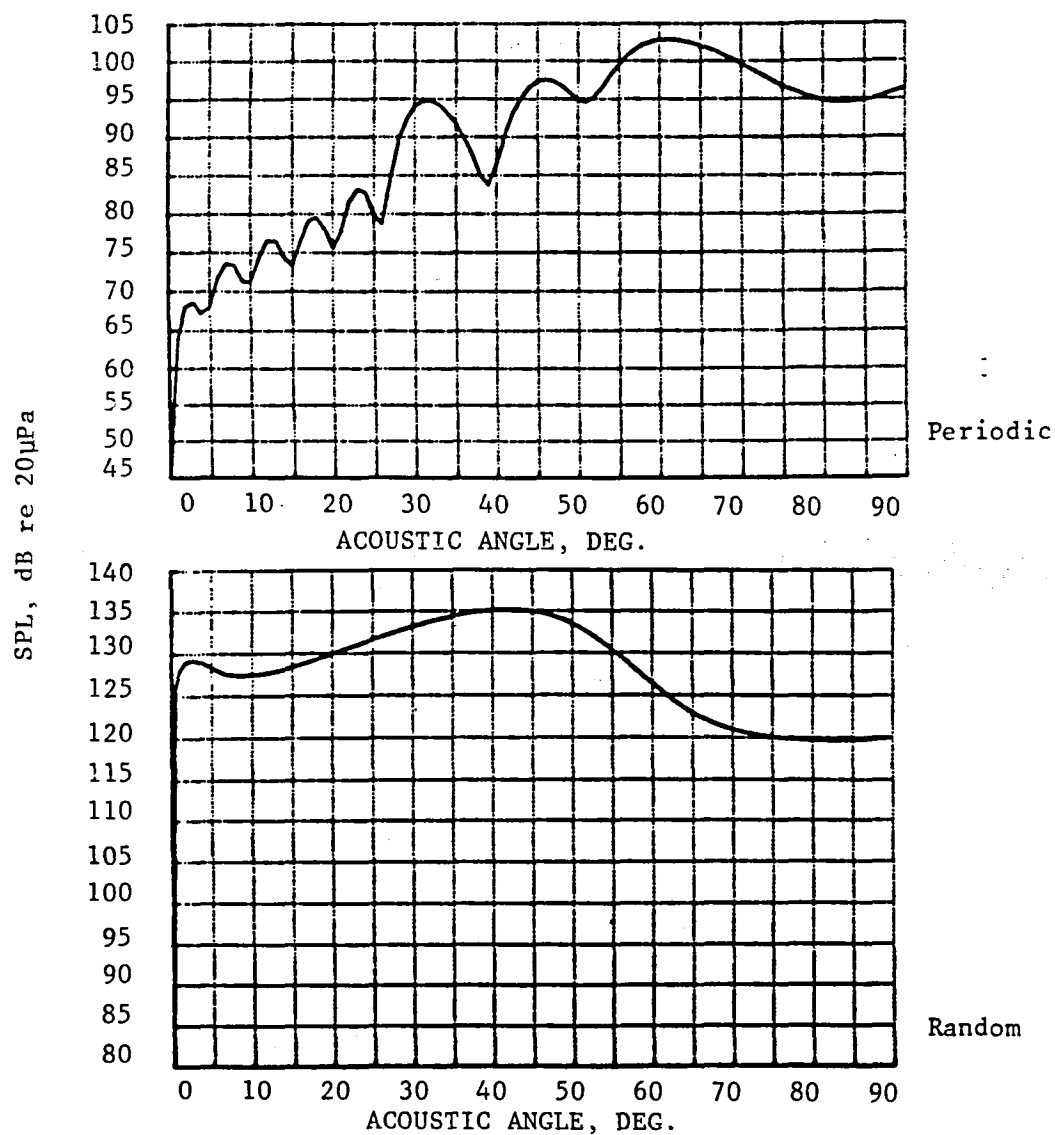
Figure 7-30. Comparison of Determined Flight BPF with BPF Predictions of Periodic and Random Acoustic Sources (13,403 RPM).

SECTION 8.0

CONCLUSIONS

8.0 CONCLUSIONS

The conclusions reached as a result of the data comparisons made and predictions accomplished are as follows:

- The broadband noise levels in flight are on the order of 5 dB lower for the flight case than for the TCS projected to flight case and 3 dB lower for the Wind Tunnel projected to flight case over the angular range from 40 to 70 degrees. At shallow angles, from 15 to 25 degrees, the flight broadband is slightly higher (<2 dB) than projected for either the TCS or Wind Tunnel cases with reasonable agreement occurring near 30° and near 90° angles.

- The BPF tone levels are in relative agreement between projected and flight measured with the following exceptions:

The TCS projected to flight tone is slightly higher than the Wind Tunnel projected to flight tone and both are generally higher than the flight measured level by a few decibels.

The Multiple Pure Tones are lower in flight than projected using TCS data and much lower than Wind Tunnel data. The disagreement in many instances is greater than 10 dB.

- Integrated noise level parameters (EPNL) are adequate for subsonic and transonic engine speeds; however, discrepancies of greater than 5 dB at supersonic speeds exist due to the large disagreement in MPT noise.

- The Blade Mounted Transducer is a useful diagnostic tool to assist in source evaluation; however, better understanding of the test results is required to make predictions of tone farfield directivities using current prediction procedures. The initial attempt to perform this evaluation can be termed encouraging; however, better BMT aerodynamic and aeromechanical understanding should lead to significant improvements in this prediction technology.

189

SECTION 9.0

REFERENCES

9.0 REFERENCES

3-1 Hodder, B.K., "An Investigation of Possible Causes for the Reduction of Fan Noise in Flight," AIAA Paper 76-585, July 1976.

3-2 Preisser, John S. and Chestnutt, David, "Flight Effects on Fan Noise with Static and Wind Tunnel Comparisons," AIAA Paper 83-0678, 8th Aeroacoustics Conference, April 11-14, 1983.

3-3 Moore, M.T., "Forward Velocity Effects on Fan Noise and the Suppression Characteristics of Advanced Inlets as Measured in the NASA-Ames 40x80 Foot Wind Tunnel," NASA CR-152328, September 1979.

3-4 McArdle, J.G., Jones, W.L., Heidelberg, L.J., and Homyak, L., "Comparison of Several Inflow Control Devices for Flight Simulation of Fan Tone Noise," NASA TMX-81505, June 1980.

3-5 Schoenster, J.A., "Fluctuating Pressure Measurements on the Fan Blades of a Turbofan Engine Purging Ground and Flight Tests," AIAA Paper 83-0679, April 11-13, 1983.

3-6 Knight, V.H. Jr., "In-Flight Jet Engine Noise Measurement System," ISA 27th International Instrumentation Symposium, April 27-30, 1981.

3-7 Holm, R.G., Horne, C., Atencio, A., and Karchmer, A., "The Influence of Inlet Design on the Aeroacoustic Performance of a JT15D Turbofan Engine as Measured in the NASA Ames 40x80 ft. Wind Tunnel," AIAA Paper 83-0681, AIAA 8th Aeroacoustic Conference, April 11-13, 1983.

4-1 Carter, G.C, Knapp, C.H. and Nutall, A.H., "Estimation of the Magnitude-Squared Coherence Function Via Overlapped Fast Fourier Transform Processing," IEEE Transactions on Audio and Electronics, Vol. AU-21, No. 4, August 1973.

4-2 Mangiarotty, R.A. and Turner, B.A., "Wave Radiation Doppler Effect Correction For Motion of a Source, Observer and the Surrounding Medium," J. Sound Vib., Vol. 6(I), pp. 110-116, 1967.

REFERENCES (Continued)

4-3   Perrachio, A.A., Ganz, U. and Gedge, M., "Studies an Proper Simulation
       During Static Testing of Forward Speed Effects on Fan Noise," NASA
       CR-165626. September 1980.

5-1   Hanson, D.B., Study of Noise and Inflow Distortion Sources in the NASA
       QF-1B Fan Using Measured Blade and Vane Pressures, NASA CR-2899,
       September 1977.

5-2   McArdle, J.G., Jones, W.L., Heidelberg, L.J., and Homyak, L.,
       Comparison of Several Inflow Control Devices for Flight Simulation of
       Fan Tune Noise Using a JT15D-1 Engine, NASA TMX-81505, June 1980.

5-3   Preisser, J.S., Schoenster, J.A., Golub, R.A. and Horne, C., "Unsteady
       Fan Blade Pressure and Acoustic Radiation from a JT15D-1 Turbofan
       Engine at Simulated Forward Speed," AIAA Paper 81-0096, January 1981.

5-4   Preisser, John S. and Chestnutt, David, "Flight Effects on Fan Noise
       with Static and Wind Tunnel Comparisons," AIAA Paper 83-0678, April
       11-14, 1983.

5-5   Holm, R.G., Langenbrunner, L.E. and McCann, E.O., Forward Velocity
       Effects on Fan Noise and the Influence of Inlet Aeroacoustic Design as
       Measured in the NASA Ames 40 x 80 Foot Wind Tunnel, NASA CR-166461,
       July 1981.

5-6   Schoenster, J.A., "Fluctuating Pressure Measurements on the Fan Blades
       of a Turbofan Engine During Ground and Flight Tests," AIAA Paper No.
       83-0679, April 1983.

6-1   Morse, Phillip M. and Ingard, K. Uno, Theoretical Acoustics, Chapter
       11, McGraw-Hill, 1968.

6-2   Kerschen, E.J. and Gliebe, P.R., Fan Noise Caused by Ingestion of
       Anisotropic Turbulence – A Model Based on Axisymmetric Turbulence
       Theory, AIAA-80-1021, AIAA 6th Aeroacoustics Conference, June 1980.

REFERENCES (Concluded)

6-3   Gliebe, P.R., <u>Analytical Study of the Effects of Wind Tunnel Turbulence on Turbofan Rotor Noise</u>, AIAA-80-1022R, AIAA 6th Aeroacoustics Conference, June 1980.

6-4   Schulten, J.B.H.M., <u>Vane Chamber and Angle of Incidence Effects in Fan Noise Generation</u>, AIAA 83-0766, April 11-14, 1983.

6-5   Rice, E.J., <u>Multimodal Farfield Acoustic Radiation Pattern - An Approximate Equation</u>, AIAA 4th Aeroacoustics Conference, October 1977.

6-6.   Mungur, P., and Gliebe, P.R., <u>Acoustic Analysis of Fan Tone Generation and Propagation</u>, AIAA 83-0769, April 11-14, 1983.

APPENDIX I

The atmospheric absorption of sound is accounted for using the procedure outlined in DOT-TST-75-87, "Review of Experimental Data in Support of a Proposed New Method for Computing Atmospheric Absorption Losses," by L. Sutherland.

α	atmospheric absorption loss coefficient (dB/ft)
α	$\alpha_{cl}' + \alpha_{rot}' + \alpha_{vib}(O_2) + \alpha_{vib}(N_2)$
α_{cl}	classical losses including thermal, viscous and diffusion losses
α_{rot}	molecular absorption losses rotational relaxation of oxygen and nitrogen molecules
$\alpha_{vib}(O_2)$ & $a_{vib}(N_2)$	molecular absorption losses for vibration relaxation of oxygen (O_2) and nitrogen (N_2) molecules respectively.
$\alpha_{cl} + \alpha_{rot}$	.672 E-10 $(f^2/P^*)/(1+^{110.4}/T))$
P^*	Barometric Pressure/29.921 (in. Hg units)
T	temperature (°K)
f	frequency Hz
α_{vib}	8.686 μ_{max} $(f/c) * (f/f_m)^2/[1+(f/f_m)^2]$
c	1087.01 * $T/273.15$ (acoustic velocity in ft/sec, dry air)
$\mu_{max}(O_2)$ $e^{-\theta o/T}/[1-e^{-\theta o/T}]^2$	$(4\pi/35) * .20948 * (\theta o/T)^2$
$\mu_{max}(N_2)$ $e^{-\theta N/T}/[1-e^{-\theta N/T}]^2$	$(4\pi/35) * .78084 * (\theta N/T)^2$
θo	2239.1 °K
θN	3352.0 °K
P_s/P_o	$10^{[20.5318 - (2929/T) - 4.922 \log (T)]}/P^*$

h $\qquad$ RH * (P_S/P_O), RH - relative humidity

fm (O_2) $\qquad$ $(24 + 44100 \ h \ [\frac{.05 + h}{.391 + h}]) * [P*/(T/293)^{0.5}]$

fm (N_2) $\qquad$ $(9 + 350 \ h \ e^{-3.763 \ [(293/T)^{1/3} - 1]}) * [P*(T/293)]$

The quantities μ_{max} and fm are the maximum loss per wavelength and the frequency at which it occurs respectively.

1. Report No. NASA CR-172322	2. Government Accession No.	3. Recipient's Catalog No.
4. Title and Subtitle JT15D SIMULATED FLIGHT DATA EVALUATION		5. Report Date Sept. 1984
		6. Performing Organization Code
7. Author(s) R. G. HOLM		8. Performing Organization Report No. —
		10. Work Unit No.
9. Performing Organization Name and Address AIRCRAFT ENGINE BUSINESS GROUP GENERAL ELECTRIC COMPANY CINCINNATI, OHIO 45215		11. Contract or Grant No. NAS1-16776
		13. Type of Report and Period Covered FINAL REPORT
12. Sponsoring Agency Name and Address NATIONAL AERONAUTIC AND SPACE ADMINISTRATION LANGLEY RESEARCH CENTER HAMPTON, VIRGINA, 23065		14. Sponsoring Agency Code

15. Supplementary Notes

LANGLEY TECHNICAL MONITOR - J. S. PREISSER
FINAL REPORT

16. Abstract   The noise characteristics of the JT15D turbo fan engine was analyzed with the objectives of (1) assessing the state-of-art ability to simulate flight acoustic data using test results acquired in wind tunnel and outdoor (turbulence controlled) environments and (2) predicting the farfield noise directivity of the blade passage frequency (BPF) tonal components using results from rotor blade mounted dynamic pressure instrumentation. Engine rotor tip speeds at subsonic, transonic, and supersonic conditions were evaluated. The ability to simulate flight results was generally within 2-3 dB for both outdoor and wind tunnel acoustic results. Some differences did occur in the broadband noise level and in the multiple-pure-tone harmonics at supersonic tip speeds.

The prediction of blade passage frequency tone directivity from dynamic pressure measurements was accomplished for the three tip speed conditions. Predictions were made of the random and periodic components of the tone directivity. The technique for estimating the random tone component used hot wire data to establish a correlation between dynamic pressure and turbulence intensity. This prediction overestimated the tone level by typically 10 dB with the greatest overestimates occurring at supersonic conditions. The periodic tone component was estimated using correlations lengths on the blade surface to determine the acoustic power level for vaious propagating modes. Conclusion is that current analytical models using dynamic measurements as the starting point to obtain farfield acoustics estimates need further refinement.

17. Key Words (Suggested by Author(s)) ACOUSTICS, FLIGHT NOISE, FAN NOISE	18. Distribution Statement

19. Security Classif. (of this report) UNCLASSIFIED	20. Security Classif. (of this page) UNCLASSIFIED	21. No. of Pages 197	22. Price

n-305